VOLUME 2 Ternary and Quaternary III-V Compounds

HANDBOOK SERIES ON

SEMICONDUCTOR PARAMETERS

Editors

M LEVINSHTEIN
S RUMYANTSEV
M SHUR

World Scientific

VOLUME 2 Ternary and Quaternary III-V Compounds

HANDBOOK SERIES ON

SEMICONDUCTOR PARAMETERS

HANDBOOK SERIES ON SEMICONDUCTOR PARAMETERS

edited by M. Levinshtein, S. Rumyantsev and M. Shur

Vol. 1: Si, Ge, C (Diamond), GaAs, GaP, GaSb, InAs, InP, InSb

Vol. 2: Ternary and Quaternary A_3B_5 Semiconductors

VOLUME 2 Ternary and Quaternary III-V Compounds

HANDBOOK SERIES ON SEMICONDUCTOR PARAMETERS

Editors

M LEVINSHTEIN
S RUMYANTSEV
Ioffe Institute

M SHUR
Rensselaer Polytechnic Institute

World Scientific
Singapore • New Jersey • London • Hong Kong

Published by

World Scientific Publishing Co. Pte. Ltd.
P O Box 128, Farrer Road, Singapore 912805
USA office: Suite 1B, 1060 Main Street, River Edge, NJ 07661
UK office: 57 Shelton Street, Covent Garden, London WC2H 9HE

British Library Cataloguing-in-Publication Data
A catalogue record for this book is available from the British Library.

HANDBOOK SERIES ON SEMICONDUCTOR PARAMETERS
VOLUME 2: Ternary and Quaternary A_3B_5 Semiconductors

Copyright © 1999 by World Scientific Publishing Co. Pte. Ltd.

All rights reserved. This book, or parts thereof, may not be reproduced in any form or by any means, electronic or mechanical, including photocopying, recording or any information storage and retrieval system now known or to be invented, without written permission from the Publisher.

For photocopying of material in this volume, please pay a copying fee through the Copyright Clearance Center, Inc., 222 Rosewood Drive, Danvers, MA 01923, USA. In this case permission to photocopy is not required from the publisher.

ISBN 981-02-1420-0 (Set)
ISBN 981-02-2935-6

This book is printed on acid-free paper.

Printed in Singapore by Uto-Print

To our friends
in many countries

PREFACE

This second volume of the Handbook Series on Semiconductor Parameters contains data on the most popular ternary and quaternary III-V compounds. To a certain extent, these compounds allow us to tailor material parameters optimizing these parameters for device applications and, at the same time, matching their lattice constants to available substrates. This is especially important for heterostructure devices, and the best semiconductor lasers and High Electron Mobility Transistors all use heterostructures based on ternary or quaternary compounds.

The technology and characterization of ternary and quaternary compounds are more complicated than for their binary counterparts. This is reflected in a variety and complexity of experimental data for the material parameters, often represented by interpolation formulas based on curve fits or on a linear regression. The parameters predicted by these formulas for the limiting values of the mole fractions ($x = 0$ or $x = 1$) may differ slightly from their values measured for the corresponding binary compounds. This should not be a cause for alarm. The situation is more serious when the differences in the values of the material parameters measured by different authors exceed the stated accuracy of the measurements. In such cases, we chose the values which we believed to be more reliable.

The data for each material in Volume II are organized in the same way, similar to how it was done in Volume I. This makes the search for information easier. We provided interpolation formulas in addition to graphs in order to make the information more quantitative. All in all, we tried to come up with a handbook, useful for every semiconductor researcher or engineer in their everyday work.

The discussion of the physical meaning of semiconductor parameters listed in this handbook may be found in "Introduction to Electronic Devices" by M. S. Shur (John Wiley and Sons, New York, 1995), which contains convenient tables summarizing the basic semiconductor equations and the definitions of basic semiconductor parameters. More detailed information is given in the two volume "Survey of Semiconductor Physics" by Karl Boer (van Nostrand, New York, 1990).

In some cases, the parameters, which one may need, are different from but related to the parameters given in this handbook. (This is especially true for parameters which are components of different tensors.) In this case, the book "Structure-Property Relations" by R. E. Newnhams (Springer-Verlag, New York, 1975) may be helpful.

The additional information about the properties of III-V ternary and quaternary compounds may be found in the book by S. Adachi, "Properties of III-V Semiconductor Compounds", John Wiley and Sons, New York, 1992. The book by T. P. Pearsal (GaInAsP Alloy Semiconductors, John Wiley and Sons, New York, 1982) describes GaInAsP and related materials. The properties of different III-V ternary and quaternary compounds are also summarized in the famous Landolt-Bornstein series, Numerical Data and Functional Relationship in Science and Technology, Springer, New York, 1982, and in the books of the Electronic Materials Information Service Datareviews Series from INSPEC (IEE Publishing). The volumes of the Datareviews Series relevant to the compounds discussed in this book are:

No. 2. Properties of Gallium Arsenide (2nd Edition, 1990)
No. 6. Properties of Indium Phosphide (1991)
No. 7. Properties of Aluminum Gallium Arsenide (1993)
No. 8. Properties of Lattice-Matched and Strained Indium Gallium Arsenide (1993)

We are grateful to our colleagues at A. F. Ioffe Institute who helped us to find information, made many excellent suggestions, and, in some cases, provided us with more accurate values of material parameters. Paraphrasing Bertrand Russell, we can say that "a parameter in science is not a fact, but an instance." Therefore, we will greatly appreciate any comments or suggestions, which can be e-mailed to M. E. Levinshtein and S. Rumyantsev (melev@nimis.ioffe.rssi.ru and sl@nimis.ioffe.rssi.ru) or to M. S. Shur (shurm@rpi.edu).

The Editors

CONTENTS

Preface vii

Chapter 1. Aluminium Gallium Arsenide ($Al_xGa_{1-x}As$) 1
Yu. A. Goldberg
1.1. Basic Parameters at 300 K 1
1.2. Band Structure and Carrier Concentration 5
1.2.1. Temperature Dependences 6
1.2.2. Dependences on Hydrostatic Pressure 8
1.2.3. Energy Gap Narrowing at High Doping Levels 9
1.2.4. Band Discontinuities at $Al_xGa_{1-x}As$/GaAs Heterointerface 10
1.2.5. Effective Masses 11
1.2.6. Donors and Acceptors 12
1.3. Electrical Properties 15
1.3.1. Mobility and Hall Effect 15
1.3.2. Two-Dimensional Electron and Hole Gas Mobility at $Al_xGa_{1-x}As$/GaAs Interface 19
1.3.3. Transport Properties in High Electric Field 21
1.3.4. Transport Properties of Electron and Hole Two-Dimensional Gas in High Electric Field 23
1.3.5. Impact Ionization 24
1.3.6. Recombination Parameters 26
1.4. Optical Properties 28
1.5. Thermal Properties 31
1.6. Mechanical Properties, Elastic Constants, Lattice Vibrations, Other Properties 33
References 35

Chapter 2. Gallium Indium Phosphide ($Ga_xIn_{1-x}P$) 37
Yu. A. Goldberg
2.1. Basic Parameters at 300 K 37
2.2. Band Structure and Carrier Concentration 40
2.2.1. Temperature Dependences 42

2.2.2. Dependences on Hydrostatic Pressure 43
2.2.3. Energy Gap Narrowing at High Doping Levels 45
2.2.4. Band Discontinuities at Heterointerface 46
2.2.5. Effective Masses 46
2.2.6. Donors and Acceptors 47
2.3. Electrical Properties 48
2.3.1. Mobility and Hall Effect 48
2.3.2. Two-Dimensional Electron Gas Mobility at $Ga_{0.51}In_{0.49}P/GaAs$ Interface 50
2.3.3. Transport Properties in High Electric Fields 51
2.3.4. Impact Ionization 52
2.3.5. Recombination Parameters 53
2.4. Optical Properties 54
2.5. Thermal Properties 56
2.6. Mechanical Properties, Elastic Constants, Lattice Vibrations, Other Properties 57
References 59

Chapter 3. Gallium Indium Arsenide ($Al_xIn_{1-x}As$) 62
Yu. A. Goldberg and Natalya M. Schmidt
3.1. Basic Parameters at 300 K 62
3.2. Band Structure and Carrier Concentration 65
3.2.1. Temperature Dependences 66
3.2.2. Dependences on Hydrostatic Pressure 68
3.2.3. Energy Gap Narrowing at High Doping Levels 69
3.2.4. Band Discontinuities at Heterointerfaces 69
3.2.5. Effective Masses 70
3.2.6. Donors and Acceptors 71
3.3. Electrical Properties 72
3.3.1. Mobility and Hall Effect 72
3.3.2. Two-Dimensional Electron and Hole Gas Mobility in Heterostructures 75
3.3.3. Transport Properties in High Electric Field 77
3.3.4. Impact Ionization 79
3.3.5. Recombination Parameters 80
3.4. Optical Properties 82
3.5. Thermal Properties 84
3.6. Mechanical Properties, Elastic Constants, Lattice Vibrations, Other Properties 85
References 87

Chapter 4. Gallium Indium Antimonide ($Ga_xIn_{1-x}Sb$) 89
Yu. A. Goldberg
4.1. Basic Parameters at 300 K 89
4.2. Band Structure and Carrier Concentration 92
4.2.1. Temperature Dependences 93
4.2.2. Dependences on Hydrostatic Pressure 94
4.2.3. Effective Masses 95
4.2.4. Donors and Acceptors 96
4.3. Electrical Properties 97
4.3.1. Mobility and Hall Effect 97
4.3.2. Transport Properties in High Electric Field 100
4.3.3. Recombination Parameters 101
4.4. Optical Properties 102
4.5. Thermal Properties 105
4.6. Mechanical Properties, Elastic Constants, Lattice Vibrations, Other Properties 107
References 109

Chapter 5. Gallium Arsenide Antimonide ($GaAs_{1-x}Sb_x$) 111
A. Ya. Vul'
5.1. Basic Parameters at 300 K 111
5.2. Band Structure and Carrier Concentration 114
5.2.1. Temperature Dependences 115
5.2.2. Dependences on Hydrostatic Pressure 116
5.2.3. Effective Masses 117
5.2.4. Donors and Acceptors 117
5.3. Electrical Properties 119
5.3.1. Mobility and Hall Effect 119
5.3.2. Impact Ionization 122
5.4. Optical Properties 123
5.5. Thermal Properties 126
5.6. Mechanical Properties, Elastic Constants, Lattice Vibrations, Other Properties 128
References 130

Chapter 6. Indium Arsenide-Antimonide ($InAs_{1-x}Sb_x$) 132
M. S. Bresler
6.1. Basic Parameters at 300 K 132
6.2. Band Structure and Carrier Concentration 135

6.2.1. Temperature Dependences 136
6.2.2. Dependences on Hydrostatic Pressure 137
6.2.3. Effective Masses 138
6.2.4. Donors and Acceptors 138
6.3. Electrical Properties 139
6.3.1. Mobility and Hall Effect 139
6.3.2. Impact Ionization 142
6.3.3. Recombination Parameters 143
6.4. Optical Properties 144
6.5. Thermal Properties 146
6.6. Mechanical Properties, Elastic Constants, Lattice Vibrations, Other Properties 148
References 151

Chapter 7. Gallium Indium Arsenide Phosphide ($Ga_xIn_{1-x}As_yP_{1-y}$) 153
Yu. A. Goldberg and Natalya M. Shmidt
7.1. Basic Parameters at 300 K 153
7.1.1. Basic Properties of $Ga_xIn_{1-x}As_yP_{1-y}$ Compositions Lattice-Matched to InP at 300 K ($x \cong 0.47y$) 154
7.2. Band Structure and Carrier Concentration 157
7.2.1. Temperature Dependences 158
7.2.2. Dependences on Hydrostatic Pressure 160
7.2.3. Band Discontinuities at GaInAsP/InP Heterostructure 160
7.2.4. Effective Masses 161
7.2.5. Donors and Acceptors 162
7.3. Electrical Properties 164
7.3.1. Mobility and Hall Effect 164
7.3.2. Transport Properties in High Electric Field 167
7.3.3. Impact Ionization 169
7.3.4. Recombination Parameters 170
7.4. Optical Properties 171
7.5. Thermal Properties 173
7.6. Mechanical Properties, Elastic Constants, Lattice Vibrations, Other Properties 175
References 178

Chapter 8. Gallium Indium Arsenide Antimonide ($Ga_xIn_{1-x}As_ySb_{1-y}$) 180
Maya P. Mikhailova
8.1. Basic Parameters at 300 K 180

8.1.1. Basic Properties of $Ga_xIn_{1-x}As_ySb_{1-y}$ Compositions Lattice-Matched to GaSb 181
8.1.2. Basic Properties of $Ga_xIn_{1-x}As_ySb_{1-y}$ Compositions Lattice-Matched to InAs 183
8.2. Band Structure and Carrier Concentration 186
8.2.1. Temperature Dependences 188
8.2.2. Band Discontinuities at GaInAsSb/GaSb and GaInAsSb/InAs Heterojunctions 191
8.2.3. Effective Masses 192
8.2.4. Donors and Acceptors 192
8.3. Electrical Properties 194
8.3.1. Mobility and Hall Effect 194
8.3.2. Impact Ionization 196
8.4. Optical Properties 197
8.5. Thermal Properties 198
8.6. Mechanical Properties, Elastic Constants, Lattice Vibrations, Other Properties 201
References 204

CHAPTER 1

ALUMINIUM GALLIUM ARSENIDE ($Al_xGa_{1-x}As$)

Yu. A. Goldberg
Ioffe Institute, St. Petersburg, Russia

1.1. Basic Parameters at 300 K

	GaAs	AlAs	$Al_xGa_{1-x}As$
Crystal structure	Zinc Blende	Zinc Blende	Zinc Blende
Space group	$F\bar{4}3m$	$F\bar{4}3m$	$F\bar{4}3m$
Number of atoms in 1 cm^3	$4.42\cdot10^{22}$	$4.25\cdot10^{22}$	$(4.42-0.17x)\cdot10^{22}$
Debye temperature (K)	370	446	$370+54x+22x^2$
Density (g/cm^3)	5.32	3.76	$5.32-1.56x$
Dielectric constant			
static	12.9	10.06	$12.90-2.84x$
high frequency	10.89	8.16	$10.89-2.73x$
Effective electron mass: **for** $x \le$ **0.41–0.45** $Al_xGa_{1-x}As$ is direct gap semiconductor ("like GaAs"). The lowest valley of the conduction band is Γ-valley m_Γ (in units of m_o)	0.063	–	$0.063+0.083x$ ($x<0.41$)
for $x>$ **0.45** $Al_xGa_{1-x}As$ is indirect gap semiconductor ("like AlAs"). The lowest valley of the conduction band is X-valley. Effective electron mass (in units of m_o)			
longitudinal m_l/m_o		1.1	
transverse m_t/m_o		0.19	

	GaAs	AlAs	$Al_xGa_{1-x}As$
Density-of-states electron mass m_{cd}/m_o		0.71	$0.85-0.14x$ ($x>0.45$)
Conductivity effective mass m_{cc}/m_o			0.26 ($0.45<x<1$)
Effective hole mass (in units of m_o)			
heavy	0.51	0.76	$0.51+0.25x$
light	0.082	0.150	$0.082+0.068x$
Electron affinity (eV)	4.07	3.5	$4.07-1.1x$ ($x<0.45x$) $3.64-0.14x$ ($0.45<x<1$)
Lattice constant (Å)	5.6533	5.6611	$5.6533+0.0078x$
Optical phonon energy (meV)	36	50	$36.25+1.83x+17.12x^2-5.11x^3$

Band structure and carrier concentration

	GaAs	AlAs	$Al_xGa_{1-x}As$
Energy gap (eV)	1.424	2.17	$1.424+1.247x$
for $x<0.45$ (direct gap)			
for $0.45<x<1$ (indirect gap)			$1.9+0.125x+0.143x^2$
Energy separation between Γ-valley and top of the valence band E_Γ (eV)	1.424	2.9	$1.424+1.155x+0.37x^2$
Energy separation between X-valley and top of the valence band E_x (eV)	1.90	2.17	$1.9+0.124x+0.144x^2$
Energy separation between L-valley and top of the valence band E_L (eV)	1.71	2.4	$1.71+0.69x$
Energy of spin-orbital splitting E_{so} (eV)	0.34	0.3	$0.34-0.04x$

	GaAs	AlAs	$Al_xGa_{1-x}As$
Intrinsic carrier concentration (cm^{-3})	$2.1\cdot10^6$	9.5	
$x=0.1$			$2.1\cdot10^5$
$x=0.3$			$2.1\cdot10^3$
$x=0.5$			$2.5\cdot10^2$
$x=0.8$			$4.3\cdot10^1$
Intrinsic resistivity (Ωcm)	$3.5\cdot10^8$	$1.6\cdot10^{15}$	
$x=0.1$			$4\cdot10^9$
$x=0.3$			10^{12}
$x=0.5$			10^{14}
$x=0.8$			$5\cdot10^{14}$
Effective conduction band density of states (cm^{-3})	$4.7\cdot10^{17}$	$1.5\cdot10^{19}$	
$x<0.41$			$2.5\cdot10^{19}\cdot(0.063+0.083x)^{3/2}$
$x>0.45$			$2.5\cdot10^{19}\cdot(0.85-0.14x)^{3/2}$
Effective valence band density of states (cm^{-3})	$9\cdot10^{18}$	$1.7\cdot10^{19}$	$2.5\cdot10^{19}\cdot(0.51-0.25x)^{3/2}$

Electrical properties

	GaAs	AlAs	$Al_xGa_{1-x}As$
Breakdown field (V/cm)	$\approx4\cdot10^5$	$\approx6\cdot10^5$	$\approx(4\div6)\cdot10^5$
Mobility ($cm^2/V\cdot s$)			
electrons	≤8500	≤200	
$x<0.45$			$8\cdot10^3-2.2\cdot10^4x+10^4x^2$
$0.45<x<1$			$-255+1160x-720x^2$
holes	≤400	≤140	$370-970x+740x^2$

	GaAs	AlAs	$Al_xGa_{1-x}As$
Diffusion coefficient (cm^2/s)			
electrons	≤ 200	≤ 5	
$x < 0.45$			$200 - 550x + 250x^2$
$0.45 < x < 1$			$-6.4 + 29x - 18x^2$
holes	≤ 10	≤ 3	$9.2 - 24x + 18.5x^2$
Electron thermal velocity (m/s)	$4.4 \cdot 10^5$	$2.3 \cdot 10^5$	
$x < 0.4$			$(4.4 - 2.1x) \cdot 10^5$
$0.45 < x < 1$			$2.3 \cdot 10^5$
Hole thermal velocity (m/s)	$1.8 \cdot 10^5$	$1.3 \cdot 10^5$	$(1.8 - 0.5x) \cdot 10^5$
Optical properties			
Infrared refractive index	3.3	2.86	$3.3 - 0.53x + 0.09x^2$
Radiative recombination coefficient (cm^3/s)	$7 \cdot 10^{-10}$	$\approx 10^{-10}$	$\sim 10^{-10}$
Thermal and mechanical properties			
Bulk modulus (dyn/cm^2)	$7.55 \cdot 10^{11}$	$7.81 \cdot 10^{11}$	$(7.55 + 0.26x) \cdot 10^{11}$
Melting point (°C)	1240	1740	$1240 - 58x + 558x^2$ (solidus curve) $1240 + 1082x - 582x^2$ (liquidus curve)
Specific heat (J/g °C)	0.33	0.45	$0.33 + 0.12x$
Thermal conductivity (W/cm °C)	0.55	0.91	$0.55 - 2.12x + 2.48x^2$
Thermal diffusivity (cm^2/s)	0.31	0.54	$0.31 - 1.23x + 1.46x^2$
Thermal expansion, linear, ($°C^{-1}$)	$5.73 \cdot 10^{-6}$	$5.2 \cdot 10^{-6}$	$(5.73 - 0.53x) \cdot 10^{-6}$

1.2. Band Structure and Carrier Concentration

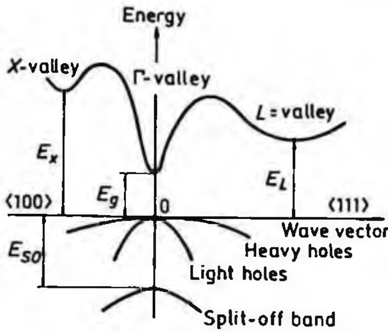

Fig. 1.2.1. Band structure of $Al_xGa_{1-x}As$ for $x \leq 0.41-0.45$. Important minima of the conduction band and maxima of the valence band.

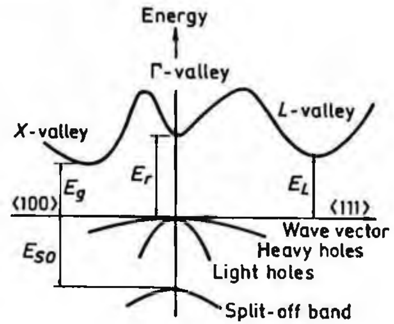

Fig. 1.2.2. Band structure of $Al_xGa_{1-x}As$ for $x \geq 0.45$. Important minima of the conduction band and maxima of the valence band.

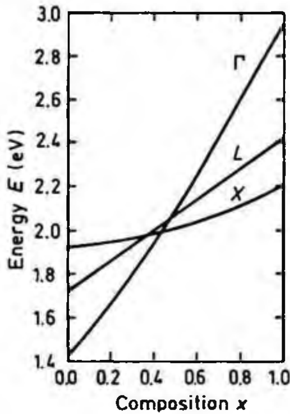

Fig. 1.2.3. Energy separations between Γ-, X-, and L-conduction band minima and top of the valence band versus composition (after Saxena [1980]).
Crossover points:

$x_c\,(L-X) = 0.35$ $E_L = E_x \cong 1.95$ eV
$x_c\,(\Gamma-X) = 0.41$ $E_\Gamma = E_x = 1.97$ eV
$x_c\,(\Gamma-L) = 0.47$ $E_\Gamma = E_L = 2.04$ eV .

(Reprinted with permission from IOP Publishing. © 1980.)

At 300 K:

$$E_\Gamma \cong 1.424 + 1.155x + 0.37x^2 \text{ (eV)} \tag{1.2.1}$$

$$E_x \cong 1.9 + 0.124x + 0.144x^2 \text{ (eV)} \tag{1.2.2}$$

$$E_L \cong 1.7 + 0.69x \text{ (eV)}\,. \tag{1.2.3}$$

According to Hava and Auslender [1993], crossover point $x_c(\Gamma - X) = 0.43$.

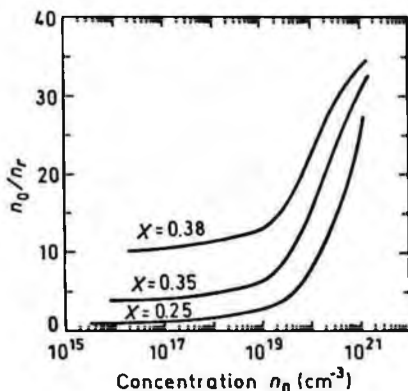

Fig. 1.2.4. Ratio of the total carrier concentration to the carrier concentration in Γ- valley as a function of equilibrium carrier concentration, 300 K (after Zarem *et al.* [1989]).

(Reprinted with permission from the American Institute of Physics, © 1989.)

1.2.1. *Temperature Dependences*

To estimate the temperature dependences of energy difference between the top of the valence band and the bottom of the Γ, *X*, and *L* valleys of the conduction band E_Γ, E_X and E_L one can use the data for GaAs (Aspnes [1976]).

$$E_\Gamma = E_\Gamma(0) - 5.41 \cdot 10^{-4} \cdot \frac{T^2}{T+204} \text{ (eV)}$$
$$E_\Gamma(0) = 1.519 + 1.155x + 0.37x^2 \text{ (eV)} \tag{1.2.4}$$

$$E_X = E_X(0) - 4.6 \cdot 10^{-4} \cdot \frac{T^2}{T+204} \text{ (eV)}$$
$$E_X(0) = 1.981 + 0.124x + 0.144x^2 \text{ (eV)} \tag{1.2.5}$$

$$E_L = E_L(0) - 6.05 \cdot 10^{-4} \cdot \frac{T^2}{T+204} \text{(eV)}$$
$$E_L(0) = 1.815 + 0.69x \text{ (eV)} , \tag{1.2.6}$$

where T is temperature in degrees K.

Effective density of states in the conduction band N_c:

$$x < 0.41$$

$$N_c \cong 4.82 \cdot 10^{15} \cdot \left(\frac{m_\Gamma}{m_o}\right)^{3/2} \cdot T^{3/2}$$

$$\cong 4.82 \cdot 10^{15} \cdot T^{3/2}(0.063 + 0.083x)^{3/2} \text{ (cm}^{-3}\text{)} \quad (1.2.7)$$

$$x > 0.45$$

$$N_c \cong 4.82 \cdot 10^{15} \cdot M \cdot \left(\frac{m_c}{m_o}\right)^{3/2} \cdot T^{3/2}$$

$$\cong 4.82 \cdot 10^{15} \cdot \left(\frac{m_{cd}}{m_o}\right)^{3/2} \cdot T^{3/2} \text{ (cm}^{-3}\text{)}$$

or

$$N_c \cong 4.82 \cdot 10^{15} \cdot T^{3/2} \cdot (0.85 - 0.14x)^{3/2} \text{ (cm}^{-3}\text{)} \quad (1.2.8)$$

$M = 3$ is the number of equivalent valleys in the conduction band.
m_c is the effective mass of the density of states in one valley of the conduction band.
m_{cd} is the effective mass of the density of states.

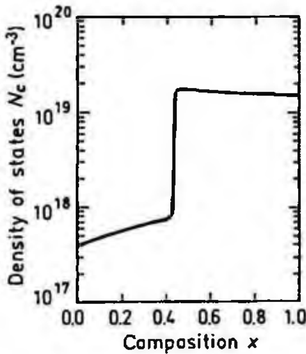

Fig. 1.2.5. Effective density of states in the conduction band versus x. Calculated according to Eqs. (1.2.7) and (1.2.8), 300 K.

Effective density of states in the valence band:

$$N_v \cong 4.82 \cdot 10^{15} \cdot T^{3/2} \cdot (0.51 + 0.25x)^{3/2} \text{ (cm}^{-3}\text{)} \quad (1.2.9)$$

Intrinsic carrier concentration:

$$n_i = (N_c \cdot N_v)^{1/2} \exp\left(-\frac{E_g}{2k_B T}\right) \tag{1.2.10}$$

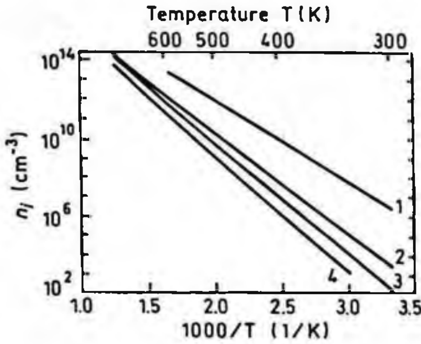

Fig. 1.2.6. The temperature dependences of the intrinsic carrier concentration.
1. $x=0$, 2. $x=0.3$, 3. $x=0.6$, 4. $x=1$.

1.2.2. *Dependences on Hydrostatic Pressure* (After Adachi [1985])

$$\frac{dE_\Gamma}{dP} = (11.5 - 1.3x)\cdot 10^{-3}\ (\text{eV/kbar})$$

$$\frac{dE_X}{dP} = -0.8\cdot 10^{-3}\cdot(\text{eV/kbar}) \tag{1.2.11}$$

$$\frac{dE_L}{dP} = 2.8\cdot 10^{-3}\ (\text{eV/kbar})$$

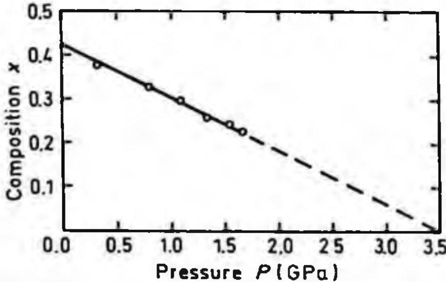

Fig. 1.2.7. Pressure dependence of the $\Gamma - X$ crossover, 300 K (after Saxena [1980]).
(Reprinted with permission from IOP Publishing, © 1980.)

1.2.3. *Energy Gap Narrowing at High Doping Levels*

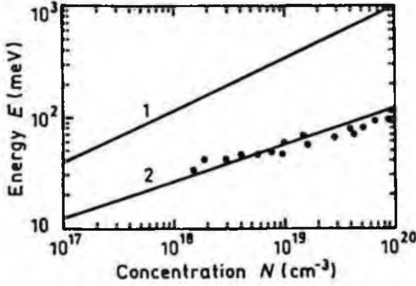

Fig. 1.2.8. Energy gap narrowing versus donor (curve 1) and acceptor (curve 2) doping density for GaAs ($x = 0$). Experimental points for *p*-GaAs are taken from four different papers (after Jain and Roulston [1991]).

(Reprinted with permission from Pergamon Press, © 1991.)

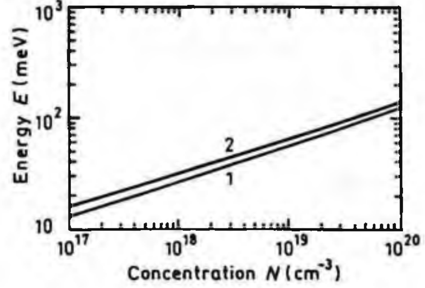

Fig. 1.2.9. Energy gap narrowing versus donor (curve 1) and acceptor (curve 2) doping density for AlAs ($x = 1$). The curves are calculated according to Jain *et al.* [1990] (see Eq. (1.2.12b)).

(Reprinted with permission from the American Institute of Physics, © 1990.)

For GaAs:

$$\Delta E_g = A\left(\frac{N}{10^{18}}\right)^{1/3} + B\left(\frac{N}{10^{18}}\right)^{1/4} + C\left(\frac{N}{10^{18}}\right)^{1/2} \text{ (meV)} \qquad (1.2.12a)$$

n-GaAs: $A = 16.3$; $B = 7.47$; $C = 90.65$

p-GaAs: $A = 9.71$; $B = 12.19$; $C = 3.88$

(after Jain and Roulston [1991]).

For AlAs:

$$\Delta E_g = 10^{-9} A_0 \cdot N^{1/3} + 10^{-7} \cdot B_0 \cdot N^{1/4} + 10^{-12} \cdot C_0 \cdot N^{1/2} \text{ (eV)} \qquad (1.2.12b)$$

n-AlAs: $A_0 = 9.76$; $B_0 = 4.33$; $C_0 = 2.93$

p-AlAs: $A_0 = 10.6$; $B_0 = 5.47$; $C_0 = 3.01$

(after Jain *et al.* [1990]).

N is carrier concentration in cm^{-3}.

1.2.4. *Band Discontinuities at $Al_xGa_{1-x}As/GaAs$ Heterointerface*

Valence band discontinuity

$$\Delta E_v \cong -0.46x \text{ (eV)} \qquad 0<x<1 \tag{1.2.13}$$

Conduction band discontinuity

$$\Delta E_c = \Delta E_g(x) - \Delta E_v$$

At 300 K:

$$\text{for } 0<x<0.41 \qquad \Delta E_c \cong 1.25x - 0.46x \cong 0.79x \text{ (eV)} \tag{1.2.14}$$

$$\text{for } 0.45<x<1 \qquad \Delta E_c \cong 0.475 - 0.335x + 0.143x^2 \text{ (eV)}$$

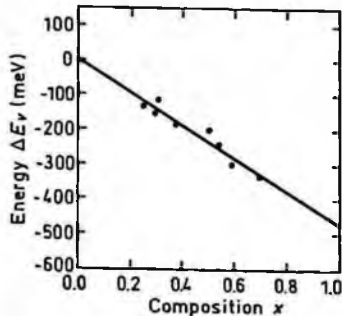

Fig. 1.2.10. Valence band edge discontinuity at $Al_xGa_{1-x}As/GaAs$ heterointerface versus x. Points represent various experimental data (after Langer and Heinrich [1985]).

(Reprinted with permission from Elsevier Science, © 1985.)

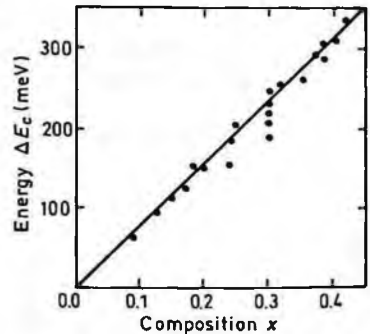

Fig. 1.2.11. Conduction band discontinuity at $Al_xGa_{1-x}As/GaAs$ heterointerface versus $x (x \le 0.45)$. Points represent experimental data (after Langer and Heinrich [1985]).

(Reprinted with permission from Elsevier Science, © 1985.)

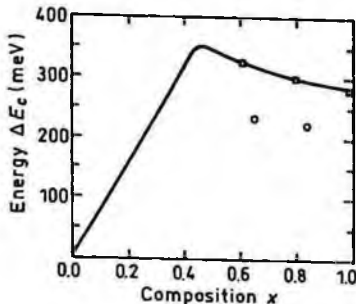

Fig. 1.2.12. Conduction band discontinuity at heterointerface versus $x(0 < x < 1)$. Solid line is calculated using Eq. (1.2.14). Experimental points are taken from Haase *et al.* [1987].

(Reprinted with permission from the American Institute of Physics, © 1987.)

1.2.5. *Effective Masses*

Electrons:

For Γ-valley: $m_\Gamma = (0.063 + 0.083x)m_o (0 < x < 1)$

For L-valleys the surfaces of equal energy are ellipsoids.

$x = 0$ (GaAs) $m_l = 1.9m_o$; $m_t = 0.075m_o$

Effective mass of density of states

$m_L = (16 m_l m_t^2)^{1/3} = 0.56m_o$

Conductivity effective mass

$$m_{cc} = \left[\frac{1}{3}\left(\frac{1}{m_l} + \frac{2}{m_t}\right)\right]^{-1} = 0.11m_o$$

$x = 1$ (AlAs) $m_l = 1.9m_o$; $m_t = 0.096m_o$

Effective mass of density of states $m_L = 0.66m_o$

Conductivity effective mass $m_{cc} = 0.14m_o$

For $0 < x < 1$

Effective mass of density of states $m_L = (0.56 + 0.1x)m_o$

Conductivity effective mass $m_{cc} = (0.11 + 0.03x)m_o$

For the *X*-valleys the surfaces of equal energy are ellipsoids.

$x = 0$ (GaAs) $m_l = 1.9m_o$; $m_t = 0.19m_o$

Effective mass of density of states

$m_x = (9 m_l m_t^2)^{1/3} = 0.85m_o$

Conductivity effective mass

$$m_{cc} = \left[\frac{1}{3}\left(\frac{1}{m_l} + \frac{2}{m_t}\right)\right]^{-1} = 0.27m_o$$

$x = 1$ (AlAs) ; $m_l = 1.1m_o$; $m_t = 0.19m_o$

Effective mass of density of states $m_x = 0.71m_o$

Conductivity effective mass $m_{cc} = 0.26m_o$

For $0 < x < 1$

Effective mass of density of states $m_x = (0.85 - 0.14x)m_o$

Conductivity effective mass $m_{cc} = (0.26 + 0.27)m_o$

Holes:

heavy $m_h = (0.51 + 0.25x)m_o$

light $m_{lp} = (0.082 + 0.068x)m_o$

split-off band $m_{so} = (0.15 + 0.09x)m_o$

1.2.6. *Donors and Acceptors*

Ionization energies of shallow donors (meV) (after Adachi [1985]):

	GaAs	AlAs	$Al_xGa_{1-x}As$
Γ-valley	5.2	20.2	$5.2 + 7.9x + 7.1x^2$
X-valley	24.8	35.3	$24.8 + 7.06x + 3.44x^2$
L-valley	8.7	19.0	$8.7 + 5.8x + 4.5x^2$

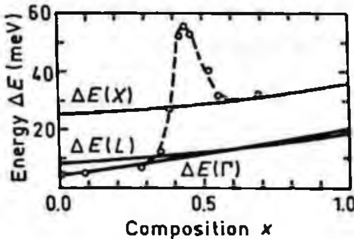

Fig. 1.2.13. Donor ionization energies $\Delta E(\Gamma)$, $\Delta E(X)$, $\Delta E(L)$ as a function of composition x. The theoretical curves (solid lines) are obtained using hydrogen approximation. Open circles are experimental data (after Adachi [1985]).

(Reprinted with permission from the American Institute of Physics, © 1985.)

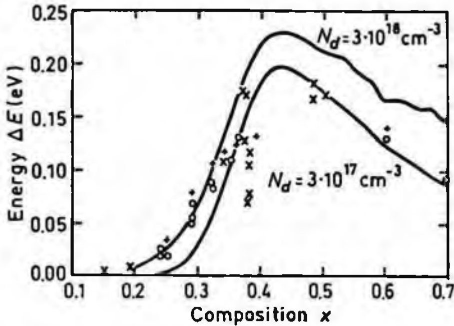

Fig. 1.2.14. Activation energy of the electron concentration in the region $T \equiv 200 \div 300$ K as a function of x for high doped AlGaAs(Si). The curves are calculated taking into account the potential fluctuations. Experimental points are taken from three different papers (after Wilamowski *et al.* [1991]).

(Reprinted with permission from IOP Publishing. © 1991.)

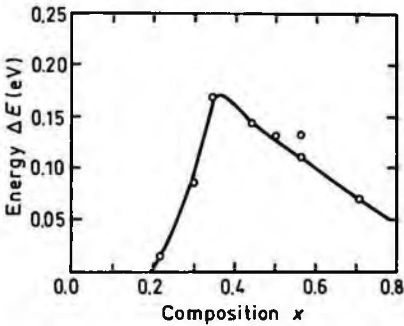

Fig. 1.2.15. Ionization energy of Sn versus x (after Kaneko *et al.* [1977]).

(Reprinted with permission from IOP Publishing. © 1977.)

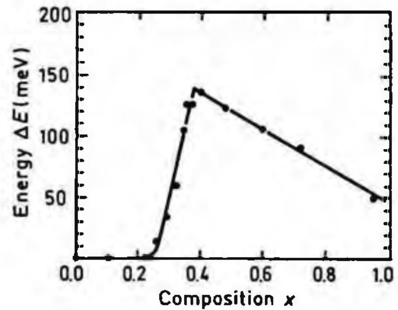

Fig. 1.2.16. Ionization energy of Te versus x (after Spring Thorpe *et al.* [1975]).

(Reprinted with permission from JOURNAL OF ELECTRONIC MATERIALS, Minerals, Metals & Materials Society, © 1975.)

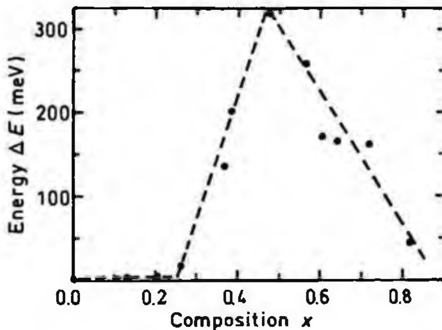

Fig. 1.2.17. Ionization energy of Se versus x (after Yang *et al.* [1982]).

(Reprinted with permission from IOP Publishing. © 1982.)

Ionization energies of shallow acceptors.

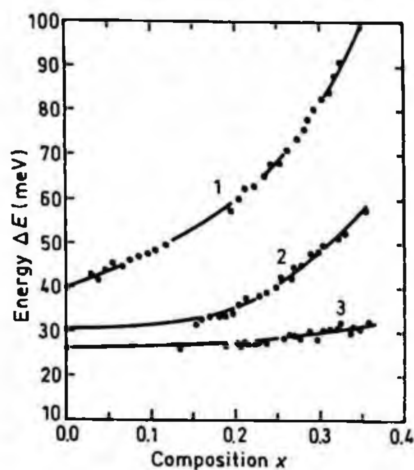

Fig. 1.2.18. Ionization energies of germanium (curve 1), zinc (curve 2) and carbon (curve 3) versus x (after Heilman and Oelgart [1990]).

(Reprinted with permission from IOP Publishing, © 1990.)

$\Delta E_{Ge} = 40.4 + 69x + 1090x^{3.34}$ (meV)

$\Delta E_{Zn} = 30.7 + 495^{2.78}$ (meV)

$\Delta E_{C} = 26.7 + 5.56x + 110x^{3.4}$ (meV) ·

($x < 0{,}4$)

1.3. Electrical Properties

1.3.1. *Mobility and Hall Effect*

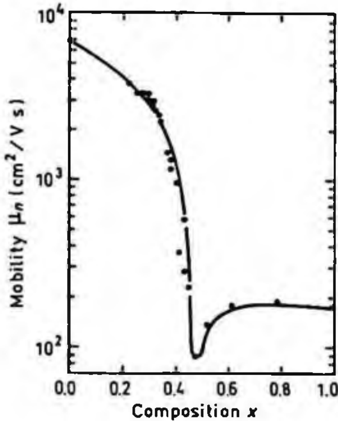

Fig. 1.3.1. Electron Hall mobility versus alloy composition x. Electron concentration $n_0 = (5-10)\cdot 10^{15}$ cm^{-3}, $T = 300$ K (after Saxena [1981b]).

(Reprinted with permission from The American Physical Society, © 1981.)

For weakly doped $Al_xGa_{1-x}As$ at 300 K electron Hall mobility:

$$\mu_H = 8000 - 22000x + 10000x^2 \qquad (\text{for } x < 0.45)$$
$$\mu_H = -255 + 1160x - 720x^2 \qquad (\text{for } 0.45 < x < 1)$$

(after Shur [1990]).

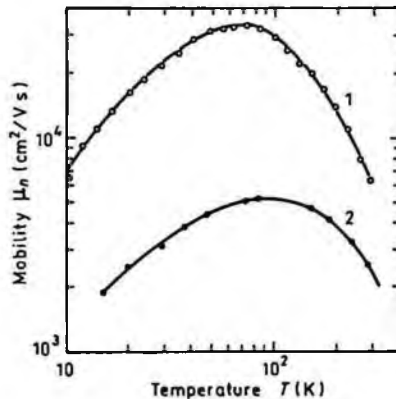

Fig. 1.3.2. Electron Hall mobility versus temperature.
Curve 1 – $x = 0$; $n_0 = 0.5\cdot 10^{16}$ cm^{-3} (after Stillman *et al.* [1970]).
Curve 2 – $x = 0.32$; $n_0 \cong (0.5 + 1)\cdot 10^{16}$ cm^{-3} (after Saxena [1981b]).

(Reprinted with permission from The American Physical Society, © 1981.)

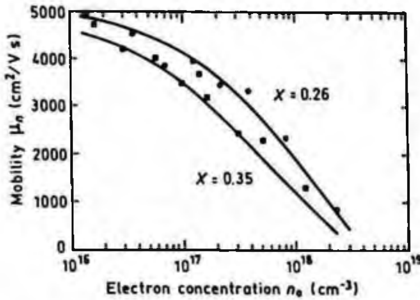

Fig. 1.3.3. Electron Hall mobility versus electron concentration for two values of x, $T = 77$ K (after Liu [1990]).

(Reprinted with permission from Chapman & Hall, © 1990.)

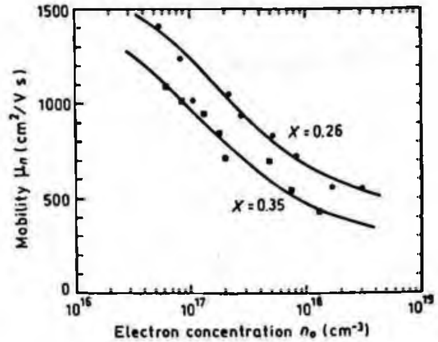

Fig. 1.3.4. Electron Hall mobility versus electron concentration for two values of x, $T = 300$ K (after Liu [1990]).

(Reprinted with permission from Chapman & Hall, © 1990.)

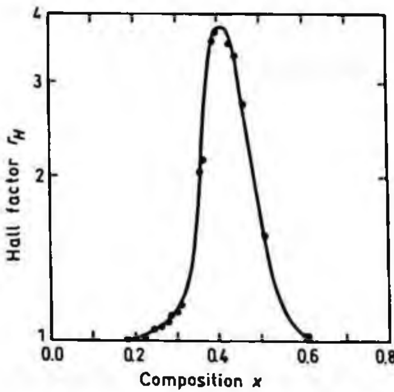

Fig. 1.3.5. Hall factor versus alloy composition x for n-type $Al_xGa_{1-x}As$. Electron concentration $n_0 \equiv (5 + 10) \cdot 10^{15}$ cm^{-3}, $T = 300$ K (after Saxena [1981a]).

(Reprinted with permission from Elsevier Science, © 1981.)

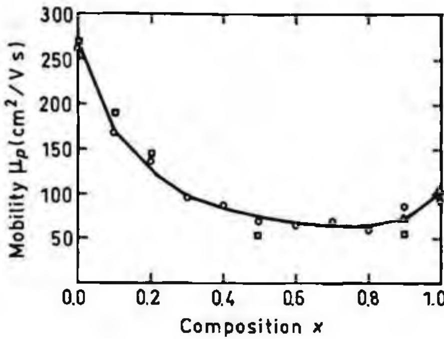

Fig. 1.3.6. Hole Hall mobility versus alloy composition x (acceptor density $N_a \approx 2.5 \cdot 10^{17}$ cm^{-3}), $T = 296$ K (after Look *et al.* [1992]).

(Reprinted with permission from the American Institute of Physics, © 1992.)

For weakly doped $Al_xGa_{1-x}As$ at 300 K hole Hall mobility:

$$\mu_H \cong 370 - 970x + 740x^2$$

(after Shur [1990]).

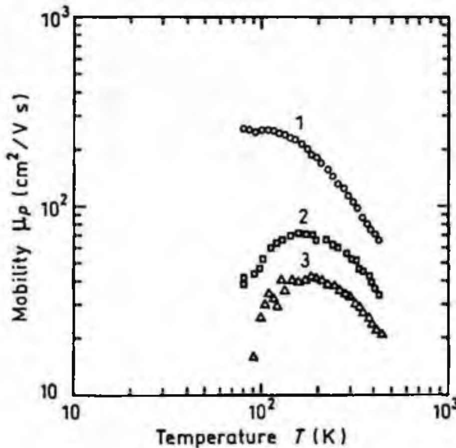

Fig. 1.3.7. Hole Hall mobility versus temperature.
Curve 1 – $x = 0$; $p_0 = 7 \cdot 10^{17}$ cm^{-3}
curve 2 – $x = 0.41$; $p_0 = 4.65 \cdot 10^{17}$ cm^{-3}
curve 3 – $x = 0.75$; $p_0 = 2.4 \cdot 10^{17}$ cm^{-3}
(after Yang *et al.* [1981]).

(Reprinted with permission from IOP Publishing, © 1981.)

Namangan davlat universiteti
inv. № 25052

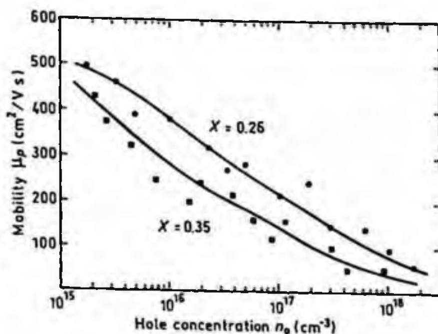

Fig. 1.3.8. Hole Hall mobility versus hole concentration for two values of x $T = 77$ K (after Liu [1990]).

(Reprinted with permission from Chapman & Hall, © 1990.)

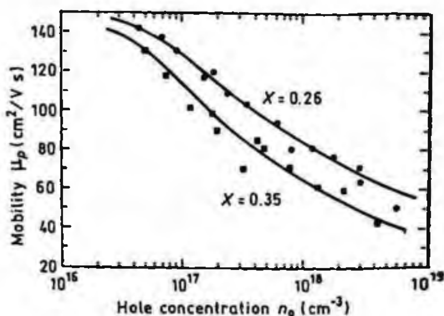

Fig. 1.3.9. Hole Hall mobility versus hole concentration for two values of x, $T = 300$ K (after Liu [1990]).

(Reprinted with permission from Chapman & Hall, © 1990.)

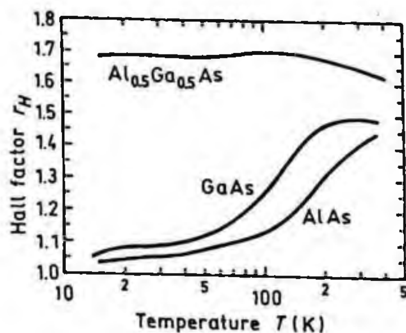

Fig. 1.3.10. Hall factor versus temperature for p-type GaAs, AlAs and $Al_{0.5}Ga_{0.5}As$. Curves are calculated for acceptor concentration $N_a = 6.5 \cdot 10^{13}$ cm^{-3} (after Look *et al.* [1992]).

(Reprinted with permission from the American Institute of Physics, © 1992.)

1.3.2. *Two-Dimensional Electron and Hole Gas Mobility at $Al_xGa_{1-x}As/GaAs$ Interface*

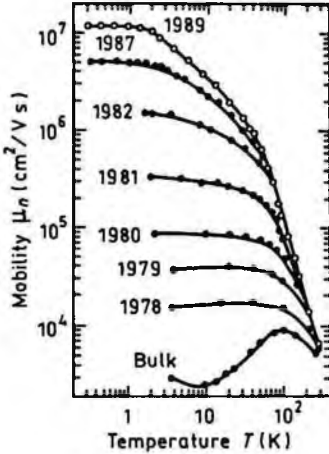

Fig. 1.3.11. Temperature dependences of the electron Hall mobility for two-dimensional gas. Landmark samples in the history of modulation-doped GaAs are shown (after Pfeiffer *et al.* [1989]).

(Reprinted with permission from the American Institute of Physics, © 1989.)

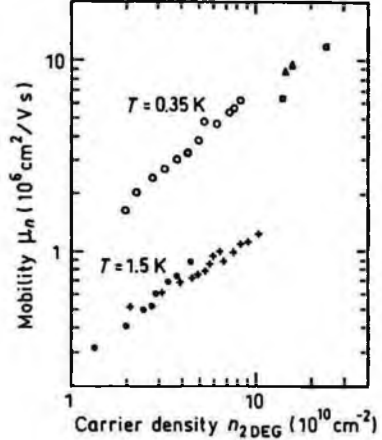

Fig. 1.3.12. Dependences of electron mobility versus surface carrier density n_{2DEG} in the modulation-doped two-dimensional gas (after Pfeiffer *et al.* [1989]).

(Reprinted with permission from the American Institute of Physics, © 1989.)

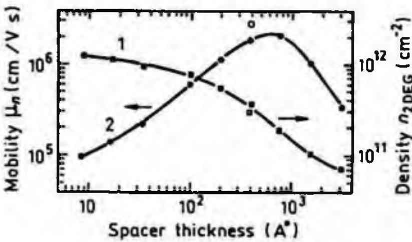

Fig. 1.3.13. Dependences of surface electron density (curve 1) and mobility (curve 2) versus undoped spacer thickness. $T = 4$ K (after Harris *et al.* [1987]).

(Reprinted with permission from the American Institute of Physics, © 1987.)

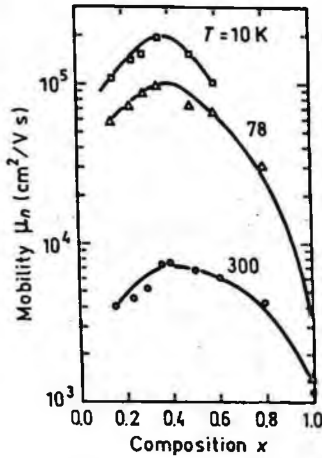

Fig. 1.3.14. Electron mobility in 2D-electron gas versus Al fraction x at three different temperatures (after Drummond *et al.* [1982]).

(Reprinted with permission from the American Institute of Physics, © 1982.)

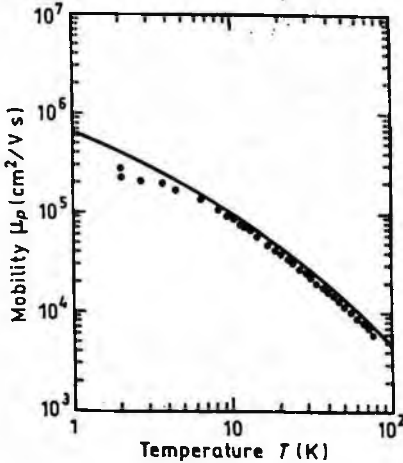

Fig. 1.3.15. Hole mobility in 2D-hole gas versus temperature. Solid line shows theoretical calculation. Points show experimental data for hole surface density $2 \cdot 10^{11}$ cm^{-2} (after Walukiewicz [1986]).

(Reprinted with permission from the American Institute of Physics, © 1986.)

1.3.3. *Transport Properties in High Electric Field*

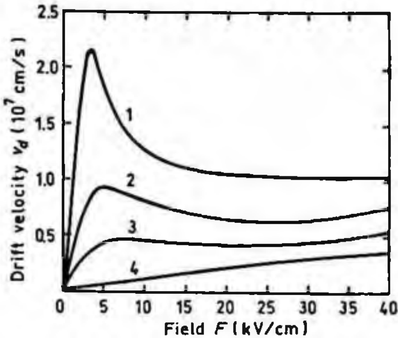

Fig. 1.3.16. Field dependences of the electron drift velocity for different values of x. Curves are calculated using displaced Maxwellian approximation, $T = 300$ K. Curve 1. $x = 0$; 2. $x = 0.225$; 3. $x = 0.325$; 4. $x = 0.5$ (after Hava and Auslender [1993]).

(Reprinted with permission from the American Institute of Physics, © 1993.)

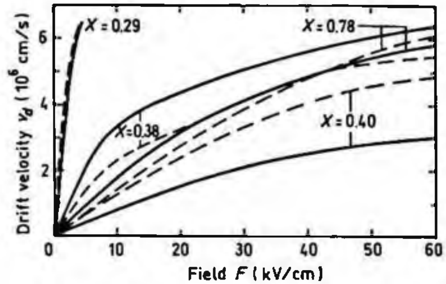

Fig. 1.3.17. Field dependences of the electron drift velocity for different values of x. Solid curves show experimental results (electron concentration $n_0 = (2 + 10) \cdot 10^{15}$ cm^{-3}. Dashed curves show results of Monte–Carlo calculations (after Hill and Robson [1981]).

(Reprinted with permission from Editions de Physique, © 1981.)

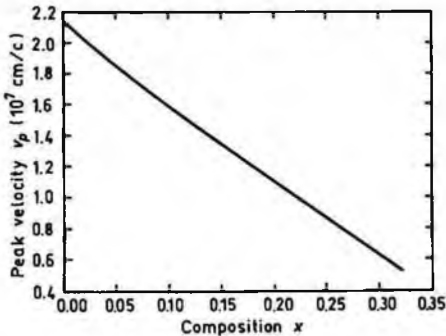

Fig. 1.3.18. Dependences of peak electron velocity versus x (after Hava and Auslender [1993]).

(Reprinted with permission from the American Institute of Physics, © 1993.)

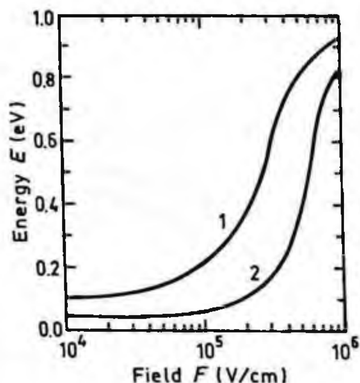

Fig. 1.3.19. Average electron energy as a function of electric field, 300 K. 1. $x = 0.25$; 2. $x = 0.45$ (after Lippens and Vanbesien [1987]).

(Reprinted with permission from IOP Publishing. © 1987.)

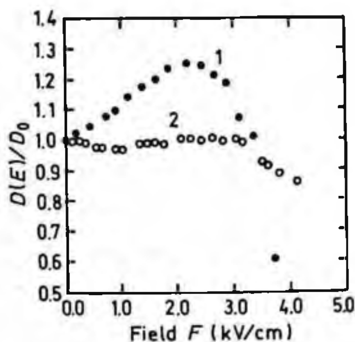

Fig. 1.3.20. The field dependences of normalized longitudinal diffusion coefficient, 300 K. 1. $x = 0$; 2. $x = 0.25$ (after de Murcia *et al.* [1993]).

(Reprinted with permission from the American Institute of Physics, © 1993.)

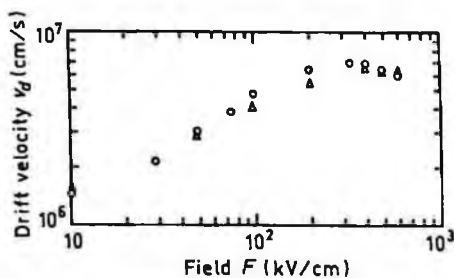

Fig. 1.3.21. Field dependence of hole drift velocity, 300 K. Monte–Carlo calculations (after Brennan and Hess [1986]).

(Reprinted with permission from the American Institute of Physics, © 1986.)

1.3.4. *Transport Properties of Electron and Hole Two-Dimensional Gas in High Electric Field*

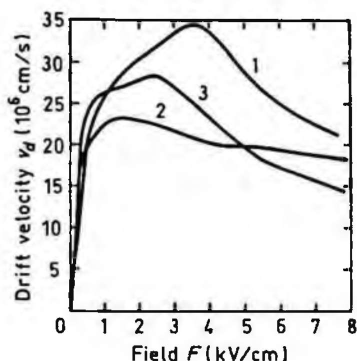

Fig. 1.3.22. Experimental field dependences of electron velocity for bulk GaAs with $n_0 = 10^{15}$ cm^{-3} (curve 1) and two-dimensional modulation-doped heterostructures $Al_xGa_{1-x}As/GaAs$ 77 K. 2. $x = 0.3$; 3. $x = 0.5$ (after Masselink [1989]).

(Reprinted with permission from IOP Publishing. © 1989.)

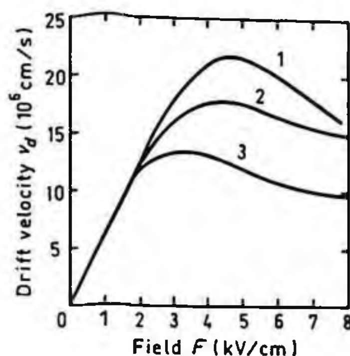

Fig. 1.3.23. Experimental field dependences of electron velocity for bulk GaAs with $n_0 = 10^{15}$ cm^{-3} (curve 1) and two-dimensional modulation-doped heterostructures, 300 K. 2. $x = 0.3$; 3. $x = 0.5$ (after Masselink [1989]).

(Reprinted with permission from IOP Publishing. © 1989.)

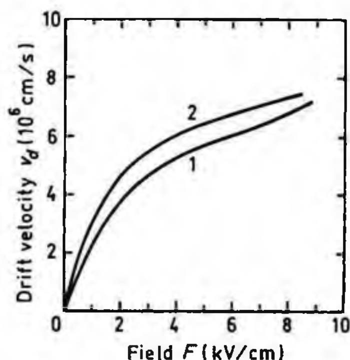

Fig. 1.3.24. Experimental field dependences of hole velocity for two-dimensional hole gas. Single heterointerface samples, $x = 0.5$, $T = 77$ K.
1. $p = 3.3 \cdot 10^{11}$ cm^{-2}, $\mu = 3300$ cm^2/Vs
2. $p = 4.2 \cdot 10^{11}$ cm^{-2}, $\mu = 4000$ cm^2/Vs
(after Masselink *et al.* [1987]).

(Reprinted with permission from IOP Publishing. © 1987.)

1.3.5. *Impact Ionization*

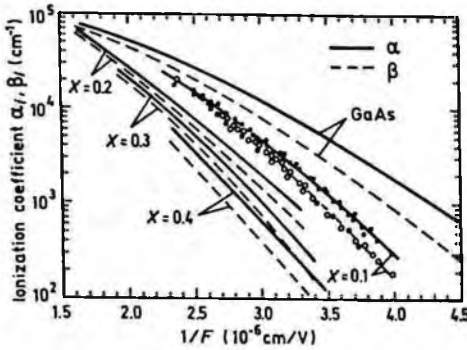

Fig. 1.3.25. Fits to experimental values of electron and hole ionization coefficients for $Al_xGa_{1-x}As$ with $x = 0.1 \div 0.4$, 300 K. Experimental points are shown only for $x = 0.1$ (after Robbins *et al.* [1988]).

(Reprinted with permission from the American Institute of Physics, © 1988.)

Electron and hole ionization coefficients, 300 K (after Robbins *et al.* [1988]).

For electrons:

$$\alpha_i = \alpha_0 \cdot \exp[-(F_{n0}/F)^m] \quad (1.3.1)$$

x	α_0 (cm^{-1})	F_{n0}(V/cm)	m
0.1	$1.81 \cdot 10^5$	$6.31 \cdot 10^5$	2.0
0.2	$1.09 \cdot 10^6$	$1.37 \cdot 10^6$	1.3
0.3	$2.21 \cdot 10^5$	$7.64 \cdot 10^5$	2.0
0.4	$1.74 \cdot 10^7$	$3.39 \cdot 10^6$	1.0

For holes:

$$\beta_i = \beta_0 \cdot \exp[-(F_{p0}/F)^n] \quad (1.3.2)$$

x	β_0 (cm^{-1})	F_{p0} (V/cm)	n
0.1	$3.05 \cdot 10^5$	$7.22 \cdot 10^5$	1.9
0.2	$6.45 \cdot 10^5$	$1.11 \cdot 10^6$	1.5
0.3	$2.79 \cdot 10^5$	$8.47 \cdot 10^5$	1.9
0.4	$3.06 \cdot 10^6$	$2.07 \cdot 10^6$	1.2

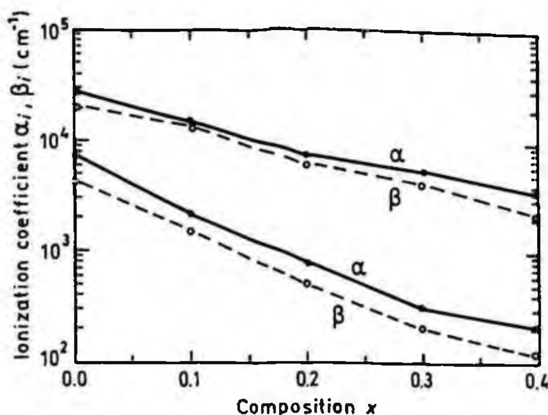

Fig. 1.3.26. Experimental ionization coefficients versus x for electric fields $3\cdot10^5$ V/cm (bottom curves) and $4\cdot10^5$ V/cm (upper curves). The lines are drawn only to connect the data points, 300 K (after Robbins *et al.* [1988]).

(Reprinted with permission from the American Institute of Physics, © 1988.)

Breakdown voltage and breakdown field of n^+-GaAs/p-$Al_{0.3}Ga_{0.7}As$ heterojunctions, 300 K

$N_a = 10^{14}$ cm^{-3}, $V_i = 2.8$ kV, $E_i = 2.8\cdot10^5$ V/cm

$N_a = 10^{16}$ cm^{-3}, $V_i = 70$ kV, $E_i = 4.5\cdot10^5$ V/cm

(after Hur *et al.* [1990]).

1.3.6. *Recombination Parameters*

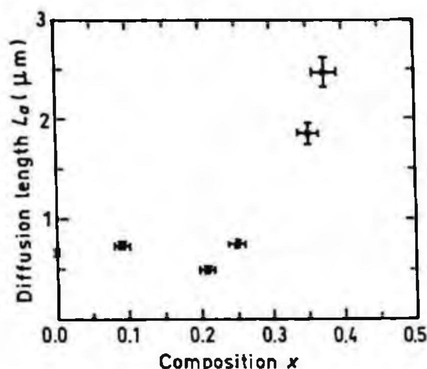

Fig. 1.3.27. Ambipolar diffusion length at a carrier density of $10^{17} + 10^{18}$ cm^{-3} versus x, 300 K. Measured by catodoluminescene technique (after Zarem *et al.* [1989]).

(Reprinted with permission from the American Institute of Physics, © 1989.)

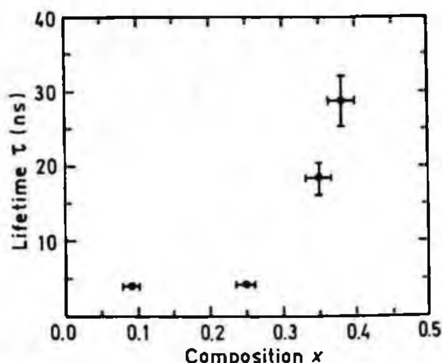

Fig. 1.3.28. Carrier lifetimes at carrier density of ~$3 \cdot 10^{18}$ cm^{-3} (high injection level) versus x, 300 K. Measured by photoluminiscence decay signal technique (after Zarem *et al.* [1989]).

(Reprinted with permission from the American Institute of Physics, © 1989.)

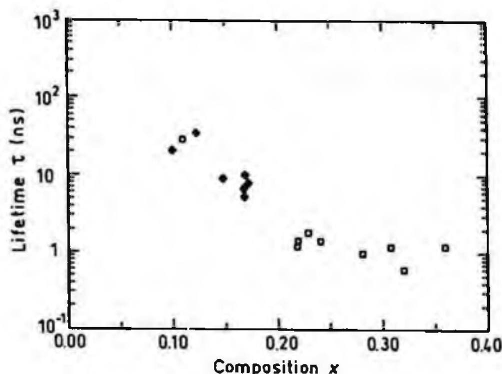

Fig. 1.3.29. Hole lifetime versus x for $n-Al_xGa_{1-x}As$ with doping level $N_d - N_a \approx 10^{15} + 10^{16}$ cm^{-3}, 300 K (after Timmons *et al.* [1988]).

(Reprinted with permission from IOP Publishing, © 1988.)

Radiative recombination coefficient at 300 K in $Al_xGa_{1-x}As \sim 10^{-10}$ cm^3/s.

Auger coefficient at 300 K (after Takeshima [1985]):

C_n (for n-doped samples)

$x = 0$	$1.9 \cdot 10^{-31}$ cm^6/s
0.1	$1.2 \cdot 10^{-31}$ cm^6/s
0.2	$0.7 \cdot 10^{-31}$ cm^6/s

C_p (for p-doped samples)

$x = 0$	$12 \cdot 10^{-31}$ cm^6/s
0.1	$8.5 \cdot 10^{-31}$ cm^6/s
0.2	$6.1 \cdot 10^{-31}$ cm^6/s.

Surface and interface recombination velocities in GaAs and $Al_xGa_{1-x}As$ (after Pavesi and Guzzi [1994]).

Al composition (x)	S (cm/s)	
0	$4 \cdot 10^5$	free surface
0	45	interface between GaAs/$Al_yGa_{1-y}As$ ($y = 0.3$)
0	450± 100	interface between GaAs/$Al_yGa_{1-y}As$ ($y = 0.5$) p-type
0.08	$4 \cdot 10^5$	free surface
0.08–0.18	$\approx 3 \cdot 10^4$	interface between $Al_xGa_{1-x}As$/$Al_yGa_{1-y}As$ ($y = 0.88$) undoped
0.28	4200	interface between $Al_xGa_{1-x}As$/$Al_yGa_{1-y}As$ ($y = 0.5$) undoped

1.4. Optical Properties

Infrared refractive index (300 K):

$$n_{\infty} = (k_{\infty})^{1/2} = 3.3 - 0.53x + 0.09x^2 \quad (1.4.1)$$

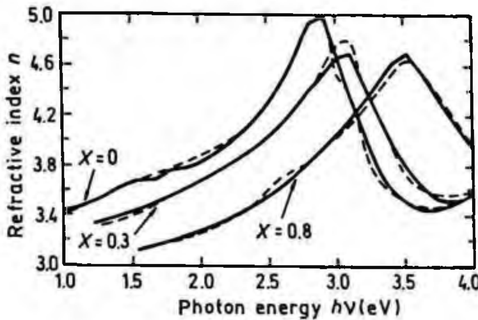

Fig. 1.4.1. Refractive index n versus photon energy for three values of x. Solid lines are calculated. Dashed lines are experimental data, 300 K (after Jenkins [1990]).

(Reprinted with permission from the American Institute of Physics, © 1990.)

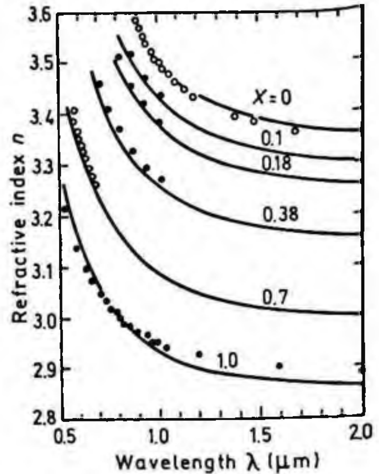

Fig. 1.4.2. Refractive index n versus wavelength for different values of x, 300 K (after Pikhtin and Yas'kov [1980]).

(Reprinted with permission from the American Institute of Physics, © 1980.)

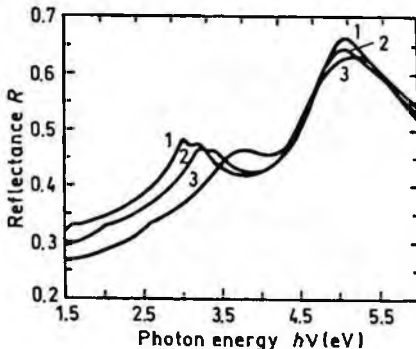

Fig. 1.4.3. Normal incidence reflectivity versus photon energy, 300 K.
Curve 1 – $x = 0.1$. Curve 2 – $x \approx 0.42$.
Curve 3 – $x = 0.8$ (after Aspnes *et al.* [1986]).

(Reprinted with permission from the American Institute of Physics, © 1986.)

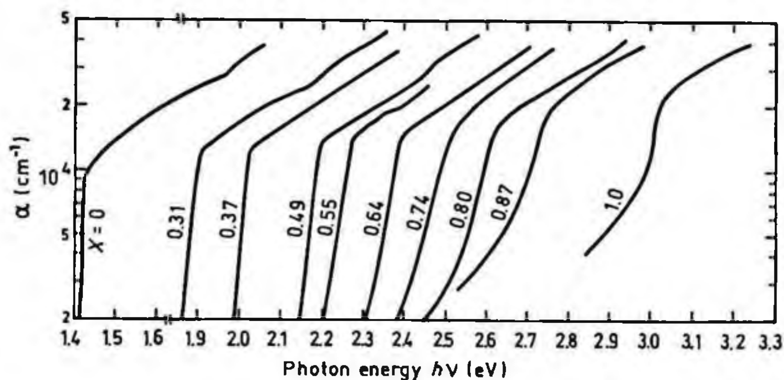

Fig. 1.4.4. Intrinsic absorption coefficient near the intrinsic absorption edge for different values of x, $T = 300$ K (after Monemar *et al.* [1976]).

(Reprinted with permission from the American Institute of Physics, © 1976.)

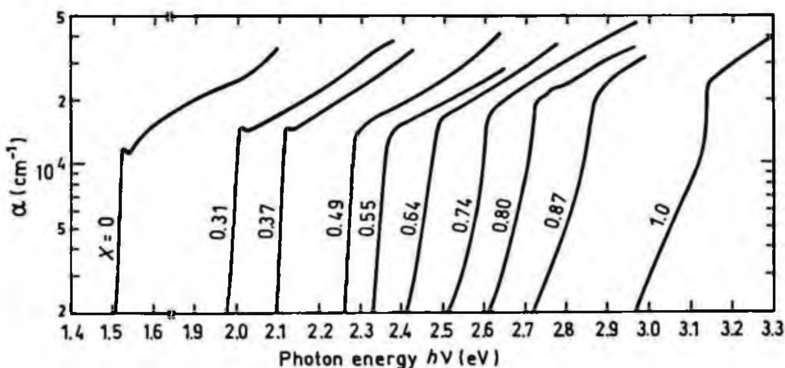

Fig. 1.4.5. Intrinsic absorption coefficient near the intrinsic absorption edge for different values of x, $T = 4$ K (after Monemar *et al.* [1976]).

(Reprinted with permission from the American Institute of Physics, © 1976.)

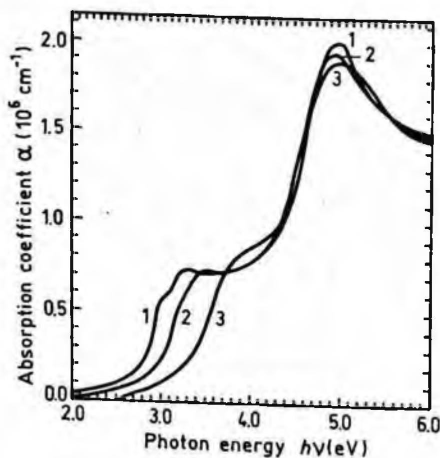

Fig. 1.4.6. The absorption coefficient versus photon energy, 300 K. Curve 1 – $x \approx 0.1$. Curve 2 – $x = 0.42$. Curve 3 – $x = 0.8$ (after Aspnes *et al.* [1986]).

(Reprinted with permission from the American Institute of Physics, © 1986.)

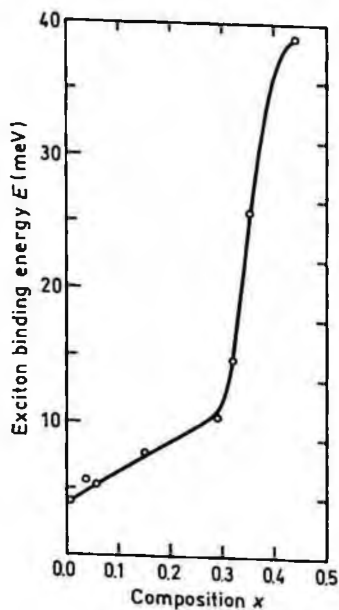

Fig. 1.4.7. Free exciton binding energy versus Al mole fraction x (after Pearah *et al.* [1985]).

(Reprinted with permission from The American Physical Society, © 1985.)

1.5. Thermal Properties

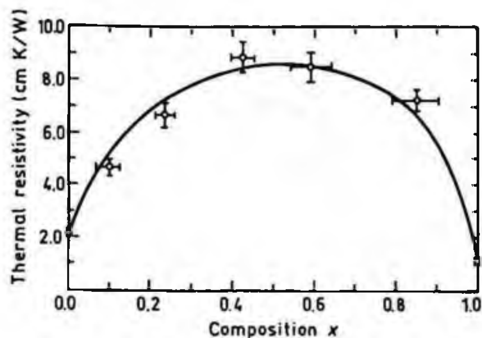

Fig. 1.5.1. Thermal resistivity versus Al fraction x. Solid curve is a theoretical fit to the experimental data, 300 K (after Afromowitz [1973]).

(Reprinted with permission from the American Institute of Physics, © 1973.)

Approximate formula for the lattice thermal resistivity:

$$R_{th} = 2.27 + 28.83x - 30x^2 \text{ (cm·K/W)}$$

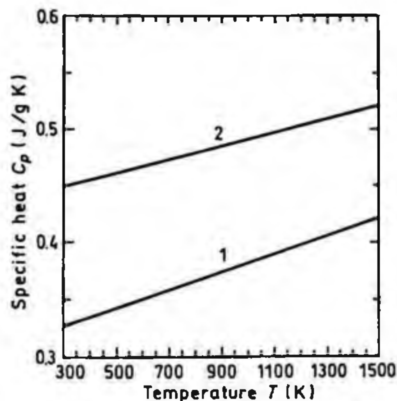

Fig. 1.5.2. Temperature dependences of specific heat at constant pressure.
Curve 1 – GaAs (after Lichter and Sommelet [1969]).
Curve 2 – AlAs (after Barin *et al.* [1977]).

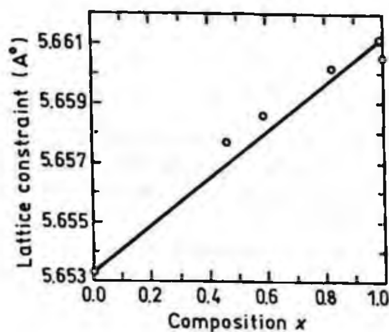

Fig. 1.5.3. Lattice constant as a function of x, 300 K (after Adachi [1985]).

(Reprinted with permission from the American Institute of Physics, © 1985.)

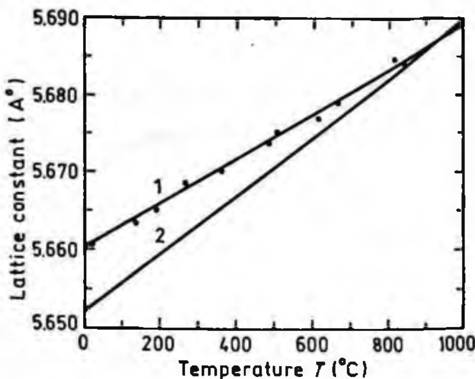

Fig. 1.5.4. Lattice constants of AlAs (line 1) and of GaAs (line 2) versus temperature (after Ettenberg and Paff [1970]).

(Reprinted with permission from the American Institute of Physics, © 1970.)

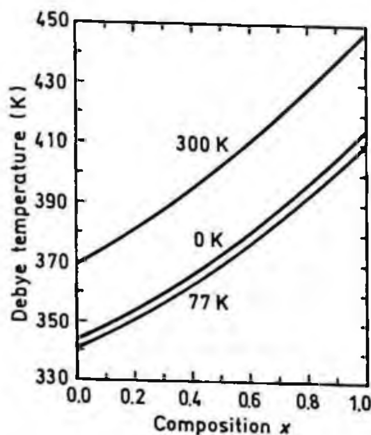

Fig. 1.5.5. Debye temperature as a function of x for three different temperatures (after Adachi [1985]).

(Reprinted with permission from the American Institute of Physics, © 1985.)

Melting point (°C):

solidus curve	$1240 - 58x + 558x^2$
liquidus curve	$1240 + 1082x - 582x^2$

1.6. Mechanical Properties, Elastic Constants, Lattice Vibrations, Other Properties

Density — $5.32-1.56x$ (g/cm^3)

Hardness — ~ 5 on the Mohs scale

Cleavage plane — {110}

Elastic constants at 300 K (after Adachi [1985]):

C_{11} — $(11.88+0.14x)\cdot 10^{11}$ dyn/cm^2

C_{12} — $(5.38+0.32x)\cdot 10^{11}$ dyn/cm^2

C_{44} — $(5.94+0.05x)\cdot 10^{11}$ dyn/cm^2

Bulk modulus (compressibility^{-1}) — $B_S = \dfrac{C_{11}+2C_{12}}{3}$ — $B_S = (7.55+0.26x)\cdot 10^{11}$ dyn/cm^2

Anizotropy factor — $A = \dfrac{C_{11}-C_{12}}{2C_{44}}$ — $A = (0.55-0.01x)$

Shear modulus — $C' = (C_{11}-C_{12})/2$ — $C' = (3.25-0.09x)\cdot 10^{11}$ dyn/cm^2

[100] Young's modulus — $Y_0 = \dfrac{(C_{11}+2C_{12})(C_{11}-C_{12})}{(C_{11}+C_{12})}$ — $Y_0 = (8.53-0.18x)\cdot 10^{11}$ dyn/cm^2

[100] Poisson ratio — $\sigma_0 = \dfrac{C_{12}}{C_{11}+C_{12}}$ — $\sigma_0 = (0.31+0.1x)$

(after Adachi [1985])

Acoustic Wave Speeds

Wave propagation direction	Wave character	Expression for wave speed	Wave speed (in units of 10^5 cm/s)
[100]	V_L	$(C_{11}/\rho)^{1/2}$	$4.73+0.68x+0.24x^2$
	V_T	$(C_{44}/\rho)^{1/2}$	$3.34+0.46x+0.16x^2$
	V_l	$[(C_{11}+C_{12}+2C_{44})/2\rho)]^{1/2}$	$5.24+0.78x+0.24x^2$
[110]	$V_{t\parallel}$	$V_{t\parallel}=V_T=(C_{44}/\rho)^{1/2}$	$3.34+0.46x+0.16x^2$
	$V_{t\perp}$	$[(C_{11}-C_{12})/2\rho)]^{1/2}$	$2.47+0.33x+0.10x^2$
[110]	V_l'	$[(C_{11}+2C_{12}+4C_{44})/3\rho)]^{1/2}$	$5.40+0.79x+0.26x^2$
	V_t'	$[(C_{11}-C_{12}+C_{44})/3\rho)]^{1/2}$	$2.79+0.38x+0.12x^2$

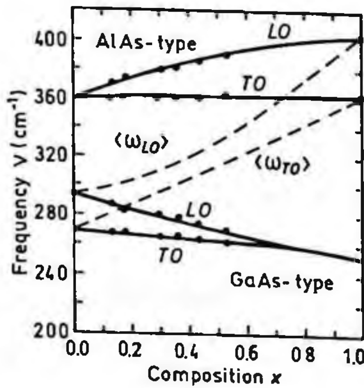

Fig. 1.6.1. Optical phonon energy as a function of x. The compositional dependence of the effective phonon energy $\langle\omega_{LO}\rangle$ and $\langle\omega_{TO}\rangle$ are shown by the dashed lines (after Adachi [1985]).

(Reprinted with permission from the American Institute of Physics, © 1985.)

Piezoelectric constant e_{14} $-(0.16+0.065x)$ C/m^2.

References

Adachi, S., *J. Appl. Phys.* **58**, 3 (1985) R1–R29.

Afromowitz, M. A., *J. Appl. Phys.* **44**, 3 (1973) 1292–1294.

Aspnes, D. E., *Phys. Rev.* **B14**, 12 (1976) 5331–5343.

Aspnes, D. E., S. M. Kelso, R. A. Logan, and R. Bhat., *J. Appl. Phys.* **60**, 2 (1986) 754–767.

Barin, I., O. Knacke, and O. Kubaschewski, *Thermochemical Properties of Inorganic Substances*, Springer, Berlin-Heidelberg-New York, 1977.

Brennan, K. and K. Hess, *J. Appl. Phys.* **59**, 3 (1986) 964–966.

de Murcia, M., D. Gasquet, E. Richard, P. Wolff, J. Zimmermann, and J. Vanbremeersch, AIP Conf. Proc. vol. **285**, *Noise in Physical Systems and 1/f Fluctuations*, St. Louis, USA, 1993, pp. 27–30.

Drummond, T. J., W. Kopp, R. Fischer, and H. Morkoč, *J. Appl. Phys.* **53**, 2 (1982) 1028–1029.

Ettenberg, M. and R. J. Paff, *J. Appl. Phys.* **41**, 10 (1970) 3926–3927.

Haase, M. A., M. A. Emanuel, S. C. Smith, J. J. Coleman, and G. E. Stillman, *Appl. Phys. Lett.* **50**, 7 (1987) 404–406.

Harris, J. J., C. T. Foxon, K. W. J. Barhkam, D. E. Lacklison, J. Hewett, and C. White, *J. Appl. Phys.* **61**, 3 (1987) 1219–1221.

Hava, S. and M. Auslender, *J. Appl. Phys.* **73**, 11 (1993) 7431–7434.

Heilman, R. and G. Oelgart, *Semicond. Sci. Technol.* **5**, 10 (1990) 1040–1045.

Hill, G. and P. N. Robson, *J. de Physique* **42**, Colloque no. 7, Suppl. au no. 10 (1981) C7-335–C7-341.

Hur, J. H., C. W. Myles, and M. A. Gundersen, *J. Appl. Phys.* **67**, 11 (1990) 6917–6923.

Jain, S. C., J. M. McGregor, and D. J. Roulston, *J. Appl. Phys.* **68**, 7 (1990) 3747–3749.

Jain, S. C. and D. J. Roulston, *Solid State Electron* **34**, 5 (1991) 453–465.

Jenkins, D. W., *J. Appl. Phys.* **68**, 4 (1990) 1848–1853.

Kaneko, K., M. Ayabe, and N. Watanabe, in *GaAs and Related Compounds*, Inst. of Phys., London, Ser. 33a, 1977, pp. 216–226.

Langer, J. M. and H. Heinrich, *Physica* **B134**, 1–3 (1985) 444–450.

Lichter, B. D. and P. Sommelet, *Trans. Metall. Soc. AIME* **245** (1969) 1021–1027.

Lippens, D. and O. Vanbesien, in *GaAs and Related Compounds*, Inst. of Phys., Bristol and Philadelphia, Ser. 91, 1987, pp. 757–760.

Liu, W.C., *J. Material Sci.* **25**, 3 (1990) 1765–1772.

Look, D. C., D. K. Lorance, J. R. Sizelove, C. E. Stutz, K. R. Evans, and D. W. Whitson, *J. Appl. Phys.* **71**, 1 (1992) 260–266.

Masselink, W. T., *Semicond. Sci. Technol.* 4, 7 (1989) 503–512.

Masselink, W. T., N. Braslau, D. LaTulipe, W. I. Wang, and S. L. Wright, in *GaAs and Related Compounds*, Inst. of Phys., Bristol and Philadelphia, Ser. 91, 1987, pp. 665–668.

Monemar, B., K. K. Shih, and G. D. Pettit, *J. Appl. Phys.* **47**, 6 (1976) 2604–2613.

Pavesi, L. and M. Guzzi, *J. Appl. Phys.* **75**, 10 (1994) 4779–4842.

Pearah, P. J., W. T. Masselink, J. Klem, T. Henderson, H. Morcoĉ, C. W. Litton, and D. C. Reynolds, *Phys. Rev.* **B32**, 6 (1985) 3857–3862.

Pfeiffer, L., K. W. West, H. L. Stormer, and K. W. Baldwin, *Appl. Phys. Lett.* **55**, 18 (1989) 1888–1890.

Pikhtin, A. N. and A. D. Yas'kov, *Sov. Phys. Semicond.* **14**, 4 (1980) 389–392.

Robbins, V. M., S. C. Smith, and G. E. Stillman, *Appl. Phys. Lett.* **52**, 4 (1988) 296–298.

Saxena, A. K., *J. Phys.* **C13**, 23 (1980) 4323–4334.

Saxena, A. K., *Solid St. Commun.* **39**, 7 (1981a) 839–842.

Saxena, A. K., *Phys. Rev.* **B24**, 6 (1981b) 3295–3302.

Shur, M., *Physics of Semiconductor Devices*, Prentice Hall, 1990.

Spring Thorpe, A. J., T. D. King, and A. J. Beck, *J. Electron. Mater.* 4, 1 (1975) 101–118.

Stillman, G. E., C. M. Wolfe, and J. O. Dimmock, *J. Phys. Chem. Solids* **31**, 6 (1970) 1199–1204.

Takeshima, M., *J. Appl. Phys.* **58**, 10 (1985) 3846.

Timmons, M. L., J. A. Hutchby, R. K. Ahrenkiel, and D. J. Dunlavy, in *GaAs and Related Compounds*, Inst. of Phys., Bristol and Philadelphia, Ser. 96, 1988, pp. 289–294.

Walukiewicz, W., *J. Appl. Phys.* **59**, 10 (1986) 3577–3579.

Wilamowski, Z., J. Kossut, W. Jantsch, and G. Ostermayer, *Semicond. Sci. Technol.* **6**, 10B (1991) B38–B46.

Yang, J. J., W. I. Simpson, and L. A. Moudy, in *GaAs and Related Compounds*, Inst. of Phys., Bristol and London, Ser. 63, 1981, pp. 107–112.

Yang, J. J., L. A. Moudy, and W. I. Simpson, *Appl. Phys. Lett.* **40**, 3 (1982) 244–46

Zarem, H. A., J. A. Lebens, K. B. Nordstrom, P. C. Sercel, S. Sanders, L. E. Eng, A. Yariv, and K. J. Vahala, *Appl. Phys. Lett.* **55**, 25 (1989) 2622–2624.

CHAPTER 2

GALLIUM INDIUM PHOSPHIDE ($Ga_xIn_{1-x}P$)

Yu. A. Goldberg
Ioffe Institute, St. Petersburg, Russia

2.1. Basic Parameters at 300 K

	InP	GaP	$Ga_{0.51}In_{0.49}P$	$Ga_xIn_{1-x}P$
Crystal structure	Zinc Blende	Zinc Blende	Zinc Blende	Zinc Blende
Space group	$F\bar{4}3m$	$F\bar{4}3m$	$F\bar{4}3m$	$F\bar{4}3m$
Number of atoms in 1 cm^3	$3.96 \cdot 10^{22}$	$4.94 \cdot 10^{22}$	$4.46 \cdot 10^{22}$	$(3.96+0.98x) \cdot 10^{22}$
Density (g/cm^3)	4.81	4.14	4.47	$4.81 - 0.67x$
Dielectric constant				
static	12.5	11.1	11.8	$12.5 - 1.4x$
high frequency	9.61	9.11	9.35	$9.61 - 0.5x$
Effective electron mass: for $x \le 0.63 \div 0.68$ $Ga_xIn_{1-x}P$ is direct semiconductor (like InP). The lowest valley of the conduction band is Γ-valley				
m_Γ (in units of m_o)	0.08	–	0.088	
for $x > 0.74 \div 0.77$ $Ga_xIn_{1-x}P$ is indirect semiconductor (like GaP). The lowest valley of the conduction band is X-valley. Effective electron mass (in units of m_o)				
longitudinal m_l/m_o	–	1.12	–	
transverse m_t/m_o	–	0.22	–	

	InP	GaP	$Ga_{0.51}In_{0.49}P$	$Ga_xIn_{1-x}P$
Density-of-states electron mass m_{cd}/m_o	0.08	0.79	0.088	$0.63 + 0.13x$ ($x > 0.74$)
Effective hole mass (in units of m_o)				
heavy	0.6	0.79	0.7	$0.6 + 0.19x$
light	0.089	0.14	0.12	$0.09 + 0.05x$
Electron affinity (eV)	4.38	3.8	4.1	$4.38 - 0.58x$
Lattice constant (Å)	5.8687	5.4505	5.653	See Fig. 2.5.3
Optical phonon energy (meV)	43	51		See Sec. 2.6

Band structure and carrier concentration

	InP	GaP	$Ga_{0.51}In_{0.49}P$	$Ga_xIn_{1-x}P$
Energy gap (eV)				
for $x < 0.63$ (direct gap)	1.344	–	1.849	$1.34 + 0.69x + 0.48x^2$
for $0.77 < x < 1$ (indirect gap)	–	2.26	–	~ 2.26
Energy separation between Γ-valley and top of the valence band E_Γ (eV)	1.344	2.78	1.849	See Figs. 2.2.3 and 2.2.4
Energy separation between X-valley and top of the valence band E_x (eV)	2.19	2.26	See Fig. 2.2.3	See Figs. 2.2.3 and 2.2.4
Energy separation between L-valley and top of the valence band E_L (eV)	1.93	2.6	2.0	$1.85 - 0.06x + 0.71x^2$
Energy of spin-orbital splitting (eV)	0.11	0.08	0.11	$0.101 + 0.042x - 0.05x^2$

	InP	GaP	$Ga_{0.51}In_{0.49}P$	$Ga_xIn_{1-x}P$
Effective conduction band density of states (cm^{-3})				
$x < 0.63$	$5.7 \cdot 10^{17}$	–	$6.5 \cdot 10^{17}$	–
$x < 0.77$	–	$1.8 \cdot 10^{19}$	–	$2.5 \cdot 10^{19} \cdot (0.66 + 0.13x)^{3/2}$
Effective valence band density of states (cm^{-3})	$1.1 \cdot 10^{19}$	$1.9 \cdot 10^{19}$	$1.45 \cdot 10^{19}$	$2.5 \cdot 10^{19} \cdot (0.6 + 0.19x)^{3/2}$
Electrical properties				
Breakdown field (V/cm)	$\approx 5 \cdot 10^5$	$\approx 1 \cdot 10^6$	$\approx (5 \div 10) \cdot 10^5$	$\approx (5 \div 10) \cdot 10^5$
Mobility ($cm^2/V \cdot s$)				
electrons				
$x < 0.63$	≤ 5400	–	See Figs. 2.3.1 – 2.3.3	
$0.77 < x < 1$	–	≤ 250	–	–
holes	≤ 200	≤ 150	See Figs. 2.3.4 – 2.3.6	
Diffusion coefficient (cm^2/s)				
electrons				
$x < 0.63$	≤ 130	–		
$x > 0.77$	–	≤ 6.5		
holes	≤ 5	≤ 4		
Optical properties				
Infrared refractive index	3.1	3.02	3.06	$3.1 - 0.08x$
Radiative recombination coefficient (cm^3/s)	$1.2 \cdot 10^{-10}$	10^{-13}	$1 \cdot 10^{-10}$	

	InP	GaP	$Ga_{0.51}In_{0.49}P$	$Ga_xIn_{1-x}P$
Thermal and mechanical properties				
Bulk modulus (dyn/cm²)	$7.1\cdot10^{11}$	$8.8\cdot10^{11}$	$8.0\cdot10^{11}$	$(7.1+1.7x)\cdot10^{11}$
Melting point (°C)	1060	1457		
Specific heat (J/g °C)	0.31	0.43	0.37	$0.31+0.12x$
Thermal conductivity (W/cm °C)	0.68	1.1	See Fig. 2.5.1	
Thermal expansion, linear (°C⁻¹)	$4.6\cdot10^{-6}$	$4.65\cdot10^{-6}$		

2.2. Band Structure and Carrier Concentration

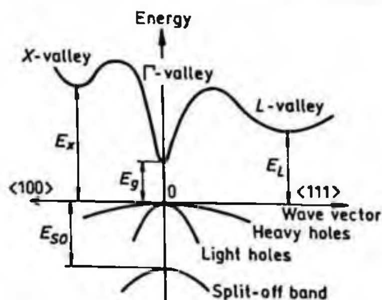

Fig. 2.2.1. Band structure of $Ga_xIn_{1-x}P$ for $x \leq 0.63 \div 0.68$. Important minima of the conduction band and maxima of the valence band.

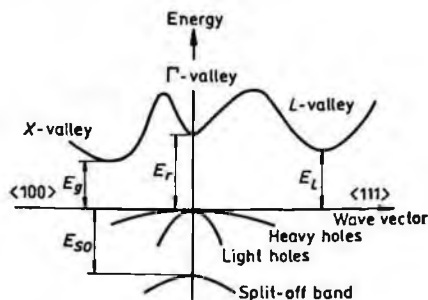

Fig. 2.2.2. Band structure of $Ga_xIn_{1-x}P$ for $x \geq 0.74 \div 0.77$. Important minima of the conduction band and maxima of the valence band.

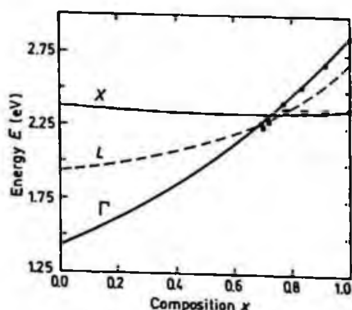

Fig. 2.2.3. Energy separations between Γ-, X-, and L-conduction band minima and top of the valence band versus composition parameter x, 10 K (after Auvergne *et al.* [1977]).

(Reprinted with permission from Elsevier Science, © 1977.)

At 10 K (after Auvergne *et al.* [1977]):

$$E_\Gamma = 1.418 + 0.77x + 0.648x^2 \text{ (eV)}$$
$$E_X \cong 2.369 - 0.152x + 0.147x^2 \text{ (eV)} \quad (2.2.1)$$

At 77 K (after Lange *et al.* [1976]):

$$E_\Gamma = 1.405 + 0.702x + 0.764x^2 \text{ (eV)}$$
$$E_X \cong 2.248 + 0.072x \text{ (eV)} \quad (2.2.2)$$

At 300 K (after Krutogolov *et al.* [1989], Lange *et al.* [1976]):

$$E_\Gamma = 1.349 + 0.668x + 0.76x^2$$
$$E_L \cong 1.85 - 0.06x + 0.71x^2 \text{ (eV)} \quad (2.2.3)$$

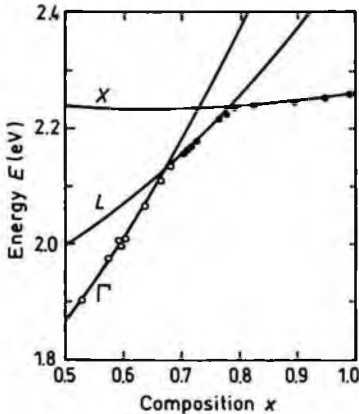

Fig. 2.2.4. Energy separation between Γ-, X-, and L conduction band minima and top of the valence band near crossover points (after Krutogolov *et al.* [1989]). Crossover points:
x_c (Γ − L) = 0.67 $E_\Gamma = E_L = 2.13$ eV
x_c (Γ − X) = 0.73 $E_\Gamma = E_X = 2.23$ eV
x_c (X − L) = 0.78 $E_X = E_L = 2.24$ eV.

Energy gap for direct gap compositions ($0 < x \leq 0.63$) at 300 K:

$$E_g \cong 1.34 + 0.69x + 0.48x^2 \text{ (eV)} \quad (2.2.4)$$

$x = 0$ (InP): $E_g = 1.344$ eV
$x = 0.51$: $E_g = 1.797$ eV (after McDermott *et al.* [1990])
$x = 0.67$: $E_g = 2.13$ eV (after Krutogolov *et al.* [1989])

For $x \geq 0.77$ (indirect compositions) at 300 K:

$$E_g \cong 2.26 \text{ eV}$$

Energy of spin-orbital splitting E_{so} at 300 K:

$$E_{so} = 0.101 + 0.042x - 0.050x^2 \quad \text{(after Lange } et\ al. \text{ [1976])} \tag{2.2.5}$$

2.2.1. *Temperature Dependences*

Temperature dependence of the energy gap E_g.
$x = 0$ (InP):

$$E_g = 1.421 - 4.9 \cdot 10^{-4} \frac{T^2}{T + 327} \text{ (eV)} \tag{2.2.6}$$

$x = 1$ (GaP):

$$E_g = 2.34 - 6.2 \cdot 10^{-4} \frac{T^2}{T + 460} \text{ (eV)} \quad \text{(after Panish and Casey [1969])} \tag{2.2.7}$$

$x = 0.5$ ($Ga_{0.5}In_{0.5}P$):

$$E_g \cong 1.937 - 6.12 \cdot 10^{-4} \frac{T^2}{T + 204} \text{ (eV)} \quad \text{(after t' Hooft } et\ al. \text{ [1992])} \tag{2.2.8}$$

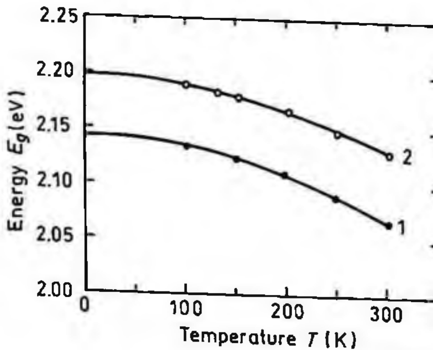

Fig. 2.2.5. Temperature dependence of the energy gap E_g for $x = 0.62$ (curve 1) and $x = 0.64$ (curve 2) (after Chin *et al.* [1993]).

(Reprinted with permission from the American Institute of Physics, © 1993.)

Effective density of states in the conduction band N_c:
$x \leq 0.63$ (direct gap)

$$N_c \cong 1.2 \cdot 10^{14} \cdot T^{3/2}\ (\mathrm{cm}^{-3}) \qquad (2.2.9)$$

$x \geq 0.78$ (indirect gap)

$$N_c \cong 4.82 \cdot 10^{15} \cdot T^{3/2}(0.66 + 0.13x)^{3/2}\ (\mathrm{cm}^{3}) \qquad (2.2.10)$$

Effective density of states in the valence band N_v:

$$N_v \cong 4.82 \cdot 10^{15} \cdot T^{3/2} \cdot (0.6 + 0.19x)^{3/2}\ (\mathrm{cm}^{-3}) \qquad (2.2.11)$$

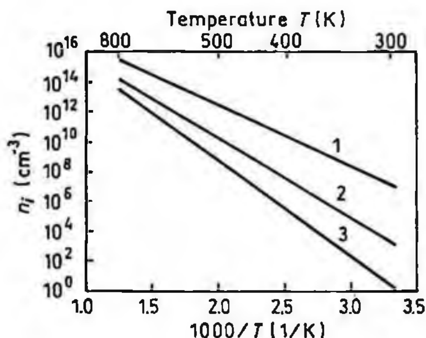

Fig. 2.2.6. The temperature dependences of the intrinsic concentration. 1. $x = 0$, 2. $x = 0.5$, 3. $x = 1$.

2.2.2. *Dependences on Hydrostatic Pressure*

$x = 0$ (InP): $E_\Gamma = 1.36 + 8.4 \cdot 10^{-3}\ P - 18 \cdot 10^{-6}\ P^2$ (eV)

$x = 0.36$ $E_\Gamma = 1.75 + 9.6 \cdot 10^{-3}\ P - 3 \cdot 10^{-5}\ P^2$ (eV)

$x = 0.5$ $E_\Gamma = 1.93 + 9.5 \cdot 10^{-3}\ P - 2.9 \cdot 10^{-5}\ P^2$ (eV)

(after Goni *et al.* [1989])

$x = 1$ (GaP): $E_X = 2.26 - 2.4 \cdot 10^{-3}\ P - 4.6 \cdot 10^{-6}\ P^2$ (eV) (after Ves *et al.* [1985]),

where P is pressure in kbar.

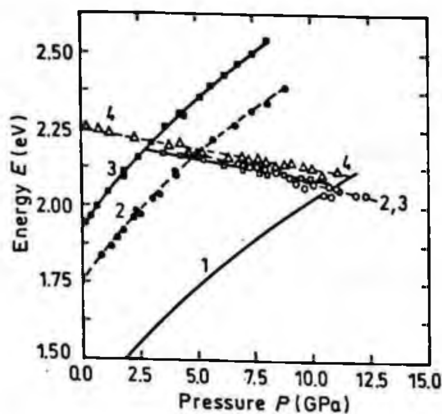

Fig. 2.2.7. Pressure dependences of the direct gap E_Γ (solid symbols) and indirect gap E_x (open symbols) for different values of composition parameter x. 1. $x = 0$ (InP), 2. $x = 0.36$, 3. $x = 0.5$, 4. $x = 1$ (GaP), 300 K (after Goni *et al.* [1989]).

(Reprinted with permission from The American Physical Society, © 1976.)

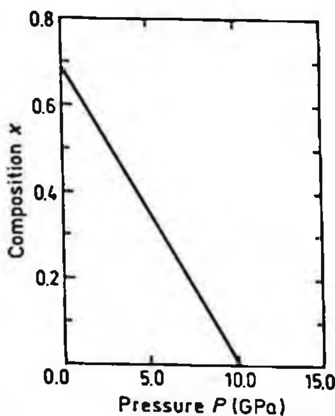

Fig. 2.2.8. Pressure dependence of the $\Gamma - X$ crossover, 300 K (after Goni *et al.* [1989]).

2.2.3. *Energy Gap Narrowing at High Doping Levels*

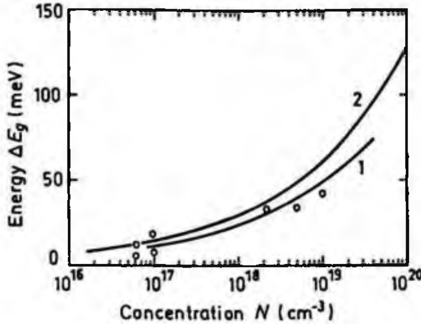

Fig. 2.2.9. Energy gap narrowing versus donor (curve 1 and experimental points) and acceptor (curve 2) doping density for $x = 0$ (InP), 300 K. Curve 1 and experimental points after Bugajski and Lewandowski [1985]. Curve 2 – after Jain *et al.* [1990].

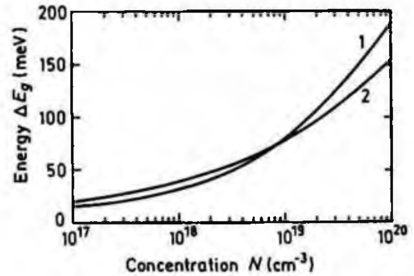

Fig. 2.2.10. Energy gap narrowing versus donor (curve 1) and acceptor (curve 2) doping density for $x = 1$ (GaP), 300 K (Calculated according to Jain *et al.* [1990]).

For InP ($x = 0$),

n-type:

$$\Delta E_g = 17.2 \cdot 10^{-9} N_d^{1/3} + 2.62 \cdot 10^{-7} \cdot N_d^{1/4} + 98.4 \cdot 10^{-12} \cdot N_d^{1/2} \qquad (2.2.12)$$

p-type:

$$\Delta E_g \cong 10.3 \cdot 10^{-9} N_a^{1/3} + 4.43 \cdot 10^{-7} N_a^{1/4} + 3.38 \cdot 10^{-12} N_a^{1/2} \text{ (eV)} \qquad (2.2.13)$$

For GaP ($x = 1$),

n-type:

$$\Delta E_g \cong 10.7 \cdot 10^{-9} N_d^{1/3} + 3.45 \cdot 10^{-7} N_d^{1/4} + 9.97 \cdot 10^{-12} N_d^{1/2} \text{ (eV)} \qquad (2.2.14)$$

p-type:

$$\Delta E_g \cong 12.7 \cdot 10^{-9} N_a^{1/3} + 5.85 \cdot 10^{-7} N_a^{1/4} + 3.90 \cdot 10^{-12} N_a^{1/2} \text{ (eV)} \qquad (2.2.15)$$

2.2.4. *Band Discontinuities at Heterointerfaces*

Lattice-matched interface $Ga_{0.51}In_{0.49}P/GaAs$:

Conduction band discontinuity $\Delta E_c = 0.2\,eV$

Valence band discontinuity $\Delta E_v = 0.28\,eV$

(after Bhattacharya *et al.* [1989]).

$Ga_{0.5}In_{0.5}P/Al_{0.5}In_{0.5}P$: $\Delta E_c = 0.43 E_g$

$\Delta E_v = 0.57 E_g$

(after O'Brien *et al.* [1988]).

$Ga_{0.5}In_{0.5}P/(Al_yGa_{1-y})_{0.51}In_{0.49}P$ $\Delta E_c = (0.6-0.7)E_g$

$Ga_xIn_{1-x}P/(Al_{0.7}Ga_{0.3})_{0.52}In_{0.48}P$: $x = 0.44$ $\Delta E_c = 0.67 E_g$

$x = 0.41$ $\Delta E_v = 0.85 E_g$

(after Dawson and Duggan [1994] and Mowbray *et al.* [1994]).

2.2.5. *Effective Masses*

Electrons:

For Γ-valley,

$x = 0$ (InP) $m_\Gamma = 0.08\,m_o$

$x = 0.5$ $m_\Gamma = (0.088 \pm 0.003)\,m_o$

(after Emanuelsson *et al.* [1994])

$x = 1$ (GaP) $m_\Gamma = 0.09 m_o$

For L-valleys,

Effective mass of density of states for all L-valleys $m_{Ld} \cong (0.63 + 0.13x)\,m_o$

For X-valleys,

Effective mass of density of states for all X-valleys $m_{Xd} \cong (0.66 + 0.13x)\,m_o$

Holes:

heavy $m_h = (0.6 + 0.19x)\,m_o$

light $m_{lp} = (0.09 + 0.05x)\,m_o$

2.2.6. *Donors and Acceptors*

Ionization energies of shallow donors (meV):

$x = 0$ (InP):	S, Si, Sn, Ge	~ 5.7
$x = 0.5$:		~ 5

Ge (amphoteric behaviour)
For donor level $E_c - E_t \cong 47$
(after Lee *et al.* [1993])

$x = 1$ (GaP):	S	~ 100
	Se	~ 100
	Te	93
	Ge	204
	Si	85
	Sn	72

Ionization energies of shallow acceptors (meV):

$x = 0$ (InP):	Zn	35
	Mg	30 (MBE)
	Mn	270
	Ge	21

$x = 0.5$:

Mg ~ 21 + 35 (after Chang *et al.* [1988]), see also Lu *et al.* [1991]).

Fig. 2.2.11. Ionization energy of Zn versus x (after Kato *et al.* [1980]).

Ge (amphoteric behaviour) for acceptor level $E_t - E_v \cong 58$ meV
(after Lee *et al.* [1993])

$x = 1$ (GaP):

Ge	265
Si	210
Be	57
Mg	60
Zn	70

2.3. Electrical Properties

2.3.1. *Mobility and Hall Effect*

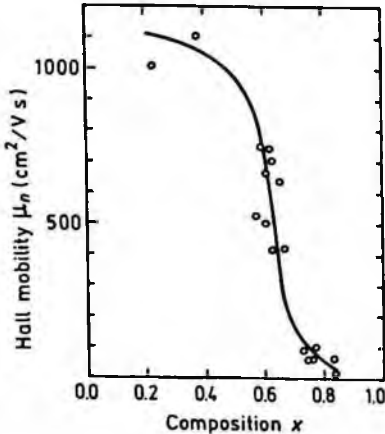

Fig. 2.3.1. Electron Hall mobility versus composition parameter x, 300 K.
Electron concentration $n_o = 10^{17} \div 1.5 \cdot 10^{18}$ cm^{-3} (after Macksey *et al.* [1973]).
(Reprinted with permission from the American Institute of Physics, © 1973.)

$x = 0$ (InP):	at 300 K	for $n_o = 3 \cdot 10^{13}$ cm^{-3},	$\mu_n \cong 5 \cdot 10^3$ cm^2/Vs
		for $n_o = 8 \cdot 10^{17}$ cm^{-3},	$\mu_n \cong 1.8 \cdot 10^3$ cm^2/Vs
$x = 1$ (GaP):	at 300 K	for $n_o = 5 \cdot 10^{16}$ cm^{-3},	$\mu_n \cong 200$ cm^2/Vs
		for $n_o = 2.5 \cdot 10^{18}$ cm^{-3},	$\mu_n \cong 100$ cm^2/Vs

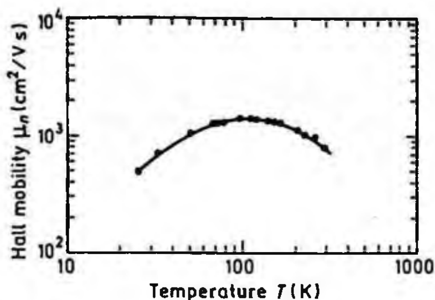

Fig. 2.3.2. Temperature dependence of electron mobility for $x = 0.5$. $n_o = 5 \cdot 10^{16}$ cm^{-3} (after Zhang *et al.* [1994]). See also Driessen *et al.* [1993].

(Reprinted with permission from Elsevier Science, © 1994.)

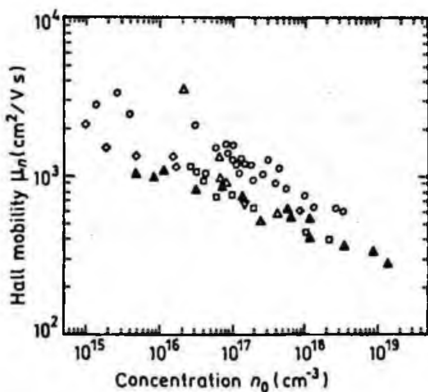

Fig. 2.3.3. Electron mobility versus electron concentration for $x = 0.52$, 300 K (after Shitara and Eberl [1994]).

(Reprinted with permission from the American Institute of Physics, © 1994.)

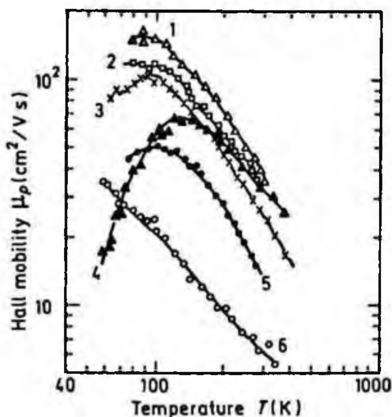

Fig. 2.3.4. Hole Hall mobility versus temperature in Zn-doped $Ga_xIn_{1-x}P$. N_a (cm^{-3}):

1. $x = 0.65$, $N_a = 2.9 \cdot 10^{17}$, $\theta = N_d/N_a = 0.26$,
2. $x = 0.32$, $N_a = 1.1 \cdot 10^{18}$, $\theta = 0.18$,
3. $x = 0.7$, $N_a = 1.9 \cdot 10^{18}$, $\theta = 0.07$,
4. $x = 0.75$, $N_a = 5.2 \cdot 10^{18}$, $\theta = 0.086$,
5. $x = 0.36$, $N_a = 9.8 \cdot 10^{17}$, $\theta = 0.18$,
6. $x = 0.55$, $N_a = 2.2 \cdot 10^{18}$, $\theta = 0.091$.

No significant dependence of the hole mobility on alloy composition is found (after Kato *et al.* [1980]).

(Reprinted with permission from the Japanese Journal of Applied Physics, © 1976.)

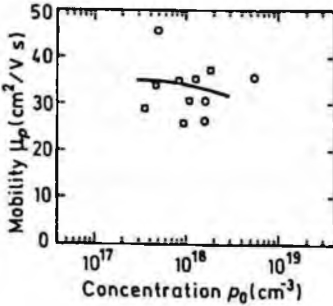

Fig. 2.3.5. Hole Hall mobility versus hole concentration for Zn-doped $Ga_{0.5}In_{0.5}P$, 300 K (after Ikedo and Kaneko [1989]).

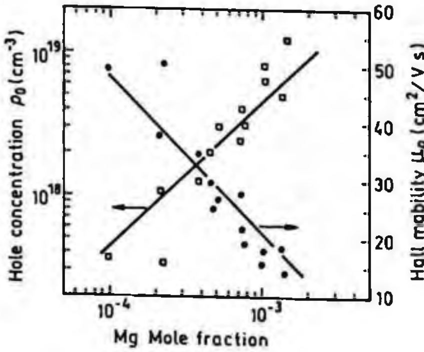

Fig. 2.3.6. Hole Hall concentration (squares) and mobility (circles) for Mg-doped $Ga_{0.5}In_{0.5}P$ as a function of Mg mole fraction in the growth solution, 300 K (after Chang *et al.* [1988]).

(Reprinted with permission from the American Institute of Physics, © 1988.)

2.3.2. *Two-Dimensional Electron Gas Mobility at $Ga_{0.51}In_{0.49}P/GaAs$ Interface (after Chan et al. [1989])*

77 K $\mu_n = 21300\ \mathrm{cm^2/V \cdot s}$ (Sheet concentration $N = 1.26 \cdot 10^{12}\ \mathrm{cm^{-2}}$)

300 K $\mu_n = 3500\ \mathrm{cm^2/V \cdot s}$ $N = 1.89 \cdot 10^{12}\ \mathrm{cm^{-2}}$

2.3.3. *Transport Properties in High Electric Fields*

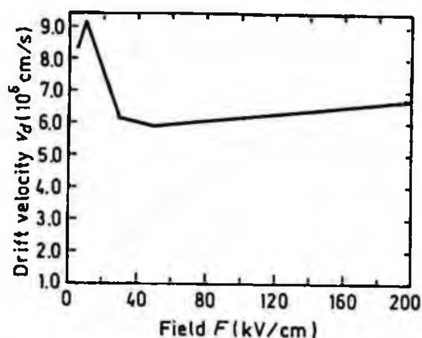

Fig. 2.3.7. Field dependence of the electron drift velocity in $Ga_{0.52}In_{0.48}P$ at 300 K. Monte-Carlo calculations (after Brennan and Chiang [1992]).

(Reprinted with permission from the American Institute of Physics, © 1992.)

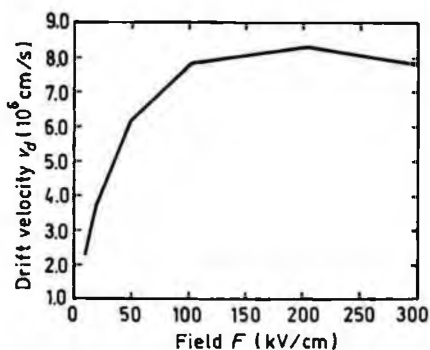

Fig. 2.3.8. Field dependence of the hole drift velocity in $Ga_{0.52}In_{0.48}P$ at 300 K. Monte-Carlo calculations (after Brennan and Chiang [1992]).

(Reprinted with permission from the American Institute of Physics, © 1992.)

2.3.4. *Impact Ionization*

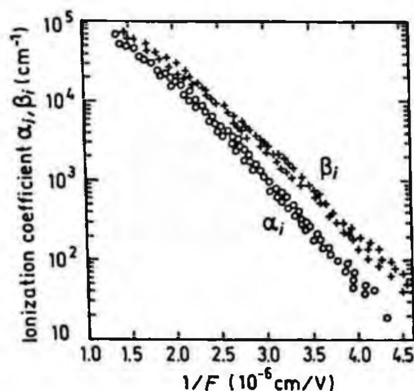

Fig. 2.3.9. The dependences of ionization rates for electrons α_i and holes β_i versus $1/F$ for $x = 0$ (InP), 300 K (after Cook *et al.* [1982]).

(Reprinted with permission from the American Institute of Physics, © 1982.)

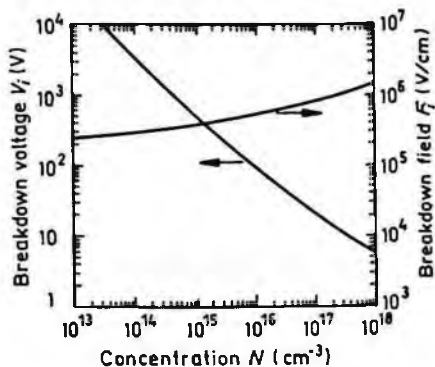

Fig. 2.3.10. Breakdown voltage and breakdown field versus doping density for an abrupt $p-n$ junction. $x = 0$ (InP), 300 K (after Kyuregyan and Yurkov [1989]).

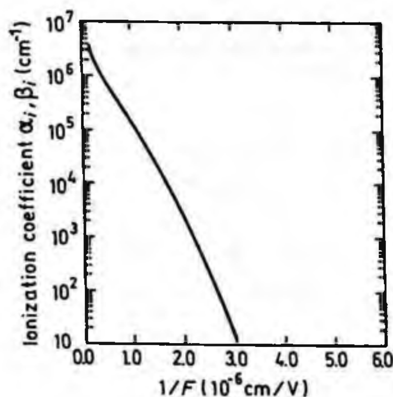

Fig. 2.3.11. The dependences of ionization rates $\alpha_i = \beta_i$ versus $1/F$ for $x = 1$ (GaP), 300 K (after Chau and Pavlidis [1992]).

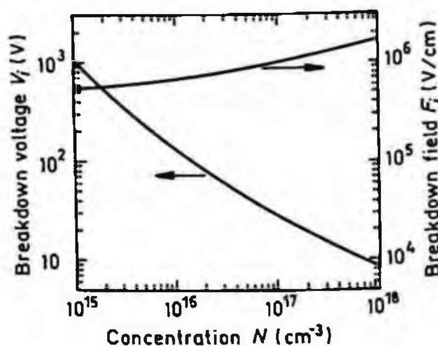

Fig. 2.3.12. Breakdown voltage and breakdown field versus doping density for abrupt $p-n$ junction. $x = 1$ (GaP), 300 K (after Sze and Gibbons [1966]).

For $x = 0.52$:

$$\alpha_i = 2.77\cdot 10^5 \exp\left[-\left(\frac{1.196\cdot 10^6}{F}\right)^{1.95}\right] \text{ (cm}^{-1}\text{)}$$

$$\beta_i = 2.75\cdot 10^5 \exp\left[-\left(\frac{1.172\cdot 10^6}{F}\right)^{1.91}\right] \text{ (cm}^{-1}\text{)},$$

where F is electric field in Vcm^{-1} (Chin *et al.* [1997]).

2.3.5. *Recombination Parameters*

Radiative recombination coefficient:

$x = 0$ (InP)	300 K – $1.2\cdot 10^{-10}$ cm^3/s
$x = 0.5$ ($Ga_{0.5}In_{0.5}P$)	300 K – $(1.0 \pm 0.3)\cdot 10^{-10}$ cm^3/s
	150 K – $(4.0 \pm 1)\cdot 10^{-10}$ cm^3/s
	(after Strauss *et al.* [1994])
$x = 1$ (GaP)	300 K:

band-to-band recombination coefficient ~ 10^{-13} cm^3/s

Auger coefficient (300 K):

$x = 0$ (InP)	~ $9\cdot 10^{-31}$ cm^6/s	
$x = 0.5$ ($Ga_{0.5}In_{0.5}P$)	~ $3\cdot 10^{-30}$ cm^6/s	(after Strauss *et al.* [1994])
$x = 1$ (GaP)	~ 10^{-30} cm^6/s	

Surface recombination velocity ($x = 0.5$, 300 K):

free surface	~ $(2 \div 5)\cdot 10^4$ cm/s (after Pearton *et al.* [1994])
interface GaInP/GaAs	1.5 cm/s (after Olson *et al.* [1989])
interface GaInP/$(Al_{0.7}Ga_{0.3})_{0.5}In_{0.5}P$	20 cm/s – undoped *n*-AlGaInP
	100 cm/s – AlGaInP with $n_o = 2.5\cdot 10^{17}$ cm^{-3} (after Domen *et al.* [1992])

2.4. Optical Properties

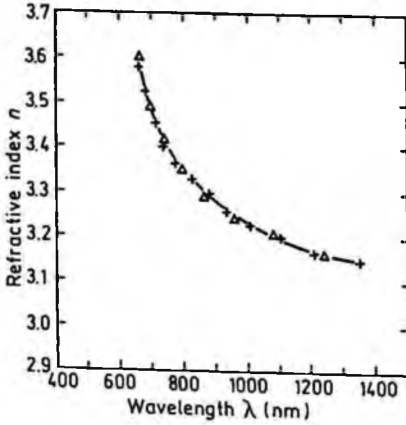

Fig. 2.4.1. Refractive index n versus wavelength for $x = 0.5$, 300 K (after Kaneko and Kishino [1994]).

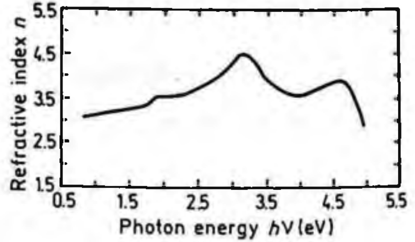

Fig. 2.4.2. Refractive index n versus photon energy for $x = 0.51$, 300 K (after Schubert *et al.* [1995]).

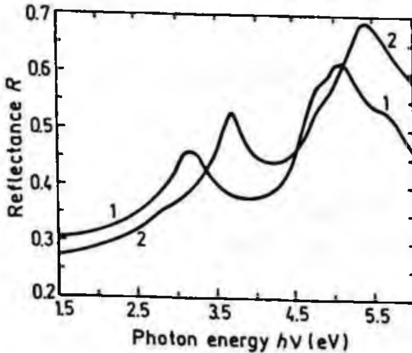

Fig. 2.4.3. Normal incidence reflectivity versus photon energy, 300 K. Curve 1 – $x = 0$ (InP). Curve 2 – $x = 1$ (GaP) (after Aspnes and Studna [1983]).

(Reprinted with permission from The American Physical Society, © 1983.)

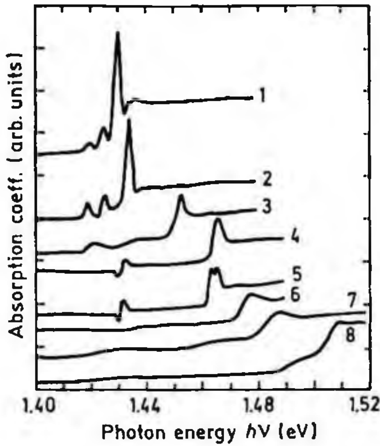

Fig. 2.4.4. Optical absorption spectra for $Ga_xIn_{1-x}P$ with different values of x, 7 K. x: 1. 0.016, 2. 0.026, 3. 0.057, 4. 0.078, 5. 0.076, 6. 0.093, 7. 0.09, 8. 0.116 (after Bensaada *et al.* [1994]). (Data for samples 4, 5 and 6 have been multiplied by a factor of 2 for presentation purposes.)

(Reprinted with permission from the American Institute of Physics, © 1994.)

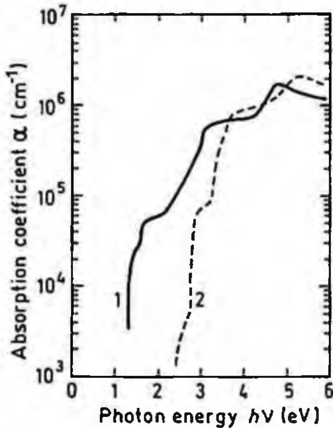

Fig. 2.4.5. The absorption coefficient versus photon energy. 1. $x = 0$ (InP) 2. $x = 1$ (GaP), 300 K (after Adachi [1989], see also Aspnes and Studna [1983]).

(Reprinted with permission from The American Physical Society, © 1983.)

2.5. Thermal Properties

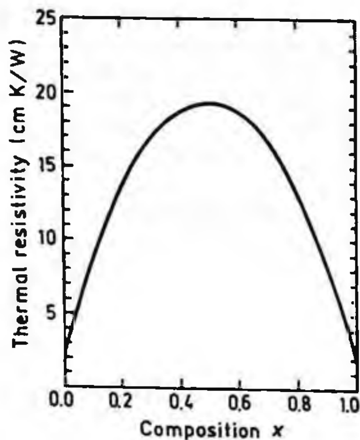

Fig. 2.5.1. Thermal resistivity versus alloy composition parameter x, 300 K (after Adachi [1983]).

(Reprinted with permission from the American Institute of Physics, © 1983.)

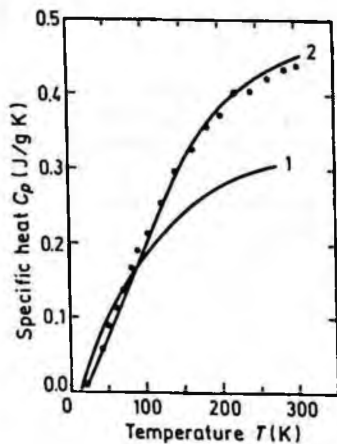

Fig. 2.5.2. Temperature dependence of specific heat at constant pressure. Curve 1 – $x = 0$ (InP) (after Piesbergen [1963]). Curve 2 – $x = 1$ (GaP) (after Sirota and Sidorov [1988]).

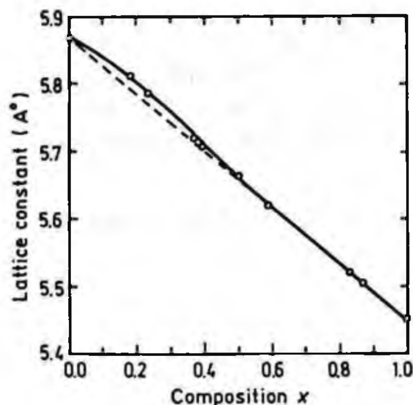

Fig. 2.5.3. Lattice constant as a function of alloy composition parameter x, 300 K (after Onton *et al.* [1971]). At $x \cong 0.5$ GaInP is lattice-matched to GaAs.

(Reprinted with permission from the American Institute of Physics, © 1971.)

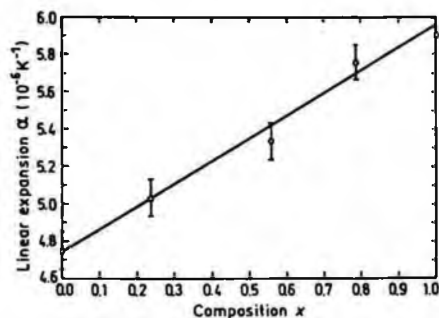

Fig. 2.5.4. Linear expansion coefficient α versus alloy composition parameter x, 300 K (after Kudman and Paff [1972]).

(Reprinted with permission from the American Institute of Physics, © 1972.)

2.6. Mechanical Properties, Elastic Constants, Lattice Vibrations, Other Properties

Density $4.81 - 0.67x$ (g/cm^3)

Hardness ~ 5 (on the Mohs scale)

Surface microhardness
(using Knoop's pyramid test)

$x = 0$ (InP) 460 kg/mm^2

$x = 1$ (GaP) 850 kg/mm^2

Elastic constants at 300 K:

C_{11}	$(10.11 + 3.94x) \cdot 10^{11}$ dyn/cm^2
C_{12}	$(5.61 + 0.59x) \cdot 10^{11}$ dyn/cm^2
C_{44}	$(4.56 + 2.47x) \cdot 10^{11}$ dyn/cm^2

Bulk modulus (compressibility^{-1}) $B_s = \frac{C_{11}+2C_{12}}{3}$ $B_s = (7.11+1.71x)\cdot 10^{11}$ dyn/cm^2

Shear modulus $C' = (C_{11} - C_{12})/2$ $C' = (2.25+1.67x)\cdot 10^{11}$ dyn/cm^2

[100] Young's modulus $Y_0 = \frac{(C_{11}+2C_{12})(C_{11}-C_{12})}{(C_{11}+C_{12})}$ $Y_0 = (6.11+4.19x)\cdot 10^{11}$ dyn/cm^2

[100] Poisson ratio $\sigma_0 = \frac{C_{12}}{C_{11}+C_{12}}$ $\sigma_0 = (0.36 - 0.05x)$

Acoustic Wave Speeds

Wave propagation direction	Wave character	Expression for wave speed	Wave speed (in units of 10^5 cm/s)
[100]	V_L	$(C_{11}/\rho)^{1/2}$	$4.58 + 1.25x$
	V_T	$(C_{44}/\rho)^{1/2}$	$3.08 + 1.04x$
[110]	V_l	$[(C_{11} + C_{12} + 2C_{44})/2\rho)]^{1/2}$	$5.08 + 1.35x$
	$V_{t\parallel}$	$V_{t\parallel} = V_T = (C_{44}/\rho)^{1/2}$	$3.08 + 1.04x$
	$V_{t\perp}$	$[(C_{11} - C_{12})/2\rho)]^{1/2}$	$2.16 + 0.92x$
[111]	V_l'	$[(C_{11} + 2C_{12} + 4C_{44})/3\rho)]^{1/2}$	$5.23 + 1.40x$
	V_t'	$[(C_{11} - C_{12} + C_{44})/3\rho)]^{1/2}$	$2.51 + 0.95x$

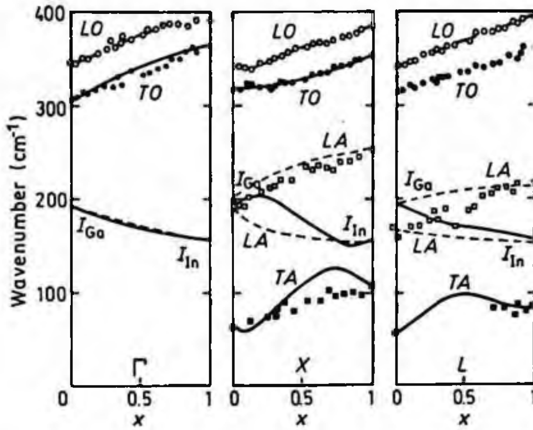

Fig. 2.6.1. Compositional dependences of longitudinal (dashed lines) and transverse (solid lines) phonon frequencies of $Ga_xIn_{1-x}P$ (after Jahne and Ulrici [1980]).

(Reprinted with permission from Akademie Verlag GmbH, © 1980.)

Phonon frequencies:
(after Lee *et al.* [1994])

ω_{LO} (GaP – like) = $404.99 - 38.97x - 18.18x^2$ (cm^{-1})

ω_{LO} (InP – like) = $394.59 - 80.36x + 30.26x^2$ (cm^{-1})

ω_{TO} (M) = $368.82 - 88.95x + 26.04x^2$ (cm^{-1})

ω_{TO} (m) = $395.02 - 54.26x + 6.72x^2$ (cm^{-1})

Piezoelectric constant e_{14} $-(0.035 + 0.065x)$ C/m^2

References

Adachi, S., *J. Appl. Phys.* **54**, 4 (1983) 1844–1848.
Adachi, S., *J. Appl. Phys.* **66**, 12 (1989) 6030–6040.
Aspnes, D. E. and A. A. Studna, *Phys. Rev.* **B27**, 2 (1983) 985–1009.
Auvergne, D., P. Merle, and H. Mathieu, *Solid State Commun.* **21**, 5 (1977) 437–439.

Bensaada, A., A. Chennouf, R. W. Cochrane, J. T. Graham, R. Leonelli, and R. A. Masut, *J. Appl. Phys.* **75**, 6 (1994) 3024–3029.

Bhattacharya, P., N. Debbar, D. Biswas, M. Razeghi, M. Defour, and F. Omnes, in *Gallium Arsenide and Related Compounds*, Inst. of Phys. Conf. Ser., Bristol and New York, vol. 106, 1989, pp. 351–356.

Brennan, K. F. and P. K. Chiang, *J. Appl. Phys.* **71**, 2 (1992) 1055–1057.

Bugajski, M. and W. Lewandowski, *J. Appl. Phys.* **57**, 2 (1985) 521–530.

Chan, Y. J., D. Pavlidis, M. Razeghi, and F. Omnes, in *Gallium Arsenide and Related Compounds*, Inst. of Phys. Conf. Ser., Bristol and New York, vol. 106, 1989, p. 891.

Chang, L. B., K. Y. Cheng, and C. C. Liu, *J. Appl. Phys.* **64**, 3 (1988) 1116–1119.

Chau, H. F. and D. Pavlidis, *J. Appl. Phys.* **72**, 2 (1992) 531–538.

Chin, R., J. P. R. David, M. Hopkinson, M. A. Pate, G. J. Rees, and P. N. Robson, *Appl. Phys. Lett.* **70**, 26 (1997) 3567–3569.

Chin, T. P., J. C. P. Chang, K. L. Kavanagh, C. W. Tu, P. D. Kirchner, and J. M. Woodall, *Appl. Phys. Lett.* **62**, 19 (1993) 2369–2371.

Cook, L. W., G. E. Bulman, and G. E. Stillman, *Appl. Phys. Lett.* **40**, 7 (1982) 589–591.

Dawson, M. D. and G. Duggan, *Appl. Phys. Lett.* **64**, 7 (1994) 892–894.

Domen, K., M. Kondo, and N. Tanahashi, in *Gallium Arsenide and Related Compounds*, (Inst. of Phys. Conf. Ser, Bristol and Philadelphia, vol. 129, 1992, pp. 447–452.

Driessen, F. A. J. M., G. J. Bauhuis, S. M. Olsthoorn, L. Y. Giling, *Phys. Rev.* **B48**, 11 (1993) 7889–7896.

Emanuelsson, P., M. Drechsler, D. M. Hofmann, B. K. Meyer, M. Moser, and F. Scholz, *Appl. Phys. Lett.* **64**, 21 (1994) 2849–2851.

Goni, A. R., K. Syassen, K. Strossner, and M. Cardona, *Phys. Rev.* **B39**, 5 (1989) 3178–3184.

t'Hooft, G. W., C. J. B. Riviere, M. P. C. M. Krijn, C. T. H. F. Liedenbaum, and A. Valster, *Appl. Phys. Lett.* **61**, 26 (1992) 3169–3171.

Ikeda, M. and K. Kaneko, *J. Appl. Phys.* **66**, 11 (1989) 5285–5289.

Jahne, E. and B. Ulrici, *Phys. Stat. Sol. (b)* **101**, 1 (1980) 169–179.

Jain, S. C., J. M. McGregor, and D. J. Roulston, *J. Appl. Phys.* **68**, 7 (1990) 3747–3749.

Kaneko, Y. and K. Kishino, *J. Appl. Phys.* **76**, 3 (1994) 1809–1818.

Kato, T., T. Matsumoto, and T. Ishida, *Jpn. J. Appl. Phys.* **19**, 12 (1980) 2367–2375.

Krutogolov, Yu. K., S. V. Dovzhenko, S. A. Diordiev, L. I. Krutogolova, Yu. I. Kunakin, and S. A. Ryzhikh, *Sov. Phys. Semicond.* **23**, 5 (1989) 557–558.

Kudman, I. and R. J. Paff, *J. Appl. Phys.* **43**, 9 (1972) 3760–3762.

Kyuregyan, A. S. and S. N. Yurkov, *Sov. Phys. Semicond.* **23**, 10 (1989) 1126–1132.

Lange, H., J. Donecker, and H. Friedrich, *Phys. Stat. Solidi (b)* **73**, 2 (1976) 633–639.
Lee, H., D. Biswas, M. V. Klein, H. Morkoc, D. E. Aspnes, B. D. Choe, J. Kim, and C. O. Griffiths, *J. Appl. Phys.* **75**, 10 (1994) 5040–5051.
Lee, J. B., I. Kim, H. K. Kwon, and B. D. Choe, *Appl. Phys. Lett.* **62**, 14 (1993) 1620–1622.
Lu, S. C., M. C. Wu, C. Y. Lee, and Y. C. Yang, *J. Appl. Phys.* **70**, 4 (1991) 2309–2312.
Macksey, H. M., N. Holonyak Jr., R. D. Dupuis, J. C. Campbell, and G. W. Zack, *J. Appl. Phys.* **44**, 3 (1973) 1333–1341.
McDermott, B. T., K. G. Reid, N. A. El-Masry, S. M. Bedair, W. M. Duncan, X. Yin, and F. H. Pollak, *Appl. Phys. Lett.* **56**, 12 (1990) 1172–1174.
Mowbray, D. J., O. P. Kowalski, M. S. Skolnick, M. C. De Long, M. Hopkinson, J. P. R. David, and A. G. Cullis, *J. Appl. Phys.* **75**, 4 (1994) 2029–2034.
O'Brien, S., D. P. Bour, and J. R. Shealy, in *Gallium Arsenide and Related Compounds*, Inst. of Phys. Conf. Ser., Bristol and Philadelphia, Ser., vol. 96, 1989, pp. 401–404.
Olson, J. M., R. K. Ahrenkiel, D. J. Dunlavy, B. Keyes, and A. E. Kibbler, *Appl. Phys. Lett.* **55**, 12 (1989) 1208–1210.
Onton, A., M. R. Lorenz, and W. Reuter, *J. Appl. Phys.* **42**, 9 (1971) 3420–3432.
Panish, M. B. and H. C. Casey Jr., *J. Appl. Phys.* **40**, 1 (1969) 163–167.
Pearton, S. J., F. Ren, W. S. Hobson, C. R. Abernathy, and U. K. Chakrabarti, *J. Vac. Sci. Technol.* **B12**, 1 (1994) 142–146.
Piesbergen, U., *Zh. Naturforschung* **18a**, 2 (1963) 141–147.
Schubert, M., V. Gottschalch, C. M. Herzinger, H. Yao, P. G. Snyder, and J. A. Woollam, *J. Appl. Phys.* **77**, 7 (1995) 3416–3419.
Shitara, T. and K. Eberl, *Appl. Phys. Lett.* **65**, 3 (1994) 356–358.
Sirota, N. N. and A. A. Sidorov, *Doklady Akademii Nauk SSSR (Soviet Physics Doklady)* **303**, 5 (1988) 1123–1126, (in Russian).
Strauss, U., W. W. Ruhle, H. J. Queisser, K. Nakano, and A. Ishibashi, *J. Appl. Phys.* **75**, 12 (1994) 8204–8206.
Sze, S. M. and G. Gibbons, *Appl. Phys. Lett.* **8**, 5 (1966) 111–113.
Ves, S., K. Strossner, C. K. Kim, and M. Cardona, *Solid State Commun.* **55**, 4 (1985) 327–331.
Zhang, B., S. Lan, L. Q. Li, W. J. Xu, C. Q. Yang, and H. D. Liu, *Solid State Commun.* **92**, 5 (1994) 419–422.

CHAPTER 3

GALLIUM INDIUM ARSENIDE ($Ga_xIn_{1-x}As$)

Yu. A. Goldberg and Natalya M. Shmidt
Ioffe Institute, St. Petersburg, Russia

3.1. Basic Parameters at 300 K

	InAs	GaAs	$Ga_{0.47}In_{0.53}As$	$Ga_xIn_{1-x}As$
Crystal structure	Zinc Blende	Zinc Blende	Zinc Blende	Zinc Blende
Space group	$F\bar{4}3m$	$F\bar{4}3m$	$F\bar{4}3m$	$F\bar{4}3m$
Number of atoms in 1 cm^3	$3.59 \cdot 10^{22}$	$4.42 \cdot 10^{22}$	$3.98 \cdot 10^{22}$	$(3.59 + 0.83x) \cdot 10^{22}$
Debye temperature (K)	280	370	330	$280 + 110x$
Density (g/cm^3)	5.68	5.31	5.50	$5.68 - 0.37x$
Dielectric constant				
static	15.15	12.9	13.9	$15.1 - 2.87x + 0.67x^2$
high frequency	12.3	10.89	11.6	$12.3 - 1.4x$
Effective electron mass: (in units of m_o)	0.023	0.063	0.041	$0.023 + 0.037x + 0.003x^2$
Effective hole mass: (in units of m_o)				
heavy	0.41	0.51	0.45	$0.41 + 0.1x$
light	0.026	0.082	0.052	$0.026 + 0.056x$
Electron affinity (eV)	4.9	4.07	4.5	$4.9 - 0.83x$
Lattice constant (Å)	6.0583	5.6533	5.8687	$6.0583 - 0.405x$
Optical phonon energy (meV)	30	36	34	See Sec. 3.6

Band structure and carrier concentration

	InAs	GaAs	$Ga_{0.47}In_{0.53}As$	$Ga_xIn_{1-x}As$
Energy gap (eV)	0.36	1.42	0.74	$0.36 + 0.63x + 0.43x^2$
Energy separation between X-valley and top of the valence band E_X (eV)	1.37	1.9	1.33	$1.37 - 0.63x + 1.16x^2$
Energy separation between L-valley and top of the valence band E_L (eV)	1.08	1.71	1.2	$1.08 - 0.02x + 0.65x^2$
Intrinsic carrier concentration (cm^{-3})	$1 \cdot 10^{15}$	$2 \cdot 10^{6}$	$6.3 \cdot 10^{11}$	See Sec. 3.2.1
Effective conduction band density of states (cm^{-3})	$8.7 \cdot 10^{16}$	$4.7 \cdot 10^{17}$	$2.1 \cdot 10^{17}$	See Sec. 3.2.1
Effective valence band density of states (cm^{-3})	$6.6 \cdot 10^{18}$	$9 \cdot 10^{18}$	$7.7 \cdot 10^{18}$	See Sec. 3.2.1
Electrical properties				
Breakdown field (V/cm)	$\approx 4 \cdot 10^4$	$\approx 4 \cdot 10^5$	$\approx 2 \cdot 10^5$	See Sec. 3.3.4
Mobility ($cm^2/V \cdot s$)				
electrons	$\leq 4 \cdot 10^4$	≤ 8500	≤ 12000	$(40 - 80.7x + 49.2x^2) \cdot 10^3$
holes	≤ 500	≤ 400	≤ 300	$\sim 300 \div 400$

	InAs	GaAs	$Ga_{0.47}In_{0.53}As$	$Ga_xIn_{1-x}As$
Diffusion coefficient (cm^2/s)				
electrons	$\leq \cdot 10^3$	≤ 200	≤ 300	$(10-20.2x+12.3x^2)\cdot 10^2$
holes	≤ 12	≤ 10	≤ 7.5	$\sim 7+12$
Electron thermal velocity (m/s)	$7.7\cdot 10^5$	$4.4\cdot 10^5$	$5.5\cdot 10^5$	$(7.7-5.9x+2.6x^2)\cdot 10^5$
Hole thermal velocity (m/s)	$2\cdot 10^5$	$1.8\cdot 10^5$	$2\cdot 10^5$	$(1.8+2)\cdot 10^5$

Optical properties

	InAs	GaAs	$Ga_{0.47}In_{0.53}As$	$Ga_xIn_{1-x}As$
Infrared refractive index	3.51	3.35	3.43	$3.51-0.16x$
Radiative recombination coefficient (cm^3/s)	$1.1\cdot 10^{-10}$	$7\cdot 10^{-10}$	$0.96\cdot 10^{-10}$	See Sec. 3.3.5

Thermal and mechanical properties

	InAs	GaAs	$Ga_{0.47}In_{0.53}As$	$Ga_xIn_{1-x}As$
Bulk modulus (dyn/cm^2)	$5.8\cdot 10^{11}$	$7.53\cdot 10^{11}$	$6.62\cdot 10^{11}$	$(5.81+1.72x)\cdot 10^{11}$
Melting point (°C)	942	1240	≈ 1100	
Specific heat (J/g °C)	0.25	0.33	0.3	See Sec. 3.5
Thermal conductivity (W/cm°C)	0.27	0.55	0.05	See Sec. 3.5
Thermal expansion, linear, ($°C^{-1}$)	$4.52\cdot 10^{-6}$	$5.73\cdot 10^{-6}$	$5.66\cdot 10^{-6}$	

3.2. Band Structure and Carrier Concentration

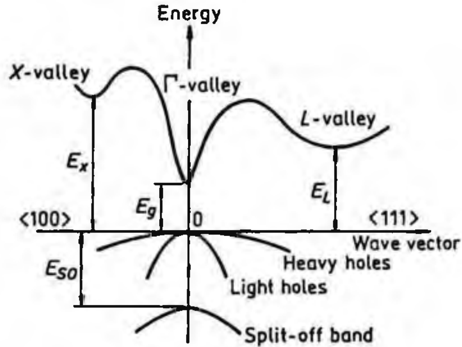

Fig. 3.2.1. Band structure of $Ga_xIn_{1-x}As$. Important minima of the conduction band and maxima of the valence band.

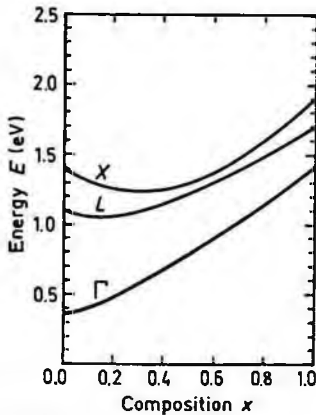

Fig. 3.2.2. Energy separations between Γ-, *X*-, and *L*-conduction band minima and top of the valence band versus composition parameter *x* (after Porod and Ferry [1983]).

At 300 K:

$$E_\Gamma = E_g \cong 0.36 + 0.63x + 0.43x^2 \text{ (eV)} \quad (3.2.1)$$

$$E_x \cong 1.37 - 0.63x + 1.16x^2 \text{ (eV)} \quad (3.2.2)$$

$$E_L \cong 1.08 - 0.02x + 0.65x^2 \text{ (eV)} \quad (3.2.3)$$

At 2 K:

$$E_\Gamma = E_g \cong 0.4105 + 0.6337x + 0.475x^2 \text{ (eV)} \quad (3.2.4)$$

(after Goetz *et al.* [1983])

Interfacial elastic strain induced by lattice parameter mismatch between epilayer and substrate results in significant band-gap shifts:

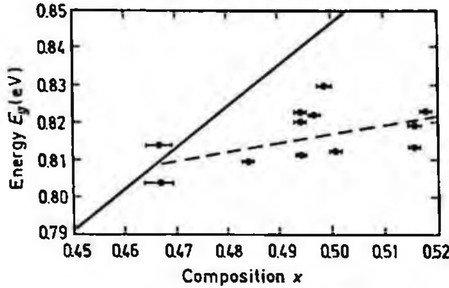

Fig. 3.2.3. Energy band gap E_g of unstrained (solid line) and strained (dashed line and experimental points) $Ga_xIn_{1-x}As$ versus composition parameter x. Solid line is calculated according to Eq. (3.2.4). Experimental points are obtained at 4 K (after Kuo *et al.* [1985]).

(Reprinted with permission from the American Institute of Physics, © 1985.)

3.2.1. *Temperature Dependences*

$$E_g(x,T) \cong 0.42 + 0.625x - \left(\frac{5.8}{T+300} - \frac{4.19}{T+271}\right) \cdot 10^{-4} T^2 x - 4.19 \cdot 10^{-4} \cdot \frac{T^2}{T+271} + 0.475x^2 \text{ (eV)} \qquad (3.2.5)$$

(after Paul *et al.* [1991]).

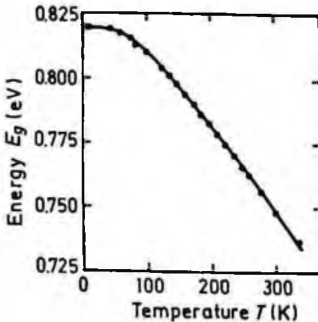

Fig. 3.2.4. Energy gap E_g versus temperature for $Ga_{0.47}In_{0.53}As$. Points are experimental data. Solid line is theoretical calculation. $E_g(0) = 821.5 \pm 0.2$ meV (after Zielinski *et al.* [1986]).

(Reprinted with permission from the American Institute of Physics, © 1986.)

For $Ga_xIn_{1-x}As$ on GaAs:

$$E_g(x,T) \cong E_g(0) - (6x^2 - 8.6x + 5.2)\cdot 10^{-4} \cdot \frac{T^2}{T + (337x^2 - 455x + 196)} \text{ (eV)} \quad (3.2.6)$$

(after Karachevtseva *et al.* [1994]).

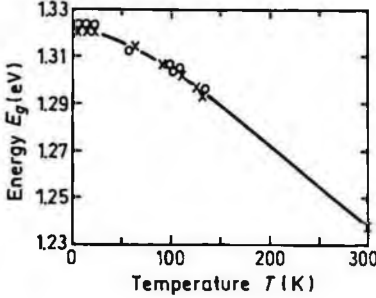

Fig. 3.2.5. Energy gap E_g versus temperature for $Ga_{0.87}In_{0.13}As$. Solid line is calculated according to equation:

$$E_g(T) = 1.321 - 4.1\cdot 10^{-4}\frac{T^2}{T+139} \text{ (eV)}$$

Points are experimental data (after Karachevtseva [1994]).

(Reprinted with permission from the American Institute of Physics, © 1994.)

Effective density of states in the conduction band N_c:

$$N_C \cong 4.82\cdot 10^{15}\cdot\left(\frac{m_\Gamma}{m_o}\right)^{3/2}\cdot T^{3/2}$$

$$\cong 4.82\cdot 10^{15}\cdot T^{3/2}\cdot(0.023 + 0.037x + 0.003x^2)^{3/2} (\text{cm}^{-3}) \quad (3.2.7)$$

Effective density of states in the valence band:

$$N_v \cong 4.82\cdot 10^{15}\cdot T^{3/2}\cdot(0.41 + 0.1x)^{3/2} \text{ (cm}^{-3}) \quad (3.2.8)$$

Intrinsic carrier concentration n_i (after Paul *et al.* [1991]):

$$n_i \cong 4.83\cdot 10^{15}[(0.41 + 0.09x)^{3/2} + (0.027 + 0.047x)^{3/2}]^{1/2} \times (0.025 + 0.043x)^{3/4}\left[T^{3/2}e^{-\nu/2}\left(1 + \frac{3.75}{\nu} + \frac{3.28}{\nu^2} - \frac{2.46}{\nu^3}\right)^{1/2}\right](\text{cm}^{-3}), \quad (3.2.9)$$

where $\nu = E_g(x,T)/kT$.

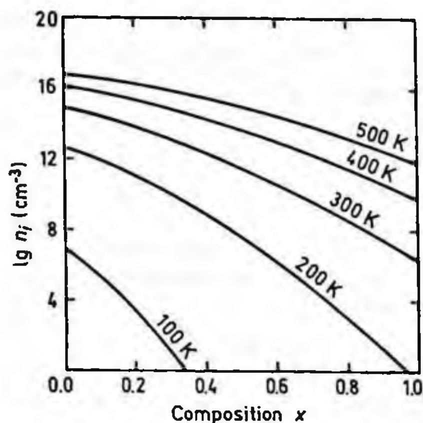

Fig. 3.2.6. Intrinsic concentration n_i versus composition parameter x for $Ga_xIn_{1-x}As$ at different temperatures (after Paul *et al.* [1991]).

(Reprinted with permission from the American Institute of Physics, © 1991.)

For $Ga_{0.47}In_{0.53}As$ at 300 K $n_i = 6.3 \cdot 10^{11}$ cm^{-3}.

3.2.2. *Dependences on Hydrostatic Pressure*

$x = 0$ (InAs):

$$E_g = E_g(0) + 4.8 \cdot 10^{-3} P \text{ (eV)}$$

$$E_L = E_L(0) + 3.2 \cdot 10^{-3} P \text{ (eV)}$$

$x = 0.47$ ($Ga_{0.47}In_{0.53}As$):

at 80 K: $E_g \cong 0.796 + 10.9 \cdot 10^{-3} P - 30 \cdot 10^{-6} P^2$ (eV)

at 300 K: $E_g \cong 0.733 + 11.0 \cdot 10^{-3} P - 27 \cdot 10^{-6} P^2$ (eV)

(after Lambkin and Dunstan [1988]).

$x = 1$ (GaAs):

$$E_g = E_g(0) + 12.6 \cdot 10^{-3} P - 37.7 \cdot 10^{-6} P^2 \text{ (eV)}$$

$$E_L = E_L(0) + 5.5 \cdot 10^{-3} P \text{ (eV)}$$

$$E_x = E_x(0) - 1.5 \cdot 10^{-3} P \text{ (eV)},$$

where P is pressure in kbar.

3.2.3. *Energy Gap Narrowing at High Doping Levels*

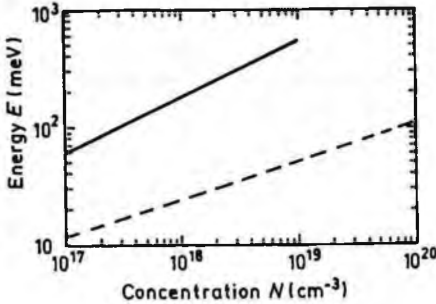

Fig. 3.2.7. Energy gap narrowing versus donor (solid line) and acceptor (dashed line) doping density for $Ga_{0.47}In_{0.53}As$, 300 K (after Jain *et al.* [1990]).

For $Ga_{0.47}In_{0.53}As$ at 300 K:

$$\Delta E_g = 10^{-9} A \cdot N^{1/3} + 10^{-7} B N^{1/4} + 10^{-12} C N^{1/2} \text{ (eV)} \quad (3.2.10)$$

$n-Ga_{0.47}In_{0.53}As$:	$A = 15.5$;	$B = 1.95$;	$C = 159$
$p-Ga_{0.47}In_{0.53}As$:	$A = 9.2$;	$B = 3.57$;	$C = 3.65$

N is carrier concentration in cm^{-3}.

3.2.4. *Band Discontinuities at Heterointerfaces*

Band discontinuities at $Ga_xIn_{1-x}As/Al_yGa_{1-y}As$ heterointerface (after Shur [1990]).

Valence band discontinuity ΔE_v:

$$\Delta E_v = 0.4 \Delta E_{gg} \text{ (eV)}, \quad (3.2.11)$$

where $\Delta E_{gg}(\text{eV}) = 1.247y + 1.5(1-x) - 0.4(1-x)^2$ (eV) is the difference between Γ-valleys in $Ga_xIn_{1-x}As$ and $Al_yGa_{1-y}As$.

Conduction band discontinuity ΔE_c:

$$\Delta E_c = \Delta E_g - \Delta E_v \quad (3.2.12)$$

Energy gap discontinuity ΔE_g:

$$\Delta E_g = \Delta E_{gg} \quad \text{for} \quad y < 0.45 \tag{3.2.13}$$

$$\Delta E_g = 0.476 + 0.125y + 0.143y^2 + 1.5(1-x) - 0.4(1-x)^2 \quad \text{for} \quad y \geq 0.45 \tag{3.2.14}$$

Band discontinuities at $Ga_{0.47}In_{0.53}As/InP$ heterointerface:

$$\Delta E_c \cong 0.22 \text{ eV}, \qquad \Delta E_v \cong 0.38 \text{ eV} \tag{3.2.15}$$

Band discontinuities at $Ga_{0.47}In_{0.53}As/Al_{0.48}In_{0.52}As$ heterointerface:

$$\Delta E_c \cong 0.52 \text{ eV}, \qquad \Delta E_v \cong 0.2 \text{ eV} \tag{3.2.16}$$

For $Ga_xIn_{1-x}As/Al_xIn_{1-x}As$ heterointerfaces:

$$\Delta E_c / \Delta E_g = 0.653 + 0.1(1-x) \text{ (eV)} \tag{3.2.17}$$

(after Wolak *et al.* [1991]).
(See also Adachi [1992] and Hybertsen [1991].)

3.2.5. *Effective Masses*

Electrons:
For Γ-valley at 300 K: $m_\Gamma / m_o = 0.023 + 0.037x + 0.003x^2$

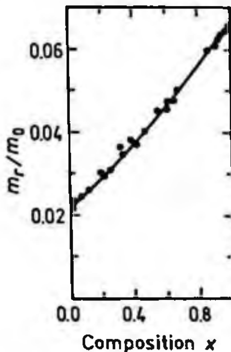

Fig. 3.2.8. Electron effective mass m_Γ versus composition parameter x for $Ga_xIn_{1-x}As$ (after Adachi [1992]).

(Reprinted with permission from John Wiley & Sons, © 1992.)

For $x = 0.47$ ($Ga_{0.47}In_{0.53}As$):

$$m_\Gamma = 0.041 m_o \quad \text{at} \quad n = 2 \cdot 10^{17}\,\text{cm}^{-3}$$
$$m_\Gamma = 0.074 m_o \quad \text{at} \quad n = 6 \cdot 10^{18}\,\text{cm}^{-3}.$$

$$m_L (L-\text{valley}): m_L/m_o = 0.29$$
$$m_X (X-\text{valley}): m_X/m_o = 0.68$$

(after Pearsall [1982]).

Holes:

heavy	$m_h \cong (0.41 + 0.1x) m_o$
light	$m_{lp} \cong (0.026 + 0.056x) m_o$
split-off band	$m_{so} \cong 0.15 m_o$

3.2.6. *Donors and Acceptors*

Ionization energies of shallow donors (meV):

$x = 0$	(InAs)	S, Se, Ge, Si, Sn, Te	≥ 1
$x = 0.47$	($Ga_{0.47}In_{0.53}As$)	Ge, Si, Sn, C	≈ 5
$x = 1$	(GaAs)	S, Se, Ge, Si, Sn, Te	≈ 6

Ionization energies of shallow acceptor (meV):

$x = 0$	(InAs)	Sn – 10, Ge – 14, Si – 20, Cd – 15, Zn – 10
$x = 0.47$	($Ga_{0.47}In_{0.53}As$)	Zn – 20, Mg – 25, Cd – 30, Mn – 50. Fe – 150 (above valence band), 280, 370, and 440 below conduction band
$x = 1$	(GaAs)	C – 20, Si – three acceptor levels ~ 30, 100, and 220, Ge – 30, Zn – 25, Sn – 20
$0 < x < 1$		Mg ~ 25, Be ~ 25, Cd – 8 ÷ 20

3.3. Electrical Properties

3.3.1. *Mobility and Hall Effect*

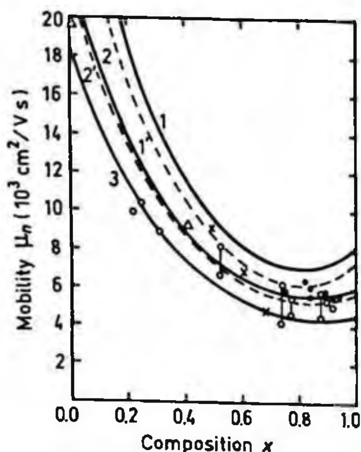

Fig. 3.3.1. Electron drift (dashed curves) and Hall (solid curves) mobility versus composition parameter x. 300 K. 1, 1'. $n = 3 \cdot 10^{15}$ cm^{-3}; 2, 2'. $n = 4 \cdot 10^{16}$ cm^{-3}, 3. $n = 2.3 \cdot 10^{17}$ cm^{-3}. For curve 3 electron Hall and drift mobility values are practically equal. Symbols are experimental data from several different papers (after Chattopadhyay *et al.* [1981]).

(Reprinted with permission from IOP Publishing, © 1981.)

For weakly doped n-$Ga_xIn_{1-x}As$ at 300 K:

$$\mu_n \cong (40 - 80.7x + 49.2x^2) \cdot 10^3 \text{ cm}^2/\text{Vs} \quad (3.3.1)$$

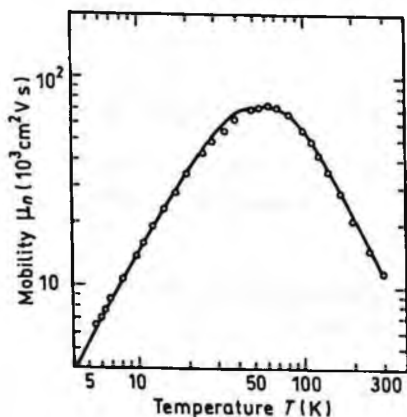

Fig. 3.3.2. Electron Hall mobility versus temperature for $Ga_{0.47}In_{0.53}As$. Electron concentration $n_o = 3.5 \cdot 10^{14}$ cm^{-3} at 300 K (after Oliver, Jr. *et al.* [1981]).

(Reprinted with permission from Elsevier Science, © 1981.)

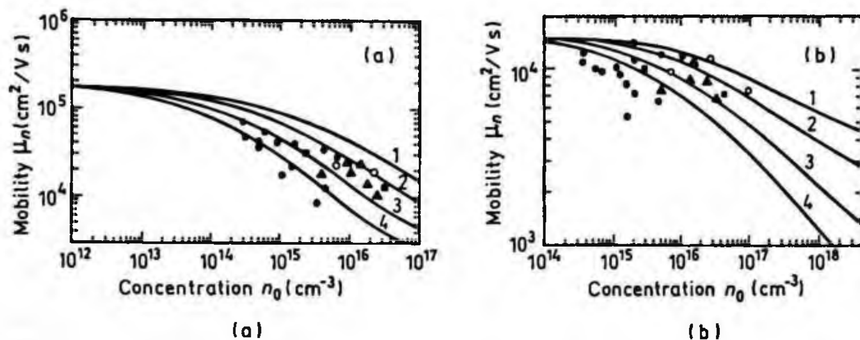

Fig. 3.3.3. Electron Hall mobility in $Ga_{0.47}In_{0.53}As$ at 77 K (a) and 300 K (b) for different compensation ratios $\theta = (N_d + N_a)/n$. 1. $\theta = 1$, 2. $\theta = 2$, 3. $\theta = 5$, 4. $\theta = 10$.
Symbols represent the experimental data from several works (after Pearsall [1982]).
(Reprinted with permission from the author.)

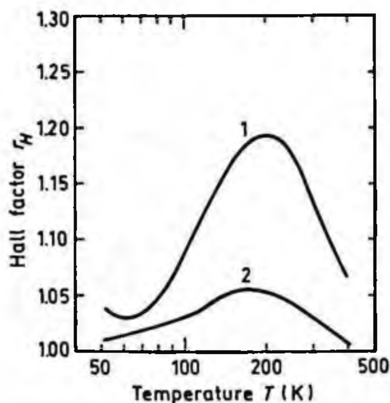

Fig. 3.3.4. Hall factor for n-type $Ga_{0.47}In_{0.53}As$ versus temperature. 1 – $n_o = 10^{15}$ cm^{-3}, 2 – $n_o = 10^{17}$ cm^{-3} (after Pearsall [1982]).
(Reprinted with permission from the author.)

For weakly doped p-$Ga_xIn_{1-x}As$ at 300 K:

$$\mu_p \leq 500\,\text{cm}^2/\text{Vs} \quad \text{at} \quad x = 0 \ \text{(InAs)}$$

$$\mu_p \leq 300\,\text{cm}^2/\text{Vs} \quad \text{at} \quad x = 0.47 \ (Ga_{0.47}In_{0.53}As)$$

$$\mu_p \leq 400\,\text{cm}^2/\text{Vs} \quad \text{at} \quad x = 1 \ \text{(GaAs)}$$

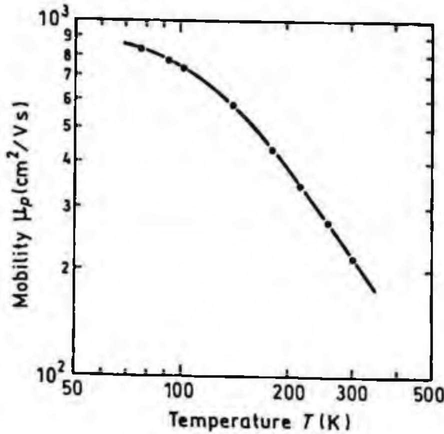

Fig. 3.3.5. Hole Hall mobility versus temperature for $Ga_{0.47}In_{0.53}As$. Hole concentration $p_o = 5.5 \cdot 10^{15}\,\text{cm}^{-3}$ at 300 K (after Novak *et al.* [1989]).

(Reprinted with permission from Elsevier Science, © 1989.)

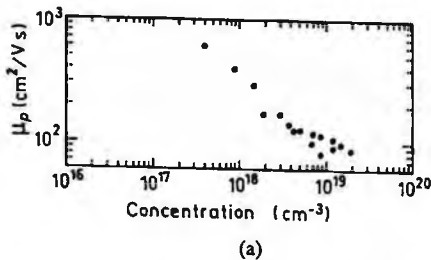

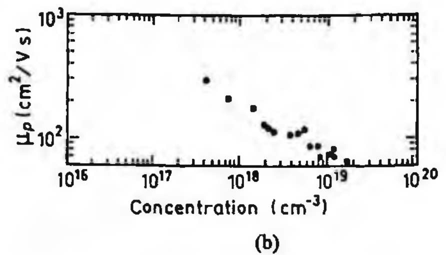

Fig. 3.3.6. Hole Hall mobility in $Ga_{0.47}In_{0.53}As$ at 77 K (a) and 295 K (b) versus total impurity concentration $N_d + N_a$ (after Pearsall and Hirtz [1981]).

(Reprinted with permission from Elsevier Science, © 1981.)

3.3.2. *Two-Dimensional Electron and Hole Gas Mobility in Heterostructures*

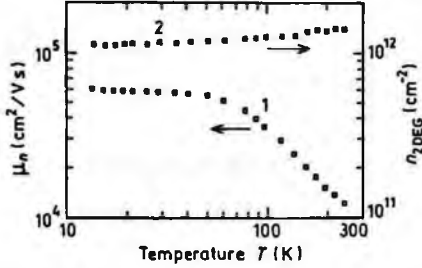

Fig. 3.3.7. Temperature dependence of the electron mobility μ_n (1) and sheet electron density n_{2DEG} (2) *in* $Ga_{0.47}In_{0.53}As/Al_{0.48}In_{0.52}As$ heterostructure. Doping density in AlInAs layer is equal to $3 \cdot 10^{17}$ cm^{-3}, 300 K (after Matsuoka *et al.* [1990]).

(Reprinted with permission from the Japanese Journal of Applied Physics, © 1990.)

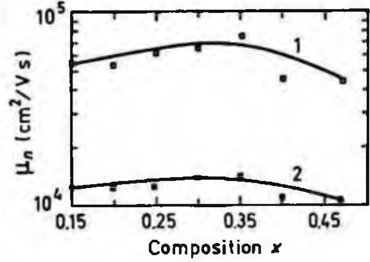

Fig. 3.3.8. Hall electron mobilities of pseudomorphic $Ga_xIn_{1-x}As/Al_{0.48}In_{0.52}As$ MODFETs at 77 K (1) and 300 K (2) (after Pamulapati *et al.* [1990]).

(Reprinted with permission from the American Institute of Physics, © 1990.)

Measured Hall data from stress compensated $Ga_xIn_{1-x}As/Al_{0.48}In_{0.52}As$ modulation-doped heterostructures (after Chin and Chang [1990]).

	μ_n (cm²/Vs)		2DEG density (cm^{-2})	
x	300 K	77 K	300 K	77 K
0.25	14100	113000	$1.71 \cdot 10^{12}$	$1.65 \cdot 10^{12}$
0.20	15200	123100	$1.84 \cdot 10^{12}$	$1.81 \cdot 10^{12}$
0.15	15300	70700	$1.84 \cdot 10^{12}$	$1.81 \cdot 10^{12}$

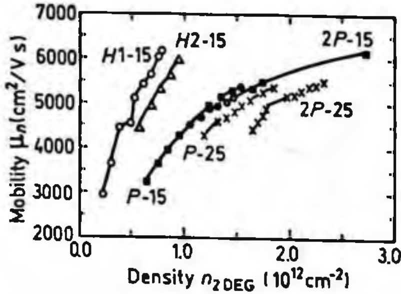

Fig. 3.3.9. Electron mobility versus 2D carrier density at 300 K for pseudomorphic HEMT structures AlGaAs/$Ga_xIn_{1-x}As$/(Al)GaAs.
H – homogeneously doped structures,
P – planar doped structures. For *H*1-15, *H*2-15, *P*-15 and 2*P*-15 samples the value of x is equal to 0.85. For *P*-25 and 2*P*-25 – $x = 0.75$ (after Gaonach *et al.* [1990]).

(Reprinted with permission from the IOP Publishing, © 1990.)

2DEG concentration and electron mobility of multiple (samples A, B, and C) and single (sample D) δ-doped GaAs/$Ga_{0.75}In_{0.25}As$/GaAs structures (after Shieh *et al.* [1994]).

	n_{2DEG} ($\times 10^{12}$ cm^{-2})		μ_n (cm^{-2}/Vs)	
	300 K	77 K	300 K	77 K
Sample A	4.3	2.5	3910	18400
Sample B	8.8	6.0	2710	6540
Sample C	6.2	4.1	4630	19100
Sample D	2.0	1.8	5600	22000

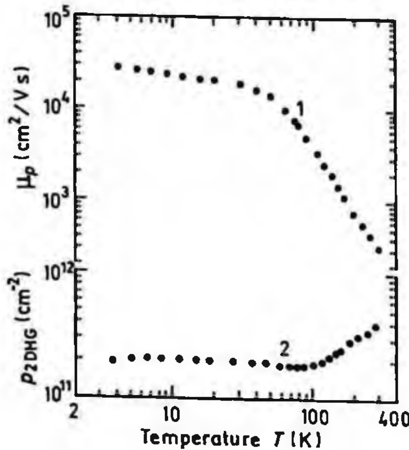

Fig. 3.3.10. Hole Hall mobility (1) and 2DHG density (2) versus temperature for single strained GaAs/$Ga_{0.8}In_{0.2}As$/GaAs quantum well structure (after Fritz *et al.* [1986]).

(Reprinted with permission from the American Institute of Physics, © 1986.)

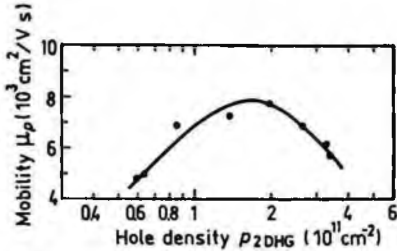

Fig. 3.3.11. Hole Hall mobility at 76 K versus 2D carrier density for 90 Å-thick $GaAs/Ga_{0.8}In_{0.2}As/GaAs$ single strained quantum well (after Fritz *et al.* [1986]).

(Reprinted with permission from the American Institute of Physics, © 1986.)

3.3.3. *Transport Properties in High Electric Field*

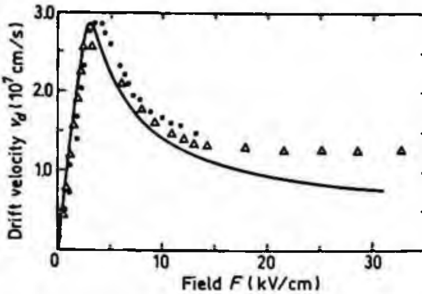

Fig. 3.3.12. Field dependence of the electron drift velocity for $Ga_{0.47}In_{0.53}As$, 300 K. Solid line represents Monte-Carlo calculation. Points and triangles are experimental data for two samples. Points: $n_o = 2.9 \cdot 10^{15}$ cm^{-3}, $\mu_o = 8500$ cm^2/Vs. Triangles: $n_o = 9 \cdot 10^{14}$ cm^{-3}, $\mu_o = 10000$ cm^2/Vs (after Balynas *et al.* [1990]).

(Reprinted with permission from Springer-Verlag GmbH, © 1990.)

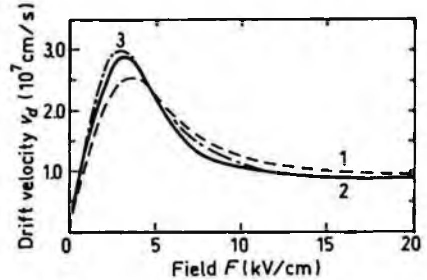

Fig. 3.3.13. Field dependence of the electron drift velocity
for $x = 0.47$ (unstrained, curve 1),
$x = 0.22$ (strained, curve 2)
and $x = 0.22$ (unstrained, curve 3), 300 K (after Thobel *et al.* [1990]).

(Reprinted with permission from the American Institute of Physics, © 1990.)

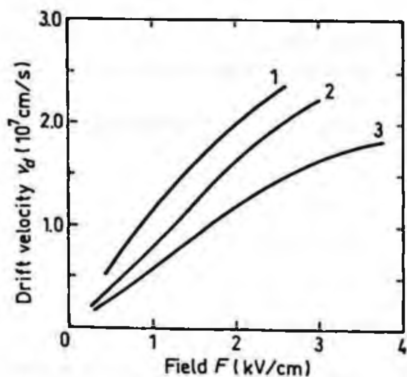

Fig. 3.3.14. Field dependence of the electron drift velocity for $Ga_{0.47}In_{0.53}As$, 300 K. Electron concentration n_o(cm^{-3}): 1. 10^{15}, 2. 10^{17}, 3. 10^{18} (after Haase *et al.* [1985]).

(Reprinted with permission from the American Institute of Physics, © 1985.)

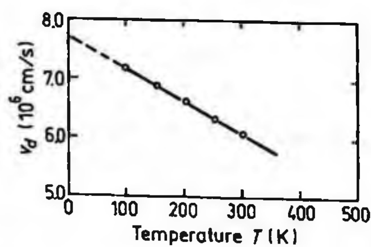

Fig. 3.3.15. Electron saturation velocity versus temperature for $Ga_{0.47}In_{0.53}As$ (after Adachi [1992]).

(Reprinted with permission from John Wiley & Sons, Inc., © 1966.)

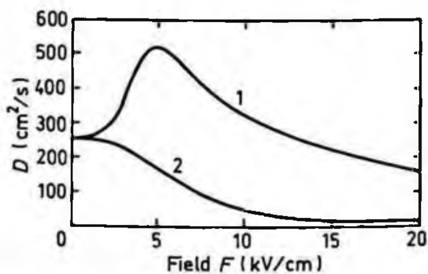

Fig. 3.3.16. The field dependence of longitudinal (1) and transverse (2) diffusion coefficient for $Ga_{0.47}In_{0.53}As$ (after Bourel *et al.* [1991]).

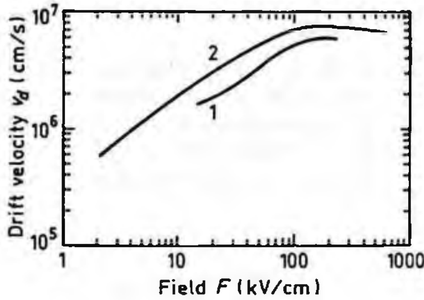

Fig. 3.3.17. Calculated field dependence of the hole drift velocity for $x = 0.47$ (curve 1) and $x = 1$ (GaAs, curve 2), 300 K (after Adachi [1992]).

(Reprinted with permission from John Wiley & Sons, Inc., © 1992.)

3.3.4. *Impact Ionization*

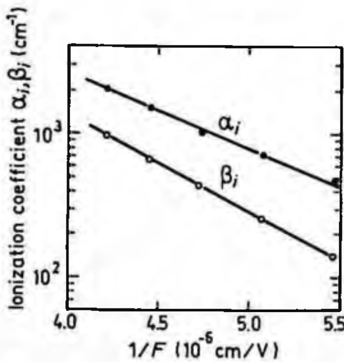

Fig. 3.3.18. Electron α_i and hole β_i ionization coefficients in $Ga_{0.47}In_{0.53}As$ versus 1/F (after Osaka *et al.* [1985]).

(Reprinted with permission from IEEE, © 1985.)

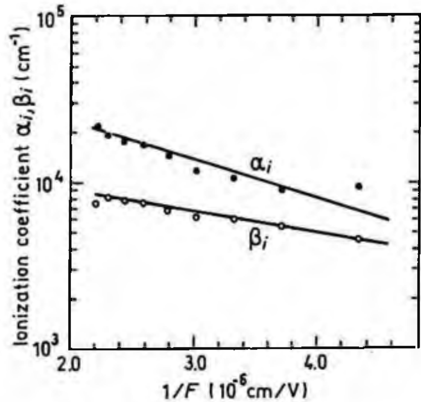

Fig. 3.3.19. Electron α_i and hole β_i ionization coefficients in $Ga_{0.8}In_{0.2}As$ – GaAs strained layer superlattice versus 1/F (after Bhattacharya *et al.* [1986]).

(Reprinted with permission from Elsevier Science, © 1986.)

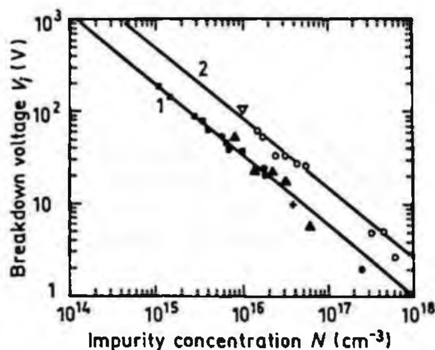

Fig. 3.3.20. Avalanche breakdown voltages for $Ga_{0.47}In_{0.53}As$ (curve 1) and InP (curve 2) p^+-n abrupt junctions versus carrier concentration (after Arnold *et al.* [1984]), 300 K.

(Reprinted with permission from IOP Publishing, © 1984.)

3.3.5. *Recombination Parameters*

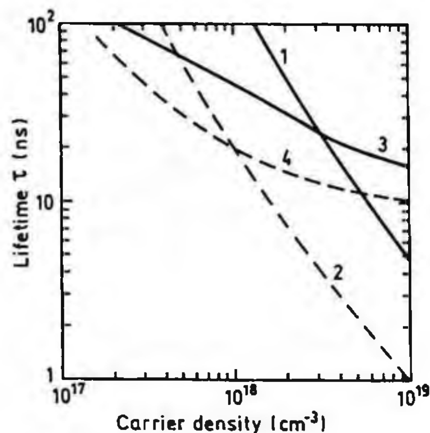

Fig. 3.3.21. Nonradiative (curves 1 and 2) and radiative (curves 3 and 4) lifetimes for $Ga_{0.47}In_{0.53}As$ versus majority carrier density. 300 K. Solid curves are dependences for n-type, dashed curves are dependences for p-type (after Henry *et al.* [1984]).

(Reprinted with permission from IEE, © 1984.)

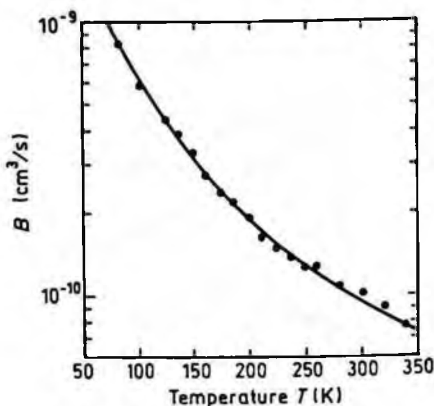

Fig. 3.3.22. Coefficient of the bimolecular recombination as a function of temperature for $Ga_{0.47}In_{0.53}As$ (after Zielinski *et al.* [1986]).

(Reprinted with permission from the American Institute of Physics, © 1986.)

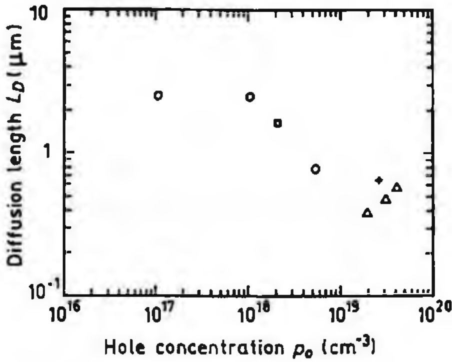

Fig. 3.3.23. Electron diffusion length in p-$Ga_{0.47}In_{0.53}As$ as a function of hole concentration (after Ambree *et al.* [1992]).

(Reprinted with permission from IOP Publishing. © 1992.)

Pure n-type $Ga_{0.47}In_{0.53}As$ ($n_o \sim 2 \cdot 10^{15}$ cm^{-3}):

The longest lifetime of holes	$\tau_p \leq 10^{-5}$ s
Diffusion length $L_p = (D_p \cdot \tau_p)^{1/2}$	$L_p \leq 100$ µm

Surface recombination velocity	$\leq 10^6$ cm/s
Radiative recombination coefficient for $Ga_{0.47}In_{0.53}As$ at 300 K	$0.96 \cdot 10^{-10}$ cm^3/s
Auger coefficient for $Ga_{0.47}In_{0.53}As$ at 300 K	$7 \cdot 10^{-29}$ cm^6/s

3.4. Optical Properties

Infrared refractive index (300 K):

$$n_{\infty} = (k_{\infty})^{1/2} = 3.51 - 0.21x$$

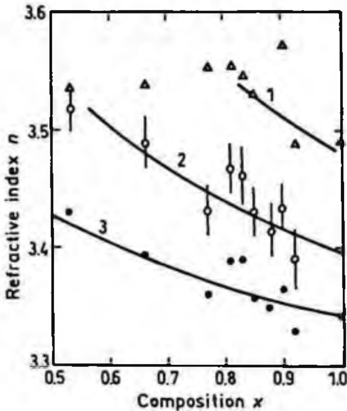

Fig. 3.4.1. Refractive index n versus alloy composition x at different photon energies hν. 1. hν = 1.2 eV, 2. hν = 0.9 eV, 3. hν = 0.6 eV (after Takagi [1978]).

(Reprinted with permission from the Japanese Journal of Applied Physics, © 1978.)

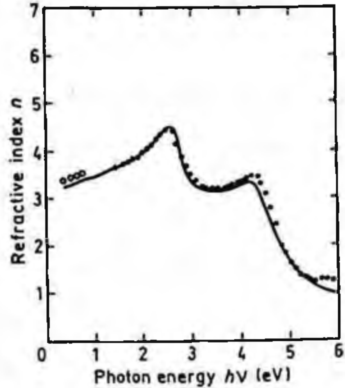

Fig. 3.4.2. Refractive index n versus photon energy for $Ga_{0.47}In_{0.53}As$. T = 300 K (after Adachi [1992]).

(Reprinted with permission from John Wiley & Sons, Inc., © 1992.)

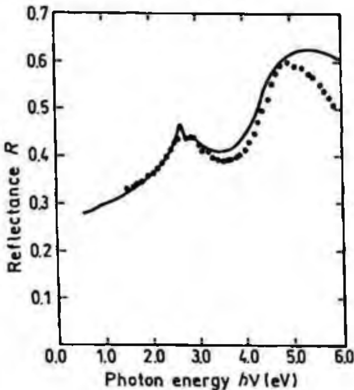

Fig. 3.4.3. Normal incidence reflectivity versus photon energy for $Ga_{0.47}In_{0.53}As$ 300 K (after Adachi [1992]).

(Reprinted with permission from John Wiley & Sons, Inc., © 1992.)

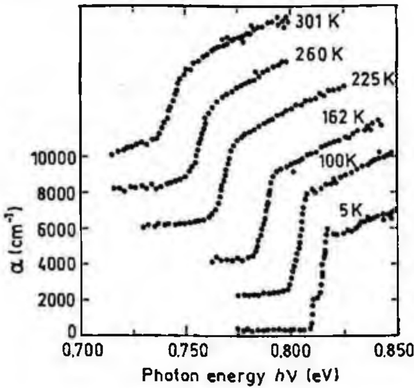

Fig. 3.4.4. The absorption coefficient versus photon energy at different temperatures for $Ga_{0.47}In_{0.53}As$. Electron concentration $n_o = 8 \cdot 10^{14}$ cm^{-3}. Curves are shifted vertically for clarity (after Zielinski *et al.* [1986]).

(Reprinted with permission from the American Institute of Physics, © 1986.)

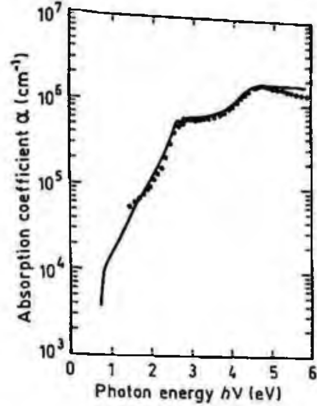

Fig 3.4.5. The absorption coefficient versus photon energy for $Ga_{0.47}In_{0.53}As$, 300 K (after Adachi [1992]).

(Reprinted with permission from John Wiley & Sons, Inc., © 1992.)

A ground state Rydberg energy $R_{x1} = 2.5$ meV (for $x = 0.47$).

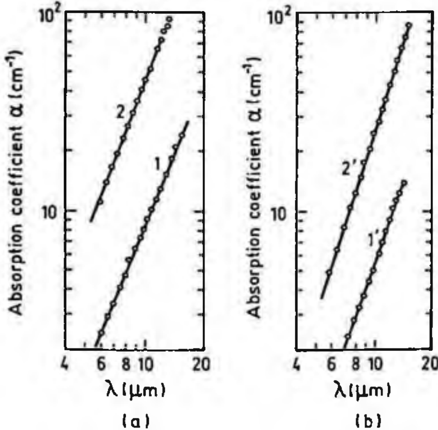

Fig. 3.4.6. Free carrier absorption coefficient versus wavelength. $a - T = 300$ K, $b - T = 92$ K. 1, 1′. $Ga_{0.08}In_{0.92}As$, $N_d = 1.4 \cdot 10^{17}$ cm^{-3}. 2, 2′. $Ga_{0.1}In_{0.9}As$, $N_d = 5.4 \cdot 10^{17}$ cm^{-3} (after Aliev *et al.* [1987]).

(Reprinted with permission from Akademie Verlag GmbH, © 1987.)

3.5. Thermal Properties

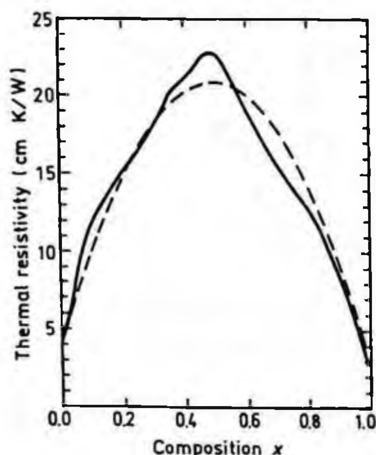

Fig. 3.5.1. Thermal resistivity versus composition parameter x in $Ga_xIn_{1-x}As$, 300 K. Solid curve shows the experimental data. Dashed curve represents the theoretical calculation (after Adachi [1983]).

(Reprinted with permission from the American Institute of Physics, © 1983.)

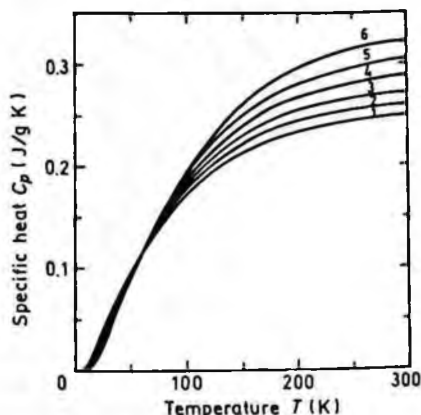

Fig. 3.5.2. Temperature dependences of specific heat at constant pressure for different values of x in $Ga_xIn_{1-x}As$.
1. $x = 0$, 2. $x = 0.2$, 3. $x = 0.4$,
4. $x = 0.6$, 5. $x = 0.8$, 6. $x = 1$
(after Sirota *et al.* [1982]).

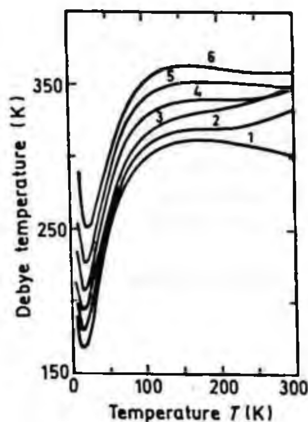

Fig. 3.5.3. Debye temperature as a function of temperature for different values of x in $Ga_xIn_{1-x}As$. (1. $x = 0$, 2. $x = 0.2$, 3. $x = 0.4$, 4. $x = 0.6$, 5. $x = 0.8$, 6. $x = 1$) (after Sirota *et al.* [1982]).

3.6. Mechanical Properties, Elastic Constants, Lattice Vibrations, Other Properties

Density $5.68 - 0.37x$ (g/cm^3)

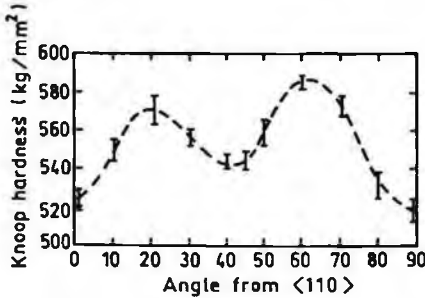

Fig. 3.6.1. Knoop microhardness anisotropy on the {100} plane for $Ga_{0.47}In_{0.53}As$ (after Adachi [1992]).

(Reprinted with permission from John Wiley & Sons, Inc., © 1992.)

Cleavage plane {110}

Elastic constants at 300 K:

C_{11}	$(8.34 + 3.56x) \cdot 10^{11}$ dyn/cm^2
C_{12}	$(4.54 + 0.8x) \cdot 10^{11}$ dyn/cm^2
C_{44}	$(3.95 + 2.01x) \cdot 10^{11}$ dyn/cm^2

Bulk modulus $B_s = \dfrac{C_{11} + 2C_{12}}{3}$ $B_s = (5.81 + 1.72x) \cdot 10^{11}$ dyn/cm^2

Anizotropy factor $A = \dfrac{C_{11} - C_{12}}{2C_{44}}$ $A = (0.48 + 0.07x)$

Shear modulus $C' = (C_{11} - C_{12})/2$ $C' = (1.9 + 1.38x) \cdot 10^{11}$ dyn/cm^2

[100] Young's modulus $Y_0 = \dfrac{(C_{11} + 2C_{12})(C_{11} - C_{12})}{(C_{11} + C_{12})}$ $Y_0 = (5.14 + 3.45x) \cdot 10^{11}$ dyn/cm^2

[100] Poisson ratio $\sigma_0 = \dfrac{C_{12}}{C_{11} + C_{12}}$ $\sigma_0 = (0.35 - 0.04x)$

Acoustic Wave Speeds

Wave propagation direction	Wave character	Expression for wave speed	Wave speed (in units of 10^5 cm/s)
[100]	V_L	$(C_{11}/\rho)^{1/2}$	$3.83+0.90x$
	V_T	$(C_{44}/\rho)^{1/2}$	$2.64+0.71x$
[110]	V_l	$[(C_{11}+C_{12}+2C_{44})/2\rho)]^{1/2}$	$4.28+0.96x$
	$V_{t\parallel}$	$V_{t\parallel}=V_T=(C_{44}/\rho)^{1/2}$	$2.64+0.71x$
	$V_{t\perp}$	$[(C_{11}-C_{12})/2\rho)]^{1/2}$	$1.83+0.65x$
[111]	V_l'	$[(C_{11}+2C_{12}+4C_{44})/3\rho)]^{1/2}$	$4.41+0.99x$
	V_t'	$[(C_{11}-C_{12}+C_{44})/3\rho)]^{1/2}$	$2.13+0.67x$

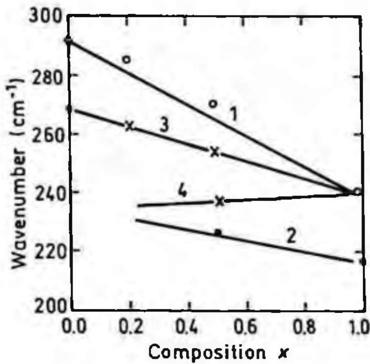

Fig. 3.6.2. Raman-active phonon modes in $Ga_xIn_{1-x}As$. The symbols show experimental results.
1. *LO* phonon behavior,
2. *TO* phonon behavior,
3, 4. mixed mode behavior (after Pearsall *et al.* [1983]).

(Reprinted with permission from the American Institute of Physics, © 1983.)

Piezoelectric constant e_{14} $\quad -(0.045+0.115x)\mathrm{C/m^2}$

References

Adachi, S., *J. Appl. Phys.* **54**, 4 (1983) 1844–1848.

Adachi, S., *Physical Properties of III-Y Semiconductor Compounds*, John Wiley and Sons, 1992.

Aliev, M. I., Kh. A. Khalilov, and G. B. Ibragimov, *Phys. Stat. Sol. (b)* **140**, 1 (1987) K83–K86.

Ambree, P., B. Gruska, and K. Wandel, *Semicond. Sci. and Technol.* **7**, 6 (1992) 858–860.

Arnold, N., R. Schmitt, and K. Heime, *J. Phys.* **D17**, 3 (1984) 443–474.

Balynas, V., A. Krotkus, A. Stalnionis, A. T. Gorelionok, N. M. Shmidt, and J. A. Tellefsen, *Appl. Phys.* **A51**, 4 (1990) 357–360.

Bhattacharya, P. K., U. Das, F. Y. Juang, Y. Nashimoto, and S. Dhar, *Solid State Electron.* **29**, 2 (1986) 261–267.

Bourel, P., J. L. Thobel, K. Bellahsni, M. Pernisek, and R. Fauquembergue, *J. de Physique, III* **1**, 4 (1991) 511–520.

Chattopadhyay, D., S. K. Sutradhar, and B. R. Nag, *J. Phys.* **C14**, 6 (1981) 891–908.

Chin, A. and T. Y. Chang, *J. Vac. Sci. Technol.* **B8**, 2 (1990) 364–366.

Fritz, I. J., T. J. Drummond, G. C. Osbourn, J. E. Schirber, and E. D. Jones, *Appl. Phys. Lett.* **48**, 24 (1986) 1678–1680.

Gaonach, C., J. Favre, E. Barbier, D. Adam, M. Champagne, C. Terrier, and D. Pons, Inst. Phys. Conf. Ser. N112, *Gallium Arsenide and Related Compounds*, Inst. of Phys., Bristol, Philadelphia and New York, 1990, pp. 441–446.

Goetz, K.-H., D. Bimberg, H. Jurgensen, J. Selders, A. V. Solomonov, G. F. Glinskii, and M. Razeghi, *J. Appl. Phys.* **54**, 8 (1983) 4543–4552.

Haase, M. A., V. M. Robbins, N. Tabatabaie, and G. E. Stillman, *J. Appl. Phys.* **57**, 6 (1985) 2295–2298.

Henry, C. H., R. A. Logan, F. R. Merritt, and C. G. Bethea, *Electron. Lett.* **20**, 9 (1984) 358–359.

Hybertsen, M. S., *Appl. Phys. Lett.* **58**, 16 (1991) 1759–1761.

Jain, S. C., J. M. McGregor, and D. J. Roulston, *J. Appl. Phys.* **68**, 7 (1990) 3747–3749.

Karatchevtseva, M. V., A. S. Ignatiev, V. G. Mokerov, G. S. Nemtsev, V. A. Strakhov, and N. G. Yaremenko, *Semiconductors* **28**, 7 (1994) 691–694.

Kuo, C. P., S. K. Vong, R. M. Cohen, and G. B. Stringfellow, *J. Appl. Phys.* **57**, 12 (1985) 5428–5432.

Lambkin, J. D. and D. J. Dunstan, *Solid State Commun.* **67**, 8 (1988) 827–830.

Matsuoka, T., E. Kobayashi, K. Taniguchi, C. Hamaguchi, and S. Sasa, *Jap. J. Appl. Phys.* **29**, 10 (1990) 2017–2025.

Novak, J., M. Kuliffayova, M. Morvic, and P. Kordos, *J. Cryst. Growth* **96**, 3 (1989) 645–648.

Oliver, Jr. J. D., L. F. Eastman, P. D. Kirchner, and W. J. Schaff, *J. Cryst. Growth* **54**, 1 (1981) 64–68.

Osaka, F., T. Mikawa, and T. Kaneda, *IEEE J. Quant. Electronics* **QE-21**, 9 (1985) 1326–1338.

Pamulapati, J., R. Lai, G. I. Ng, Y. C. Chen, P. R. Berger, P. K. Bhattacharya, J. Singh, and D. Pavlidis, *J. Appl. Phys*. **68**, 1 (1990) 347–350.

Paul, S., J. B. Roy, and P. K. Basu, *J. Appl. Phys*. **69**, 2 (1991) 827–829.

Pearsall, T. P. and J. P. Hirtz, *J. Cryst. Growth* **54**, 1 (1981) 127–131.

Pearsall, T. P. (ed.), *GaInAsP Alloy Semiconductors*, John Wiley and Sons, 1982.

Pearsall, T. P., R. Carles, and J. C. Portal, *Appl. Phys. Lett*. **42**, 5 (1983) 436–438.

Porod, W. and D. K. Ferry, *Phys. Rev*. **B27**, 4 (1983) 2587–2589.

Sirota, N. N., V. V. Novikov, and A. M. Antiukhov, *Doklady Akademii Nauk SSSR* **263**, 1 (1982) 96–100.

Shieh, H.-M., C.-L. Wu, W.-Ch. Hsu, Y.-H. Wu, and M.-J. Kao, *Jap. J. Appl. Phys*. **33**, 4a (1994) 1778–1780.

Shur, M., *Physics of Semiconductor Devices*, Prentice Hall, 1990.

Takagi, T., *Jap. J. Appl. Phys*. **17**, 10 (1978) 1813–1817.

Thobel, J. L., L. Baudry, A. Cappy, P. Bourel, and R. Fauquembergue, *Appl. Phys. Lett*. **56**, 4 (1990) 346–348.

Wolak, E., J. C. Harmand, T. Matsuno, K. Inoue, and T. Narusawa, *Appl. Phys. Lett*. **59**, 1 (1991) 111–113.

Zielinski, E., H. Schweizer, K. Streubel, H. Eisele, and G. Weimann, *J. Appl. Phys*. **59**, 6 (1986) 2196–2204.

CHAPTER 4

GALLIUM INDIUM ANTIMONIDE ($Ga_xIn_{1-x}Sb$)

Yu. A. Goldberg

Ioffe Institute, St. Petersburg, Russia

4.1. Basic Parameters at 300 K

	InSb	GaSb	$Ga_xIn_{1-x}Sb$
Crystal structure	Zinc Blende	Zinc Blende	Zinc Blende
Space group	$F\bar{4}3m$	$F\bar{4}3m$	$F\bar{4}3m$
Number of atoms in 1 cm³	$2.94 \cdot 10^{22}$	$3.53 \cdot 10^{22}$	$(2.94 + 0.59x) \cdot 10^{22}$
Debye temperature (K)	160	266	
Density (g/cm³)	5.77	5.61	$5.77 - 0.16x$
Dielectric constant			
static	16.8	15.7	$16.8 - 1.1x$
high frequency	15.7	14.4	$15.7 - 1.3x$
Effective electron mass: (in units of m_o)	0.014	0.041	$0.014 + 0.0178x + 0.0092x^2$
Effective hole mass: (in units of m_o)			
heavy hole	0.43	0.4	$0.43 - 0.03x$
light hole	0.015	0.05	$0.015 + 0.01x + 0.025x^2$
Electron affinity (eV)	4.59	4.06	$4.59 - 0.53x$
Lattice constant (Å)	6.479	6.096	$6.479 - 0.383x$
Optical phonon energy (eV)	0.025	0.0297	See Sec. 4.6

Band structure and carrier concentration

	InSb	GaSb	$Ga_xIn_{1-x}Sb$
Energy gap (eV)	0.172	0.726	$0.172 + 0.139x + 0.415x^2$
Energy separation between Γ-valley and L valleys $E_{\Gamma L}$ (eV)	0.51	0.084	See Fig. 4.2.4
Energy separation between Γ-valley and X valleys $E_{\Gamma X}$ (eV)	0.83	0.31	See Fig. 4.2.4
Energy of spin-orbital splitting E_{so} (eV)	~ 0.8	~ 0.8	See Fig. 4.2.5
Intrinsic carrier concentration (cm^{-3})	$2\cdot10^{16}$	$1.5\cdot10^{12}$	See Fig. 4.2.7
Effective conduction band density of states (cm^{-3})	$4.2\cdot10^{16}$	$2.1\cdot10^{17}$	$2.5\cdot10^{19}(0.014 + 0.0178x + 0.0092x^2)^{3/2}$
Effective valence band density of states (cm^{-3})	$7.3\cdot10^{18}$	$1.8\cdot10^{19}$	

Electrical properties

	InSb	GaSb	$Ga_xIn_{1-x}Sb$
Breakdown field (V/cm)	$\sim 10^3$	$\sim 5\cdot10^4$	$\sim (1\div50)\cdot10^3$
Mobility (cm^2/V·s)			
electrons	$\le 7.7\cdot10^4$	$\le 3\cdot10^3$	See Fig. 4.3.1
holes	≤ 850	≤ 1000	≤ 1000

	InSb	GaSb	$Ga_xIn_{1-x}Sb$
Diffusion coefficient (cm^2/s)			
electrons	$\leq 2\cdot 10^3$	≤ 75	
holes	≤ 22	≤ 25	
Electron thermal velocity (m/s)	$9.8\cdot 10^5$	$5.8\cdot 10^5$	$(9.8-4x)\cdot 10^5$
Hole thermal velocity (m/s)	$1.8\cdot 10^5$	$2.1\cdot 10^5$	$(1.8+0.3x)\cdot 10^5$
Optical properties			
Infrared refractive index	4.0	3.8	$4.0-0.2x$
Radiative recombination coefficient (cm^3/s)	$5\cdot 10^{-11}$	$\approx 10^{-10}$	
Thermal and mechanical properties			
Bulk modulus (dyn/cm^2)	$4.66\cdot 10^{11}$	$5.62\cdot 10^{11}$	$(4.66+0.96x)\cdot 10^{11}$
Melting point (°C)	527	712	See Fig. 4.5.6
Specific heat (J/g°C)	0.2	0.25	
Thermal conductivity (W/cm °C)	0.18	0.32	See Fig. 4.5.1
Thermal diffusivity (cm^2/s)	0.16	0.23	
Thermal expansion, linear, ($°C^{-1}$)	$5.37\cdot 10^{-6}$	$7.75\cdot 10^{-6}$	

4.2. Band Structure and Carrier Concentration

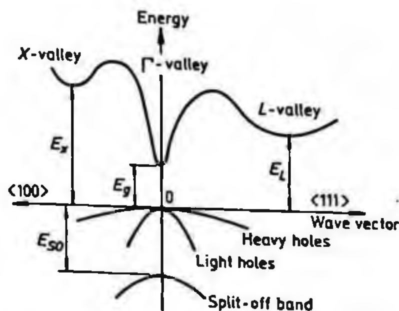

Fig. 4.2.1. Band structure of InSb ($x = 0$). Important minima of the conduction band and maxima of the valence band.
$E_g = 0.17$ eV, $E_L = 0.68$ eV
$E_x = 1.0$ eV, $E_{so} = 0.8$ eV.

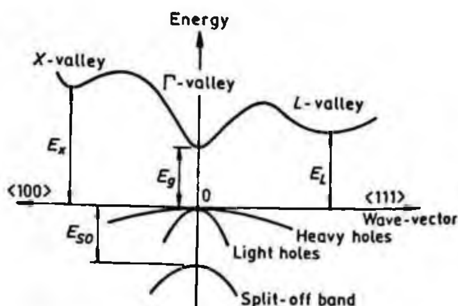

Fig. 4.2.2. Band structure of GaSb ($x = 1$). Important minima of the conduction band and maxima of the valence band.
$E_g = 0.73$ eV, $E_L = 0.81$ eV
$E_x = 1.03$ eV, $E_{so} = 0.8$ eV.

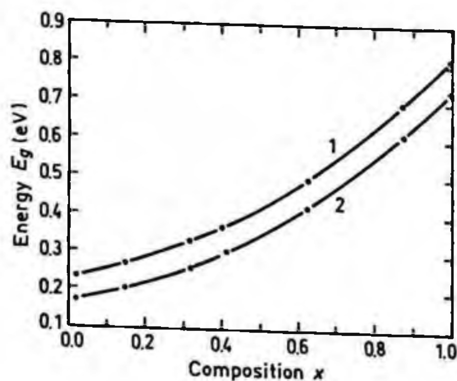

Fig. 4.2.3. Energy gap E_g of $Ga_xIn_{1-x}Sb$ as a function of composition parameter x. 1. $T = 80$ K, 2. $T = 300$ K (after Auvergne *et al.* [1974]).
(Reprinted with permission from Elsevier Science, © 1974.)

At 300: $$E_g = 0.172 + 0.139x + 0.415x^2 \text{ (eV)} \quad (4.2.1)$$

At 80: $$E_g = 0.234 + 0.154x + 0.415x^2 \text{ (eV)} \quad (4.2.2)$$

(after Auvergne *et al.* [1974])

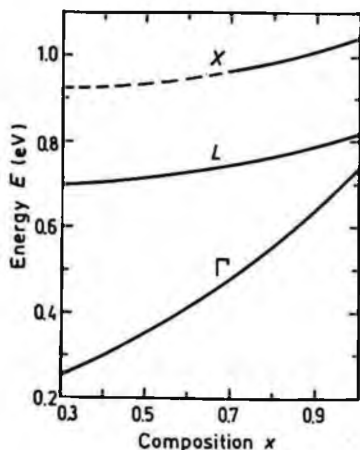

Fig. 4.2.4. Energy separation between Γ, X and L-conduction band minima and top of the valence band versus alloy composition parameter x. 300 K (after Zitouni *et al.* [1986]).

(Reprinted with permission from The American Physical Society, © 1986.)

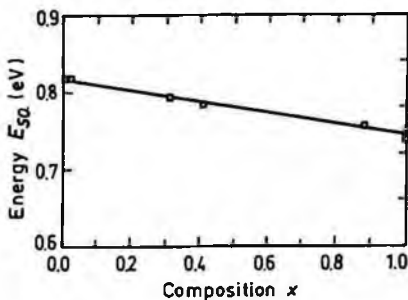

Fig. 4.2.5. Energy of spin-orbital splitting E_{so} versus composition parameter x, 77 K (after Auvergne *et al.* [1974]).

(Reprinted with permission from Elsevier Science, © 1974.)

4.2.1. *Temperature Dependences*

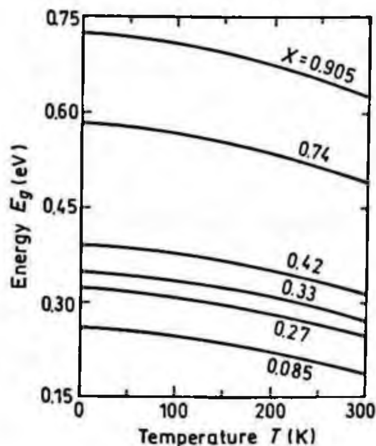

Fig. 4.2.6. Temperature dependences of energy gap E_g for different $Ga_xIn_{1-x}Sb$ compositions (after Roth *et al.* [1980]).

(Reprinted with permission from CISTI/Research Press, © 1980.)

$$E_g(x,T) = E_g(x,0) - 6.2\cdot10^{-4}\cdot T^2x\frac{1}{T+260} - 3.8\cdot10^{-4}T^2(1-x)\frac{1}{T+200} + 5\cdot10^{-5}Tx(1-x)\ \text{(eV)} \quad (4.2.3)$$

$E_g(x, 0) = 0.235 + 0.1653x + 0.413x^2$ (eV)
(after Roth *et al.* [1980])

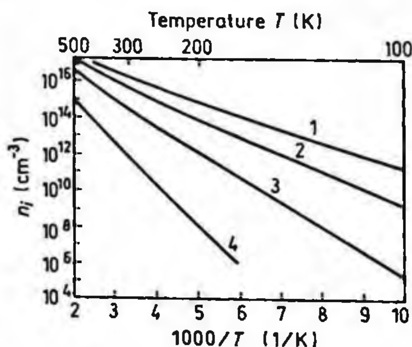

Fig. 4.2.7. The temperature dependences of the intrinsic carrier concentration.
1. $x = 0$, 2. $x = 0.3$, 3. $x = 0.6$, 4. $x = 1$.

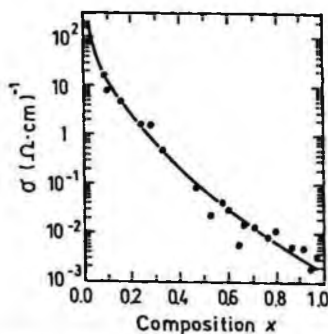

Fig. 4.2.8. Composition dependence of the intrinsic conductivity at 300 K (after Wooley and Gillet [1960]).

(Reprinted with permission from Elsevier Science, © 1960.)

4.2.2. Dependences on Hydrostatic Pressure (After Zitouni et al. [1986])

$$\frac{dE_g}{dP} = (15 - 0.5x)\cdot10^{-3}\text{eV/kbar}$$

$$\frac{dE_L}{dP} = (5.5 - 0.5x)\cdot10^{-3}\text{eV/kbar} \quad (4.2.4)$$

$$\frac{dE_x}{dP} = -1.5\cdot10^{-3}\text{eV/kbar}$$

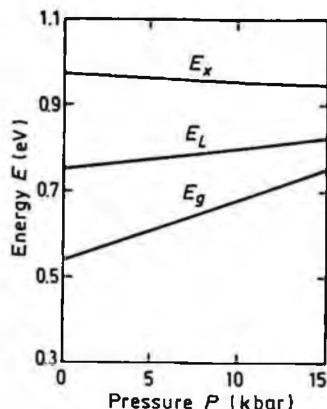

Fig. 4.2.9. Energy separation between Γ-, L-, X-conduction band minima and top of the valence band for $Ga_{0.78}In_{0.22}Sb$ versus hydrostatic pressure. 300 K (after Zitouni *et al.* [1986]).

(Reprinted with permission from The American Physical Society, © 1986.)

4.2.3. *Effective Masses*

Electrons:

For Γ-valley $\quad m_\Gamma = (0.014 + 0.0178x + 0.0092x^2) \cdot m_o \quad$ (4.2.5)

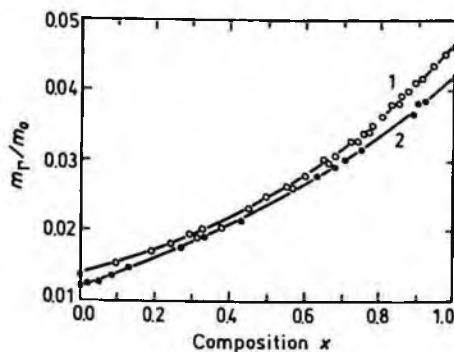

Fig. 4.2.10. Effective electron mass versus composition parameter x at 300 K (curve 1), and 6 K (curve 2). Experimental results have been taken from five experimental works (after Roth and Fortin [1978]).

(Reprinted with permission from CISTI/Research Press, © 1978.)

Holes:

heavy	$m_h = 0.4m_o$
light	$m_{lp} \cong (0.015 + 0.01x + 0.025x^2)m_o$
split-off band	$m_{so} \cong (0.12 + 0.02x)m_o$

4.2.4. *Donors and Acceptors*

Ionization energies of shallow donors (meV):

$x = 0$ (InSb):	*S*, Se, Te	≤ 0.7
$x = 1$ (GaSb):	*S*(*L*)	150,
	S(*X*)	300
	Se(*L*)	50
	Se(*X*)	230
	Te(*L*)	20
	Te(*X*)	≤ 80

Ionization energies of shallow acceptors (meV):

$x = 0$ (InSb):	Cd – 10,	Zn – 10,	Cr – 70,	Cu^{o} – 28,	Cu^{-} – 56
$x = 1$ (GaSb):	$E_{a1} = 30$,	$E_{a2} = 100$,	Si ~ 10,	Ge ~ 9,	Zn ~ 37

4.3. Electrical Properties

4.3.1. *Mobility and Hall Effect*

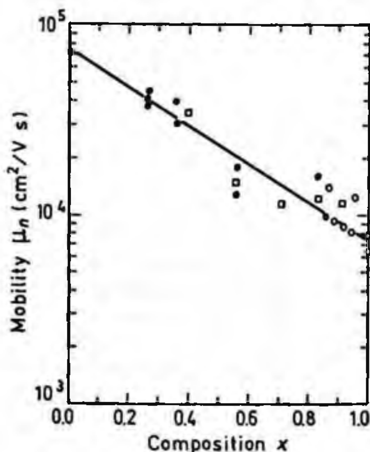

Fig. 4.3.1. Electron mobility versus composition parameter x for $Ga_xIn_{1-x}Sb$, 300 K. Circles represent the data by Miki *et al.* [1975]. Full circles – InSb substrate, open circle – GaSb substrate. Squares represent the data by Kawashima and Kataoka [1979].

(Reprinted with permission from the Japanese Journal of Applied Physics, © 1979.)

Electron concentration n_0 ~ 10^{15} + 10^{16} cm^{-3}.

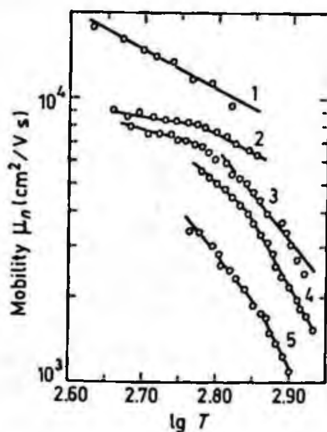

Fig. 4.3.2. Electron Hall mobility versus temperature for $Ga_xIn_{1-x}Sb$ 1. x = 0.10, 2. x = 0.47, 3. x = 0.70, 4. x = 0.86, 5. x = 0.91 (after Wooley and Gillett [1960]. See also Coderre and Woolley [1969]).

(Reprinted with permission from Elsevier Science, © 1960.)

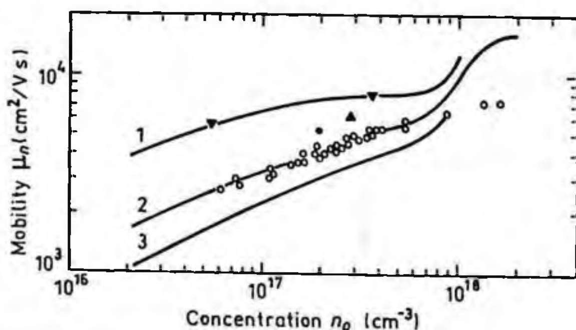

Fig. 4.3.3. Electron Hall mobility versus electron concentration for GaSb ($x = 1$). $T = 77$ K. Open circles represent measurements with a group of samples having approximately the same residual acceptor concentrations N_a. Full symbols: specimens with lower residual acceptor concentrations. Solid lines represent the theoretical calculations for different values of compensating acceptor densities – either singly (N_a^-) or doubly (N_a^{--}) ionized.
1. $N_a^- = 1.2 \cdot 10^{17}$ or $N_a^{--} = 0.4 \cdot 10^{17}$ cm^{-3}, 2. $N_a^- = 2.85 \cdot 10^{17}$ or $N_a^{--} = 0.95 \cdot 10^{17}$ cm^{-3},
3. $N_a^- = 4.5 \cdot 10^{17}$ or $N_a^{--} = 1.5 \cdot 10^{17}$ cm^{-3} (after Baxter *et al.* [1967]).

(Reprinted with permission from The American Physical Society, © 1967.)

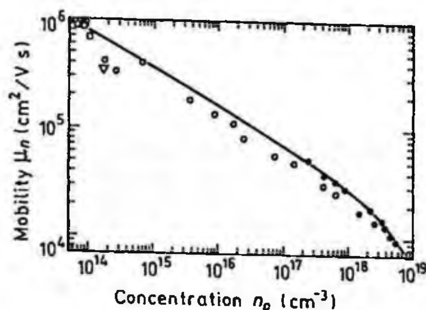

Fig. 4.3.4. Electron mobility versus electron concentration for InSb ($x = 0$), 77 K (after Litwin-Staszewska *et al.* [1981]).

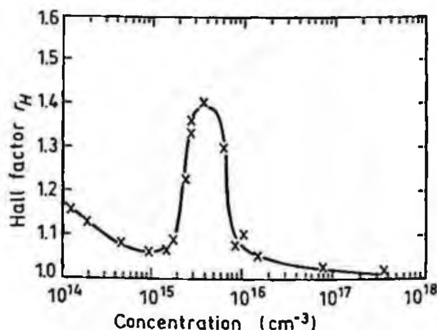

Fig. 4.3.5. The electron Hall factor versus carrier concentration for InSb ($x = 0$), 77 K (after Baranskii and Gorodnichii [1969]).

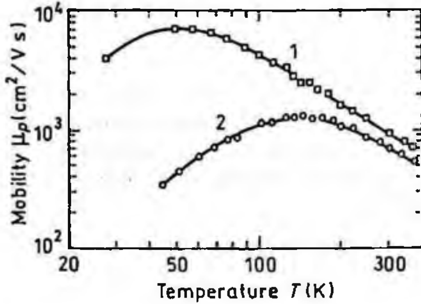

Fig. 4.3.6. Hole Hall mobility versus temperature for GaSb ($x = 1$). MBE technique. Carrier concentration p_o at 300 K:
1. $2.28 \cdot 10^{16}$ cm^{-3},
2. $1.9 \cdot 10^{16}$ cm^{-3}
(after Johnson *et al.* [1988]).

(Reprinted with permission from IOP Publishing, © 1988.)

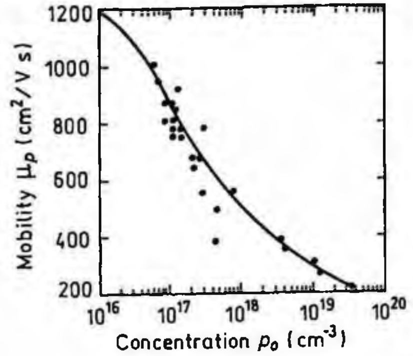

Fig. 4.3.7. Hole Hall mobility versus hole concentration for GaSb ($x = 1$), 300 K. Experimental data are taken from five different papers (after Wiley [1975]).

(Reprinted with permission from Academic Press, © 1975.)

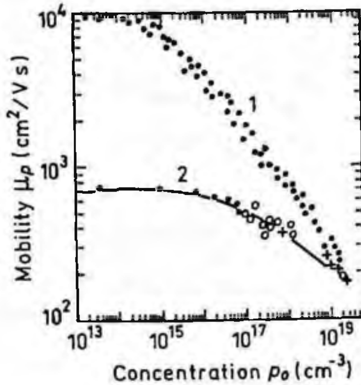

Fig. 4.3.8. Hole Hall mobility versus hole concentration for InSb ($x = 0$).
1. 77 K (after Filipchenko and Bolshakov [1976]).
2. 290 K (after Wiley [1975]).

(Reprinted with permission from Academic Press, © 1975.)

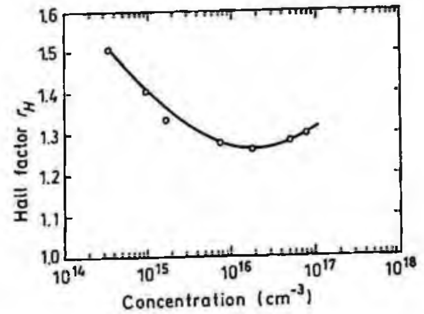

Fig. 4.3.9. The hole Hall factor versus carrier concentration for InSb ($x = 0$), 77 K (after Baranskii and Gorodnichii [1969]).

(Reprinted with permission from Akademie Verlag GmbH, © 1969.)

4.3.2. Transport Properties in High Electric Field

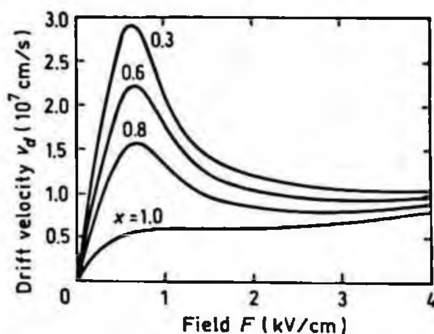

Fig. 4.3.10. Field dependences of the electron drift velocities calculated by Monte Carlo method for different values of x, 300 K (after Ikoma *et al.* [1977]).

(Reprinted with permission from the Japanese Journal of Applied Physics, © 1977.)

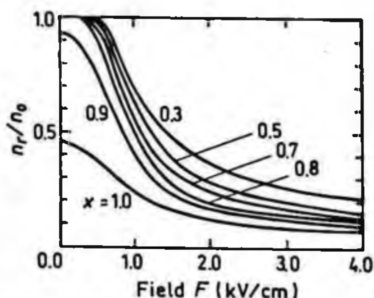

Fig. 4.3.11. Fraction of electrons in the Γ-valley as a function of field for different values of x (after Ikoma *et al.* [1977]).

(Reprinted with permission from the Japanese Journal of Applied Physics, © 1977.)

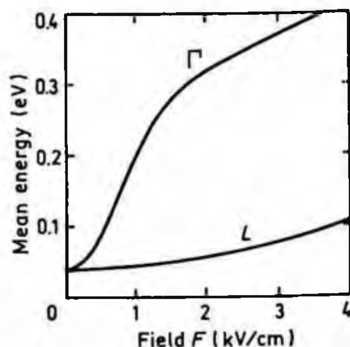

Fig. 4.3.12. Electron mean energies in the Γ- and L-valleys of $Ga_{0.5}In_{0.5}Sb$ as a function of field, 300 K (after Ikoma *et al.* [1977]).

(Reprinted with permission from the Japanese Journal of Applied Physics, © 1977.)

4.3.3. *Recombination Parameters*

For $x = 0$ (InSb)

For pure InSb at $T \geq 250$ K lifetime of carries (electron and holes) is determined by the Auger recombination

$$\tau_n = \tau_p = 1/Cn_i^2 ,$$

where $C \cong 5 \cdot 10^{-26}$ cm^6/s is Auger coefficient, n_i is intrinsic concentration.

For 300 K: $\tau_n = \tau_p \approx 5 \cdot 10^{-8}$ s

At 77 K for pure InSb	n-type: the lifetime of holes	$\tau_p \sim 10^{-6}$ s
	p-type: the lifetime of electrons	$\tau_n \sim 10^{-10}$ s
Radiative recombination coefficient		$5 \cdot 10^{-11}$ cm^3/s
Auger coefficient		$C = 5 \cdot 10^{-26}$ cm^6/s

For $x = 1$ (GaSb)

Fig. 4.3.13. Electron radiative (squares) and nonradiative (triangles) lifetime versus acceptor concentration for p-GaSb ($x = 1$), 77 K (after Titkov *et al.* [1986]).

Radiative recombination coefficient		$\sim 10^{-10}$ cm^3/s
Auger coefficient	77 K	$2 \cdot 10^{-29}$ cm^6/s
	300 K	$5 \cdot 10^{-30}$ cm^6/s
Auger coefficient in In As/$Ga_xIn_{1-x}Sb$	77 K	$1.3 \cdot 10^{-27}$ cm^6/s
superlattices (after Youngdale [1994])	300 K	$8 \cdot 10^{-25}$ cm^6/s
Surface recombination velocity for $Ga_{0.6}In_{0.4}Sb$ (after Mbow *et al.* [1993])		$2 \cdot 10^7$ cm/s

4.4. Optical Properties

Infrared refractive index (300 K):

$$n_\infty = (k_\infty)^{1/2} \cong 4.0 - 0.2x$$

Long wave *TO* phonon energy at 300 K (meV):

$x = 0$ (InSb) 22.9

$x = 1$ (GaSb) 27.8

Long wave *LO* phonon energy at 300 K (meV):

$x = 0$ (InSb) 24.4

$x = 1$ (GaSb) 28.9

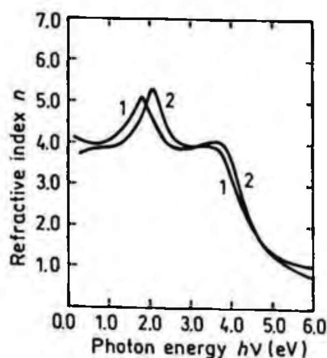

Fig. 4.4.1. Refractive index n versus photon energy for $x = 0$ (InSb, curve 1) and $x = 1$ (GaSb, curve 2), 300 K (after Adachi [1989]). See also Paskov [1997].

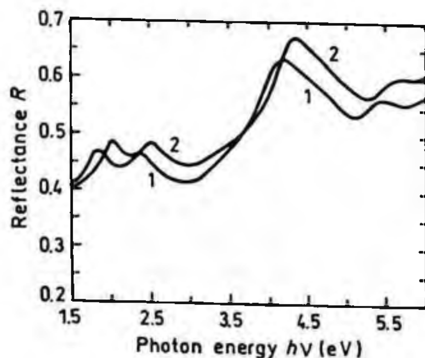

Fig. 4.4.2. Normal incidence reflectivity versus photon energy for $x = 0$ (InSb, curve 1) and $x = 1$ (GaSb, curve 2), 300 K (after Aspnes and Studna [1983]).

(Reprinted with permission from The American Physical Society, © 1983.)

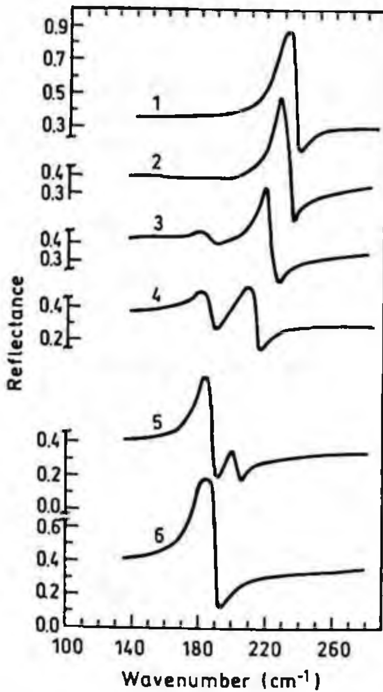

Fig. 4.4.3. Wavenumber dependence of the reflectance for different alloy compositions of $Ga_xIn_{1-x}Sb$, 300 K. 1. $x = 1$, 2. $x = 0.84$, 3. $x = 0.6$ 4. $x = 0.3$, 5. $x = 0.05$, 6. $x = 0$ (after Brodsky *et al.* [1970]).

(Reprinted with permission from The American Physical Society, © 1970.)

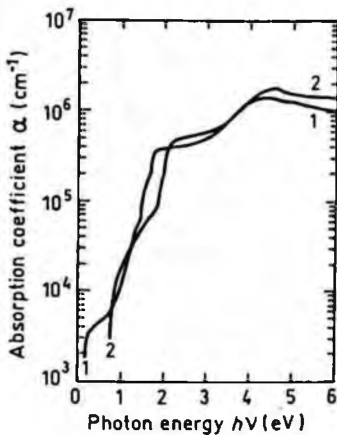

Fig. 4.4.4. The absorption coefficient versus photon energy for $x = 0$ (InSb, curve 1) and $x = 1$ (GaSb, curve 2), 300 K (after Adachi [1989]). (See also Aspnes and Studna [1983]).

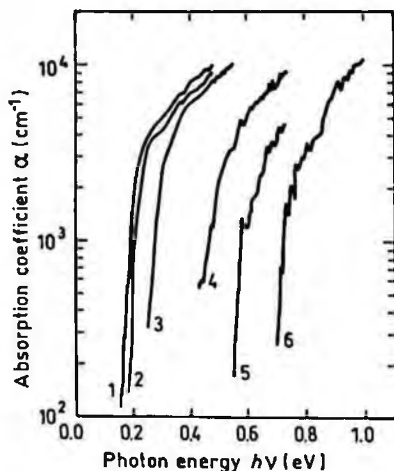

Fig. 4.4.5. Intrinsic absorption edge for different alloy compositions of n-type $Ga_xIn_{1-x}Sb$ (curves 1, 2) and p-type $Ga_xIn_{1-x}Sb$ (curves 3–6). $T = 300$ K.
1. $x = 0$, 2. $x = 0.07$, 3. $x = 0.36$,
4. $x = 0.7$, 5. $x = 0.78$, 6. $x = 0.97$
For n-type samples electron concentration
$n_o \approx 2 \cdot 10^{17} \div 10^{18}$ cm^{-3}.
For p-type samples hole concentration
$p_o \approx 10^{18} \div 6 \cdot 10^{19}$ cm^{-3}.
(after Rousina *et al.* [1990])

(Reprinted with permission from the American Institute of Physics, © 1990.)

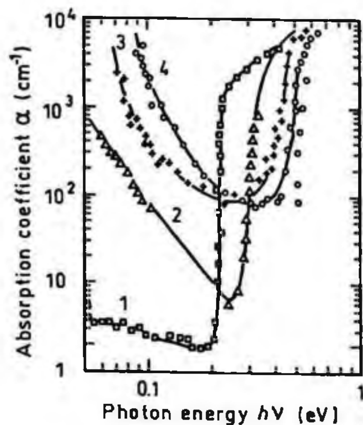

Fig. 4.4.6. Absorption coefficient versus photon energy for different doping levels. $x = 0$. (n-InSb). $T = 130$ K. n_o (cm^{-3}):
1. $6.6 \cdot 10^{13}$, 2. $7.5 \cdot 10^{17}$,
3. $2.6 \cdot 10^{18}$, 4. $6 \cdot 10^{18}$
(after Ukhanov [1977]).

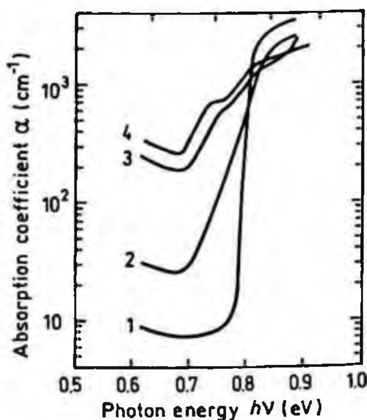

Fig. 4.4.7. Absorption coefficient versus photon energy for different doping levels. $x = 1$. (p-GaSb). $T = 77$ K. N_a (cm^{-3}):
1. $2.9 \cdot 10^{17}$, 2. $5 \cdot 10^{18}$,
3. $1.8 \cdot 10^{19}$, 4. $3 \cdot 10^{19}$ (after Iluridze *et al.* [1987]).

4.5. Thermal Properties

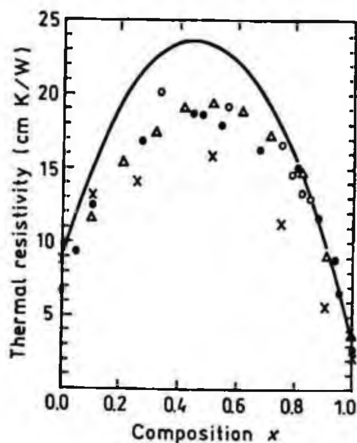

Fig. 4.5.1. Thermal resistivity versus composition parameter x. Solid curve shows the theoretical calculation (after Adachi [1983]). Points represent experimental data of different authors (after Briggs *et al.* [1970]).

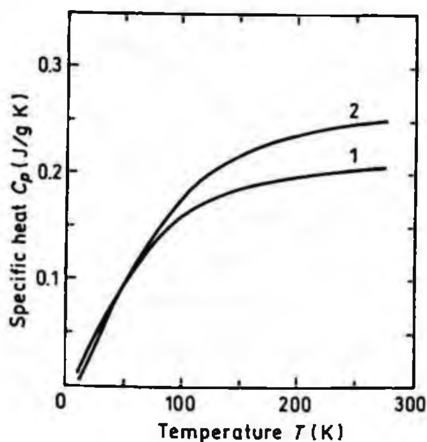

Fig. 4.5.2. Temperature dependence of the specific heat at constant pressure (low temperatures).
1. $x = 0$ (InSb), 2. $x = 1$ (GaSb)
(after Piesbergen [1963]).

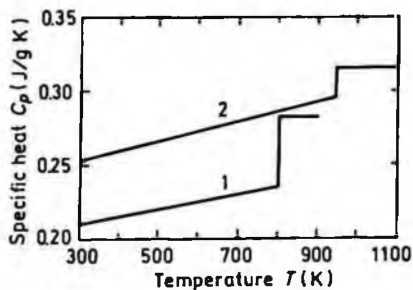

Fig. 4.5.3. Temperature dependence of specific heat at constant pressure (high temperatures).
1. $x = 0$ (InSb), 2. $x = 1$ (GaSb)
(after Okhotin *et al.* [1972]).

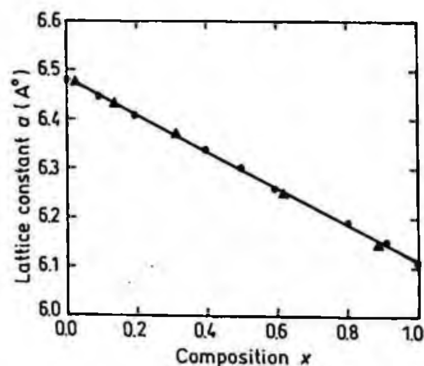

Fig. 4.5.4. Lattice constant as a function of composition parameter x for $Ga_xIn_{1-x}Sb$ (after Auvergne *et al.* [1974]).

(Reprinted with permission from Elsevier Science, © 1974.)

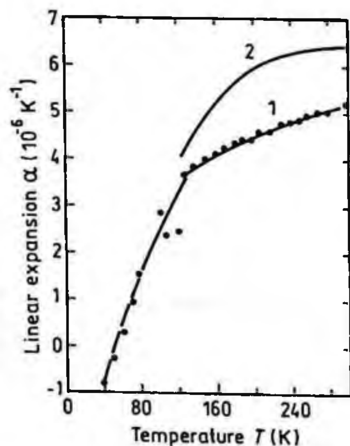

Fig. 4.5.5. Temperature dependence of linear expansion coefficient.
1. $x = 0$ (InSb) (after Gibbons [1958]).
2. $x = 1$ (GaSb) (after Novikova and Abrikosov [1963]).

(Reprinted with permission from The American Physical Society, © 1958.)

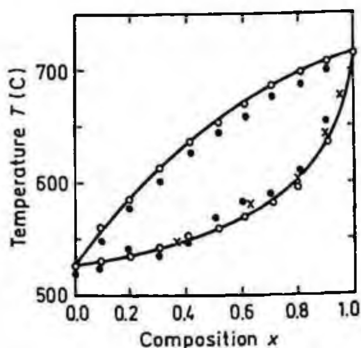

Fig. 4.5.6. Pseudobinary phase diagram for $Ga_xIn_{1-x}Sb$ system. (after Ufimtsev *et al.* [1971]).

4.6. Mechanical Properties, Elastic Constants, Lattice Vibrations, Other Properties

Density		$(5.77 - 0.16x)$ g/cm^3
Surface microhardness (using Knoop's pyramid test)		$x = 0$ (InSb) – 220 kg/mm^2 $x = 1$ (GaSb) – 450 kg/mm^2
Cleavage planes		{110} {111}
Elastic constants at 300 K:		
C_{11}		$(6.67 + 2.16x) \cdot 10^{11}$ dyn/cm^2
C_{12}		$(3.65 + 0.37x) \cdot 10^{11}$ dyn/cm^2
C_{44}		$(3.02 + 1.30x) \cdot 10^{11}$ dyn/cm^2
Bulk modulus	$B_s = \frac{C_{11} + 2C_{12}}{3}$	$B_s = (4.66 + 0.96x) \cdot 10^{11}$dyn/cm^2
Anizotropy factor	$A = \frac{C_{11} - C_{12}}{2C_{44}}$	$A = 0.5 + 0.06x$
Shear modulus	$C' = (C_{11} - C_{12})/2$	$C' = (1.51 + 0.89x) \cdot 10^{11}$dyn/cm^2
[100] Young's modulus	$Y_0 = \frac{(C_{11} + 2C_{12})(C_{11} - C_{12})}{(C_{11} + C_{12})}$	$Y_0 = (4.09 + 2.22x) \cdot 10^{11}$dyn/cm^2
[100] Poisson ratio	$\sigma_0 = \frac{C_{12}}{C_{11} + C_{12}}$	$\sigma_0 = 0.35 - 0.04x$

Acoustic Wave Speeds

Wave propagation direction	Wave character	Expression for wave speed	Wave speed (in units of 10^5 cm/s)
[100]	V_L	$(C_{11}/\rho)^{1/2}$	$3.40+0.57x$
	V_T	$(C_{44}/\rho)^{1/2}$	$2.29+0.48x$
[110]	V_l	$[(C_{11}+C_{12}+2C_{44})/2\rho)]^{1/2}$	$3.76+0.62x$
	$V_{t\parallel}$	$V_{t\parallel}=V_T=(C_{44}/\rho)^{1/2}$	$2.29+0.48x$
	$V_{t\perp}$	$[(C_{11}-C_{12})/2\rho)]^{1/2}$	$1.62+0.45x$
[111]	V_l'	$[(C_{11}+2C_{12}+4C_{44})/3\rho)]^{1/2}$	$3.88+0.62x$
	V_t'	$[(C_{11}-C_{12}+C_{44})/3\rho)]^{1/2}$	$1.87+0.46x$

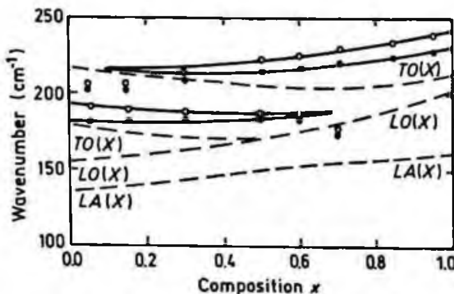

Fig. 4.6.1. Γ- and X-phonons as a function of composition parameter x for $Ga_xIn_{1-x}Sb$. Solid and dashed curves show Γ- and X-phonons, respectively. Open and full circles show $LO(\Gamma)$ and $TO(\Gamma)$ phonons, respectively (after Kleinert [1984]).

Piezoelectric constant e_{14} $-(0.07+0.06x)\ \mathrm{C/m^2}$

References

Adachi, S., *J. Appl. Phys.* **54**, 4 (1983) 1844–1848.

Adachi, S., *J. Appl. Phys.* **66**, 12 (1989) 6030–3040.

Aspnes, D. E. and A. A. Studna, *Phys. Rev.* **B27**, 2 (1983) 985–1009.

Auvergne, D., J. Camassel, H. Mathieu, and A. Joullie, *J. Phys. Chem. Solids* **35**, 2 (1974) 133–140.

Baranskii, P. I. and O. P. Gorodnichii, *Phys. Stat. Solidi* **35**, 2 (1969) K123–K126.

Baxter, R. D., F. J. Reid, and A. C. Beer, *Phys. Rev.* **162**, 3 (1967) 718–727.

Briggs, A. G., L. J. Challis, and F. W. Sheard, *J. Phys.* **C3**, 3 (1970) 687–695.

Brodsky, M. H., G. Lucovsky, M. F. Chen, and T. S. Plaskett, *Phys. Rev.* **B2**, 8 (1970) 3303–3311.

Coderre, W. M. and J. C. Woolley, *Canadian J. of Phys.* **47**, 22 (1969) 2553–2564.

Filipchenko, A. S. and L. P. Bolshakov, *Phys. Stat. Solidi (b)* **77**, 1 (1976) 53–58.

Gibbons, D. F., *Phys. Rev.* **112**, 1 (1958) 136–140.

Ikoma, T., K. Sakai, Y. Adachi, and H. Yanai, *Jap. J. Appl. Phys.* **16**, 8 (1977) 1379–1387.

Iluridze, G. N., A. N. Titkov, and E. I. Chaikina, *Sov. Phys. Semicond.* **21**, 1 (1987) 47–50.

Johnson, G. R., B. C. Cavenett, T. M. Kerr, P. B. Kirby, and C. E. C. Wood, *Semicond. Sci. and Technol.* **3**, (1988) 1157–1165.

Kawashima, M. and Sh. Kataoka, *Jap. J. Appl. Phys.* **18**, 7 (1979) 1311–1316.

Kleinert, P., *Phys. Stat. Sol. (b)* **122**, 1 (1984) 81–89.

Litwin-Staszewska, E., W. Szymanska, and P. Piotrzkowski, *Phys. Stat. Solidi (b)* **106**, 2 (1981) 551–559.

Mbow, B., N. Rezzoug, C. Peremarti, A. Mezerreg, and C. Llinares, *J. de Physique III* **3**, 9 (1993) 1777–1782.

Miki, H., K. Segawa, M. Otsubo, K. Shirahata, and K. Fujibayashi, in *GaAs and Related Compounds* Inst. Phys. Conf. Ser. no. 24, Inst. of Phys., London and Bristol, 1975, pp. 16–21.

Novikova, S. I. and N. Kh. Abrikosov, *Sov. Phys. Solid State* **5**, 8 (1963) 1558.

Okhotin, A. S., A. S. Pushkarskii, and V. V. Gorbachev, *Thermophysical Properties of Semiconductors*, Moscow, "Atom" Publ. House, 1972, (in Russian).

Paskov P. P., *J Appl. Phys.* **81**, 4 (1997) 1890–1898.

Piesbergen, V. U., *Zeit fur Naturforschung* **18a**, 2 (1963) 141–147.

Roth, A. P. and E. Fortin, *Canadian J. of Phys.* **56**, 11 (1978) 1468–1475.

Roth, A. P., W. J. Keeler, and E. Fortin, *Canadian J. of Phys.* **58**, 4 (1980) 560–564.

Rousina, R., C. Halpin, and J. B. Webb, *J. Appl. Phys.* **68**, 5 (1990) 2181–2186.

Titkov, A. N., G. N. Iluridze, I. F. Mironov, and V. A. Cheban, *Sov. Phys. Semicond.* **20**, 1 (1986) 16–21.

Ukhanov, Yu. I. *Optical Properties of Semiconductors*, Moscow, "Nauka" Publ. Co., 1977, (in Russian).

Ufimtsev, V. B., A. S.Timoshin, and G. V. Kostin, *Izv. Akad. Nauk SSSR, Neorg. Mat.* **7**, 11 (1971) 2090–2091.

Wiley, J. D., *Semiconductors and Semimetals*, eds. by R. K. Willardson and A. C. Beer, Academic Press, N.Y., Vol. 10, 1975, p. 91.

Woolley, J. C. and C. M. Gillett, *J. Phys. Chem. Solids* **17**, 1/2 (1960) 34–43.

Youngdale, E. R., J. R. Meyer, C. A. Hoffman, F. J. Bartoli, C. H. Grain, P. M. Young, H. Ehrenreich, R. H. Miles, and D. H. Chow, *Appl. Phys. Lett.* **64**, 23 (1994) 3160–3162.

Zitouni, K., A. Kadri, and R. L. Aulombard, *Phys. Rev.* **B34**, 4 (1986) 2638–2648.

CHAPTER 5

GALLIUM ARSENIDE ANTIMONIDE ($GaAs_{1-x}Sb_x$)

A. Ya. Vul'
Ioffe Institute, St. Petersburg, Russia

5.1. Basic Parameters at 300 K

	GaAs	GaSb	$GaAs_{1-x}Sb_x$
Crystal structure	Zinc Blende	Zinc Blende	Zinc Blende
Space group	$F\bar{4}3m$	$F\bar{4}3m$	$F\bar{4}3m$
Number of atoms in 1 cm^3	$4.42 \cdot 10^{22}$	$3.53 \cdot 10^{22}$	$(4.42-0.89x) \cdot 10^{22}$
Debye temperature (K)	360	266	
Density (g/cm^3)	5.32	5.61	$5.32 + 0.29x$
Dielectric constant			
static	12.9	15.7	$12.90 + 2.8x$
high frequency	10.89	14.4	$10.89 + 3.51x$
Effective electron mass: (in units of m_o)	0.063	0.041	$0.063 - 0.0495x + 0.0258x^2$
Effective hole mass: (in units of m_o)			
heavy hole	0.51	0.4	$0.51 - 0.11x$
light hole	0.082	0.05	$0.082 - 0.032x$
Electron affinity (eV)	4.07	4.06	4.07
Lattice constant (Å)	5.6532	6.0959	See Sec. 5.5
Optical phonon energy (eV)	0.035	0.03	See Sec. 5.6

Band structure and carrier concentration

	GaAs	GaSb	$GaAs_{1-x}Sb_x$
Energy gap (eV)	1.424	0.726	$1.42 - 1.9x + 1.2x^2$ (for $0 < x < 0.3$)
Energy separation between Γ-valley and L-valleys $E_{\Gamma L}$ (eV)	0.29	0.084	See Fig. 5.2.4
Energy separation between Γ-valley and X-valleys $E_{\Gamma X}$ (eV)	0.48	0.31	
Energy of spin-orbital splitting E_{so} (eV)	0.34	0.8	
Intrinsic carrier concentration (cm^{-3})	$2.1 \cdot 10^6$	$1.5 \cdot 10^{12}$	See Sec. 5.2.1
Effective conduction band density of states (cm^{-3})	$4.7 \cdot 10^{17}$	$2.1 \cdot 10^{17}$	$2.5 \cdot 10^{19}(0.063 - 0.0495x + 0.0258x^2)^{3/2}$
Effective valence band density of states (cm^{-3})	$9 \cdot 10^{18}$	$1.8 \cdot 10^{19}$	

Electrical properties

	GaAs	GaSb	$GaAs_{1-x}Sb_x$
Breakdown field (V/cm)	$\approx 4 \cdot 10^5$	$\approx 5 \cdot 10^4$	See Sec. 5.3.2
Mobility (cm^2/V·s)			
electrons	≤ 8500	≤ 3000	See Sec. 5.3.1
holes	≤ 400	≤ 1000	

	GaAs	GaSb	$GaAs_{1-x}Sb_x$
Diffusion coefficient (cm^2/s)			
electrons	≤ 200	≤ 75	
holes	≤ 10	≤ 25	
Electron thermal velocity (m/s)	$4.4 \cdot 10^5$	$5.8 \cdot 10^5$	$4.4 \cdot 10^5(1+0.4x-0.09x^2)$
Hole thermal velocity (m/s)	$1.8 \cdot 10^5$	$2.1 \cdot 10^5$	$(1.8+0.3x) \cdot 10^5$
Optical properties			
Infrared refractive index	3.3	3.8	$3.3 + 0.5x$
Rediative recombination coefficient (cm^3/s)	$7 \cdot 10^{-10}$	$\approx 10^{-10}$	
Thermal and mechanical properties			
Bulk modulus (dyn/cm^2)	$7.53 \cdot 10^{11}$	$5.63 \cdot 10^{11}$	$(7.53-1.9x) \cdot 10^{11}$
Melting point (°C)	1240	712	See Sec. 5.5
Specific heat (J/g°C)	0.33	0.25	
Thermal conductivity (W/cm °C)	0.55	0.32	
Thermal diffusivity (cm^2/s)	0.31	0.23	
Thermal expansion, linear, ($°C^{-1}$)	$5.73 \cdot 10^{-6}$	$7.75 \cdot 10^{-6}$	

5.2. Band Structure and Carrier Concentration

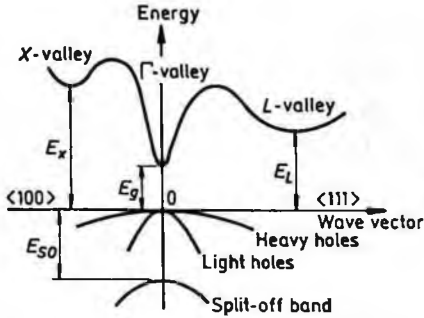

Fig. 5.2.1. Band structure of GaAs ($x = 0$). Important minima of the conduction band and maxima of the valence band.
$E_g = 1.42$ eV, $E_L = 1.71$ eV
$E_x = 1.90$ eV, $E_{so} = 0.34$ eV.

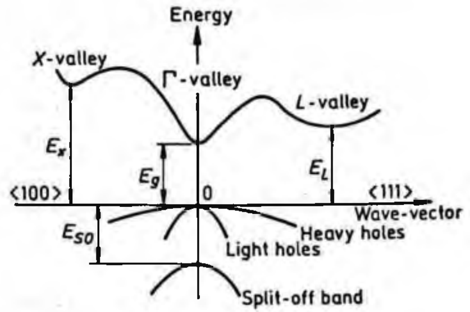

Fig. 5.2.2. Band structure of GaSb ($x = 1$). Important minima of the conduction band and maxima of the valence band.
$E_g = 0.73$ eV, $E_L = 0.81$ eV
$E_x = 1.03$ eV, $E_{so} = 0.8$ eV.

There is a miscibility gap in the composition range, $0.39 < x < 0.62$.

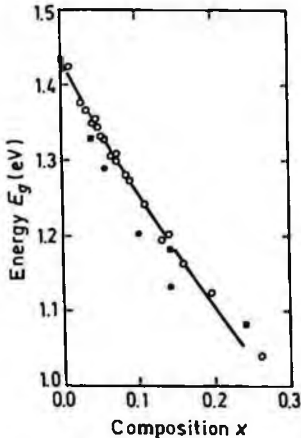

Fig. 5.2.3. Variation of energy gap E_g with composition x for $GaAs_{1-x}Sb_x$ (after Biryulin *et al.* [1979a]).

(Reprinted with permission from the American Institute of Physics, © 1979.)

For $0 < x < 0.3$ at 300 K:

$$E_g = 1.42 - 1.9x + 1.2x^2 \quad (5.2.1)$$

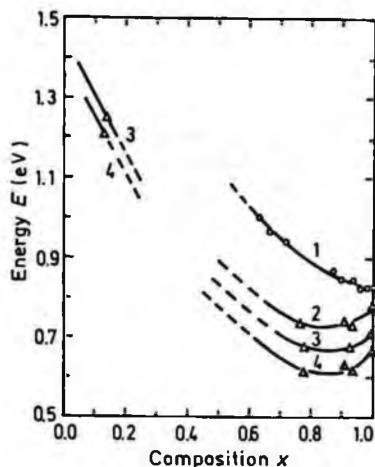

Fig. 5.2.4. Energy separation between L-valley of conduction band and top of the valence band (curve 1, after Rosenbaum and Woolley [1975]) and energy gap (curves 2–4, after Taylor and Fortin [1970]) versus composition x.
2. $T = 100$ K, 3. $T = 210$ K,
1,4. $T = 300$ K.

5.2.1. *Temperature Dependences*

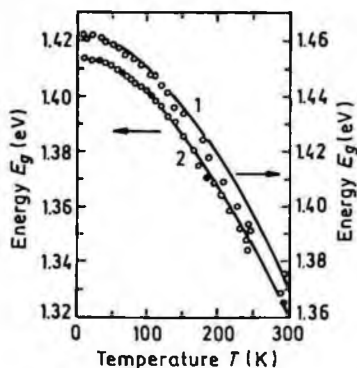

Fig. 5.2.5. Temperature dependences of energy gap E_g for $GaAs_{1-x}Sb_x$.
1. $x = 0.026$, 2. $x = 0.05$ (after Biryulin *et al.* [1979b]).

(Reprinted with permission from the American Institute of Physics. © 1979.)

For GaAs ($x = 0$): $$E_g = 1.519 - 5.405 \cdot 10^{-4} \cdot \frac{T^2}{T + 204} \text{ (eV)} \tag{5.2.2}$$

For GaSb ($x = 1$): $$E_g = 0.813 - 3.78 \cdot 10^{-4} \cdot \frac{T^2}{T + 94} \text{ (eV)} \tag{5.2.3}$$

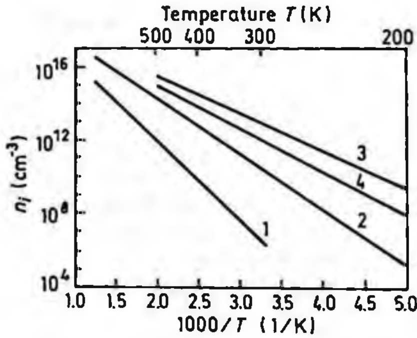

Fig. 5.2.6. The temperature dependences of the intrinsic carrier concentration.
1. $x = 0$ (GaAs), 2. $x = 0.3$,
3. $x = 0.8$, 4. $x = 1$ (GaSb).

5.2.2. *Dependences on Hydrostatic Pressure*

$x = 0$ (GaAs):

$$E_g = E_g(0) + 0.0126P - 3.77 \cdot 10^{-5} \cdot P^2 \text{ (eV)}$$

$$E_L = E_L(0) + 5.5 \cdot 10^{-3} \cdot P \text{ (eV)} \quad (5.2.6)$$

$$E_x = E_x(0) - 1.5 \cdot 10^{-3} \cdot P \text{ (eV)}$$

$x = 1$ (GaSb):

$$E_g = E_g(0) + 0.0145P \text{ (eV)}$$

$$E_L = E_L(0) + 5 \cdot 10^{-3} \cdot P \text{ (eV)} \quad (5.2.7)$$

$$E_x = E_x(0) - 1.5 \cdot 10^{-3} \cdot P \text{ (eV)},$$

where P is pressure in kbar.

5.2.3. *Effective Masses*

Electrons:

$$m_\Gamma \cong (0.063 - 0.0495x + 0.0258x^2) \cdot m_o \qquad (5.2.8)$$

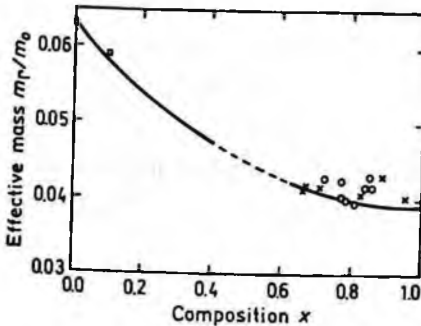

Fig. 5.2.7. Dependence of electron effective mass m_Γ on composition parameter x. The curve is calculated according to Eq. (5.2.8). Dashed part of the curve corresponds to the miscibility gap. Symbols are experimental data taken from Delvin *et al.* [1981].

Holes:

heavy	$m_h = (0.51 - 0.11x)m_o$
light	$m_{lp} = (0.082 - 0.032x)m_o$
split-off band	$m_{so} \cong 0.15m_o$

5.2.4. *Donors and Acceptors*

Ionization energies of shallow donors (meV):

$x = 0$ (GaAs):	$S - 6$,	Se − 6,	Te − 30
$x = 1$ (GaSb):	$S\,(L) \sim 150$,	Se $(L) \sim 50$	Te $(L) \sim 20$
	$S\,(X) \sim 300$	Se $(X) \sim 230$	Te $(X) \leq 80$

For typical donor concentrations $N_d \geq 10^{17}$ cm^{-3} the shallow donor states in GaSb connected with Γ-valley do not appear.

Ionization energies of shallow acceptors (meV).

$x = 0$ (GaAs):	Si -	three acceptor levels ~ 30, 100 and 220
	Zn	~ 25
	Ge	~ 30
$x = 1$ (GaSb):	Si	~ 10
	Zn	~ 37
	Ge	~ 9

The dominant acceptor of undoped GaSb seems to be a native defect. This acceptor is doubly ionizable: $E_{a1} = 30$ meV, $E_{a2} = 100$ meV.

5.3. Electrical Properties

5.3.1. *Mobility and Hall Effect*

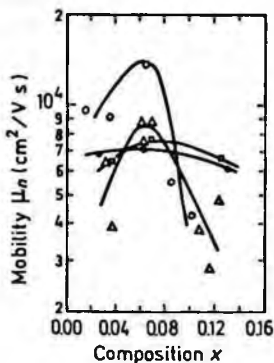

Fig. 5.3.1. Electron Hall mobility versus x for four sets of samples, 77 K. Electron concentration $n_0 \le 5 \cdot 10^{16}$ cm^{-3} (after Biryulin *et al.* [1981]).

(Reprinted with permission from the American Institute of Physics, © 1981.)

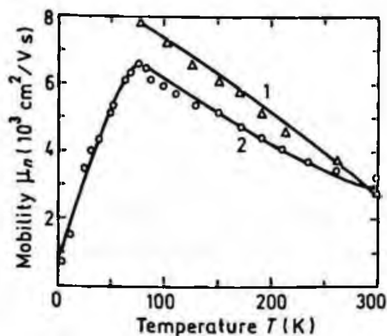

Fig. 5.3.2. Temperature dependences of electron Hall mobility for $GaAs_{1-x}Sb_x$. Electron concentration $n_0 \le 5 \cdot 10^{16}$ cm^{-3}. 1. $x = 0.07$, 2. $x = 0.12$ (after Biruylin *et al.* [1981]).

(Reprinted with permission from the American Institute of Physics, © 1981.)

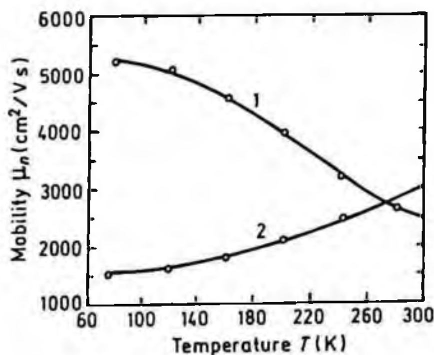

Fig. 5.3.3. Temperature dependences of electron Hall mobility for GaSb ($x = 1$). 1. $N_d = 1.7 \cdot 10^{18}$ cm^{-3}, 2. $N_d = 2.8 \cdot 10^{17}$ cm^{-3} (after Mathur and Jain [1979]).

(Reprinted with permission from The American Physical Society, © 1979.)

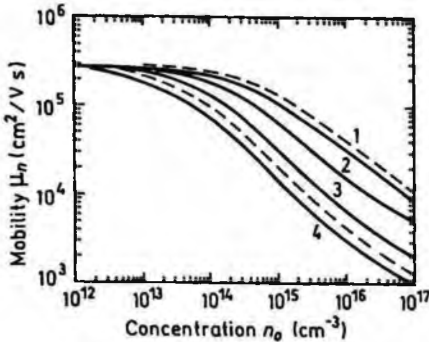

Fig. 5.3.4. Electron drift (solid curves) and Hall (dashed curves) mobilities versus electron concentration n_0 for GaAs ($x = 0$) for different degrees of compensation, 77 K. $(N_d + N_a)/n_0$: 1. 1, 2. 2, 3. 5, 4. 10 (after Rode [1975]).

(Reprinted with permission from Academic Press, © 1975.)

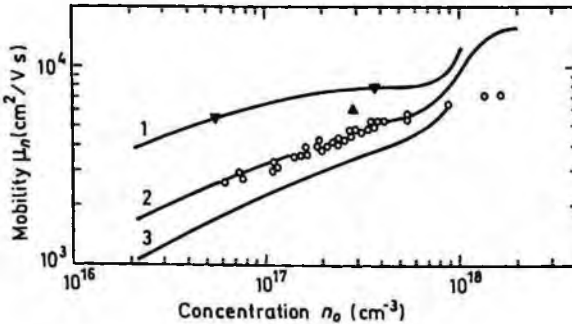

Fig. 5.3.5. Electron Hall mobility versus electron concentration n_0 for GaSb ($x = 1$), $T = 77$ K. Open circles represent measurements with a group of samples having approximately the same residual acceptor concentrations N_a. Full symbols: specimens with lower residual acceptor concentrations. Solid lines represent the theoretical calculations for different values of compensating acceptor densities – either singly (N_a^-) or doubly (N_a^{--}) ionized.

1. $N_a^- = 1.2 \cdot 10^{17}$ cm^{-3} or $N_a^{--} = 0.4 \cdot 10^{17}$ cm^{-3}, 2. $N_a^- = 2.85 \cdot 10^{17}$ cm^{-3} or $N_a^{--} = 0.95 \cdot 10^{17}$ cm^{-3},
3. $N_a^- = 4.5 \cdot 10^{17}$ cm^{-3} or $N_a^{--} = 1.5 \cdot 10^{17}$ cm^{-3} (after Baxter *et al.* [1967]).

(Reprinted with permission from The American Physical Society, © 1967.)

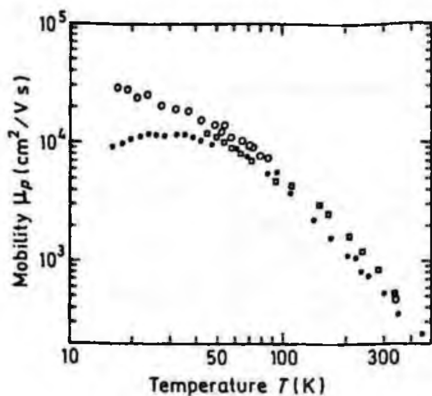

Fig. 5.3.6. Temperature dependences of hole Hall mobility for three high-purity GaAs ($x = 0$) samples (after Wiley [1975]).

(Reprinted with permission from Academic Press, © 1975.)

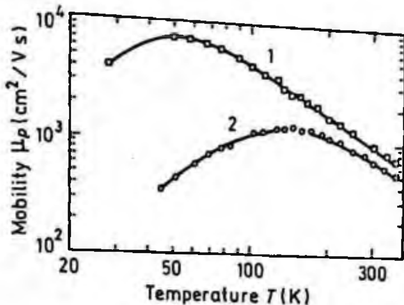

Fig. 5.3.7. Temperature dependences of hole Hall mobility for two GaSb ($x = 1$) samples. MBE technique. Hole concentration at 300 K: 1. $2.28 \cdot 10^{16}$ cm^{-3}, 2. $1.9 \cdot 10^{19}$ cm^{-3} (after Johnson *et al.* [1988]).

(Reprinted with permission from IOP Publishing, © 1988.)

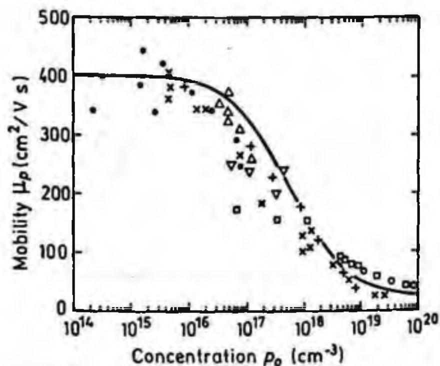

Fig. 5.3.8. Hole Hall mobility versus hole concentration p_o for GaAs ($x = 0$), 300 K (after Wiley [1975]).

(Reprinted with permission from Academic Press, © 1975.)

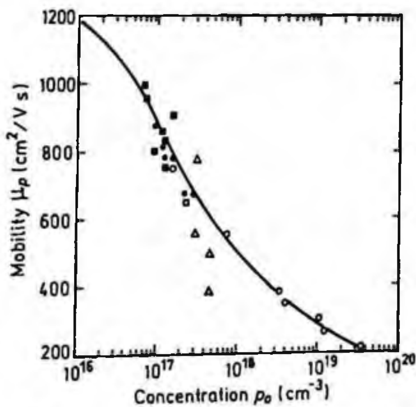

Fig. 5.3.9. Hole Hall mobility versus hole concentration p_o for GaSb ($x = 1$), 300 K (after Wiley [1975]).

(Reprinted with permission from Academic Press, © 1975.)

5.3.2. *Impact Ionization*

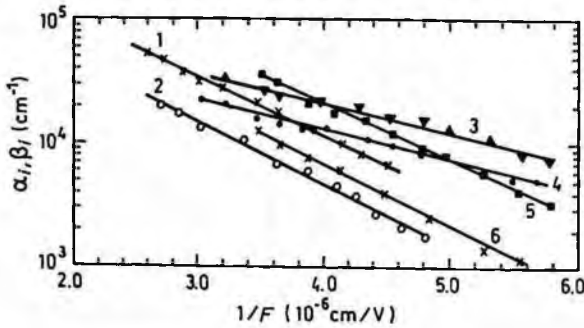

Fig. 5.3.10. The dependences of ionization rates for electrons α_i and holes β_i versus $1/F$. curves 1–4. $x = 0.10$, curves 5, 6. $x = 0.125$, curves 1, 3, 5 show $\alpha\,(1/F)$ dependences, curves 2, 4, 6 show $\beta\,(1/F)$ dependences. Temperature $T(K)$: 1, 2, 5, 6 – 300, 3, 4 – 77 (after Andreev *et al.* [1981]).

(Reprinted with permission from the American Institute of Physics, © 1981.)

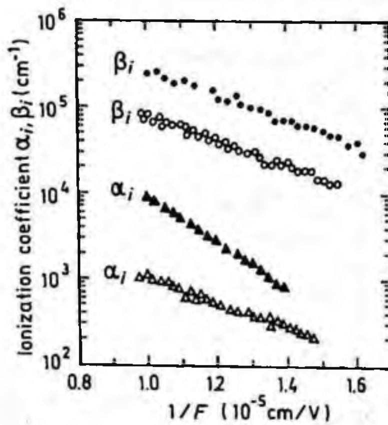

Fig. 5.3.11. The dependences of α_i and β_i versus $1/F$ for GaSb ($x = 1$), 77 K.
Open symbols: $F||(111)$.
Filled symbols: $F||(100)$ (after Zhingarev *et al.* [1981]).

(Reprinted with permission from the American Institute of Physics, © 1981.)

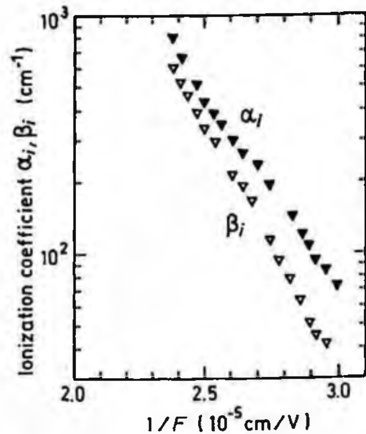

Fig. 5.3.12. The dependences of α_i and β_i versus $1/F$ for GaSb ($x = 1$), 300 K. $F\,||\,(100)$ (after Hildebrand *et al.* [1980]).

(Reprinted with permission from the American Institute of Physics, © 1980.)

5.4. Optical Properties

Infrared refractive index (300 K):

$$n_\infty = (k_\infty)^{1/2} \cong 3.3 + 0.5x$$

Long wave *TO* phonon energy at 300 K (meV):

$$h\nu_{TO} \cong 33.2 - 5.4x$$

Long wave *LO* phonon energy at 300 K (meV):

$$x = 0\,(\text{GaAs})\; 36.1$$
$$x = 1\,(\text{GaSb})\; 28.9$$

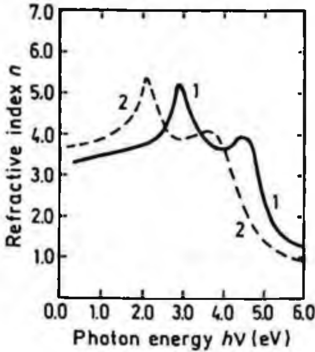

Fig. 5.4.1. Refractive index n versus photon energy for $x = 0$ (GaAs, curve 1) and $x = 1$ (GaSb, curve 2), 300 K (after Adachi [1989]).

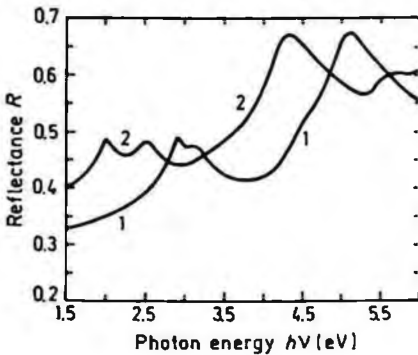

Fig. 5.4.2. Normal incidence reflectivity versus photon energy for $x = 0$ (GaAs, curve 1) and $x = 1$ (GaSb, curve 2), 300 K (after Aspnes and Studna [1983]).

(Reprinted with permission from The American Physcial Society, © 1983.)

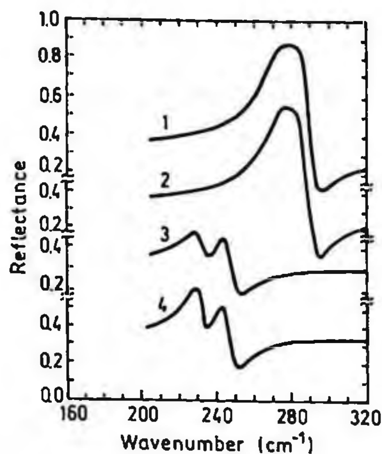

Fig. 5.4.3. Wavenumber dependences of the reflectance for four alloy compositions of $GaAs_{1-x}Sb_x$, 300 K.
1. $x = 0.07$, 2. $x = 0.09$,
3. $x = 0.89$, 4. $x = 0.93$ (after Lucovsky and Chen [1970]).

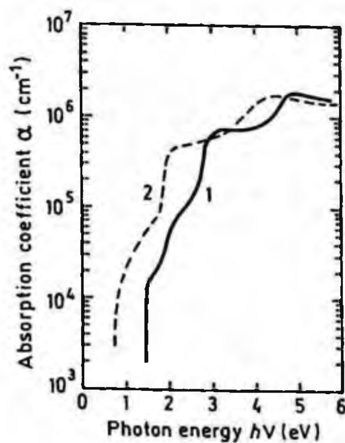

Fig. 5.4.4. The absorption coefficient versus photon energy for $x = 0$ (GaAs, curve 1) and $x = 1$ (GaSb, curve 2) 300 K (after Adachi [1989]).

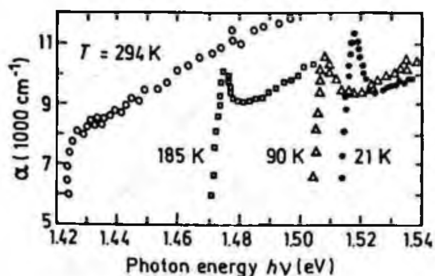

Fig. 5.4.5. Absorption coefficient near the intrinsic absorption edge for $x = 0$ (GaAs) (after Sturge [1962]).

(Reprinted with permission from The American Physical Society, © 1962.)

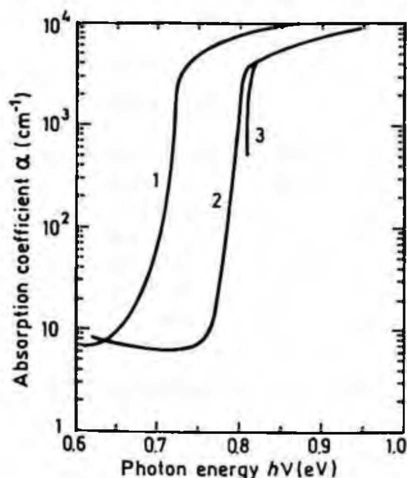

Fig. 5.4.6. Intrinsic absorption coefficient near the intrinsic absorption edge for $x = 1$ (GaSb). $T(K)$: 1. 300, 2. 77, 3. 4.2 (after Becker *et al.* [1961]).

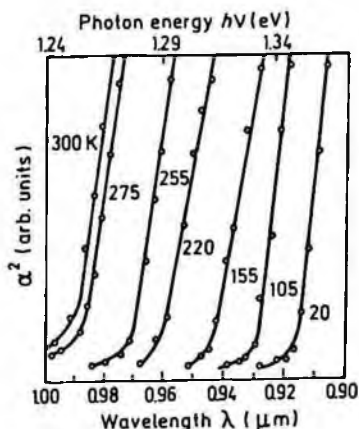

Fig. 5.4.7. Absorption edge of $GaAs_{0.9}Sb_{0.1}$ ($x = 0.1$) at different temperatures (after Swarup *et al.* [1981]).

(Reprinted with permission from Akademie Verlag, © 1981.)

A ground state Rydberg energy R_{x1} (meV):

$x = 0$ (GaAs)	– 4.2
$x = 1$ (GaSb)	– 2.8

5.5. Thermal Properties

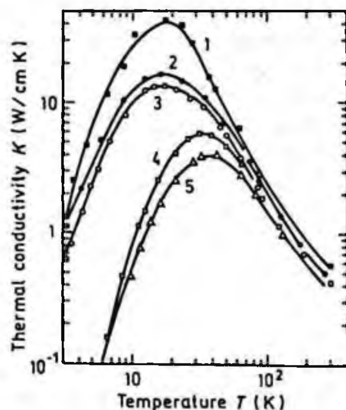

Fig. 5.5.1. Temperature dependences of the thermal conductivity for $x = 0$ (GaAs). 1 ÷ 3 – n-type samples. n_o (cm^{-3}): 1. 10^{16}, 2. 1.4×10^{16}, 3. 10^{18}, 4, 5. p-type samples. p_o (cm^{-3}): 4. $3 \cdot 10^{18}$, 5. $1.2 \cdot 10^{19}$ (after Carlson *et al.* [1965]).

(Reprinted with permission from the American Institute of Physics, © 1965.)

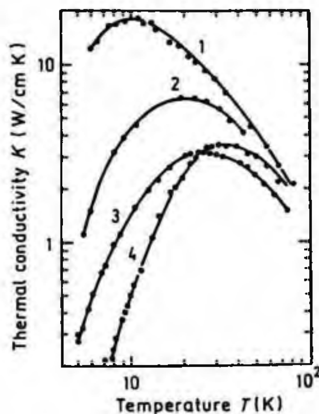

Fig. 5.5.2. Temperature dependences of the thermal conductivity for $x = 1$ (GaSb). 1 ÷ 3 – n-type samples. n_o (300 K), cm^{-3}: 1. $1.6 \cdot 10^{17}$, 2. $8.6 \cdot 10^{17}$, 3. $1.8 \cdot 10^{18}$. 4. p-type sample. p_o (300 K) $= 1.4 \cdot 10^{17}$ cm^{-3} (after Poudjade and Albany [1969]). For $300 < T < 800$ K, $K \cong 0.32\,(T/300)^{-1.6}$ (W/cmK).

The essential decrease of the thermal conductivity has been usually observed for intermediate alloy compositions $0 < x < 1$ (See Chaps. 1, 3 and 7).

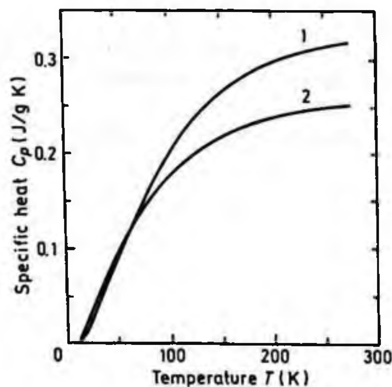

Fig. 5.5.3. Temperature dependences of specific heat at constant pressure. 1. $x = 0$ (GaAs), 2. $x = 1$ (GaSb) (after Piesbergen [1963]).

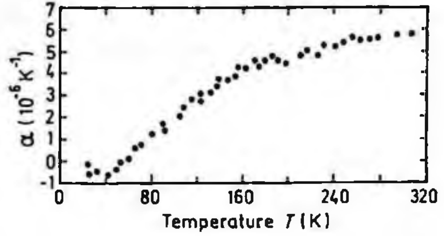

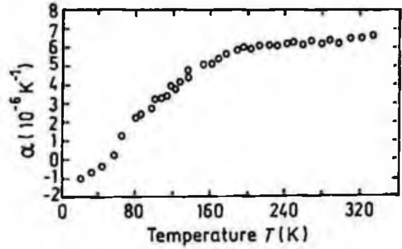

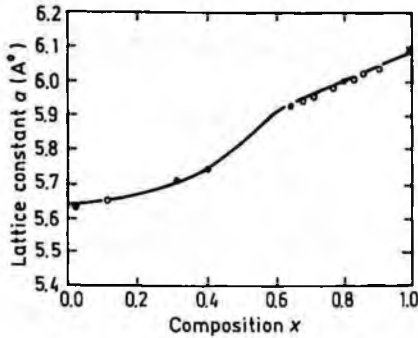

Fig. 5.5.4. Lattice constant as a function of x (after Lendvay [1984]).

Fig. 5.5.5. Temperature dependences of linear expansion coefficient. (a) $x = 0$ (GaAs) (after Novikova [1961]). (b) $x = 1$ (GaSb) (after Novikova and Abrikosov [1963]).

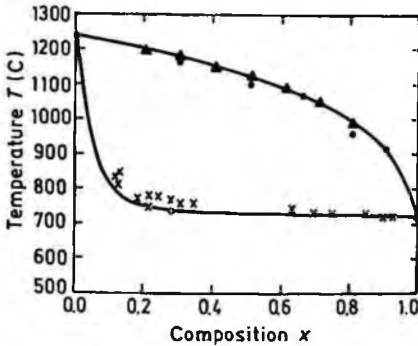

Fig. 5.5.6. Pseudobinary phase diagram for $GaAs_{1-x}Sb_x$ system (after Gratton and Woolley [1980]).

5.6. Mechanical Properties, Elastic Constants, Lattice Vibrations, Other Properties

Density		$5.32 + 0.29x$ (g/cm^3)
Hardness		between 4 and 5 on the Mohs scale
Surface mocrohardness (using Knoop's pyramid test)		$x = 0$ (GaAs) – 750 kg/mm^2 $x = 1$ (GaSb) – 450 kg/mm^2
Cleavage plane		{110}
Elastic constants at 300 K:		
C_{11}		$(11.9 - 3.07x) \cdot 10^{11}$ dyn/cm^2
C_{12}		$(5.34 - 1.32x) \cdot 10^{11}$ dyn/cm^2
C_{44}		$(5.96 - 1.64x) \cdot 10^{11}$ dyn/cm^2
Bulk modulus	$B_s = \frac{C_{11}+2C_{12}}{3}$	$B_s = (7.53 - 1.9x) \cdot 10^{11}$ dyn/cm^2
Anisotropy factor	$A = \frac{C_{11}-C_{12}}{2C_{44}}$	$A \cong 0.55$
Shear modulus	$C' = (C_{11} - C_{12})/2$	$C' = (3.28 - 0.88x) \cdot 10^{11}$ dyn/cm^2
[100] Young's modulus	$Y_0 = \frac{(C_{11}+2C_{12})(C_{11}-C_{12})}{(C_{11}+C_{12})}$	$Y_0 = (8.59 - 2.28x) \cdot 10^{11}$ dyn/cm^2
[100] Poisson ratio	$\sigma_0 = \frac{C_{12}}{C_{11}+C_{12}}$	$\sigma_0 \cong 0.31$

Acoustic Wave Speeds

Wave propagation direction	Wave character	Expression for wave speed	Wave speed (in units of 10^5 cm/s)
[100]	V_L	$(C_{11}/\rho)^{1/2}$	$4.73-0.76x$
	V_T	$(C_{44}/\rho)^{1/2}$	$3.35-0.58x$
	V_l	$[(C_{11}+C_{12}+2C_{44})/2\rho)]^{1/2}$	$5.24-0.86x$
[110]	$V_{t\parallel}$	$V_{t\parallel}=V_T=(C_{44}/\rho)^{1/2}$	$3.35-0.58x$
	$V_{t\perp}$	$[(C_{11}-C_{12})/2\rho)]^{1/2}$	$2.48-0.41x$
[111]	V_l'	$[(C_{11}+2C_{12}+4C_{44})/3\rho)]^{1/2}$	$5.40-0.90x$
	V_t'	$[(C_{11}-C_{12}+C_{44})/3\rho)]^{1/2}$	$2.80-0.47x$

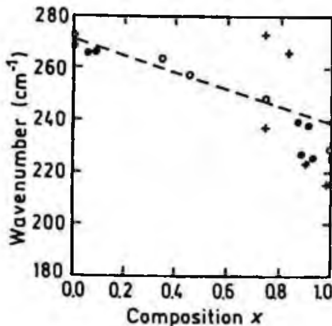

Fig. 5.6.1. Optical phonon energy as a function of x. Full and open circles show TO phonon frequencies (after Lucovsky and Chen [1970]). Crosses show LO phonon frequencies (data are taken from Filion and Fortin [1974]).

Piezoelectric constant e_{14} $-(0.16-0.03x)$ C/m^2

References

Adachi, S., *J. Appl. Phys.* **66**, 12 (1989) 6030–6040.

Andreev, V. M., M. Z. Zhingarev, O. O. Ivent'eva, V. I. Korol'kov, and M. P. Mikhailova, *Sov. Phys. Semicond.* **15**, 6 (1981) 701–702.

Aspnes, D. E. and A. A. Studna, *Phys. Rev.* **B27**, 2 (1983) 985–1009.

Baxter, R. D., F. J. Reid, and A. C. Reer, *Phys. Rev.* **162**, 3 (1967) 718–727.

Becker, W. M., A. K. Randas, and H. Y. Fan, *J. Appl. Phys.* **32** (Suppl.), 10 (1961) 2094–2102.

Biryulin, Yu. F., R. R. Ichkitidze, V. G. Krigel, and Yu. V. Shmartsev, *Sov. Phys. Semicond.* **13**, 6 (1979a) 727–728.

Biryulin, Yu. F., R. R. Ichkitidze, V. G. Krigel, V. V. Chaldyshev, and Yu. V. Shmartsev, *Sov. Phys. Semicond.* **13**, 11 (1979b) 1334–1336.

Biryulin, Yu. F., V. N. Karyaev, I. Yu. Novikova, T. A. Polyanskaya, V. V. Chaldyshev, and Yu. V. Shmartsev, *Sov. Phys. Semicond.* **15**, 11 (1981) 1330–1332.

Carlson, R. O., G. A. Slack, and S. J. Silverman, *J. Appl. Phys.* **36**, 2 (1965) 505.

Delvin, P., H. M. Heravi, and J. C. Woolley, *Can. J. Phys.* **59**, 7 (1981) 939–944.

Filion, A. and E. Fortin, *Can. J. Phys.* **52**, 8 (1974) 743–747.

Gratton, M. F. and J. C. Woolley, *J. Electrochemical Soc.* **127**, 1 (1980) 55–62.

Hildebrand, O., W. Kuebart, and P. H. Pilkuhn, *Appl. Phys. Lett.* **37**, 9 (1980) 800–803.

Johnson, G. R., B. C. Cavenett, and T. M. Kerr, *Semicond. Sci. and Technol.* **3** (1988) 1157–1165.

Lendvay, E., *Prog. Cryst. Growth and Chemist.* **8** (1984) 371–425.

Lucovsky, G. and M. F. Chen, *Solid State Commun.* **8**, 17 (1970) 1397–1401.

Mathur, P. C. and S. Jain, *Phys. Rev.* **B19**, 6 (1979) 3159–3166.

Novikova, S. I., *Sov. Phys. Solid State* **3**, 1 (1961) 129.

Novikova, S. I. and N. Kh. Abrikosov, *Sov. Phys. Solid State* **3** (1963) 1558.

Piesbergen, V., *Zeit. fur Naturforschung*, **18a**, 2 (1963) 141–147.

Poudjade, A. M. and H. J. Albany, *Phys. Rev.* **182**, 3 (1969) 802–807.

Rode, D. L., *Semiconductors and Semimetals*, ed. by R. K. Willardson and A. C. Beer, Academic Press, N.Y., Vol. 10, 1975, p. 1.

Rosenbaum, S. D. and J. C. Woolley, *Can. J. Phys.* **53**, 11 (1975) 1071–1077.

Sturge, M. D., *Phys. Rev.* **127**, 3 (1962) 768.

Swarup, P., R. K. Jain, S. N. Verma, Sh. Charan, and D. M. Tandle, *Phys. Stat. Sol. (a)* **65** (1981) K183–K187.

Taylor, A. E. and E. Fortin, *Can. J. Phys.* **48**, 16 (1970) 1874–1878.

Wiley, J. D., *Semiconductors and Semimetals*, ed. by R. K. Willardson and A. C. Beer, Academic Press, N.Y., Vol. 10, 1975, p. 91.

Zhingarev, M. Z., V. I. Korolkov, M. P. Mikhailova, and V. V. Sazonov, *Sov. Techn. Phys. Lett.* **7**, 12 (1981) 637–638.

CHAPTER 6

INDIUM ARSENIDE-ANTIMONIDE ($InAs_{1-x}Sb_x$)

M. S. Bresler

Ioffe Institute, St. Petersburg, Russia

6.1. Basic Parameters at 300 K

	InAs	InSb	$InAs_{1-x}Sb_x$
Crystal structure	Zinc Blende	Zinc Blende	Zinc Blende
Space group	$F\bar{4}3m$	$F\bar{4}3m$	$F\bar{4}3m$
Number of atoms in 1 cm^3	$3.59\cdot10^{22}$	$2.94\cdot10^{22}$	$(3.59-0.65x)\cdot10^{22}$
Debye temperature (K)	280	160 250 (at 77 K)	
Density (g/cm^3)	5.68	5.77	$5.68+0.09x$
Dielectric constant			
static	15.15	16.8	$15.15+1.65x$
high frequency	12.3	15.7	$12.3+3.4x$
Effective electron mass: (in units of m_o)	0.023	0.014	$0.023-0.039x+0.03x^2$
Effective hole mass: (in units of m_o)			
heavy hole	0.41	0.43	$0.41+0.02x$
light hole	0.026	0.015	$0.026-0.011x$
Electron affinity (eV)	4.9	4.59	$4.9-0.31x$
Lattice constant (Å)	6.0583	6.479	$6.0583+0.4207x$
Optical phonon energy (eV)	0.030	0.025	See Sec. 6.6

Band structure and carrier concentration

	InAs	InSb	$InAs_{1-x}Sb_x$
Energy gap (eV)	0.354	0.17	$0.351 - 0.774x + 0.598x^2$
Energy separation between Γ-valley and L-valleys $E_{\Gamma L}$ (eV)	0.73	0.51	
Energy separation between Γ-valley and X-valleys $E_{\Gamma X}$ (eV)	1.02	0.83	
Energy of spin-orbital splitting E_{so} (eV)	0.41	0.80	$0.39 - 0.75x + 1.17x^2$
Intrinsic carrier concentration (cm^{-3})	$1 \cdot 10^{15}$	$2 \cdot 10^{16}$	See Sec. 6.2.1
Effective conduction band density of states (cm^{-3})	$8.7 \cdot 10^{16}$	$4.2 \cdot 10^{16}$	$2.5 \cdot 10^{19} \cdot (0.023 - 0.039x + 0.03x^2)^{3/2}$
Effective valence band density of states (cm^{-3})	$6.6 \cdot 10^{18}$	$7.1 \cdot 10^{18}$	$2.5 \cdot 10^{19} \cdot (0.41 + 0.02x)^{3/2}$
Electrical properties			
Breakdown field (V/cm)	$\approx 4 \cdot 10^4$	$\approx 10^3$	$5 \cdot 10^2 < F_i < 4 \cdot 10^4$
Mobility ($cm^2/V \cdot s$)			
electrons	$\leq 4 \cdot 10^4$	$\leq 7.7 \cdot 10^4$	See Sec. 6.3.1
holes	$\leq 5 \cdot 10^2$	$\leq 8.5 \cdot 10^2$	$\leq 5 \cdot 10^2$

	InAs	InSb	$InAs_{1-x}Sb_x$
Diffusion coefficient (cm^2/s)			
electrons	$\le 10^3$	$\le 2\cdot10^3$	$\le 10^3$
holes	≤ 13	≤ 22	≤ 10
Electron thermal velocity (m/s)	$7.7\cdot10^5$	$9.8\cdot10^5$	$7.7\cdot10^5(1+1.18x-0.91x^2)$
Hole thermal velocity (m/s)	$1.8\cdot10^5$	$1.8\cdot10^5$	$1.8\cdot10^5\ (0<x<1)$
Optical properties			
Infrared refractive index	3.51	4.0	
Rediative recombination coefficient (cm^3/s)	$8\cdot10^{-11}$	$4.9\cdot10^{-11}$	See Sec. 6.3.3
Thermal and mechanical properties			
Bulk modulus (dyn/cm^2)	$5.8\cdot10^{11}$	$4.7\cdot10^{11}$	$(5.8-1.1x)\cdot10^{11}$
Melting point (°C)	942	527	See Sec. 6.5
Specific heat (J/g°C)	0.25	0.2	
Thermal conductivity (W/cm °C)	0.27	0.18	
Thermal diffusivity (cm^2/s)	0.19	0.16	
Thermal expansion, linear ($°C^{-1}$)	$4.52\cdot10^{-6}$	$5.37\cdot10^{-6}$	

6.2. Band Structure and Carrier Concentration

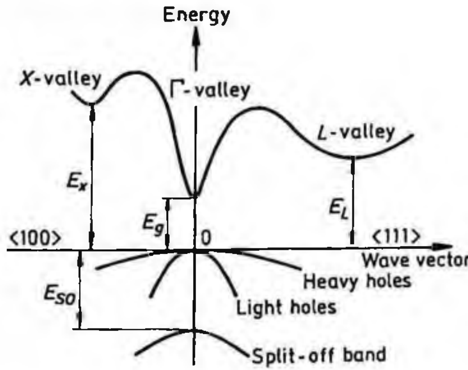

Fig. 6.2.1. Band structure of $InAs_{1-x}Sb_x$. Important minima of the conduction band and maxima of the valence band.

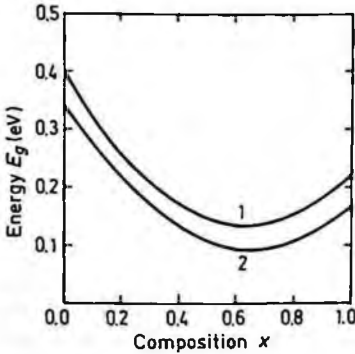

Fig. 6.2.2. Variation of energy gap E_g with composition x for $InAs_{1-x}Sb_x$ at 77 K(1) and 300 K(2) (after Rogalski [1989]).

(Reprinted with permission from Elsevier Science. © 1989.)

At 300 K:

$$E_g = 0.351 - 0.774x + 0.598x^2 \text{ (eV)} \tag{6.2.1}$$

At 10 K:

$$E_g = 0.415(1-x) - 0.672x(1-x) + 0.235x \text{ (eV)} \tag{6.2.2}$$

(after Fang *et al.* [1990]).

Energy of spin-orbital splitting E_{so} (eV), 300 K:

$$E_{so} = 0.39 - 0.75x + 1.17x^2 \tag{6.2.3}$$

6.2.1. *Temperature Dependences*

Temperature dependence of energy gap (after Wieder and Clawson, [1973])

$$E_g(x,T) = 0.411 - 3.4\cdot10^{-4}\cdot\frac{T^2}{T+210} - 0.876x + 0.70x^2 + 3.4\cdot10^{-4}\cdot x\cdot T\cdot(1-x)\ (\text{eV})$$
$$\text{for}\quad 77 < T < 300\ \text{K} \qquad (6.2.4)$$

Effective density of state in the conduction band:

$$N_c \cong 4.82\cdot10^{15}\cdot\left(\frac{m_\Gamma}{m_o}\right)^{3/2}\cdot T^{3/2}$$
$$\cong 4.82\cdot10^{15}\cdot T^{3/2}(0.023 - 0.039x + 0.03x^2)^{3/2}\ (\text{cm}^{-3}) \qquad (6.2.5)$$

Effective density of state in the valence band:

$$N_v = 4.82\cdot10^{15}\cdot\left(\frac{m_{cd}}{m_o}\right)^{3/2}\cdot T^{3/2} = 4.82\cdot10^{15}\cdot T^{3/2}\cdot(0.41 + 0.02x)^{3/2}\ (\text{cm}^{-3}) \qquad (6.2.6)$$

Intrinsic carrier concentration:

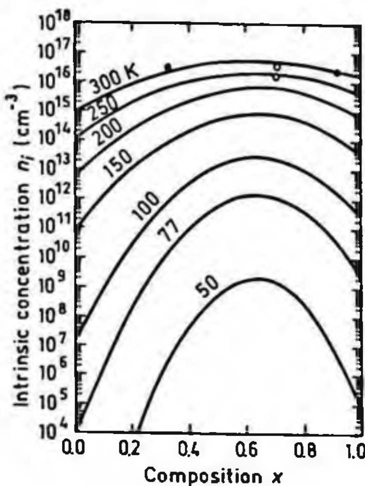

Fig. 6.2.3. Intrinsic carrier concentration in $InAs_{1-x}Sb_x$ as a function of composition for various temperatures. Points represent the experimental data taken from several papers (after Rogalski and Jozwikowski [1989]).

(Reprinted with permission from Elsevier Science, © 1989.)

For all $InAs_{1-x}Sb_x$ compositions there is a temperature T_c below the solidus temperature at which the band gap passes through zero and the band gap structure passes from a normal to an inverted form.

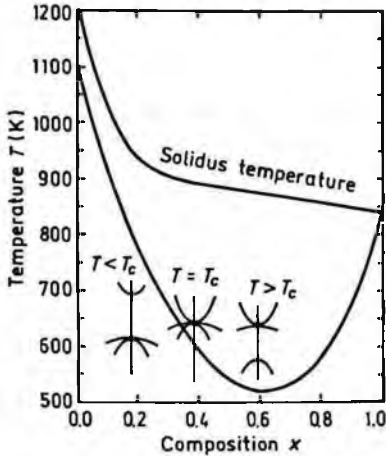

Fig. 6.2.4. Variation of normal-inverted transition temperatures T_c and solidus temperature T_s with composition parameter x (after Rogalski [1989]).

6.2.2. *Dependences on Hydrostatic Pressure*

$x = 0$ (InAs):

$$E_g \cong E_g(0) + 4.8 \cdot 10^{-3}P \text{ (eV)} \tag{6.2.7}$$

$$E_L \cong E_L(0) + 3.2 \cdot 10^{-3}P \text{ (eV)}$$

$x = 1$ (InSb):

$$E_g \cong E_g(0) + 13.7 \cdot 10^{-3}P - 3.6 \cdot 10^{-5}P^2 \text{ (eV)}$$

$$E_L \cong E_L(0) + 4.7 \cdot 10^{-3}P - 1.1 \cdot 10^{-5}P^2 \text{ (eV)} \tag{6.2.8}$$

$$E_X \cong E_X(0) - 3.5 \cdot 10^{-3}P + 0.64 \cdot 10^{-5}P^2 \text{ (eV)},$$

where P is pressure in kbar.

6.2.3. *Effective Masses*

Electrons:

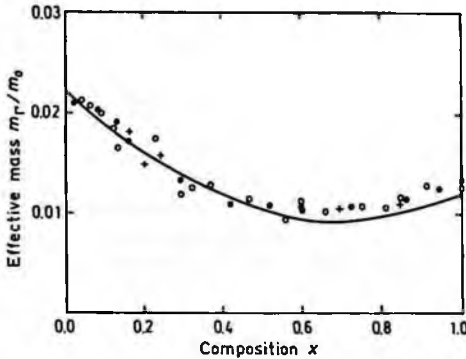

Fig. 6.2.5. Dependence of electron effective mass m_Γ on composition parameter x for $InAs_{1-x}Sb_x$ (after Rogalski [1989]).
(Reprinted with permission from Elsevier Science. © 1989.)

$$m_\Gamma/m_o \approx 0.023 - 0.039x + 0.03x^2 \tag{6.2.9}$$

Non-parabolicity: $E(1+\alpha E) = \dfrac{\hbar^2 k^2}{2m\Gamma}$; $x = 0$ (InAs) $\alpha = 1.4$ (eV^{-1})
$x = 1$ (InSb) $\alpha = 4.1$ (eV^{-1})

Holes:

heavy	$m_h \approx (0.41 + 0.02x)m_o$
light	$m_{lp} \approx (0.026 - 0.011x)m_o$
split-off band	$m_{so} \approx (0.16 - 0.04x)m_o$

6.2.4. *Donors and Acceptors*

Ionization energies of shallow donors ΔE_d (meV): $0.5 \le \Delta E_d \le 1$

Ionization energies of shallow acceptors ΔE_a: (after Yen *et al.* [1988])

for $x = 0.04$	$\Delta E_a = 21.8$ meV
for $x = 0.13$	$\Delta E_a = 13.4$ meV

6.3. Electrical Properties

6.3.1. *Mobility and Hall Effect*

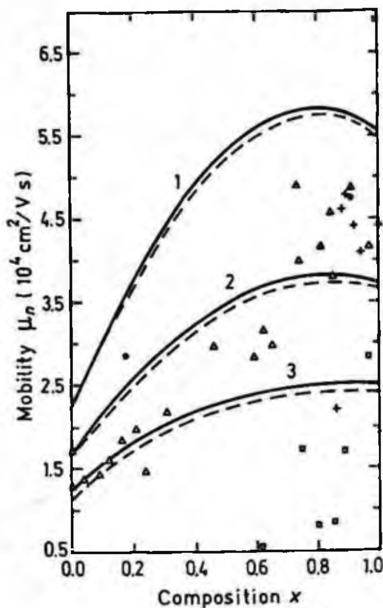

Fig. 6.3.1. Electron drift mobility (dashed curves) and Hall mobility (solid curves) versus x for $InAs_{1-x}Sb_x$, 300 K. Electron concentration $n = 5 \cdot 10^{16}$ cm^{-3} for all curves. Ionized impurity concentration N_I (cm^{-3}): 1. $5 \cdot 10^{16}$, 2. $1.25 \cdot 10^{17}$, 3. $2.5 \cdot 10^{17}$. Experimental points (triangles, full circles, and crosses) are taken from three different papers for $n \cong 5 \cdot 10^{16}$ cm^{-3} (after Chattopadhyay *et al.* [1981]). Squares are experimental results for $n \cong 5 \cdot 10^{15}$ cm^{-3} (from Tsukamoto *et al.* [1990]).

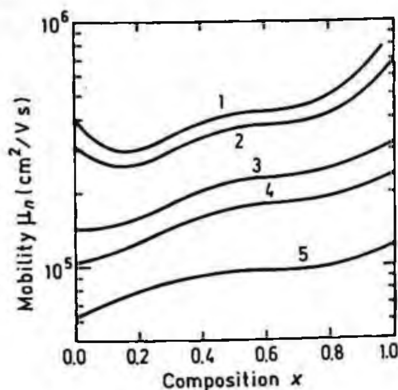

Fig. 6.3.2. Electron drift mobility of $InAs_{1-x}Sb_x$ versus x at 77 K. Ionized impurity concentration (cm^{-3}): 1. $5 \cdot 10^{14}$, 2. 10^{15}, 3. $5 \cdot 10^{15}$, 4. 10^{16}, 5. $5 \cdot 10^{16}$ (after Chin *et al.* [1992]).

(Reprinted with permission from the American Institute of Physics, © 1992.)

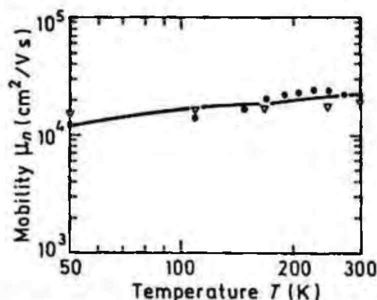

Fig. 6.3.3. Temperature dependence of electron mobility for $InAs_{1-x}Sb_x$. Solid line represents theoretical calculation. A dislocation density of $1.5 \cdot 10^8$ cm^{-2} and a compensation ratio 0.5 are included.
Open triangles: $x = 0.78$
Full circles: $x = 0.76$
$n \cong 10^{17}$ cm^{-3} (after Egan *et al.* [1994]).

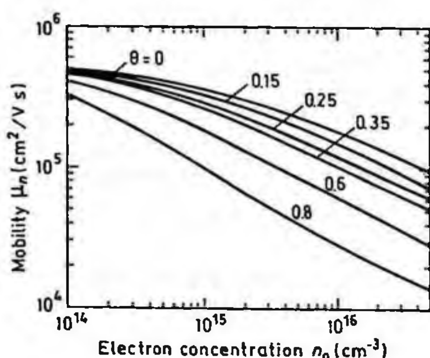

Fig. 6.3.4. Electron mobility versus electron concentration $n = N_d - N_a$ with series of compensation ratios $\theta = N_a/N_d$ for $x = 0.6$, 77 K (after Chin *et al.* [1992]).

(Reprinted with permission from the American Institute of Physics, © 1992.)

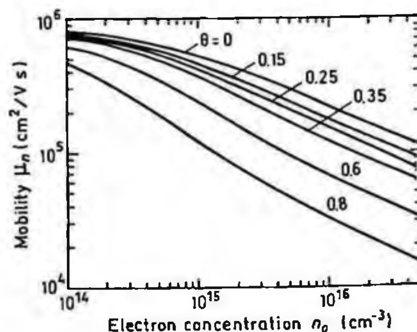

Fig. 6.3.5. Electron mobility versus electron concentration $n = N_d - N_a$ with series of compensation ratios $\theta = N_a/N_d$ for $x = 0.9$, 77 K (after Chin *et al.* [1992]).

(Reprinted with permission from the American Institute of Physics, © 1992.)

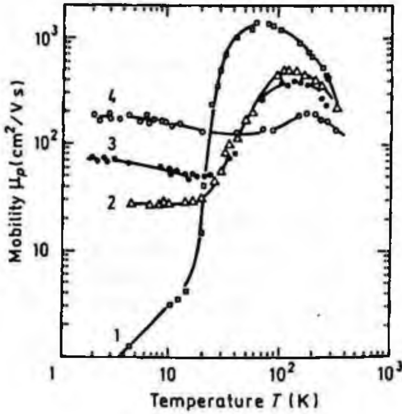

Fig. 6.3.6. Hole Hall mobility ($R \cdot \sigma$) versus temperature for different acceptor densities. $x = 0$ (InAs) (after Kesamanly *et al.* [1968]). Hole concentration at 300 K p_o(cm^{-3}): 1. $5.7 \cdot 10^{16}$, 2. $2.6 \cdot 10^{17}$, 3. $4.2 \cdot 10^{17}$, 4. $1.3 \cdot 10^{18}$.

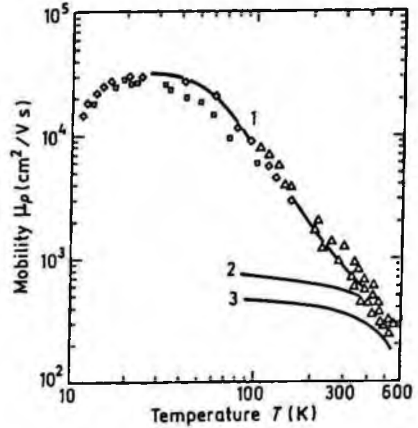

Fig. 6.3.7. Hole Hall mobility versus temperature for different hole concentrations. $x = 1$ (InSb) p_o(cm^{-3}): 1. $8 \cdot 10^{14}$, 2. $3.15 \cdot 10^{18}$, 3. $2.5 \cdot 10^{19}$ (after Zimpel *et al.* [1989] and Filipchenko and Bolshakov [1976]).

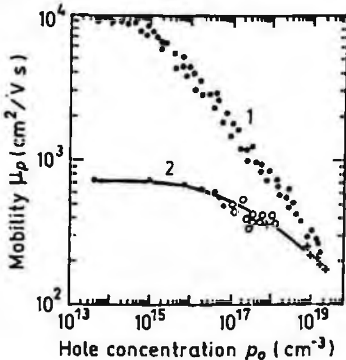

Fig. 6.3.8. Hole mobility versus hole concentration 1. 77 K (after Filipchenko and Bolshakov [1976]), 2. 290 K (after Wiley [1975]). $x = 1$ (InSb).

6.3.2. *Impact Ionization*

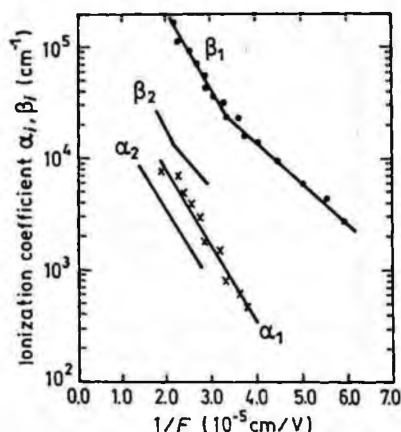

Fig. 6.3.9. The dependences of ionization rates for electrons (α) and holes (β) versus 1/F, 77 K. α_1, β_1 – for $x = 0$ (InAs) (after Mikhailova *et al.* [1976]). α_2, β_2 – for $x = 0.12$ (after Matveev *et al.* [1979]).

For electrons:

$$\alpha_i = \alpha_o \exp(-F_{no}/F) \tag{6.3.1}$$

$x = 0$ $\alpha_o = 1.8 \cdot 10^5$ cm^{-1}, $F_{no} = 1.6 \cdot 10^5$ V/cm (77 K)

$x = 0.12$ $\alpha_o = 0.7 \cdot 10^5$ cm^{-1}, $F_{no} = 1.5 \cdot 10^5$ V/cm (77 K)

For holes:

$$\beta_i = \beta_o \exp(-F_{po}/F) \tag{6.3.2}$$

$x = 0$ $1.5 \cdot 10^4$ V/cm $< F < 3 \cdot 10^4$ V/cm -
$\beta_o = 4.7 \cdot 10^5$ cm^{-1}, $F_{po} = 0.85 \cdot 10^5$ V/cm (77 K)

$3 \cdot 10^4$ V/cm $< F < 6 \cdot 10^4$ V/cm -
$\beta_o = 4.5 \cdot 10^6$ cm^{-1}, $F_{po} = 1.54 \cdot 10^5$ V/cm (77 K)

$x = 0.12$ $F < 4.5 \cdot 10^4$ V/cm $\beta_o = 1.1 \cdot 10^5$ cm^{-1}, $F_{po} = 1.0 \cdot 10^5$ V/cm
$F > 4.5 \cdot 10^4$ V/cm $\beta_o = 6 \cdot 10^5$ cm^{-1}, $F_{po} = 1.75 \cdot 10^5$ V/cm

6.3.3. *Recombination Parameters*

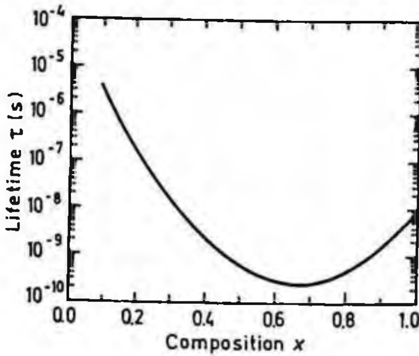

Fig. 6.3.10. Carrier lifetime in intrinsic $InAs_{1-x}Sb_x$ versus x (for Auger recombination), 300 K (after Rogalski and Orman [1985]).

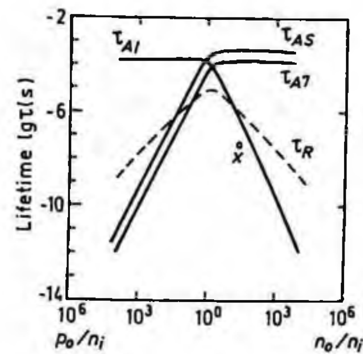

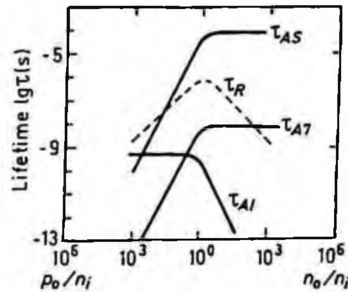

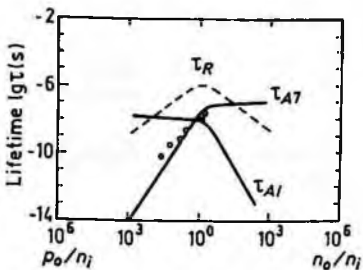

Fig. 6.3.11. Dependence of carrier lifetime on normalized doping concentration for (a) $x = 0$ (InAs), (b) $x = 0.65$, (c) $x = 1$ (InSb), 300 K. n_i is the intrinsic concentration. Dashed lines represent radiative lifetimes. Solid lines represent Auger recombination lifetimes for different components of Auger processes. Symbols represent the experimental data (after Rogalski and Orman [1985]).

6.4. Optical Properties

Infrared refractive index $n_\infty = (k_\infty)^{1/2}$ at 300 K:

$x = 0$	3.51
$x = 1$	4.0

Long wave *TO* phonon energy $h\nu_{TO}$ at 300 K (meV):

$x = 0$	27
$x = 1$	≈ 22.9

Long wave *LO* phonon energy $h\nu_{LO}$ at 300 K (meV):

$x = 0$	29
$x = 1$	≈ 24.4

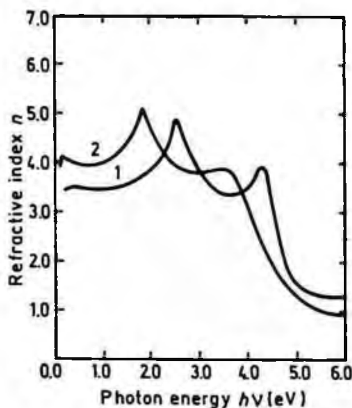

Fig. 6.4.1. Refractive index n versus photon energy for $x = 0$ (InAs) – curve 1 and $x = 1$ (InSb) – curve 2, 300 K (after Adachi [1989]).

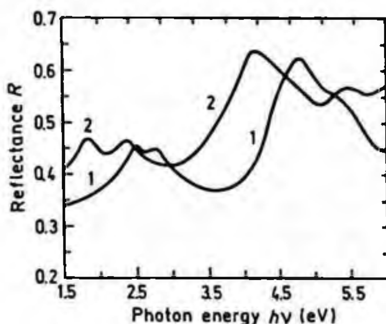

Fig. 6.4.2. Normal incidence reflectivity versus photon energy for $x = 0$ (InAs) – curve 1 and $x = 1$ (InSb) – curve 2, 300 K (after Aspnes and Studna [1983]).

(Reprinted with permission from The American Physical Society, © 1983.)

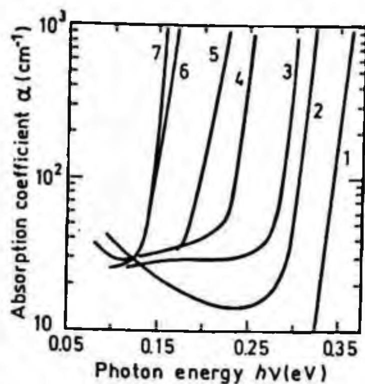

Fig. 6.4.3. Optical absorption coefficient versus photon energy for different values of x. 1. $x = 0$, 2. $x = 0.05$, 3. $x = 0.07$, 4. $x = 0.15$, 5. $x = 0.21$, 6. $x = 0.31$, 7 - $x = 0.89$ (after Stringfellow and Greene [1971]).

(Reprinted with permission from the Electrochemical Society, Inc., © 1971.)

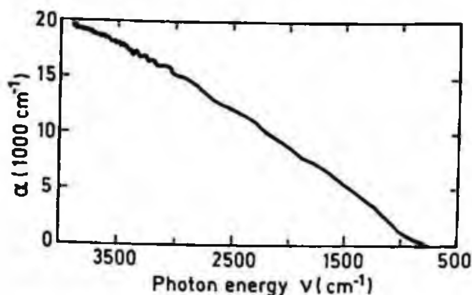

Fig. 6.4.4. Absorption coefficient of $InAs_{0.22}Sb_{0.78}$ versus photon energy, 300 K (after Bethea *et al.* [1988]).

(Reprinted with permission from the American Institute of Physics, © 1988.)

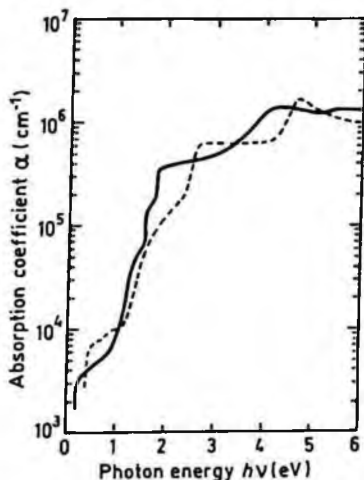

Fig. 6.4.5. Absorption coefficient versus photon energy for $x = 0$ (InAs) and $x = 1$ (InSb), 300 K Dashed line – $x = 0$. Solid line – $x = 1$ (after Adachi [1989]).

6.5. Thermal Properties

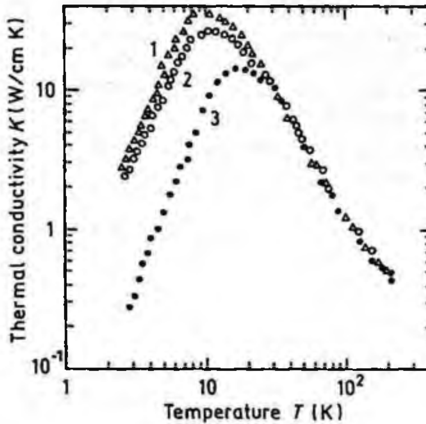

Fig. 6.5.1. Temperature dependences of thermal conductivity for $x=0$ (InAs). 1, 2. n-type samples. 1. $n_o=1.6\cdot10^{16}$ cm^{-3}, 2. $n_o=2\cdot10^{17}$ cm^{-3}. 3. p-type sample, $p_o=2\cdot10^{17}$ cm^{-3} (after Tamarin and Shalyt [1971]).

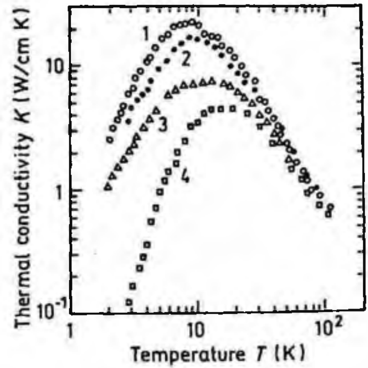

Fig. 6.5.2. Temperature dependences of thermal conductivity for $x=1$ (InSb). 1 – 3. n-type samples. Electron concentration n_o (cm^{-3}) at 78 K: 1. $2\cdot10^{14}$, 2. $4.8\cdot10^{16}$, 3. $4\cdot10^{18}$. 4. p-type sample. Hole concentration at 78 K, $p_o\sim6\cdot10^{18}$ cm^{-3} (after Kosarev *et al.* [1971]).

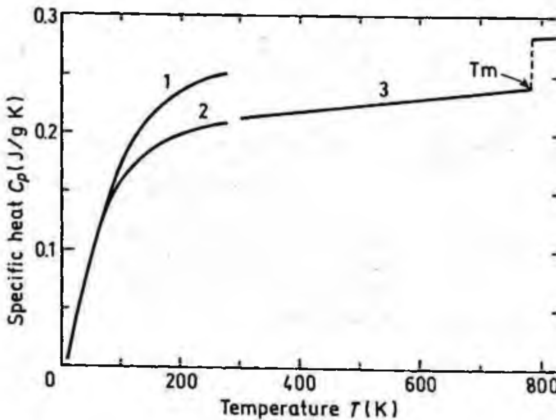

Fig. 6.5.3. Temperature dependences of specific heat at constant pressure. 1. $x=0$ (InAs) (after Piesbergen [1963]). 2, 3. $x=1$ (InSb) 2. after Piesbergen [1963], 3. after Okhotin *et al.* [1972].

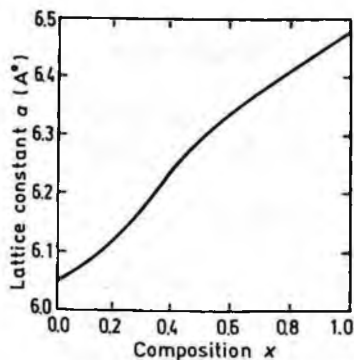

Fig. 6.5.4. Lattice constant as a function of x (after Rogalski [1989]).

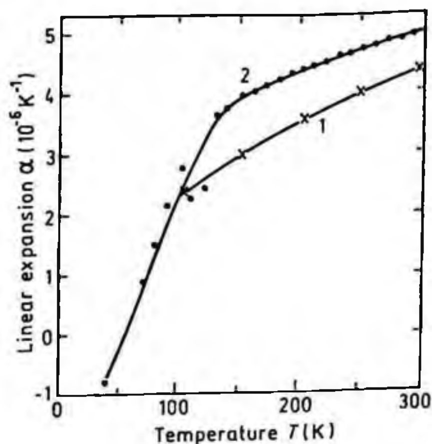

Fig. 6.5.5. Temperature dependences of linear expansion coefficient for $x = 0$ (InAs) and $x = 1$ (InSb). 1. $x = 0$ (after Sirota and Berger [1959]), 2. $x = 1$ (after Gibbons [1958]).

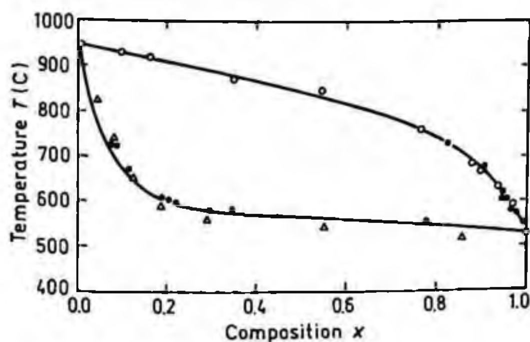

Fig. 6.5.6. Pseudobinary phase diagram for $InAs_{1-x}Sb_x$ system (after Stringfellow and Greene [1971]).

6.6. Mechanical Properties, Elastic Constants, Lattice Vibrations, Other Properties

Density		$5.68 + 0.09x$ (g/cm^3)
Hardness		~ 4 (on the Mohs scale)
Surface microhardness (using Knoop's pyramid test)		$x = 0$ (InAs) – 430 kg/mm^2 $x = 1$ (InSb) – 220 kg/mm^2
Cleavage plane		{110}, {111}
Elastic constants at 300 K:		
C_{11}		$(8.34 - 1.67x) \cdot 10^{11}$ dyn/cm^2
C_{12}		$(4.54 - 0.89x) \cdot 10^{11}$ dyn/cm^2
C_{44}		$(3.95 - 0.93x) \cdot 10^{11}$ dyn/cm^2
Bulk modulus	$B_s = \frac{C_{11} + 2C_{12}}{3}$	$B_s = (5.81 - 1.15x) \cdot 10^{11}\text{dyn/cm}^2$
Anizotropy factor	$A = \frac{C_{11} - C_{12}}{2C_{44}}$	$A \cong 0.5$
Shear modulus	$C' = (C_{11} - C_{12})/2$	$C' = (1.9 - 0.39x) \cdot 10^{11}\text{dyn/cm}^2$
[100] Young's modulus	$Y_0 = \frac{(C_{11} + 2C_{12})(C_{11} - C_{12})}{(C_{11} + C_{12})}$	$Y_0 = (5.14 - 1.05x) \cdot 10^{11}\text{dyn/cm}^2$
[100] Poisson ratio	$\sigma_0 = \frac{C_{12}}{C_{11} + C_{12}}$	$\sigma_0 \cong 0.35$

Acoustic Wave Speeds

Wave propagation direction	Wave character	Expression for wave speed	Wave speed (in units of 10^5 cm/s)
[100]	V_L	$(C_{11}/\rho)^{1/2}$	$3.83 - 0.43x$
	V_T	$(C_{44}/\rho)^{1/2}$	$2.64 - 0.35x$
[110]	V_l	$[(C_{11}+C_{12}+2C_{44})/2\rho)]^{1/2}$	$4.28 - 0.52x$
	$V_{t\parallel}$	$V_{t\parallel} = V_T = (C_{44}/\rho)^{1/2}$	$2.64 - 0.35x$
	$V_{t\perp}$	$[(C_{11}-C_{12})/2\rho)]^{1/2}$	$1.83 - 0.21x$
[111]	V_l'	$[(C_{11}+2C_{12}+4C_{44})/3\rho)]^{1/2}$	$4.41 - 0.53x$
	V_t'	$[(C_{11}-C_{12}+C_{44})/3\rho)]^{1/2}$	$2.13 - 0.26x$

Phonon frequencies (in units of 10^{12} Hz):

	$x = 0$ (InAs)	$x = 1$ (InSb)
$\nu_{LO}(\Gamma)$	7.01	5.90
$\nu_{TO}(\Gamma)$	6.44	5.54
$\nu_{TA}(X)$	1.70	1.12
$\nu_{LA}(X)$	4.94	4.30
$\nu_{LO}(X)$	6.20	4.75
$\nu_{TO}(X)$	6.47	5.38
$\nu_{TA}(L)$	1.50	0.98
$\nu_{LA}(L)$	4.46	3.81
$\nu_{LO}(L)$	6.26	4.82
$\nu_{TO}(L)$	6.44	5.31

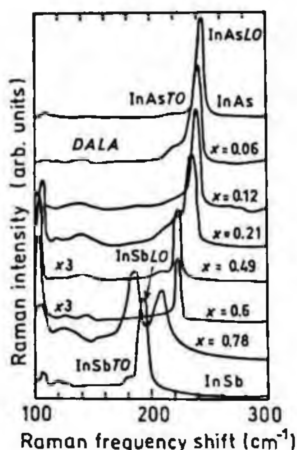

Fig. 6.6.1. Raman scattering spectra for $InAs_{1-x}Sb_x$ (DALA-disorder-activated longitudinal acoustic phonon) (after Cherng *et al.* [1988]).
(Reprinted with permission from the American Institute of Physics, © 1988.)

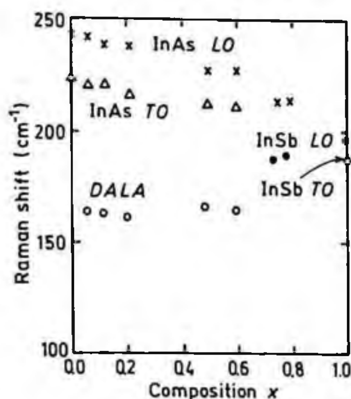

Fig. 6.6.2. Raman frequency shift versus composition parameter x (after Cherng *et al.* [1988]).
(Reprinted with permission from the American Institute of Physics, © 1988.)

Raman frequencies (cm^{-1}):

	$x = 0$ (InAs)	$x = 1$ (InSb)
LO	242	193
TO	220	185

Piezoelectric constant e_{14} (C/m^2):	$x = 0$ (InAs)	$-4.5 \cdot 10^{-2}$
	$x = 1$ (InSb)	$-7.0 \cdot 10^{-2}$
Electron g-factor:	$x = 0$ (InAs)	-17.5
	$x = 1$ (InSb)	-50.6

References

Adachi, S., *J. Appl. Phys.* **66**, 12 (1989) 6030–6040.

Aspnes, D. E. and A. A. Studna, *Phys. Rev.* **B27**, 2 (1983) 985–1009.

Bethea, C. G., B. F. Levine, M. Y. Yen, and A. Y. Cho, *Appl. Phys. Lett.* **53**, 4 (1988) 291–292.

Chattopadhyay, D., S. K. Sutradhar, and R. P. Nag, *J. Phys C: Solid State Phys.* **14**, 6 (1981) 891–908.

Cherng, Y. T., K. Y. Ma, and G. B. Stringfellow, *Appl. Phys. Lett.* **53**, 10 (1988) 886–887.

Chin, V. W., R. J. Egan, and T. L. Tansley, *J. Appl. Phys.* **72**, 4 (1992) 1410–1415.

Egan, R. J., V. W. Chin, and T. L. Tansley, *J. Appl. Phys.* **75**, 5 (1994) 2473–2476.

Fang, Z. M., K. Y. Ma, D. H. Jaw, R. M. Cohen, and G. B. Stringfellow, *J. Appl. Phys.* **67**, 11 (1990) 7034–7039.

Filipchenko, A. S. and L. P. Bolshakov, *Phys. Stat. Solidi (b)* **77**, 1 (1976) 53–58.

Gibbons, D. F., *Phys. Rev.* **112**, 1 (1958) 136–140.

Kesamanly, F. P., T. S. Lagunova, D. N. Nasledov, L. A. Nikolaeva, and M. N. Pivovarov, *Fiz. Tekh. Poluprov.* **2**, 1 (1968) 56–63 (in Russian).

Kosarev, V. V., P. V. Tamarin, and S. S. Shalyt, *Phys. Stat. Solidi (b)* **44**, 2 (1971) 525–534.

Matveev, B. A., M. P. Mikhailova, S. V. Slobodchikov, N. N. Smirnova, N. M. Stus', and G. N. Talalakin, *Sov. Phys. Semicond.* **13**, 3 (1979) 294–297.

Mikhailova, M. P., A. A. Rogachev, and I. N. Yassievich, *Sov. Phys. Semicond.* **10**, 8 (1976) 866–871.

Okhotin, A. S., A. S. Pushkarskii, and V. V. Gorbachev, *Thermophysical Properties of Semiconductors* Moskow, "Atom" Publ. House, 1972, (in Russian).

Piesbergen, U., *Zeit. fur Naturforschung* **18a**, 2 (1963) 141–147.

Rogalski A. and Z. Orman, *Infrared Phys.* **25**, 3 (1985) 551–560.

Rogalski, A., *Prog. Quant. Electr.* **13**, (1989) 191–231.

Rogalski, A. and K. Jozwikowski, *Infrared Physics* **29**, 1 (1989) 35–42.

Sirota, N. N. and L. I. Berger, *Inzh. Fiz. Zhurnal, Akad. Nauk Beloruss. SSR* **2** (1959) 104.

Stringfellow, G. B. and P. E. Greene, *J. Electrochem. Soc.* **118**, 5 (1971) 805–810.

Tamarin, P. V. and S. S. Shalyt, *Sov. Phys. Semicond.* **5**, 5 (1971) 1097–1098.

Tsukamoto, S., P. Bhattacharya, Y. C. Chen, and J. H. Kim, *J. Appl. Phys.* **67**, 11 (1990) 6819–6822.

Wieder, H. H. and A. R. Clawson, *Thin Solid Films* **15**, 2 (1973) 217–221.

Wiley, J. D., *Semiconductors and Semimetals*, ed. by R. K. Willardson and A. C. Beer, Academic Press, NY, vol. 10, 1975, p. 91.

Yen, M. Y., R. People, K. W. Wecht, and A. Y. Cho, *Appl. Phys. Lett.* **52**, 6 (1988) 489–491.

Zimpel, M., M. Oszwadowski, and J. Goc, *Acta Phys. Polonica* **A75**, 2 (1989) 297–300.

CHAPTER 7

GALLIUM INDIUM ARSENIDE PHOSPHIDE ($Ga_xIn_{1-x}As_yP_{1-y}$)

Yu. A. Goldberg and Natalya M. Shmidt

Ioffe Institute, St. Petersburg, Russia

7.1. Basic Parameters at 300 K

Crystal structure	Zinc blende
Group of symmetry	$T_d^2 - F\bar{4}3m$

To estimate the value of any parameter b of $Ga_xIn_{1-x}As_yP_{1-y}$ one can use an approximate formula (after Adachi [1982]):

$$b(x,y) \cong (1-x)y \cdot b_{InAs} + (1-x)(1-y) \cdot b_{InP} + xy \cdot b_{GaAs} + x(1-y) \cdot b_{GaP} \qquad (7.1.1)$$

Lattice constant a (Å) 5.4505 (GaP) ÷ 6.0583 (InAs)

$$a \cong 5.8688 - 0.4176x + 0.1896y + 0.0125xy \text{ (Å)} \text{ (after Adachi [1982])} \qquad (7.1.2)$$

For compositions lattice-matched:

to InP $\left(x \cong \dfrac{0.1894y}{0.4184 - 0.013y} \cong 0.47y\right)$ $a = 5.8687$ Å

to GaAs $\left(x \cong \dfrac{1+y}{2.08}\right)$ $a = 5.65325$ Å

to ZnSe $\left(x \cong \dfrac{1.06+y}{2.06}\right)$ $a = 5.6676$ Å

Energy gap E_g (eV)	0.354 (InAs) ÷ 2.27 (GaP)
Direct energy gap (eV)	
min	0.354 (InAs)
max	2.17

For direct energy gap compositions:

$$E_g \cong 1.35 + 0.668x - 1.068y + 0.758x^2 + 0.078y^2 - 0.069xy - 0.332x^2y + 0.03xy^2 \text{ (eV)} \quad (7.1.3)$$

7.1.1. *Basic Properties of* $Ga_xIn_{1-x}As_yP_{1-y}$ *Compositions Lattice-Matched to InP at 300 K* ($x \cong 0.47y$)

	$y=0$ (InP)	$y=1$ ($Ga_{0.47}In_{0.53}As$)	$0<y<1$
Number of atoms in 1 cm^3	$3.96 \cdot 10^{22}$	$3.96 \cdot 10^{22}$	$3.96 \cdot 10^{22}$
Auger recombination coefficient (cm^6/s)	$9 \cdot 10^{-31}$		
$y=0.24$			$1.1 \cdot 10^{-31}$
$y=0.6$			$2.9 \cdot 10^{-30}$
Debye temperature (K)	425	322	$425 - 103y$
Density (g/cm^3)	4.81	5.50	$4.81 + 0.552y + 0.138y^2$
Dielectric constant			
static	12.5	13.94	$12.5 + 1.44y$
high frequency	9.61	11.61	$9.61 + 2y$

	$y = 0$ (InP)	$y = 1$ ($Ga_{0.47}In_{0.53}As$)	$0 < y < 1$
Effective electron mass (in units of m_o)	0.08	0.041	$0.08 - 0.039y$
Effective hole mass: (in units of m_o)			
heavy	0.6	0.42	$0.6 - 0.18y$
light	0.12	0.051	$0.12 - 0.099y + 0.03y^2$
Lattice constant (Å)	5.8687	5.8687	5.8687
Optical phonon energy (meV)	43		

Band structure and carrier concentration

Energy gap (eV)	1.344	0.74	$1.344 - 0.738y + 0.138y^2$
Energy separation between X-valley and top of the valence band E_X (eV)	2.19	1.33	$2.19 - 0.86y$
Energy separation between L-valley and top of the valence band E_L (eV)	1.93	1.2	$1.93 - 0.73y$
Energy separation of spin-orbital splitting E_{so} (eV)	0.11	0.35	$0.11 + 0.24y$
Intrinsic carrier concentration (cm^{-3})	$1.3 \cdot 10^7$	$6.7 \cdot 10^{11}$	
$y = 0.27$			$4.3 \cdot 10^8$
$y = 0.47$			$4.4 \cdot 10^9$
$y = 1$			$6.7 \cdot 10^{11}$
Effective conduction band density of states (cm^{-3})	$5.7 \cdot 10^{17}$	$2.1 \cdot 10^{17}$	$2.5 \cdot 10^{19}(0.08 - 0.039y)^{3/2}$

	$y=0$ (InP)	$y=1$ ($Ga_{0.47}In_{0.53}As$)	$0<y<1$
Effective valence band density of states (cm^{-3})	$1.1\cdot10^{19}$	$6.8\cdot10^{18}$	$2.5\cdot10^{19}(0.6-0.18y)^{3/2}$
Electrical properties			
Breakdown field (V/cm)	$\approx 5\cdot10^5$	$\approx 2\cdot10^5$	$\approx(5\div2)\cdot10^5$
Mobility ($cm^2/V{\cdot}s$)			
electrons	≤ 5400	≤ 12000	$\leq(5400-7750y+14400y^2)$
holes	≤ 200	≤ 300	$\leq(200-400y+500y^2)$
Diffusion coefficient (cm^2/s)			
electrons	≤ 130	≤ 300	$\leq(130-190y+360y^2)$
holes	≤ 5	≤ 7.5	$\leq(5-10y+12.5y^2)$
Electron thermal velocity (m/s)	$3.9\cdot10^5$	$5.5\cdot10^5$	$(3.9+1.6y)\cdot10^5$
Hole thermal velocity (m/s)	$1.7\cdot10^5$	$2\cdot10^5$	$(1.7+0.3y)\cdot10^5$
Optical properties			
Infrared refractive index	3.1	3.56	$3.1+0.46y$
Radiative recombination coefficient (cm^3/s)	$1.2\cdot10^{-10}$		
$y=0.24$			$1.2\cdot10^{-10}$
$y=0.6$			$1.1\cdot10^{-10}$
Thermal and mechanical properties			
Bulk modulus (dyn/cm^2)	$7.1\cdot10^{11}$	$6.61\cdot10^{11}$	$(7.1-0.516y+0.02y^2)\cdot10^{11}$
Melting point (°C)	1060	≈ 1100	≈ 1100
Specific heat (J/g °C)	0.31	0.34	$0.31+0.038y-0.008y^2$
Thermal conductivity (W/cm °C)	0.68	0.05	$0.68-1.77y+1.25y^2$
Thermal expansion, linear, (°C^{-1})	$4.6\cdot10^{-6}$	$5.66\cdot10^{-6}$	$(4.6+1.06y)\cdot10^{-6}$

7.2. Band Structure and Carrier Concentration

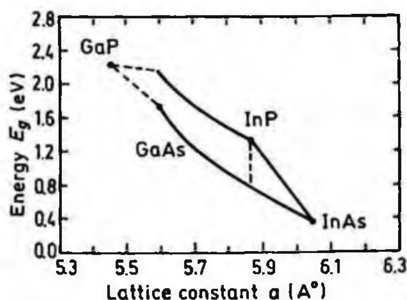

Fig. 7.2.1. Energy gap E_g of $Ga_xIn_{1-x}As_yP_{1-y}$ versus lattice constant. Solid lines represent direct band region. Dashed lines represent indirect band region (after Foyt [1981]).

(Reprinted with permission from Elsevier Science, © 1981.)

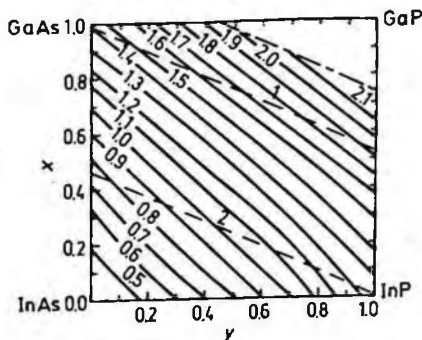

Fig. 7.2.2. Energy gap E_g of $Ga_xIn_{1-x}As_yP_{1-y}$ versus x and y, 300 K. Dashed lines represent the compositions lattice-matched to GaAs (1) and InP (2) (after Gorelenok *et al.* [1981]).

(Reprinted with permission from the American Institute of Physics, © 1981.)

For direct band region (300 K):

$$E_g \cong 1.35 + 0.668x - 1.068y + 0.758x^2 + 0.078y^2 \\ - 0.069xy - 0.332x^2y + 0.03xy^2 \text{ (eV)} \tag{7.2.1}$$

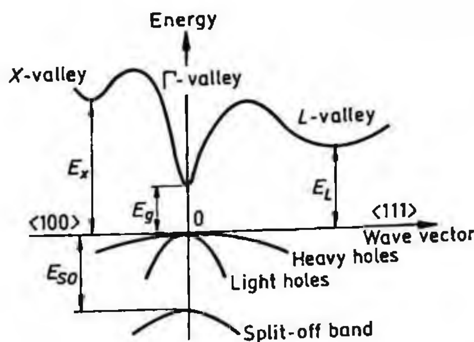

Fig. 7.2.3. Band structure of $Ga_xIn_{1-x}As_yP_{1-y}$ alloys lattice-matched to InP. Important minima of the conduction band and maxima of the valence band.

For compositions lattice-matched to InP (300 K):

$$E_g \cong 1.344 - 0.738y + 0.138y^2 \text{ (eV)} \tag{7.2.2}$$

For compositions lattice-matched to InP (4.2 K):

$$E_g \cong 0.41(1-x)y + 1.42(1-x)(1-y) + 1.51xy + 2.34x(1-y) \\ - 0.54x(1-x) - 0.17y(1-y) \cong 1.42 - y + 0.37y^2 \text{ (eV)} \tag{7.2.3}$$

(after Benzaquen *et al.* [1994])

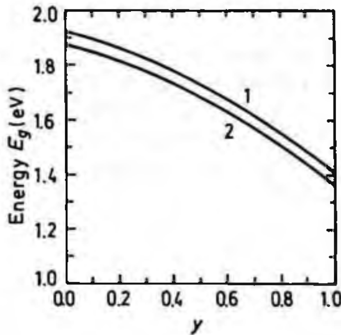

Fig. 7.2.4. Energy gap E_g as a function of y for $Ga_xIn_{1-x}As_yP_{1-y}$ lattice-matched to GaAs (1) and ZnSe (2), 300 K (after Adachi [1982]).

(Reprinted with permission from the American Institute of Physics, © 1982.)

7.2.1. *Temperature Dependences*

Temperature dependence of the energy gap for $Ga_xIn_{1-x}As_yP_{1-y}$ lattice-matched to InP (after Satzke *et al.* [1988]):

$$E_g = E_g(0) - 4.3 \cdot 10^{-4} \cdot \frac{T^2}{T + 224} \text{ (eV)} \tag{7.2.4}$$

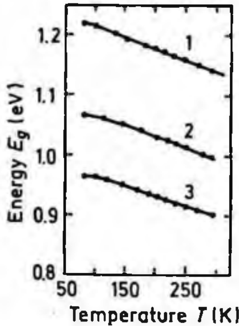

Fig. 7.2.5. The temperature dependences of the energy gap E_g for three $Ga_xIn_{1-x}As_yP_{1-y}$ compositions lattice-matched to InP. 1. $y = 0.3$, 2. $y = 0.48$, 3. $y = 0.69$ (after Yamazoe *et al.* [1981]).
(Reprinted with permission from IEEE, © 1981.)

Temperature dependence of lasing wavelength λ_0 for GaInAsP/InP double-heterostructure lasers:

$$\frac{d\lambda_0}{dT} \cong 4 \text{ Å/K} \quad \text{at} \quad \lambda_0 = 1.3\,\mu\text{m} \;\; (y = 0.6)$$

(after Arai *et al.* [1980])

$$\frac{d\lambda_0}{dT} \cong 5 \text{ Å/K} \quad \text{at} \quad \lambda_0 = 1.55\,\mu\text{m} \;\; (y = 0.9)$$

Effective density of states in the conduction band N_c (for GaInAsP alloys lattice-matched to InP):

$$N_c \cong 4.82 \cdot 10^{15} \left(\frac{m_\Gamma}{m_o}\right)^{3/2} T^{3/2}$$
$$= 4.82 \cdot 10^{15} \cdot T^{3/2} (0.08 - 0.039y)^{3/2} \text{ (cm}^{-3}\text{)} \qquad (7.2.5)$$

Effective density of states in the valence band N_v (for GaInAsP alloys lattice-matched to InP):

$$N_v \cong 4.82 \cdot 10^{15} \cdot T^{3/2} \left(\frac{m_h}{m_o}\right)^{3/2}$$
$$= 4.82 \cdot 10^{15} \cdot T^{3/2} (0.6 - 0.18y)^{3/2} \text{ (cm}^{-3}\text{)} \qquad (7.2.6)$$

Intrinsic carrier concentration:

$$n_i = (N_c \cdot N_v)^{1/2} \exp\left(-\frac{E_g}{2k_B T}\right) \qquad (7.2.7)$$

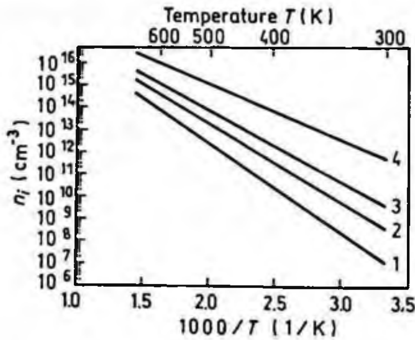

Fig. 7.2.6. The temperature dependences of the intrinsic carrier concentration for $Ga_xIn_{1-x}As_yP_{1-y}$ alloys lattice-matched to InP. 1. $y = 1$, 2. $y = 0.47$, 3. $y = 0.27$, 4. $y = 0$.

7.2.2. *Dependence on Hydrostatic Pressure*

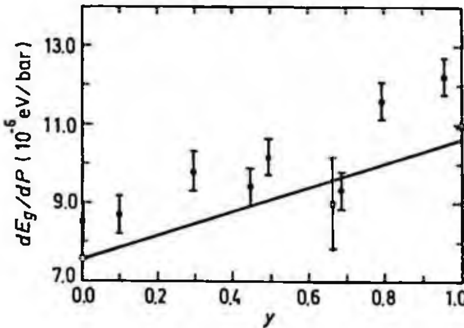

Fig.7.2.7. Hydrostatic-pressure coefficient dependence of the energy gap E_g as a function of y for $Ga_xIn_{1-x}As_yP_{1-y}$ lattice-matched to InP (after Adachi [1992]).

(Reprinted with permission from John Wiley & Sons, Inc., © 1992.)

7.2.3. *Band Discontinuities at GaInAsP/InP Heterostructure*

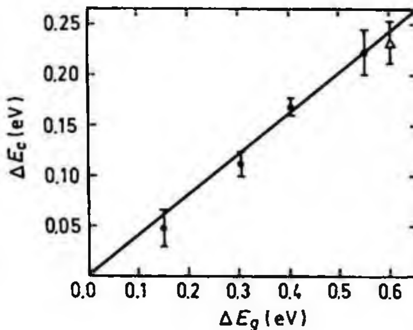

Fig.7.2.8. The conduction-band discontinuities ΔE_c versus band-gap differences ΔE_g between $Ga_xIn_{1-x}As_yP_{1-y}$ composition and InP for GaInAsP/InP heterojunctions, 300 K (after Forrest *et al.* [1984]).

(Reprinted with permission from the American Institute of Physics, © 1984.)

At 77 K:

$$\Delta E_c = 268y + 3y^2 \quad \text{(meV)}$$
$$\Delta E_v = 502y - 152y^2 \quad \text{(meV)}$$

(after Adachi [1992]).

Band discontinuities at $Ga_{0.47}In_{0.53}As$ and $Al_{0.48}In_{0.52}As$ heterojunction at 300 K:

$$\Delta E_c \cong 520 \quad \text{(meV)}$$

(see also Adachi [1992]).

7.2.4. *Effective Masses*

Electrons:

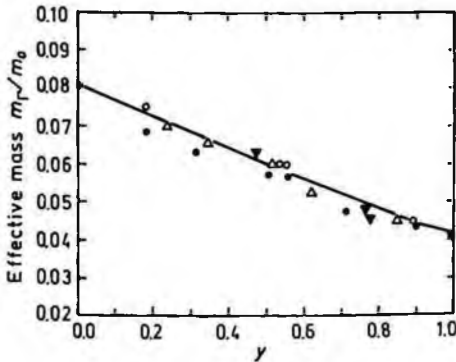

Fig. 7.2.9. Electron effective mass m_Γ in GaInAsP alloys as a function of y for compositions lattice-matched to InP (after Pearsall [1982]).

For alloys lattice-matched to InP at 300 K:

$$m_\Gamma/m_o \cong 0.08 - 0.05y + 0.017y^2 \cong 0.08 - 0.039y \tag{7.2.8}$$

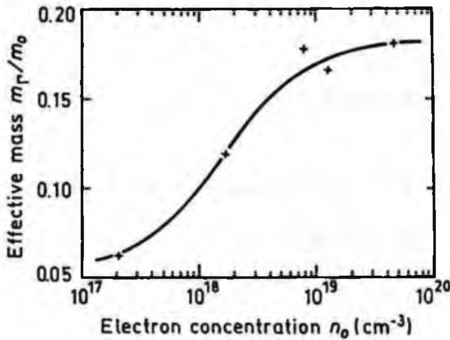

Fig. 7.2.10. Electron effective mass m_Γ in $Ga_{0.1}In_{0.9}As_{0.3}P_{0.7}$ alloy versus electron concentration, 80 K (after Vilkotsky *et al.* [1986]).
(Reprinted with permission from the American Institute of Physics, © 1986.)

Holes:

heavy	$m_h \cong (0.6 - 0.18y)m_o$
light	$m_{lp} \cong (0.12 - 0.099y + 0.03y^2)m_o$
split-off band	$m_{so} \cong (0.21 - 0.01y - 0.05y^2)m_o$

7.2.5. *Donors and Acceptors*

For composition alloys lattice-matched to InP,

Ionization energies of shallow donors (meV):

Sn, Ge, Si, Te, S ~5

Ionization energies of shallow acceptors (meV):

Zn - from 37.5 to 22 for $y = 0.3 \div 0.9$
Cd - from ~60 to 30 for $y = 0.2 \div 0.9$
Be ~40
Mg ~35

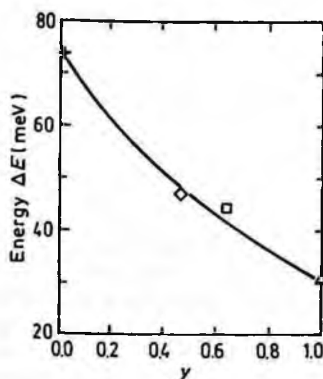

Fig. 7.2.11. Ionization energy of Cd versus y for GaInAsP alloys lattice-matched to InP (after Wehmann *et al.* [1986]).

(Reprinted with permission from IEE Publishing, © 1986.)

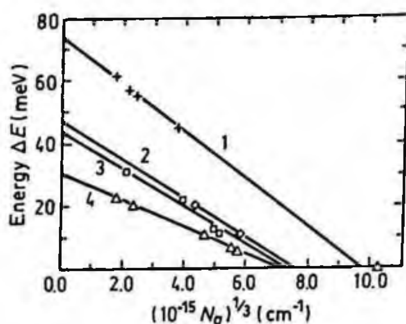

Fig. 7.2.12. Ionization energy of Cd versus acceptor concentration N_a for four GaInAsP alloys lattice-matched to InP, 77 K. 1. $y = 0$ (InP); 2. $y = 0.47$; 3. $y = 0.64$; 4. $y = 1$ (after Wehmann *et al.* [1986]).

(Reprinted with permission from IEE Publishing, © 1986.)

7.3. Electrical Properties

7.3.1. *Mobility and Hall Effect*

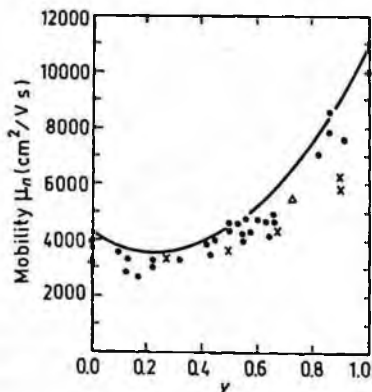

Fig. 7.3.1. Electron mobility versus alloy composition parameter y for $Ga_xIn_{1-x}As_yP_{1-y}$ lattice-matched to InP, 300 K. The experimental points correspond to samples with electron concentration $n_o = (1 \div 5) \cdot 10^{16}$ cm^{-3}. Full curve shows calculations for $n_o = 10^{15}$ cm^{-3} (after Pearsall [1982]).

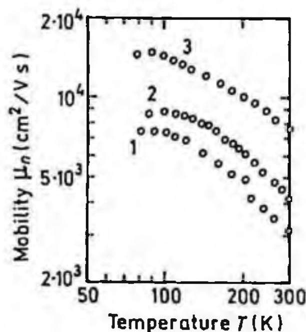

Fig. 7.3.2. Electron mobility versus temperature for $Ga_xIn_{1-x}As_yP_{1-y}$ alloys lattice-matched to InP. Electron concentration $n_o = (1 \div 5) \cdot 10^{16}$ cm^{-3}.
Curve 1. $y = 0.31$
Curve 2. $y = 0.50$
Curve 3. $y = 0.91$ (after Pearsall [1982]).

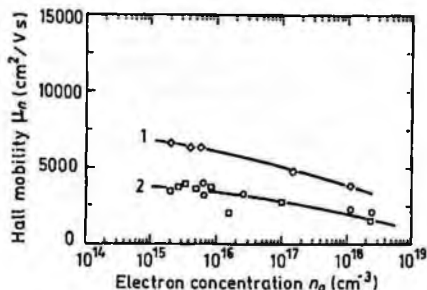

Fig. 7.3.3. Electron Hall mobility versus electron concentration for three $Ga_xIn_{1-x}As_yP_{1-y}$ alloy compositions lattice-matched to InP, 300 K.
1. $y \cong 0.9$ ($\lambda \cong (1.239/E_g) = 1.55$ μm)
2. $y \cong 0.6$ ($\lambda = 1.3$ μm, circles) and $y \cong 0.3$ ($\lambda = 1.1$ μm, squares) (after Tappura [1993]).

(Reprinted with permission from the American Institute of Physics, © 1993.)

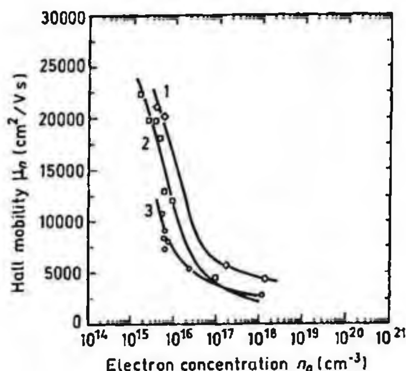

Fig. 7.3.4. Electron Hall mobility versus electron concentration for three $Ga_xIn_{1-x}As_yP_{1-y}$ alloy compositions lattice-matched to InP, 77 K.
1. $y \cong 0.9$ ($\lambda = 1.55$ μm)
2. $y \cong 0.3$ ($\lambda = 1.1$ μm)
3. $y \cong 0.6$ ($\lambda = 1.3$ μm) (after Tappura [1993]).

(Reprinted with permission from the American Institute of Physics, © 1993.)

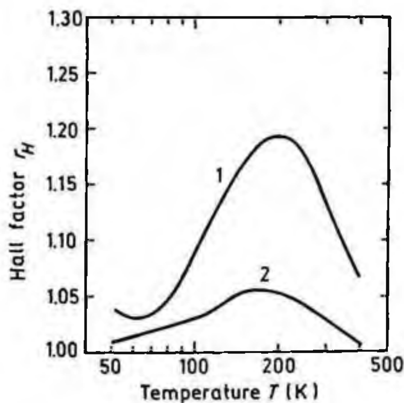

Fig. 7.3.5. Hall factor for n-type $Ga_{0.47}In_{0.53}As$ ($y = 1$) versus temperature.
1. $n_0 = 10^{15}$ cm^{-3}
2. $n_0 = 10^{17}$ cm^{-3} (after Pearsall [1982]).

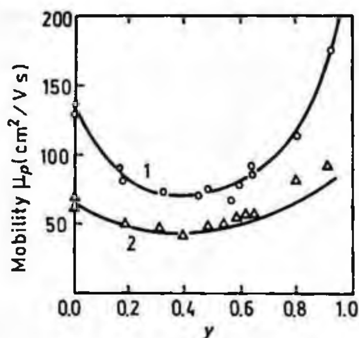

Fig. 7.3.6. Hole mobility versus alloy composition parameter y for $Ga_xIn_{1-x}As_yP_{1-y}$ lattice-matched to InP, $T = 300$ K. Hole concentration:
curve 1. $p_0 = 4 \cdot 10^{16}$ cm^{-3}
curve 2. $p_0 = 2 \cdot 10^{18}$ cm^{-3} (after Pearsall [1982]).

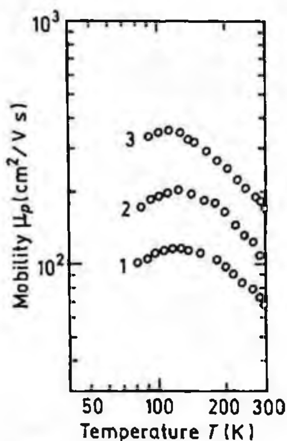

Fig. 7.3.7. Hole mobility versus temperature for $Ga_xIn_{1-x}As_yP_{1-y}$ lattice-matched to InP.
Curve 1. $y = 0.64$
Curve 2. $y = 0.8$
Curve 3. $y = 0.91$ (after Hayes *et al.* [1982]).

(Reprinted with permission from JOURNAL OF ELECTRONIC MATERIALS, a publication of the Minerals, Metals & Materials Society, Warrendale, Pennsylvania 15086.)

7.3.2. *Transport Properties in High Electric Field*

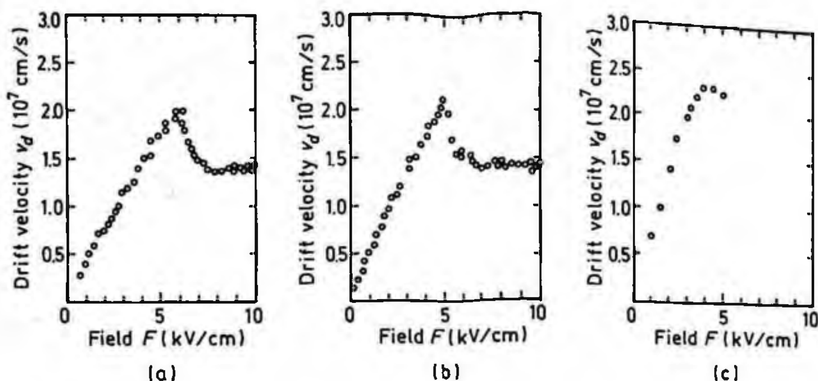

Fig. 7.3.8. Field dependences of the electron drift velocity for three GaInAsP composition alloys lattice-matched to InP, 300 K.
a. $y = 0.42$, $n_0 = 10^{15}$ cm^{-3}, b. $y = 0.65$. $n_0 = 8 \cdot 10^{15}$ cm^{-3}, c. $y = 0.8$. $n_0 = 2.5 \cdot 10^{14}$ cm^{-3} (after Galvanauskas *et al.* [1988]).

(Reprinted with permission from the American Institute of Physics, © 1988.)

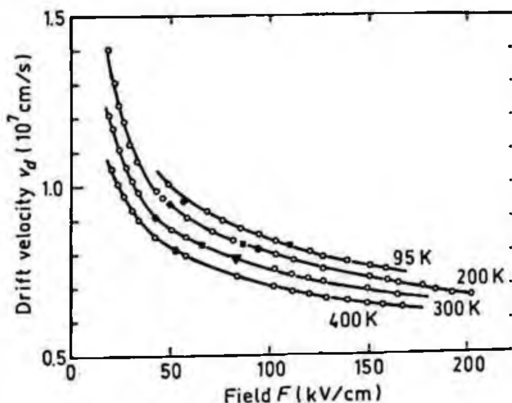

Fig. 7.3.9. Field dependences of the electron drift velocity in high electric fields. $Ga_{0.2}In_{0.8}As_{0.44}P_{0.56}$ ($\lambda_g = 1.2$ μm) (after Windhorn *et al.* [1982]).

(Reprinted with permission from the American Institute of Physics, © 1982.)

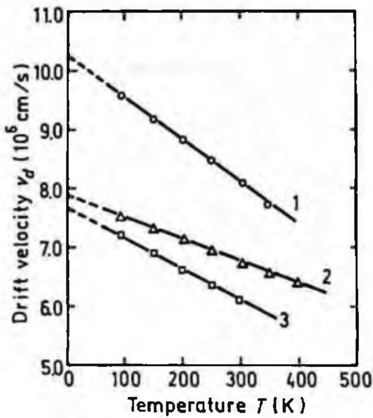

Fig. 7.3.10. Temperature dependence of the electron saturation velocity for three different composition alloys lattice-matched to InP.
1. $y = 0$, 2. $y = 0.44$, 3. $y = 1$ (after Adachi [1992]).

(Reprinted with permission from John Wiley & Sons, Inc., © 1992.)

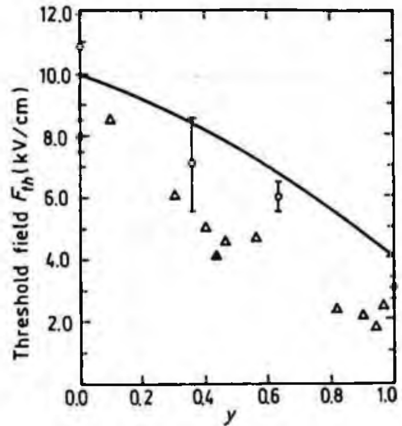

Fig. 7.3.11 Composition dependence of the threshold electric field E_{th} for the $Ga_xIn_{1-x}As_yP_{1-y}$ lattice-matched to InP, 300 K. Experimental data are taken from different papers (after Adachi [1992]).

(Reprinted with permission from John Wiley and Sons, Inc., © 1992.)

7.3.3. *Impact Ionization*

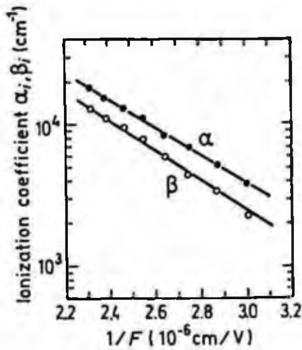

Fig. 7.3.12. Field dependence of electron (α_i) and hole (β_i) ionization coefficients for $Ga_{0.33}In_{0.67}As_{0.7}P_{0.3}$, 300 K (after Osaka *et al.* [1984]).

(*Reprinted with permission from the American Institute of Physics, © 1984.*)

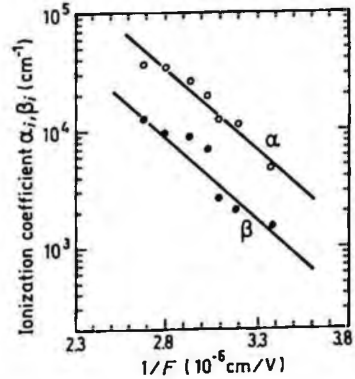

Fig. 7.3.13. Field dependence of electron (α_i) and hole (β_i) ionization coefficients for $Ga_{0.11}In_{0.89}As_{0.74}P_{0.26}$, 300 K (after Takanashi and Horikoshi [1979]).

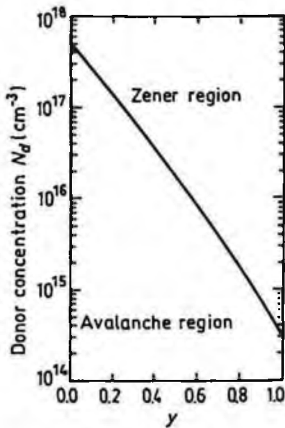

Fig. 7.3.14. Calculated donor concentration for the avalanche-Zener breakdown transition as a function of y for GaInAsP alloys lattice-matched to InP, 300 K (after Pearsall [1982]).

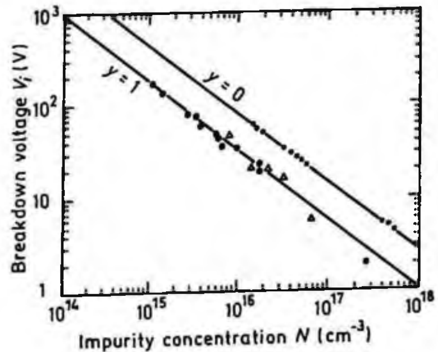

Fig. 7.3.15. Calculated avalanche breakdown voltage for InP ($y = 0$) and $Ga_{0.47}In_{0.53}As$ ($y = 1$) abrupt $p-n$ junctions, 300 K (after Pearsall [1982]).

7.3.4. *Recombination Parameters*

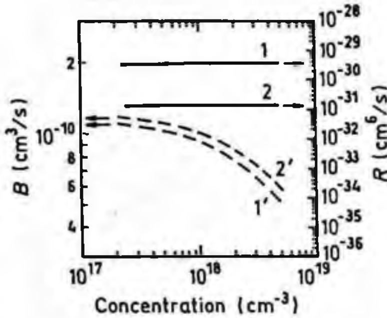

Fig. 7.3.16. Calculated dependences of Auger coefficients R (solid lines) and radiative recombination coefficients B (dashed lines) versus electron-hole concentration for two composition alloys lattice-matched to InP, 300 K. $\Delta n = \Delta p$. 1, 1'. $y = 0.6$, 2, 2'. $y = 0.24$ (after Garbuzov *et al.* [1984]).

(Reprinted with permission from the American Institute of Physics, © 1984.)

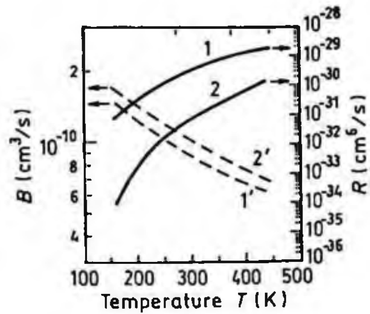

Fig. 7.3.17. Calculated dependences of Auger coefficients R (solid lines) and radiative recombination coefficients B (dashed lines) versus temperature for two composition alloys lattice-matched to InP. 1, 1'. $y = 0.6$, 2, 2'. $y = 0.24$ $\Delta n = \Delta p = 2\cdot 10^{18}$ cm^{-3} (after Garbuzov *et al.* [1984]).

(Reprinted with permission from the American Institute of Physics, © 1984.)

Characteristic surface recombination rates $\sim 10^4 \div 10^5$ cm/s

7.4. Optical Properties

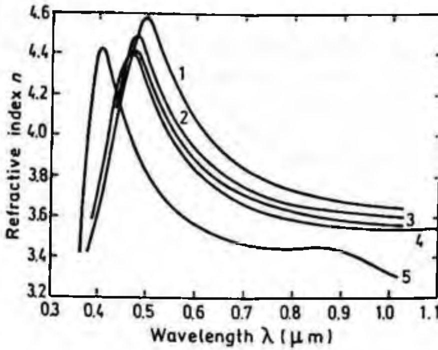

Fig. 7.4.1. Refractive index n versus wavelength for different composition alloys lattice-matched to InP, 300 K (after Burkhard *et al.* [1982]). 1. $y = 1$, 2. $y = 0.7$, 3. $y = 0.61$, 4. $y = 0.54$, 5. $y = 0$.

(Reprinted with permission from the American Institute of Physics, © 1982.)

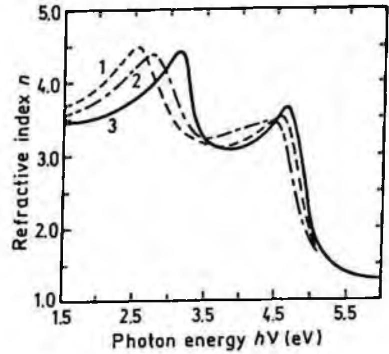

Fig. 7.4.2. Refractive index n versus photon energy for different composition alloys lattice-matched to InP, 300 K (after Kelso *et al.* [1982]). 1. $y = 1$, 2. $y = 0.55$, 3. $y = 0$.

(Reprinted with permission from The American Physical Society, © 1982.)

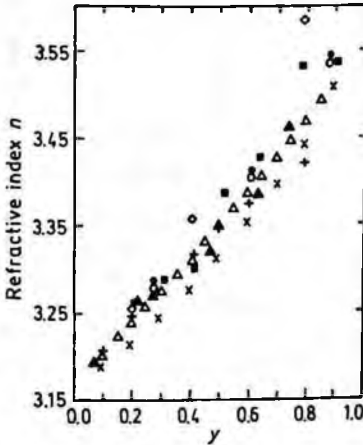

Fig. 7.4.3. Refractive index n for composition alloys lattice-matched to InP versus composition parameter y at wavelength $\lambda = 1.55$ μm. Symbols represent the experimental and calculated data from several papers (after Amiotti and Landgren [1993]).

(Reprinted with permission from the American Institute of Physics, © 1993.)

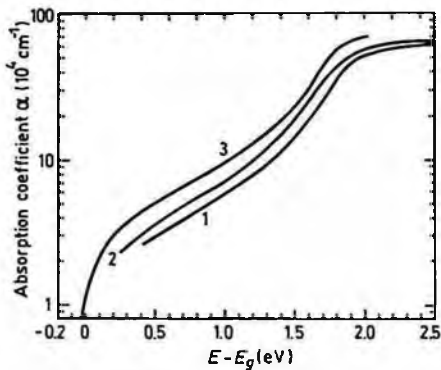

Fig. 7.4.4. The absorption coefficient versus energy difference $E-E_g$ (E_g is an energy gap) for different composition alloys of GaInAsP lattice-matched to InP, 300 K. 1. $y=1$ ($E_g \cong 0.75$ eV), 2. $0.54 < y < 0.7$, 3. $y=0$ ($E_g \cong 1.35$ eV) (after Burkhard *et al.* [1982]).

(Reprinted with permission from the American Institute of Physics, © 1982.)

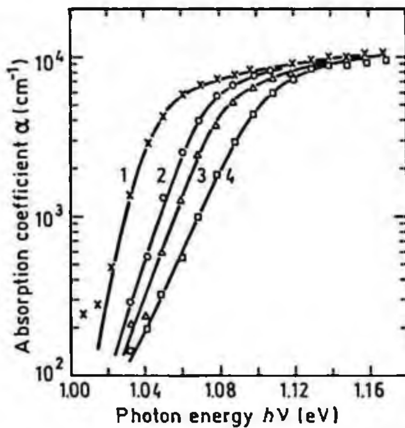

Fig. 7.4.5. The absorption coefficient near the intrinsic absorption edge for $Ga_{0.28}In_{0.72}As_{0.6}P_{0.4}$ (Ge doped, composition alloy lattice-matched to InP) versus photon energy at different doping levels N, 80 K. 1. $N=2\cdot10^{16}$ cm^{-3}, 2. $N=3.5\cdot10^{17}$ cm^{-3}, 3. $N=9.8\cdot10^{17}$ cm^{-3}, 4. $N=2.4\cdot10^{18}$ cm^{-3} (after Rajalakshmi and Arora [1990]).

(Reprinted with permission from the American Institute of Physics, © 1990.)

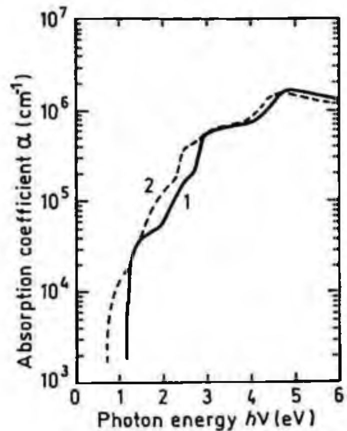

Fig. 7.4.6. The absorption coefficient versus photon energy for $Ga_xIn_{1-x}As_yP_{1-y}$ composition alloys lattice-matched to InP, 300 K. 1. $y=0.24$, 2. $y=1$ (after Adachi [1989]).

(Reprinted with permission from the American Institute of Physics, © 1989.)

7.5. Thermal Properties

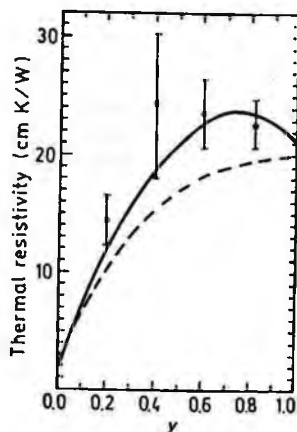

Fig.7.5.1. Thermal resistivity versus composition parameter y for $Ga_xIn_{1-x}As_yP_{1-y}$ lattice-matched to InP, 300 K. The solid circles are experimental data. The solid and dashed lines are the results calculated according to two different models (after Adachi [1992]).

(Reprinted with permission from John Wiley & Sons, Inc., © 1992.)

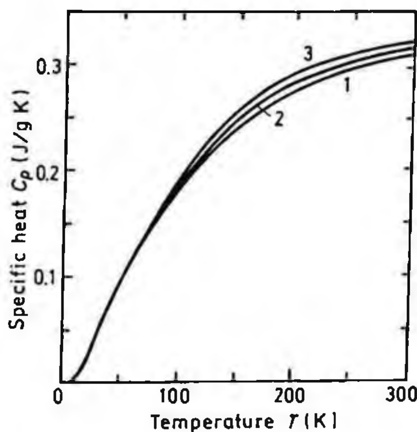

Fig. 7.5.2. Temperature dependence of specific heat at constant pressure for different $Ga_xIn_{1-x}As_yP_{1-y}$ alloys (after Sirota *et al.* [1982]). 1. $x = y = 0.2$; 2. $x = y = 0.4$; 3. $x = y = 0.8$.

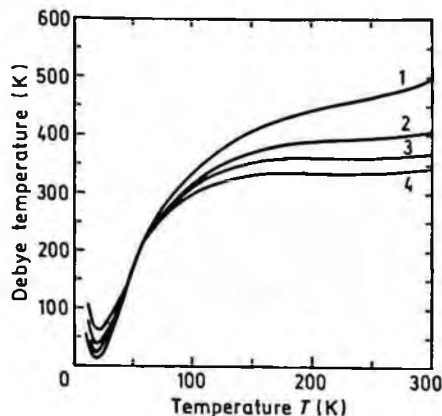

Fig. 7.5.3. Debye temperature as a function of temperature for different $Ga_xIn_{1-x}As_yP_{1-y}$ alloys (after Sirota *et al.* [1982]). 1. $x = y = 0.2$; 2. $x = y = 0.4$; 3. $x = y = 0.6$; 4. $x = y = 0.8$.

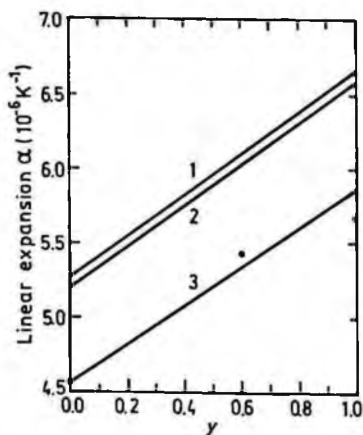

Fig. 7.5.4. Thermal expansion coefficients as a function of the y-composition parameter for $Ga_xIn_{1-x}As_yP_{1-y}$ lattice-matched to GaAs (curve 1), ZnSe (curve 2) and InP (curve 3) (after Adachi [1982]).

(*Reprinted with permission from the American Institute of Physics, © 1982.*)

1.6. Mechanical Properties, Elastic Constants, Lattice Vibrations, Other Properties

Density (for $Ga_xIn_{1-x}As_yP_{1-y}$ lattice-matched to InP) $4.81 + 0.552y + 0.138y^2$ (g/cm³)

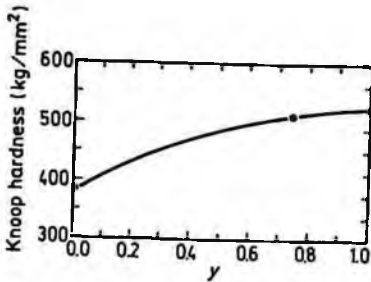

Fig. 7.6.1. Surface microhardness (using Knoop's pyramid test) measured on (100) plane along the ⟨100⟩ direction as a function of y for the undoped $Ga_xIn_{1-x}As_yP_{1-y}$ lattice-matched to InP (after Watts and Willoughby [1984]).

(Reprinted with permission from the American Institute of Physics, © 1984.)

Elastic constants at 300 K,
for $Ga_xIn_{1-x}As_yP_{1-y}$ lattice-matched to InP (after Adachi [1992]):

C_{11}	$(10.11 - 0.12y) \cdot 10^{11}$ dyn/cm²
C_{12}	$(5.61 - 0.68y) \cdot 10^{11}$ dyn/cm²
C_{44}	$(4.56 + 0.33y) \cdot 10^{11}$ dyn/cm²

Bulk modulus $B_s = \dfrac{C_{11} + 2C_{12}}{3}$ $B_s = (7.11 - 0.516y + 0.02y^2) \cdot 10^{11}$ dyn/cm²

Anizotropy factor $A = \dfrac{C_{11} - C_{12}}{2C_{44}}$ $A = 0.493 + 0.035y - 0.01y^2$

Shear modulus $C' = (C_{11} - C_{12})/2$ $C' = (2.25 + 0.28y) \cdot 10^{11}$ dyn/cm²

[100] Young's modulus	$Y_0 = \frac{(C_{11}+2C_{12})(C_{11}-C_{12})}{(C_{11}+C_{12})}$	$Y_0 = (6.106 + 0.976y - 0.344y^2)\cdot 10^{11}$ dyn/cm^2
[100] Poisson ratio	$\sigma_0 = \frac{C_{12}}{C_{11}+2C_{12}}$	$\sigma_0 = 0.357 - 0.033y + 0.006y^2$

(after Adachi [1992])

Acoustic Wave Speeds (after Adachi [1992])

Wave propagation direction	Wave character	Expression for wave speed	Wave speed (in units of 10^5 cm/s)
[100]	V_L	$(C_{11}/\rho)^{1/2}$	$4.594 - 0.334y$
	V_T	$(C_{44}/\rho)^{1/2}$	$3.085 - 0.104y$
[110]	V_l	$[(C_{11}+C_{12}+2C_{44})/2\rho)]^{1/2}$	$5.092 - 0.355y$
	$V_{t\parallel}$	$V_{t\parallel} = V_T = (C_{44}/\rho)^{1/2}$	$3.085 - 0.104y$
	$V_{t\perp}$	$[(C_{11}-C_{12})/2\rho)]^{1/2}$	$2.167 - 0.023y$
[111]	V_l'	$[(C_{11}+2C_{12}+4C_{44})/3\rho)]^{1/2}$	$5.247 - 0.362y$
	V_t'	$[(C_{11}-C_{12}+C_{44})/3\rho)]^{1/2}$	$2.511 - 0.056y$

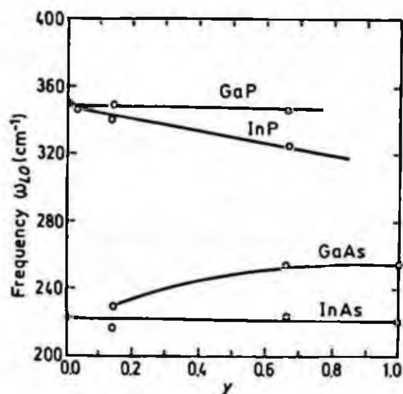

Fig. 7.6.2. Longitudinal optical phonon frequency ω_{LO} versus composition y for $Ga_xIn_{1-x}As_yP_{1-y}$ lattice-matched to InP (after Adachi [1992]).

(Reprinted with permission from John Wiley & Sons, Inc., © 1992.)

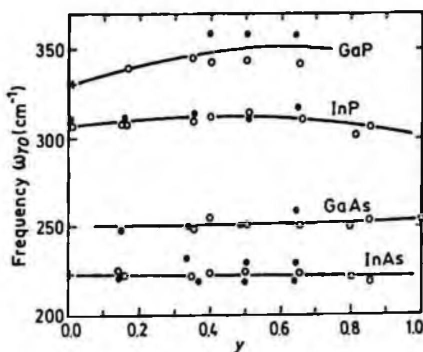

Fig. 7.6.3. Transverse optical phonon frequency ω_{TO} versus composition y for $Ga_xIn_{1-x}As_yP_{1-y}$ lattice-matched to InP (after Adachi [1992]).

(Reprinted with permission from John Wiley & Sons, Inc., © 1992.)

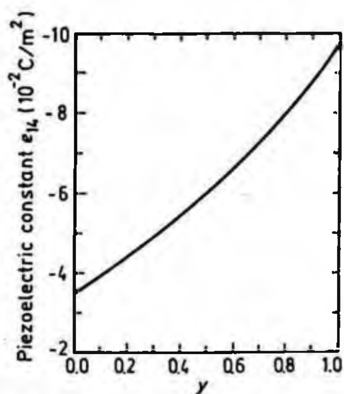

Fig. 7.6.4. Piezoelectric constant e_{14} as a function of composition parameter y for $Ga_xIn_{1-x}As_yP_{1-y}$ lattice-matched to InP (after Adachi [1982]).

(Reprinted with permission from the American Institute of Physics, © 1982.)

References

Adachi, S., *J. Appl. Phys.* **53**, 12 (1982) 8775–8792.

Adachi, S., *J. Appl. Phys.* **66**, 12 (1989) 6030–6040.

Adachi, S., *Physical Properties of III-V Semiconductor Compounds*, John Wiley and Sons, 1992.

Amiotti, M. and G. Landgren, *J. Appl. Phys.* **73**, 6 (1993) 2965–2971.

Arai, S., Y. Suematsu, and Y. Itaya, *IEEE J. of Quant. Electron.* **QE-16**, 2 (1980) 197–205.

Benzaquen, R., S. Clarbonneau, N. Sawadsky, A. P. Roth, R. Leonelli, L. Hobbs, and G. Knight, *J. Appl. Phys.* **75**, 5 (1994) 2633–2639.

Burkhard, H., H. W. Dinges, and E. Kuphal, *J. Appl. Phys.* **53**, 1 (1982) 655–662.

Forrest, S. R., P. H. Schmidt, R. B. Wilson, and M. L. Kaplan, *Appl. Phys. Lett.* **45**, 11 (1984) 1199–1201.

Foyt, A. G., *J. Cryst. Growth.* **54**, 1 (1981) 1–8.

Galvanauskas, A., A. Gorelenok, Z. Dobrovol'skis, S. Kershulis, Yu. Pozhela, A. Reklaitis, and N. Shmidt, *Sov. Phys. Semicond.* **22**, 9 (1988) 1055–1058.

Garbuzov, D. Z., V. V. Agaev, Z. N. Sokolova, V. B. Khalfin, and V. P. Chalyi, *Sov. Phys. Semicond.* **18**, 6 (1984) 665–669.

Gorelenok, A. T., A. G. Dzigasov, P. P. Moskvin, V. S. Sorokin, and I. S. Tarasov, *Sov. Phys. Semicond.* **15**, 12 (1981) 1400–1402.

Hayes, J. R., D. Patel, A. R. Adams, and P. D. Greene, *J. Electron. Mater.* **11**, 1 (1982) 155–189.

Kelso, S. M., D. E. Aspnes, M. A. Pollack, and R. E. Nahory, *Phys. Rev.* **B26**, 12 (1982) 6669–6681.

Nahory, R. E., M. A. Pollack, W. D. Johnston, Jr., and R. L. Barns, *Appl. Phys. Lett.* **33**, 7 (1978) 659–661.

Osaka, F., T. Mikawa, and T. Kaneda, *Appl. Phys. Lett.* **45**, 3 (1984) 292–293.

Pearsall, T. P., *GaInAsP Alloy Semiconductors*, John Wiley and Sons, 1982.

Rajalakshmi, R. and B. M. Arora, *J. Appl. Phys.* **67**, 7 (1990) 3533–3538.

Satzke, K., G. Weiser, R. Hoger, and W. Thulke, *J. Appl. Phys.* **63**, 11 (1988) 5485–5490.

Sirota, N. N., A. M. Antiukhov, V. V. Novikov, and A. A. Sidorov, *Doklady Akademii Nauk SSSR (Soviet Physics Doklady)*, **266**, 1 (1982) 105–108, (in Russian).

Takanashi, Y., and Y. Horikoshi, *Jap. J. Appl. Phys.* **18**, 11 (1979) 2173–2174.

Tappura, K., *J. Appl. Phys.* **74**, 7 (1993) 4565–4570.

Vilkotsky, V. A., D. S. Domanevsky, F. Ugerek, Ya. Kovach, and M. V. Prokopenya, *Sov. Phys. Semicond.* **20**, 8 (1986) 966–967.

Watts, D. Y. and A. F. W. Willoughby, *J. Appl. Phys.* **56**, 6 (1984) 1869–1871.

Wehmann, H. H., F. Fiedler, and A. Schlachetzki, *Electron. Lett.* **22**, 25 (1986) 1338–1340.

Windhorn, T. H., L. W. Cook, and G. E. Stillman, *Appl. Phys. Lett.* **41**, 11 (1982) 1065–1067.

Yamazoe, Y., T. Nishino, and Y. Hamakawa, *IEEE J. of Quant. Electron.* **QE-17**, 2 (1981) 139–144.

CHAPTER 8

GALLIUM INDIUM ARSENIDE ANTIMONIDE ($Ga_xIn_{1-x}As_ySb_{1-y}$)

Maya P. Mikhailova
Ioffe Institute, St. Petersburg, Russia

8.1. Basic Parameters at 300 K

Crystal structure	Zinc blende
Group of symmetry	$T_d^2 - F\bar{4}3m$

To estimate the value of any parameter b of $Ga_xIn_{1-x}As_ySb_{1-y}$ one can use an approximate formula (after Adachi [1987]):

$$b(x,y) \cong xyb_{GaAs} + x(1-y)b_{GaSb} + (1-x)yb_{InAs} + (1-x)(1-y)b_{InSb} \qquad (8.1.1)$$

Lattice constant a (Å) 6.0959 (GaSb) – 6.0583 (InAs)

For compositions lattice-matched:

to **GaSb** $$y = \frac{0.3835 - 0.3835x}{0.4210 + 0.216x} \qquad (0 \le x \le 1) \qquad a = 6.0959\ \text{Å} \qquad (8.1.2)$$

to **InAs** $$y = \frac{0.4210 - 0.3835x}{0.4210 + 0.0216x} \qquad (0 \le x \le 1) \qquad a = 6.0583\ \text{Å} \qquad (8.1.3)$$

(after Adachi [1987])

8.1.1. *Basic Properties of* $Ga_xIn_{1-x}As_ySb_{1-y}$ *Compositions Lattice-Matched to GaSb*

	$x = 0$ ($InAs_{0.91}Sb_{0.09}$)	$x = 1$ (GaSb)	$0 < x < 1$
Number of atoms in 1 cm^3	$3.53 \cdot 10^{22}$	$3.53 \cdot 10^{22}$	$3.53 \cdot 10^{22}$
Auger recombination coefficient (cm^6/s)	$\sim 2 \cdot 10^{-27}$	$5 \cdot 10^{-30}$	
Debye temperature (K)	~ 280	266	~ 270
Density (g/cm^3)	5.69	5.61	$5.69 - 0.08x$
Dielectric constant			
static	15.3	15.7	$15.3 + 0.4x$
high frequency	12.6	14.4	$12.6 + 1.8x$
Effective electron mass (in units of m_o)	0.022	0.041	$0.022 + 0.03x - 0.012x^2$
Effective hole mass (in units of m_o)			
heavy hole	0.4	0.4	0.4
light hole	0.025	0.05	$0.025 + 0.025x$
Electron affinity (eV)	4.87	4.06	$4.87 - 0.81x$
Lattice constant (Å)	6.0959	6.0959	6.0959
Optical phonon energy (eV)	~ 0.03	~ 0.03	~ 0.03

Band structure and carrier concentration

	$x = 0$ ($InAs_{0.91}Sb_{0.09}$)	$x = 1$ (GaSb)	$0 < x < 1$
Energy gap (eV)	0.29	0.726	$0.29 - 0.165x + 0.6x^2$
Energy separation between X-valley and top of the valence band E_X (eV)	1.37	1.03	See Fig. 8.2.4
Energy separation between L-valley and top of the valence band E_L (eV)	1.02	0.81	See Fig. 8.2.4
Energy of spin-orbital splitting E_{so} (eV)	0.33	0.76	See Fig. 8.2.5
Effective conduction band density of states (cm^{-3})	$8 \cdot 10^6$	$2.1 \cdot 10^{17}$	$2.5 \cdot 10^{19}(0.022 + 0.03x - 0.012x^2)^{3/2}$
Effective valence band density of states (cm^{-3})	$6.6 \cdot 10^{18}$	$1.8 \cdot 10^{19}$	$2.5 \cdot 10^{19}(0.41 + 0.16x + 0.23x^2)^{3/2}$

Electrical properties

Breakdown field (V/cm)	$\sim 4 \cdot 10^4$	$\sim 5 \cdot 10^4$	$\sim 5 \cdot 10^4$
Mobility (cm^2/V·s):			
electrons	$\leq 4 \cdot 10^4$	≤ 3000	See Sec. 8.3.1
holes	≤ 500	≤ 1000	
Diffusion coefficient (cm^2/s):			
electrons	$\leq 10^3$	≤ 75	
holes	≤ 13	≤ 25	

Optical properties

	$x = 0$ ($InAs_{0.91}Sb_{0.09}$)	$x = 1$ (GaSb)	$0 < x < 1$
Infrared refractive index	3.5	3.8	See Fig. 8.4.1
Radiative recombination coefficient (cm^3/s)	$\sim 10^{-10}$	$\sim 10^{-10}$	

Thermal and mechanical properties

Bulk modulus (dyn/cm^2)	$5.7 \cdot 10^{11}$	$5.7 \cdot 10^{11}$	$5.7 \cdot 10^{11}$
Melting point (°C)	~ 700	~ 712	See Sec. 8.5
Specific heat (J/g°C)	~ 0.25	~ 0.25	

8.1.2. *Basic Properties of* $Ga_xIn_{1-x}As_ySb_{1-y}$ *Compositions Lattice-Matched to InAs*

	$x = 0$ (InAs)	$x = 1$ ($GaAs_{0.08}Sb_{0.92}$)	$0 < x < 1$
Number of atoms in 1 cm^3	$3.59 \cdot 10^{22}$	$3.59 \cdot 10^{22}$	$3.59 \cdot 10^{22}$
Debye temperature (K)	280	~ 270	~ 270
Density (g/cm^3)	5.68	5.59	See Sec. 8.6
Dielectric constant:			
static	15.15	15.5	$15.15 + 0.35x$
high frequency	12.3	14.1	$12.3 + 1.8x$

	$x = 0$ (InAs)	$x = 1$ ($GaAs_{0.08}Sb_{0.92}$)	$0 < x < 1$
Effective electron mass (in units of m_o)	0.023	0.041	$0.023 + 0.032x - 0.012x^2$
Effective hole mass: (in units of m_o)			
heavy hole	0.41	0.41	0.41
light hole	0.026	0.052	$0.026 + 0.026x$
Electron affinity (eV)	4.9	4.07	$4.9 - 0.83x$
Lattice constant (Å)	6.0583	6.0583	6.0583
Optical phonon energy (eV)	0.03	~ 0.03	~ 0.03
Band structure and carrier concentration			
Energy gap (eV)	0.36	0.60	$0.36 - 0.23x + 0.54x^2$
Energy separation between X-valley and top of the valence band E_X (eV)	1.38	1.07	See Fig. 8.2.7
Energy separation between L-valley and top of the valence band E_L (eV)	1.09	0.82	See Fig. 8.2.7
Energy of spin-orbital splitting E_{so} (eV)	0.41	0.76	
Effective conduction band density of states (cm^{-3})	$8.7 \cdot 10^{16}$	$2.2 \cdot 10^{17}$	$2.5 \cdot 10^{19}(0.023 + 0.032x - 0.012x^2)^{3/2}$

	$x=0$ ($InAs_{0.91}Sb_{0.09}$)	$x=1$ (GaSb)	$0<x<1$
Effective valence band density of states (cm^{-3})	$6.6\cdot10^{18}$	$1\cdot10^{19}$	$2.5\cdot10^{19}(0.41+0.14x+0.23x^2)^{3/2}$
Electrical properties			
Breakdown field (V/cm)	$\sim4\cdot10^4$	$\sim4\cdot10^4$	$\sim4\cdot10^4$
Mobility (cm^2/V·s):			
electrons	$\le4\cdot10^4$	$\le2\cdot10^4$	
holes	≤500	≤500	
Diffusion coefficient (cm^2/s)			
electrons	$\le10^3$	≤500	
holes	≤12	≤12	
Optical properties			
Infrared refractive index	3.51	3.76	$3.51+0.25x$
Radiative recombination coefficient (cm^3/s)	$\sim10^{-10}$	$\sim10^{-10}$	
Thermal and mechanical properties			
Bulk modulus (dyn/cm^2)	$5.8\cdot10^{11}$	$5.8\cdot10^{11}$	$5.8\cdot10^{11}$
Melting point (°C)	942	715	
Specific heat (J/g°C)	0.25	~0.25	~0.25

8.2. Band Structure and Carrier Concentration

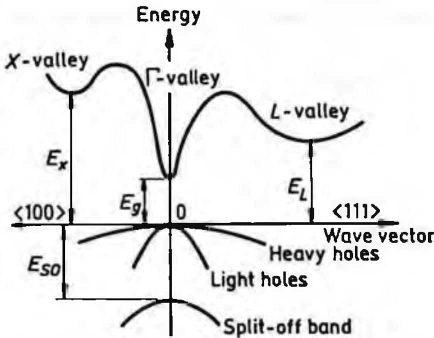

Fig. 8.2.1. Band structure of $Ga_xIn_{1-x}As_ySb_{1-y}$. Important minima of the conduction band and maxima of the valence band.

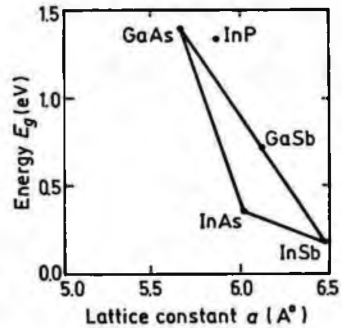

Fig. 8.2.2. Energy gap E_g of $Ga_xIn_{1-x}As_ySb_{1-y}$ versus lattice constant.

Within the whole range of the compositions the $Ga_xIn_{1-x}As_ySb_{1-y}$ is a direct gap semiconductor.

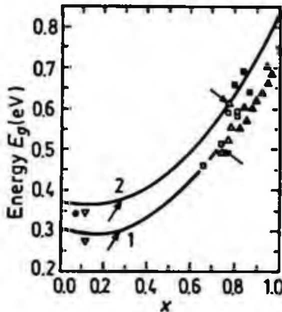

Fig. 8.2.3. Energy gap E_g as a function of x for $Ga_xIn_{1-x}As_ySb_{1-y}$ lattice-matched to GaSb. Experimental points are taken from five different papers. Arrows show the region of the miscibility gap. $T(K)$: 1. 300, 2. 77 (after Mikhailova and Titkov [1994]).

For $Ga_xIn_{1-x}As_ySb_{1-y}$ compositions lattice-matched to GaSb there is a miscibility gap for $0.25 \leq x \leq 0.75$ with a critical temperature estimated to be 1467°C (after Cherng *et al.* [1986]).

For $Ga_xIn_{1-x}As_ySb_{1-y}$ compositions lattice-matched to GaSb (after Karouta *et al.* [1987]):

$$T = 300\text{ K} \qquad E_g \cong 0.725x + 0.290(1-x) - 0.6x(1-x) \quad \text{(eV)} \qquad (8.2.1)$$

$$T = 77\text{ K} \qquad E_g \cong 0.801x + 0.354(1-x) - 0.6x(1-x) \quad \text{(eV)} \qquad (8.2.2)$$

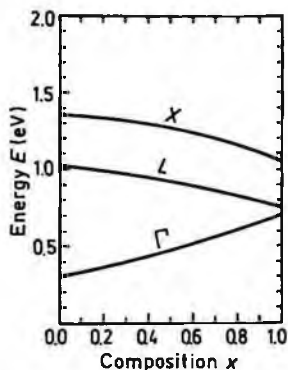

Fig. 8.2.4. Energy separations between Γ, L and X conduction band minima and top of the valence band versus composition parameter x for $Ga_xIn_{1-x}As_ySb_{1-y}$ lattice-matched to GaSb (after Adachi [1987]).

(Reprinted with permission from the American Institute of Physics, © 1987.)

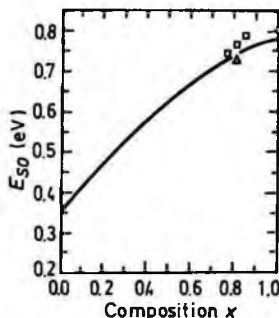

Fig. 8.2.5. Energy of spin-orbital splitting E_{so} versus composition parameter x for GaInAsSb lattice-matched to GaSb (after Tournie [1990]).

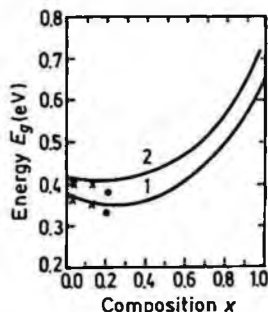

Fig. 8.2.6. Energy gap E_g as a function of x for $Ga_xIn_{1-x}As_ySb_{1-y}$ lattice-matched to InAs. $T(K)$: 1. 300, 2. 77 (after Voronina *et al.* [1991a]).

For $Ga_xIn_{1-x}As_ySb_{1-y}$ compositions lattice-matched to InAs:

$$T = 300\ \text{K} \qquad E_g \cong 0.36 - 0.23x + 0.54x^2 \quad (\text{eV}) \tag{8.2.3}$$

$$T = 77\ \text{K} \qquad E_g \cong 0.41 - 0.29x + 0.66x^2 \quad (\text{eV}) \tag{8.2.4}$$

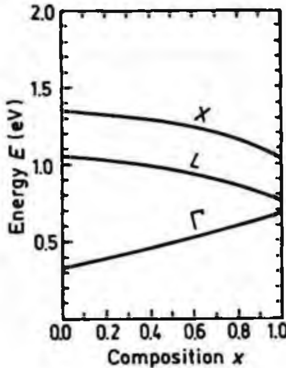

Fig. 8.2.7. Energy separation between Γ, L and X conduction band minima and top of the valence band versus composition parameter x for $Ga_xIn_{1-x}As_ySb_{1-y}$ lattice-matched to InAs (after Adachi [1987]).

(Reprinted with permission from the American Institute of Physics, © 1987.)

8.2.1. *Temperature Dependences*

Temperature dependence of the energy gap for GaSb $(x = 1, y = 0)$:
(after Wu and Chen [1992])

$$E_g \cong 0.813 - 3.78 \cdot 10^{-4} \cdot \frac{T^2}{T + 94} \quad (\text{eV}) \tag{8.2.5}$$

Temperature dependence of the energy gap for InAs $(x = 0, y = 1)$:
(after Fang *et al.* [1990])

$$E_g \cong 0.415 - 2.76 \cdot 10^{-4} \cdot \frac{T^2}{T + 83} \quad (\text{eV}) \tag{8.2.6}$$

Temperature dependence of the energy gap for $Ga_{0.07}In_{0.93}A_{0.88}Sb_{0.12}$:
(after Gong *et al.* [1994])

$$E_g \cong 0.378 - 4.27 \cdot 10^{-4} \cdot \frac{T^2}{T + 288} \quad (\text{eV}) \tag{8.2.7}$$

Effective density of states in the conduction band N_c for GaInAsSb lattice-matched to GaSb:

$$N_c \cong 4.82 \cdot 10^{15} \left(\frac{m_\Gamma}{m_o}\right)^{3/2} T^{3/2} = 4.82 \cdot 10^{15} \cdot T^{3/2} (0.022 + 0.03x - 0.012x^2)^{3/2} \quad (\text{cm}^{-3}) \tag{8.2.8}$$

Effective density of states in the valence band N_v for GaInAsSb lattice-matched to GaSb:

$$N_v \cong 4.82 \cdot 10^{15} \cdot T^{3/2} \left(\frac{m_h}{m_o}\right)^{3/2} = 4.82 \cdot 10^{15} \cdot T^{3/2} (0.41 + 0.16x + 0.23x^2)^{3/2} \quad (\text{cm}^{-3}) \tag{8.2.9}$$

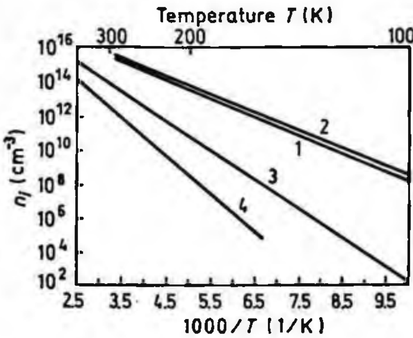

Fig. 8.2.8. The temperature dependences of the intrinsic carrier concentration for $Ga_xIn_{1-x}As_ySb_{1-y}$ alloys lattice-matched to GaSb. 1. $x = 0$, 2. $x = 0.2$, 3. $x = 0.8$, 4. $x = 1$.

Effective density of states in the conduction band N_c for GaInAsSb lattice-matched to InAs:

$$N_c \cong 4.82 \cdot 10^{15} \left(\frac{m_\Gamma}{m_o}\right)^{3/2} T^{3/2} = 4.82 \cdot 10^{15} \cdot T^{3/2} (0.023 + 0.032x - 0.012x^2)^{3/2} \quad (\text{cm}^{-3}) \tag{8.2.10}$$

Effective density of states in the valence band N_v for GaInAsSb lattice-matched to InAs:

$$N_v \cong 4.82 \cdot 10^{15} \cdot T^{3/2} \left(\frac{m_h}{m_o} \right)^{3/2}$$
$$= 4.82 \cdot 10^{15} \cdot T^{3/2} (0.41 + 0.14x + 0.23x^2)^{3/2} \quad (\mathrm{cm}^{-3}) \tag{8.2.11}$$

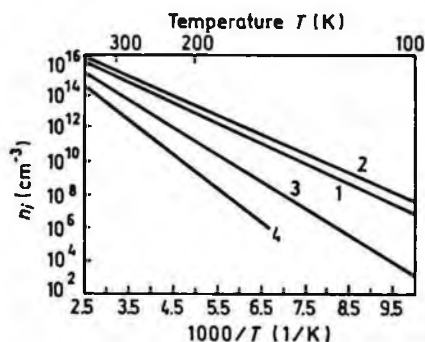

Fig. 8.2.9. The temperature dependences of the intrinsic carrier concentration for $Ga_xIn_{1-x}As_ySb_{1-y}$ alloys lattice-matched to InAs. 1. $x = 0$, 2. $x = 0.2$, 3. $x = 0.8$, 4. $x = 1$.

8.2.2. Band Discontinuities at GaInAsSb/GaSb and GaInAsSb/InAs Heterojunctions

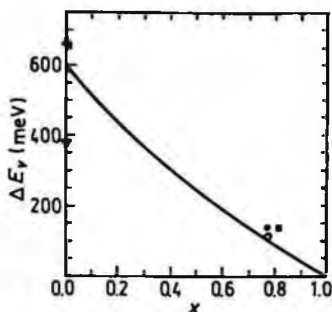

Fig. 8.2.10. Valence band offset ΔE_v versus composition parameter x for lattice-matched $Ga_xIn_{1-x}As_ySb_{1-y}$/GaSb heterostructure (after Mebarki *et al.* [1993]).

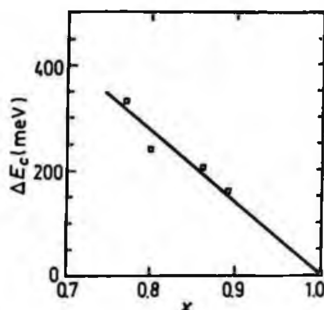

Fig. 8.2.11. Conduction band offset ΔE_c versus composition parameter x for lattice-matched $Ga_xIn_{1-x}As_ySb_{1-y}$/GaSb heterostructure (after Mikhailova and Titkov [1994]).

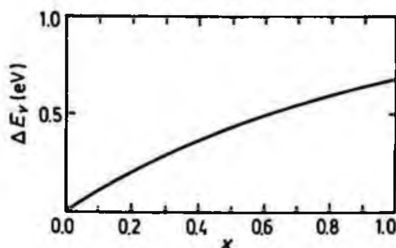

Fig. 8.2.12. Valence band offset ΔE_v versus composition parameter x for lattice-matched $Ga_xIn_{1-x}As_ySb_{1-y}$/InAs heterostructure (after Nakao *et al.* [1984]).

(Reprinted with permission from Elsevier Science, © 1984.)

8.2.3. *Effective Masses*

Electrons:

For GaInAsSb lattice-matched to GaSb (estimated according to Eq. (8.1.1)):

$$m_\Gamma/m_o \cong 0.022+0.03x-0.012x^2 \quad (8.2.11)$$

For GaInAsSb lattice-matched to InAs (estimated according to Eq. (8.1.1)):

$$m_\Gamma/m_o \cong 0.023+0.032x-0.012x^2 \quad (8.2.12)$$

Holes:

Effective mass of density of states m_v for GaInAsSb lattice-matched to GaSb (estimated according to Eq. (8.1.1)):

$$m_v/m_o \cong 0.41+0.16x+0.23x^2 \quad (8.2.13)$$

Effective mass of density of states m_v for GaInAsSb lattice-matched to InAs (estimated according to Eq. (8.1.1)):

$$m_v/m_o \cong 0.41+0.14x+0.23x^2 \quad (8.2.14)$$

8.2.4. *Donors and Acceptors*

$Ga_xIn_{1-x}As_ySb_{1-y}$ $(0 < x \leq 0.2)$
(after Baranov *et al.* [1990], Voronina *et al.* [1991b])

Undoped $Ga_xIn_{1-x}As_ySb_{1-y}$ compositions $(0 < x \leq 0.2)$ have the conductivity of *p*-type. Three native acceptor traps have been observed for these compositions:

$$E_t - E_v \cong 0.01 \text{ eV}$$
$$E_t - E_v \cong 0.03+0.035 \text{ eV}$$
$$E_t - E_v \cong 0.07 \text{ eV}$$

Ge, Cd - $(E_t - E_v) \cong 0.01$ eV (acceptor)
$Ge + V_{ac}$ - $(E_t - E_v) \cong 0.017$ eV (acceptor)
$Cd + V_{ac}$ - $(E_t - E_v) \cong 0.017$ eV (acceptor)
Zn - $(E_t - E_v) \cong 0.1 \div 0.15$ eV (acceptor)
Te - $(E_c - E_t) \cong 5 \cdot 10^{-3}$ eV (donor)
$(E_c - E_t) \cong 0.04 \div 0.05$ eV (donor)

$Ga_xIn_{1-x}As_ySb_{1-y}$ ($x \geq 0.8$).
(after Voronina *et al.* [1991a])
Undoped $Ga_xIn_{1-x}As_ySb_{1-y}$ compositions ($0.76 \leq x \leq 1$) have the conductivity of *n*-type. Native donor trap has been observed for these compositions:

$(E_c - E_t) \cong 0.09 \div 0.1$ eV
Mn - $(E_t - E_v) \cong 0.02 \div 0.025$ eV (acceptor)

8.3. Electrical Properties

8.3.1. *Mobility and Hall Effect*

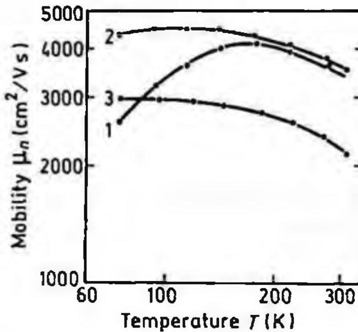

Fig. 8.3.1. Temperature dependences of the electron Hall mobility for $Ga_xIn_{1-x}As_ySb_{1-y}$ (Te). $x \cong 0.1$. For all samples acceptor concentration $N_a \cong 5 \cdot 10^{16}$ cm^{-3}. Donor concentration (Te). N_d (cm^{-3}): 1. $2.5 \cdot 10^{17}$, 2. $8.5 \cdot 10^{17}$, 3. $4 \cdot 10^{18}$ (after Voronina *et al.* [1991b]).

(Reprinted with permission from the American Institute of Physics, © 1991.)

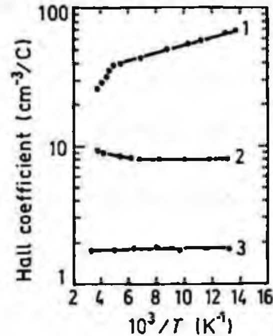

Fig. 8.3.2. Temperature dependences of the Hall coefficient for the same samples as in Fig. 8.3.1 (after Voronina *et al.* [1991b]).

(Reprinted with permission from the American Institute of Physics, © 1991.)

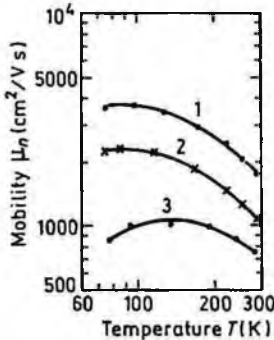

Fig. 8.3.3. Temperature dependences of the electron Hall mobility for $Ga_xIn_{1-x}As_ySb_{1-y}$. $x \cong 0.8$. For all samples donor concentration $N_d \cong 5 \cdot 10^{18}$ cm^{-3}. Acceptor concentration (Mn) N_a (cm^{-3}): 1. $4.4 \cdot 10^{17}$, 2. $6 \cdot 10^{17}$, 3. $7.8 \cdot 10^{17}$ (after Voronina *et al.* [1991a]).

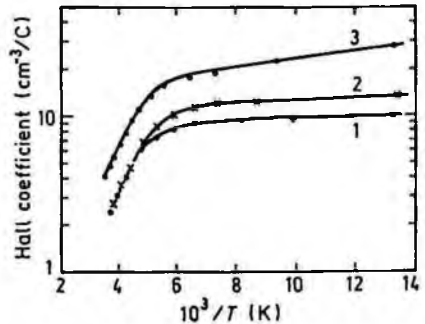

Fig. 8.3.4. The temperature dependences of the Hall coefficient for the same samples as in Fig. 8.3.3 (after Voronina *et al.* [1991a]).

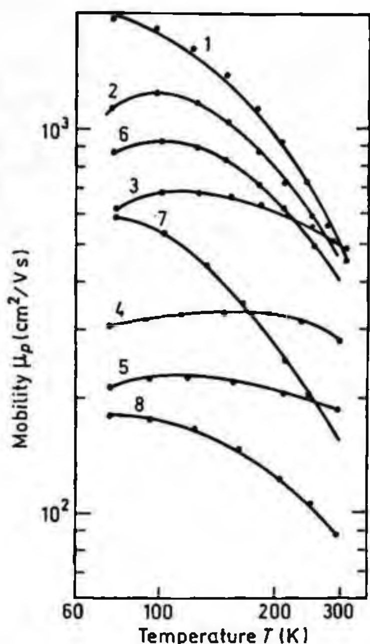

Fig. 8.3.5. Temperature dependences of the hole Hall mobility for $Ga_xIn_{1-x}As_ySb_{1-y}$ for different dopants and different doping levels. $x \cong 0.1$. 1. undoped: $N_a - 4.4 \cdot 10^{16}$ cm^{-3}, $N_d - 1.7 \cdot 10^{16}$ cm^{-3}; 2–5. samples doped with Ge. N (cm^{-3}): 2. $N_a - 1.9 \cdot 10^{17}$, $N_d - 5 \cdot 10^{16}$, 3. $N_a - 6.4 \cdot 10^{17}$, $N_d - 2 \cdot 10^{17}$, 4. $N_a - 3.4 \cdot 10^{18}$, $N_d - 6 \cdot 10^{17}$, 5. $N_a - 1.6 \cdot 10^{19}$, $N_d - 2 \cdot 10^{18}$, 6. Sample doped with Cd. $N_a - 9 \cdot 10^{16}$ cm^{-3}, $N_d - 2 \cdot 10^{16}$ cm^{-3}. 7–8. Samples doped with Zn. N (cm^{-3}): 7. $N_a - 4.2 \cdot 10^{17}$, $N_d - 2 \cdot 10^{16}$, 8. $N_a - 6.2 \cdot 10^{17}$, $N_d - 2 \cdot 10^{16}$ (after Voronina *et al.* [1991b]).

(Reprinted with permission from the American Institute of Physics, © 1991.)

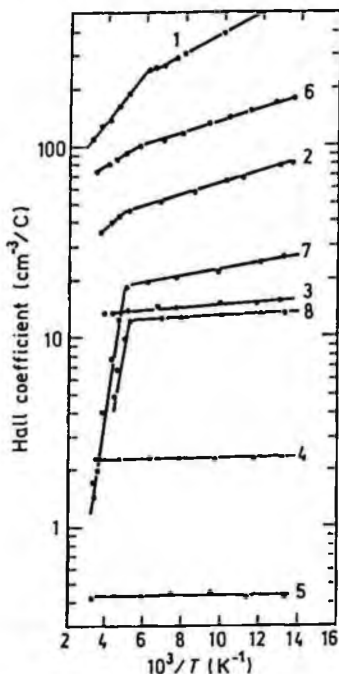

Fig. 8.3.6. Temperature dependences of the Hall coefficient for the same samples as in Fig. 8.3.5 (after Voronina *et al.* [1991b]).

(Reprinted with permission from the American Institute of Physics, © 1991.)

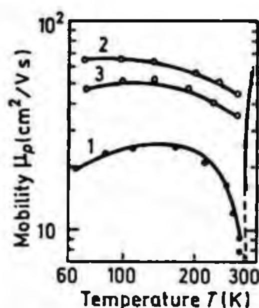

Fig. 8.3.7. Temperature dependences of the hole Hall mobility for $Ga_xIn_{1-x}As_ySb_{1-y}$, $x \cong 0.8$. For all samples donor concentration $N_d \equiv 10^{18}$ cm^{-3}, Acceptor concentration (Mn) (cm^{-3}): 1. $1.7 \cdot 10^{18}$, 2. $2.3 \cdot 10^{18}$, 3. $5 \cdot 10^{18}$ (after Voronina *et al.* [1991a]).

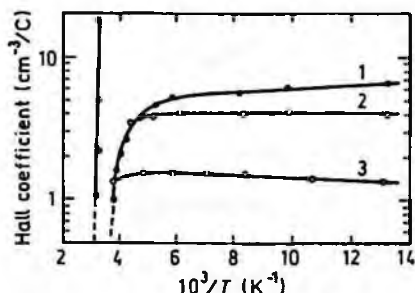

Fig. 8.3.8. Temperature dependences of the Hall coefficient for the same samples as in Fig. 8.3.7 (after Voronina *et al.* [1991a]).

8.3.2. *Impact Ionization*

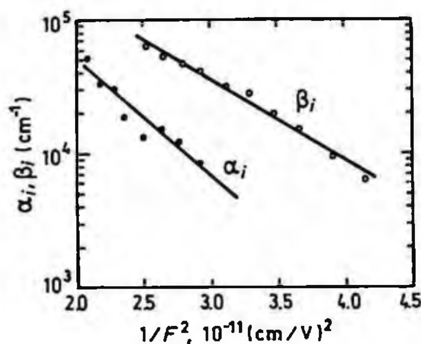

Fig. 8.3.9. Field dependences of electron (α) and hole (β) ionization coefficients for $Ga_{0.8}In_{0.2}As_{0.17}Sb_{0.83}$, 230 K (after Andreev *et al.* [1991]).

$$\alpha = \alpha_\infty \exp(-F_{n0}/F)^2. \quad (8.3.1)$$

$\alpha_\infty = 2.41 \cdot 10^6$ cm^{-1}, $F_{n0} = 4.45 \cdot 10^5$ V/cm

$$\beta = \beta_\infty \exp(-F_{p0}/F)^2. \quad (8.3.2)$$

$\beta_\infty = 1.98 \cdot 10^6$ cm^{-1}, $F_{p0} = 3.69 \cdot 10^5$ V/cm

8.4. Optical Properties

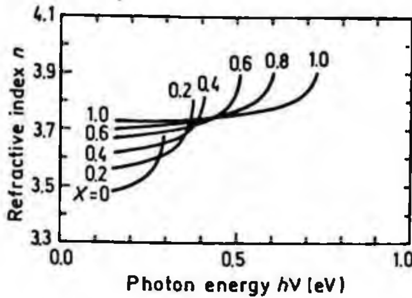

Fig. 8.4.1. Refractive index n versus photon energy for $Ga_xIn_{1-x}As_ySb_{1-y}$ lattice-matched to GaSb (after Adachi [1987]).

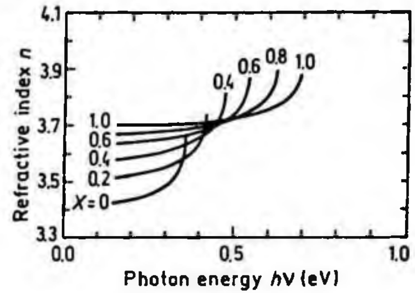

Fig. 8.4.2. Refractive index n versus photon energy for $Ga_xIn_{1-x}As_ySb_{1-y}$ lattice-matched to InAs (after Adachi [1987]).

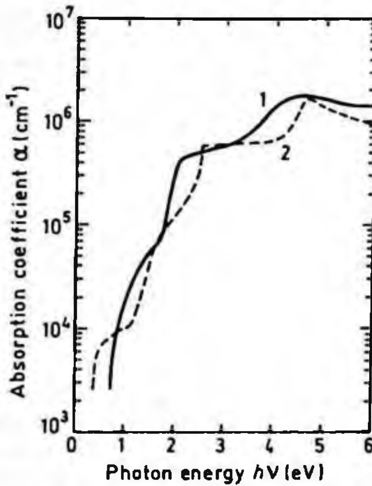

Fig. 8.4.3. The absorption coefficient versus photon energy, 300 K. Curve 1: $x = 1, y = 0$ (GaSb), Curve 2: $x = 0, y = 1$ (InAs) (after Adachi [1989]).

8.5. Thermal Properties

Thermal resistivity for several GaInAsSb compositions ($y \approx 1 - x$), 300 K (after Both *et al.* [1990]).

Composition	E_g (eV)	Thermal resistivity (cm K/W)
$Ga_{0.94}In_{0.06}As_{0.05}Sb_{0.95}$	0.67	5.5
$Ga_{0.85}In_{0.15}As_{0.13}Sb_{0.87}$	0.59	7.1
$Ga_{0.81}In_{0.19}As_{0.16}Sb_{0.83}$	0.56	10.4

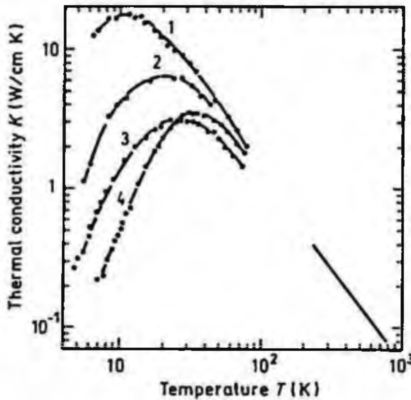

Fig. 8.5.1. Temperature dependences of thermal conductivity. $x = 1$, $y = 0$. (GaSb). 1 ÷ 3 – *n*-type samples. n (300 K), cm^{-3}: 1. $1.6 \cdot 10^{17}$, 2. $8.6 \cdot 10^{17}$, 3. $1.8 \cdot 10^{18}$, 4. *p*-type sample. p (300 K) = $1.4 \cdot 10^{17}$ cm^{-3} (after Poudjade and Albany [1969] and Okhotin *et al.* [1972]).

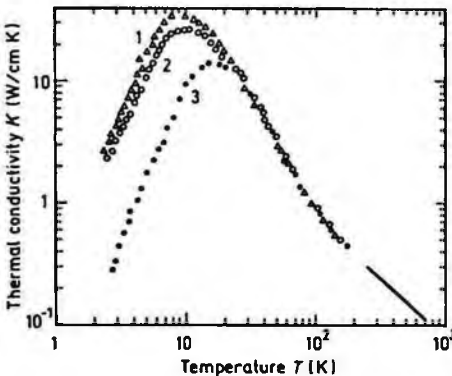

Fig. 8.5.2. Temperature dependences of thermal conductivity. $x = 0$, $y = 1$. (InAs). 1, 2 – *n*-type samples. 1. $n_0 = 1.6 \cdot 10^{16}$ cm^{-3}, 2. $n_0 = 2 \cdot 10^{17}$ cm^{-3}, 3. *p*-type sample, $p_0 = 2 \cdot 10^{17}$ cm^{-3} (after Tamarin and Shalyt [1971] and Okhotin *et al.* [1972]).

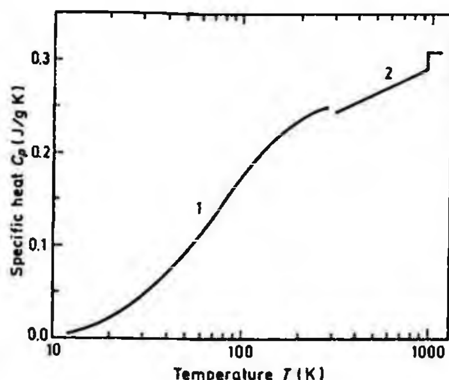

Fig. 8.5.3. Temperature dependence of specific heat $x = 1, y = 0$ (GaSb) 1. after Piesbergen [1963], 2. after Okhotin *et al.* [1972].

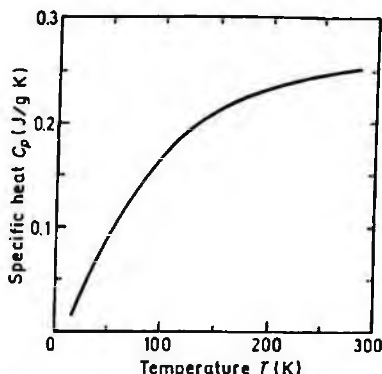

Fig. 8.5.4. Temperature dependence of specific heat at constant pressure. $x = 0, y = 1$ (InAs) (after Piesbergen [1963]). For $298 < T < 1215$ K. $C_p = 0.24 + 3.97 \cdot 10^{-5}\, T$ (J/gK) (after Barin *et al.* [1977]).

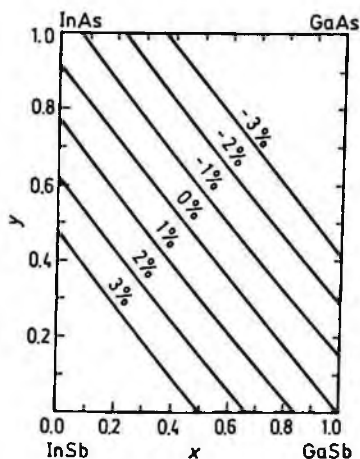

Fig. 8.5.5. Contours of constant lattice-mismatch as a function of x and y in a GaInAsSb system grown on a GaSb substrate (after Ghiti and O'Reilly [1993]).

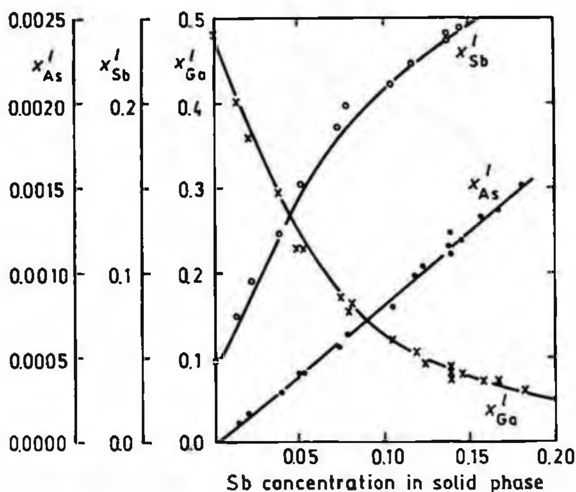

Fig. 8.5.6. Phase diagram for GaInAsSb at 530°C. Experimental points: ∘ – concentration of Sb in liquid phase x^l_{Sb}, • – x^l_{As}, × – x^l_{Ga}. Solid phase is lattice matched to GaSb (after Guseinov *et al.* [1989]).

(Reprinted with permission from the American Institute of Physics, © 1989.)

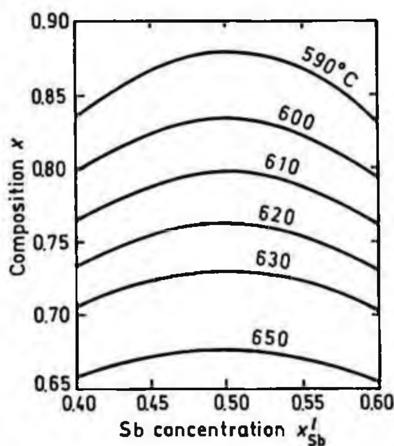

Fig. 8.5.7. Solidus isothermes for several GaInAsSb compositions lattice-matched to GaSb as a function of the Sb concentration in liquid phase x^l_{Sb} (after Tournie [1990]).

8.6. Mechanical Properties, Elastic Constants, Lattice Vibrations, Other Properties

Density (g/cm^3)	GaSb - 5.61	InAs - 5.68
	GaAs - 5.32	InSb - 5.77
Hardness on the Mohs scale	GaSb - 4.5	InAs - 3.8
	GaAs - between 4 and 5	
Surface microhardness (kg/mm^2)	GaSb - 450	InAs - 430
(using Knoop's pyramid test)	GaAs - 750	InAs - 220

Elastic constant at 300 K:

for compositions lattice-matched to GaSb (estimated according to Eq. (8.1.1)):

C_{11}	$(8.19 + 0.64x) \cdot 10^{11}$ dyn/cm^2
C_{12}	$(4.46 - 0.44x) \cdot 10^{11}$ dyn/cm^2
C_{44}	$(3.89 + 0.43x) \cdot 10^{11}$ dyn/cm^2

for compositions lattice-matched to InAs (estimated according to Eq. (8.1.1)):

C_{11}	$(8.34 + 0.73x) \cdot 10^{11}$ dyn/cm^2
C_{12}	$(4.54 - 0.42x) \cdot 10^{11}$ dyn/cm^2
C_{44}	$(3.95 + 0.50x) \cdot 10^{11}$ dyn/cm^2

	For GaInAsSb compositions lattice-matched to GaSb	For GaInAsSb compositions lattice-matched to InAs
Bulk modulus ($\cdot 10^{11}$ dyn/cm^2)	~5.7	~5.8
Shear modulus ($\cdot 10^{11}$ dyn/cm^2)	$1.86 + 0.54x$	$1.9 + 0.57x$
[100] Young's modulus ($\cdot 10^{11}$ dyn/cm^2)	$5.04 + 1.27x$	$5.14 + 1.35x$
[100] Poisson ratio	$0.35 - 0.04x$	$0.35 - 0.04x$

Acoustic Wave Speeds

Wave propagation direction	Wave character	Wave speed (in units of 10^5 cm/s) for GaInAsSb compositions lattice-matched to GaSb	Wave speed (in units of 10^5 cm/s) for GaInAsSb compositions lattice-matched to InAs
[100]	V_L	$3.79 + 0.18x$	$3.83 + 0.2x$
	V_T	$2.61 + 0.16x$	$2.64 + 0.17x$
[110]	V_l	$4.23 + 0.15x$	$4.28 + 0.17x$
	$V_{t\parallel}$	$2.61 + 0.16x$	$2.64 + 0.17x$
	$V_{t\perp}$	$1.81 + 0.26x$	$1.83 + 0.27x$
[111]	V_l'	$4.36 + 0.14x$	$4.41 + 0.16x$
	V_t'	$2.11 + 0.22x$	$2.13 + 0.24x$

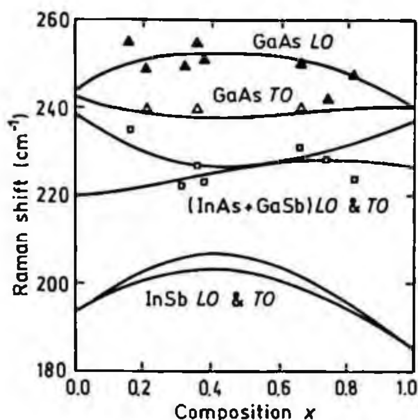

Fig. 8.6.1. Frequencies of the *LO* and *TO* phonons in $Ga_xIn_{1-x}As_ySb_{1-y}$ as a function of the composition *x* for $y = 1 - x$. The solid curves represent the calculated results using the modified REI model (after Jaw *et al.* [1989]).

(Reprinted with permission from the American Institute of Physics, © 1989.)

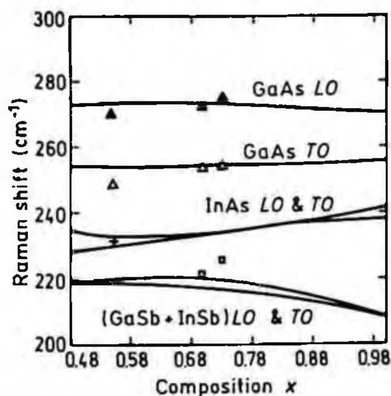

Fig. 8.6.2. Frequencies of the *LO* and *TO* phonons in $Ga_xIn_{1-x}As_ySb_{1-y}$ as a function of the composition *x* for $y = 1.48 - x$. The solid curves represent the calculated results using the modified REI model (after Jaw *et al.* [1989]).

(Reprinted with permission from the American Institute of Physics, © 1989.)

References

Adachi, S., *J. Appl. Phys.* **61**, 10 (1987) 4869–4876.

Adachi, S., *J. Appl. Phys.* **66**, 12 (1989) 6030–6040.

Andreev, I. A., M. P. Mikhailova, S. V. Melnikov, Yu. P. Smorchkova, and Yu. P. Yakovlev, *Sov. Phys. Semicond.* **25**, 8 (1991) 861–865.

Baranov, A. N., A. N. Dakhno, B. E. Dzhurtanov, T. S. Lagunova, M. A. Sipovskaya, and Yu. P. Yakovlev, *Sov. Phys. Semicond.* **24**, 1 (1990) 59–62.

Barin, I., O. Knacke, and O. Kubaschewski, *Thermochemical Properties of Inorganic Substances*, Springer, Berlin, Heidelberg, New York, 1977.

Both, W., A. Bochkarev, A. Drakin, and B. Sverdlov, *Electron. Lett.* **26**, (1990) 418–419.

Chemg, M. J., G. B. Stringfellow, D. W. Kisker, A. K. Srivastava, and J. L. Zyskind, *Appl. Phys. Lett.* **48**, 6 (1986) 419–421.

Fang, Z. M., K. Y. Ma, D. H. Jaw, R. M. Cohen, and G. B. Stringfellow, *J. Appl. Phys.* **67**, 11 (1990) 7034–7039.

Ghiti A. and E. P. O'Reilly, *Semicond. Sci. Technol.* **8** (1993) 1655–1661.

Gong, X., H. Kan, T. Yamaguchi, I. Suzuki, M. Aoyama, M. Kumagawa, N. L. Rowell, A. Wang, and R. Rinfret, *Jpn. J. Appl. Phys.* **33** (1994) 1740–1746.

Guseinov, A. A., B. E. Dzhurtanov, A. M. Litvak, M. A. Mirsagatov, N. A. Charykov, V. V. Sherstnev, and Yu. P. Yakovlev, *Sov. Techn. Phys. Lett.* **15**, 6 (1989) 483–485.

Jaw, D. H., Y. T. Chemg and G. B. Stringfellow, *J. Appl. Phys.* **66**, 5 (1989) 1965–1967.

Karouta, F., H. Mani, J. Bhan, Fan Jia Hua, and A. Joullie, *Revue Phys. Appl.* **22** (1987) 1459–1467.

Mebarki, M., D. Boukredimi, S. Sadik, and J.L. Lazzari, *J. Appl. Phys.* **73**, 5 (1993) 2360–2363.

Mikhailova, M. P. and A. N. Titkov, *Semicond. Sci. Technol.* **9** (1994) 1279–1295.

Mikhailova, M. P., G. G. Zegrya, K. D. Moiseev, I. N. Timchenko, and Yu. P. Yakovlev, *Semiconductors* **29**, 4 (1995) 357–361.

Nakao, N., S. Yoshida, and S. Gonda, *Solid State Commun.* **49** (1984) 663.

Okhotin, A. S., A. S. Pushkarskii, and V. V. Gorbachev, *Thermophysical Properties of Semiconductors*, Moscow, "Atom" Publ. House, 1972, (in Russian).

Piesbergen, U., *Zeit. fur Naturforschung* **18a**, 2 (1963) 141–147.

Poudjade, A. M. and H. J. Allbany, *Phys. Rev.* **182**, 3 (1969) 802–807.

Tamarin, P. V. and S. S. Shalyt, *Sov. Phys. Semicond.* **5**, 5 (1971) 1097–1098.

Tournie, E., Thesis, University of Montpellier 2, 1990.

Voronina, T. I., T. S. Lagunova, M. P. Mikhailova, M. A. Sipovskaya, V. V. Sherstnev, and Yu. P. Yakovlev, *Sov. Phys. Semicond.* 25, 2 (1991a) 167–171.

Voronina, T. I., B. E. Dzhurtanov, T. S. Lagunova, and Yu. P. Yakovlev, *Sov. Phys. Semicond.* 25, 2 (1991b) 171–174.

Wu, M. C. and C. C. Chen, *J. Appl. Phys.* 72, 9 (1992) 4275–4280.

About the book

The Handbook Series on Semiconductor Parameters includes data of the most popular semiconductor materials. These volumes aim to be a basic reference for scientists, engineers, students and technicians working in semiconductor materials and devices. The books have been kept compact but comprehensive and contain the values of frequently needed parameters, selected and commented by leading experts on these materials. The second volume will include data on Ternary and Quaternary III-V Compounds.

2046 hc

http://www.worldscientific.com/